SLOPE FAILURE IN LOESS
A
DETAILED INVESTIGATION
ALLANDALE, BANKS PENINSULA

A
Thesis
submitted in partial fulfillment
of the requirements for the Degree
of
Master of Science in Engineering Geology
in the
University of Canterbury
by
Stefan Goldwater

University of Canterbury
1990

The human race cannot exist without taking risks- after all, most of us drive motorcars. Asking one of us (the N.Z. Geomechanics Soceity) for an assurance that a piece of sloping ground will not become flatter is like asking a doctor of medicine for a certificate that we will not die- the only question in both cases is "when".

Opening session to the Symposium on Stability of Slopes in Natural Ground, Nelson, Nov. 1984.
D.K. Taylor, Chairman, N.Z. Geomechanics Society.

Appropriately the only significant failure during this thesis investigation involved a University of Canterbury motor vehicle.

ABSTRACT

This study investigates a slope failure complex in loess at Allandale, Lyttelton Harbour. Literature relevant to the slope stability and strength of Banks Peninsula loessial soils is reviewed.

Laboratory and in situ strength testing shows that both C and P layer loess in a partially saturated state displays a significant reduction in undrained shear strength with increasing degree of saturation. Strength reduction can be attributed to reduced pore water tension due to capillary suction which results from an increased degree of saturation. The moisture controlled strength component in partially saturated loess can be defined by any two of dry density, moisture content and degree of saturation. When comparing loess C and P layer remoulded strengths with peak strengths, the P layer is significantly more sensitive to remoulding than C layer.

Drained direct shear testing of C layer loess produces remoulded and peak strength parameters of $c'=0$, $\phi'=28.4°$ and $c'=6$kPa, $\phi'=28.4°$ respectively. Drained direct shear testing of P layer loess produced remoulded and peak shear strength parameters of $c'=0$, $\phi'=28.4°$ and $c'=20$kPa, $\phi'=28.4°$ respectively.

The slope failure complex investigated has been formed by an earthflow initiated by a tension crack in C layer loess (which acts as an unconfined leaky aquifer). Subsequent retrogressive upslope and lateral migration of the slope failure complex involves "turfmat slides" in S layer loess which also acts as an unconfined leaky aquifer, and more tension crack initiated earth flows in C layer loess. Back analysis suggests both forms of slope movement may have failed by translational sliding at the base of their respective loess layer, with a piezometric level coincident with the ground surface. Mobilisation of the "turfmat slide", requires drained remoulded shear strengths, whereas mobilisation of the earth flow is more likely to involve drained peak shear strengths.

CONTENTS

2 Banks Peninsula Geology, Loess, Slope stability -A Review

3 Site Investigation

4 Laboratory Investigations

5 Analysis of Strength Behaviour

6 Slope Stability

7 Conclusions

List of Figures

List of Tables

List of Map Enclosure

List of Symbols

Vw	volume of water
Va	volume of air
Vs	volume of solids
Vv	volume of voids
v	velocity
g	acceleration due to gravity
γ_w	unit weight of water
γ_d	dry unit weight
z	elevation above a reference point
H	hydraulic head
P	pressure
ρ	bulk density
ρ_d	dry density
σ'	effective stress
σ	total stress
u	pore water pressure
c′	effective cohesion
ϕ'	effective angle of friction
S	degree of saturation
X	partially saturated parameter
w	moisture content
s_u	undrained shear strength
q_f	unconfined compressive strength (failure)
u_a	pore air pressure
u_w	pore water pressure
τ	shear strength
ß	downslope exit failure surface angle relative to slope angle
δ	slope angle
ppm	parts per million
ϵ_f	strain at failure
E_{tan}	tangent modulus
E	compactive effort

Chapter 1

INTRODUCTION

1.1 Background

Discussions with Dr D.M. Elder and M.D. Yetton from Soils and Foundations Limited, Christchurch, revealed that qualitative assessment of slope instability is becoming less acceptable to local Authorities. Recently, more local Authorities have required quantitative slope stability analysis to prove an adequate "Factor of Safety". However, it would appear there is no consensus among Geotechnical Engineers as to what shear strength parameters should be used for calculating the factor of safety for loessial soils from Banks Peninsula.

A thesis study site at Allandale on Banks Peninsula (figure 1.1) was selected with the aid of M.D. Yetton and D.H. Bell, for the following reasons:

1) The presence of a pre-existing slope failure contained entirely in loessial soils;
2) The slope failure appeared typical of those encountered elsewhere on Banks Peninsula in loessial soils.

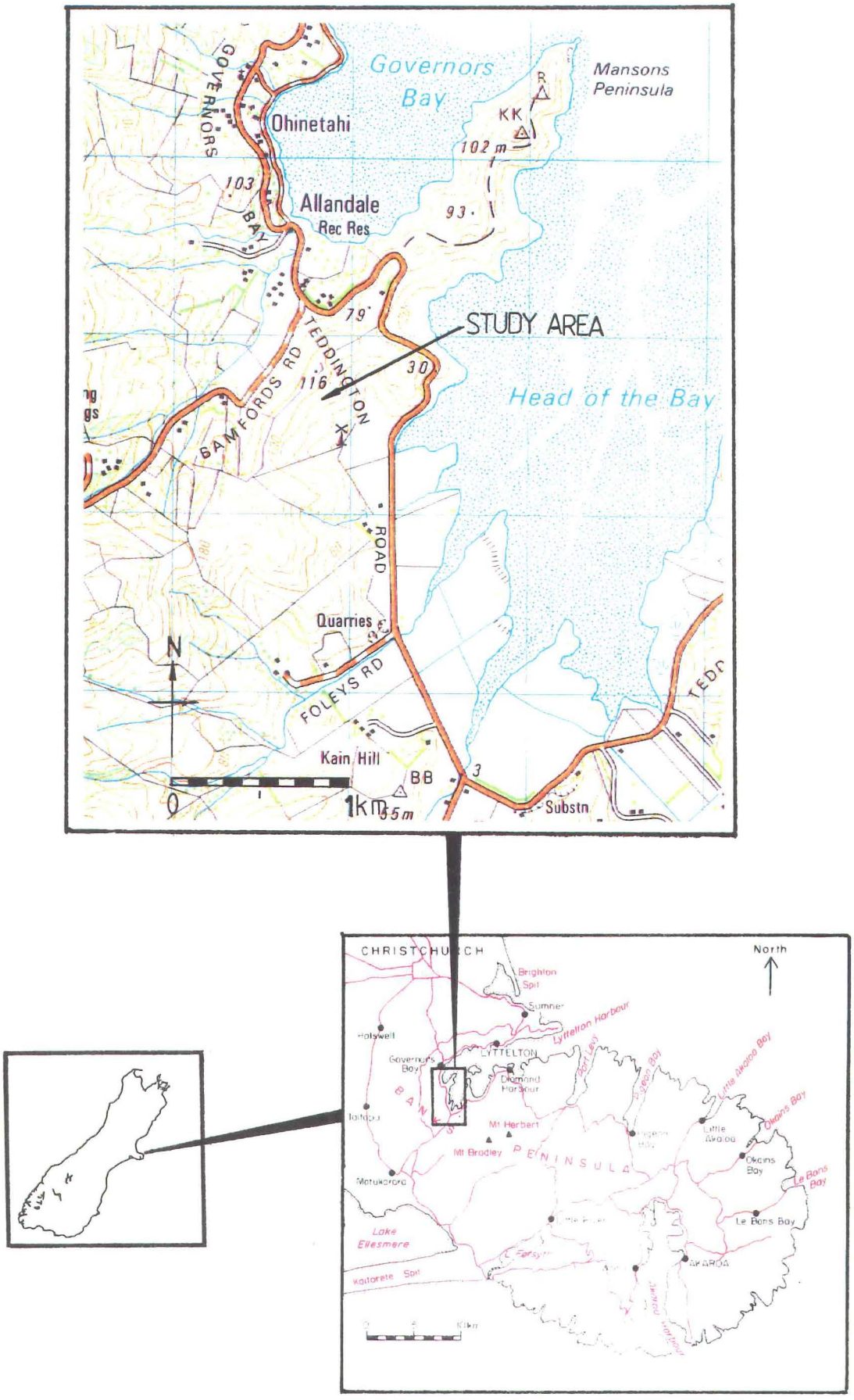

Figure 1.1 Location Map

1.2 Thesis Objectives

The principal objectives of this study are:

1) To determine the causes and mechanism of slope failure identified at Allandale;
2) To develop engineering geological models of the hillslope hydrogeology and stability;
3) To obtain and compare shear strength parameters determined from back analysis of the pre-existing hillslope failure, with shear strength parameters determined by in situ and laboratory testing.

1.2.1 Scope of Research

This study is intended to enhance the understanding of the strength behaviour and slope failure causes and mechanisms of loessial soils from Banks Peninsula. In particular, it is intended to obtain shear strength parameters that are representative of the loessial soils investigated, to enable a soundly based quantitative assessment of slope instability.

1.3 Thesis Methodology

To meet the thesis objectives the author has carryed out detailed engineering geological mapping/logging, installation of appropriate field instrumentation, laboratory and in situ strength testing, and a review of the relevant literature.

1.4 Thesis Organisation

Chapter 2 presents: 1) a literature review of Banks Peninsula engineering geology; 2) a review of loessial soils both locally and worldwide; 3) a review of slope stability concepts relevant to this study, thereby setting the background to the investigations carried out.

Chapter 3 attempts to identify the development and nature of the investigated slope instability. A hydrogeological model of the hillslope is presented and the slope failures are classified.

Chapter 4 presents the laboratory methodology and the results obtained from testing.

Chapter 5 analyses in detail the strength results presented in chapter 4.

Chapter 6 mathematically models the observed instability, compares this with the site investigation findings and presents a schematic model of the slope failures at Allandale.

Chapter 7 presents conclusions drawn from this thesis study and makes recommendations for further research.

Chapter 2

Banks Peninsula Geology, Loess, Slope stability - A Review

2.1 Introduction

This chapter reviews Banks Peninsula geology, loessial soils generally, and the slope stability concepts, relevant to this study. A review of the previous work sets the framework for the investigations carried out.

2.2 Geological Setting

In summary, the present form of Banks Peninsula developed in four phases of volcanic activity: Lyttelton, Mt Herbert, Akaroa, and Diamond Harbour Volcanic Phases, which formed two major composite volcanoes (Lyttelton and Akaroa) (see figures 2.1 and 2.2). Rapid erosion, both during and after successive volcanic episodes, formed anteconsequent radial drainage patterns. By the end of the volcanism both the Lyttelton and Akaroa volcanoes had been breached by the sea.

During the Pleistocene, glacial outwash sediments accumulated to form the Canterbury Plains, and transformed the once volcanic island into a peninsula. Aeolian silt (loess) was blown from the Canterbury Plains and accumulated in gullies and on many slopes on the peninsula.

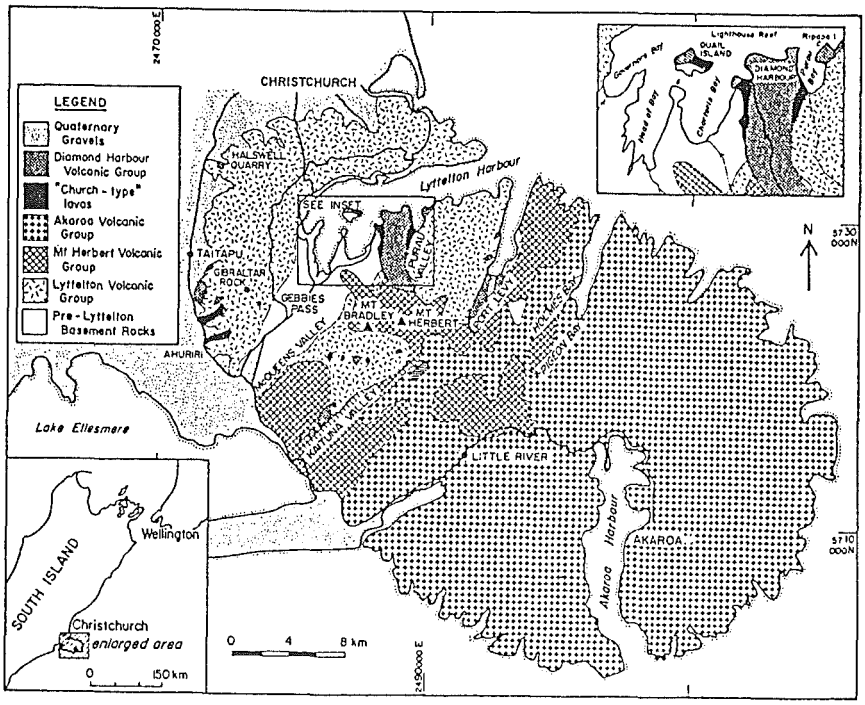

Figure 2.1 Simplified Geological Map of Miocene Volcanic Rock of Banks Peninsula (after Sewell, 1988).

AGE millions of years before present		BANKS PENINSULA GEOLOGY	
		GEOLOGICAL UNIT	LITHOLOGY
QUATERNARY	0		
	1	Recent deposits	loess, gravels and alluvium
		break in succession	no rocks of Pliocene age known
MIOCENE	6	Diamond Harbour Volcanics	basalt lavas
	8	Akaroa Volcano	basalt - trachyte lavas, dikes, gabbro - syenite
		Mt Herbert Volcanics	basalt lavas, pyroclastics and lake sediments
	10	Lyttelton Volcano	basalt - trachyte lavas and dikes
	12	Governors Bay Volcanics	andesite flows and rhyolite domes
	14		
		break in succession	no rocks of Eocene - Oligocene age known
PALEOCENE	50		
	60	Charteris Bay Sandstone	marine, buff - coloured quartz - sandstone
CRETACEOUS		break in succession	no rocks known
	90	McQueens Volcanics	andesite flows and rhyolite domes
	100	break in succession folding of Torlesse rocks	no rocks of Jurassic age known
TRIASSIC	210		
	230	Torlesse Terrain	marine, grey sandstones and mudstones, and red cherts

Figure 2.2 Stratigraphic Column of Banks Peninsula (after Weaver et al., 1985).

A more detailed geological history of Banks Peninsula is described by: Bradshaw et al., 1981; Thiele, 1983; Weaver et al., 1985; Browne and Field, 1988; Sewell, 1988; Sewell et al., 1988; Weaver et al., 1989; and Shelly, 1989.

2.3 Loess Deposits

2.3.1 Introduction

Loessial soils are the predominant slope deposit on Banks Peninsula, particularly on the lower slopes of the Port Hills, where residential housing is concentrated. The aim of this study is to extend the understanding of slope failure on Banks Peninsula by evaluating the fundamental parameters affecting strength and stability of hillslope loess deposits. This section begins with a general discussion of loess, and culminates in a discussion of Banks Peninsula loess.

2.3.2 A General Overview

Loess (derived from the German *löss* or *lösch* = loose), is a fine grained aeolian sediment which covers approximately 10% of the world's land surface and generally occurs between latitudes 24° and 55° North in the northern Hemisphere, and between latitudes 24° and 47° South, in the southern Hemisphere (Kriger, 1985) (figure 2.3). The thickest and most extensive loess deposits are found in China, Soviet central Asia, the Ukraine, Siberia, central Europe, Argentina and the Great Plains of North America. Small deposits occur in Israel, Iran, Iraq and New Zealand, but true loess is rare in Australia and Africa (Pye, 1984).

There are many reported studies of loess deposits of the world. However, owing to linguistic problems and the diversity of research interest, it is often difficult to obtain the relevant literature of most interest. There appear to be at least five main languages in which discussion about loess has been written: Russian; English; German; French; Chinese; and it is also discussed in various other central European languages. This often results in misinterpretation from translations and a general lack of communication between researchers from different countries. This is especially evident between Russian and English speaking scientists. In addition, there is a wide diversity of specialised interest in loess research (For example: Engineering, Agriculture, Geology, Archaeology, Anthropology, and History), (Smalley, 1983).

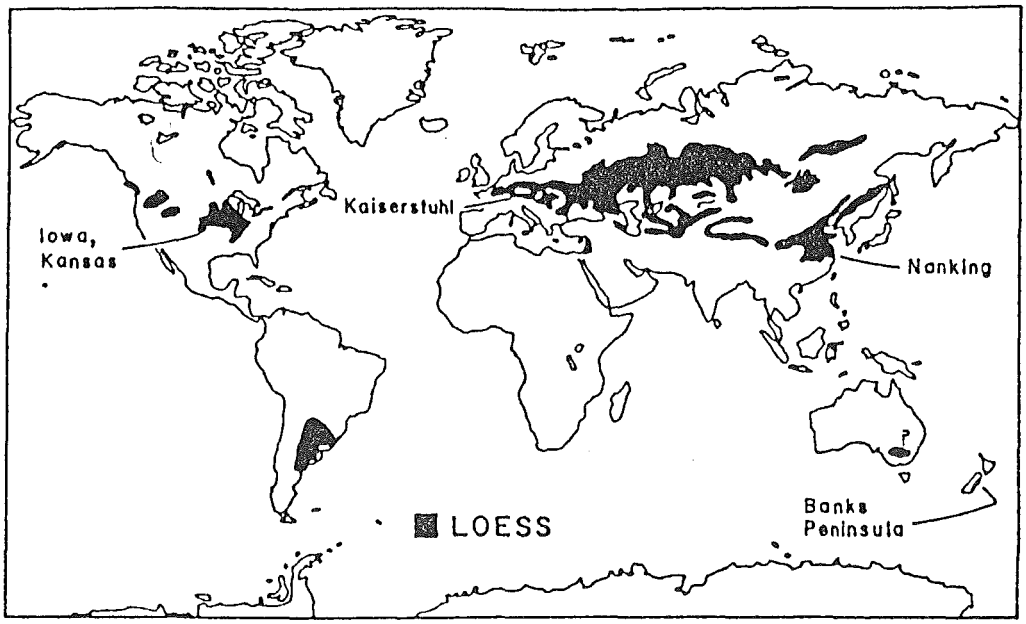

Figure 2.3 Map Showing the Distribution of Loess Deposits. Loess covers approximately 10% of the world's land surface (after Tatlor et al., 1983).

The majority of loess-size material (2-60 μm) is produced by two major mechanisms-glacial grinding and frost weathering (Smalley and Smalley, 1983). Limited amounts of loess material are derived from other sources such as high energy rivers. The two major mechanisms produce two primary types of loess:

1) ice-sheet loess (IS) - associated with major continental glaciations and produced by glacial grinding and;
2) mountain loess - produced by frost weathering.

Table 2.1 shows in a generalised form the type and source region for loess deposits of various parts of the world.

Table 2.1 **Loess deposits in various parts of the world - type and source** (modified after Smalley and Smalley, 1983)

Place	Type	Source Region
Central North America	IS	northern glaciers
North European Band	IS	northern glaciers
China, North China & inland	Mountain	Himalayan & Tibetan uplands
New Zealand, North Island	Mountain	Tararua Mts.
	(& tephric)	Ruahine Mts.
New Zealand, South Island	Mountain & IS	Southern Alps
Europe, Rhineland	Mountain	European Alps
Europe, East-Central	Mountain & IS	Alps and northern glaciers
Soviet Central Asia	Mountain	Tien Shan Mts.
Kashmir	Mountain	Himalayas
England, S.E.	IS	northern glaciers
Argentina	Mountain	Andes

There is no single, universally accepted definition of loess. Pye (1984) states:

> There have been many attempts to define loess and no single definition, including that proposed by the INQUA (International Union for Quaternary Research) Loess Commission, has gained universal acceptance.

Pye gives his definition of loess, which is very similar to most European definitions, as:

> ...loess is defined simply as a windblown silt deposit consisting chiefly of quartz, feldspar, mica, clay minerals and carbonate grains... Loess is typically homogeneous, non-stratified and highly porous...

This definition, like many others, would exclude New Zealand loess. It is not always highly porous, generally not calcareous or non-stratified and the soil mass is not typically homogeneous. For the purposes of this thesis, Raeside's (1964) definition will be adopted. It is essentially:

> ...any fine-textured deposit of aeolian origin other than sand dunes or tephra. It thus embraces all aeolian deposits where transport has been primarily by suspension, irrespective of content of organic matter, mineralogical composition, calcium carbonate content, degree of compaction, or texture.

Table 2.2 gives the general properties and characteristics of loessial deposits worldwide.

Table 2.2 General Characteristics of Loessial Deposits (after Bell, 1978)

COLOUR	- usually yellow-brown or buff, but varies as a function of organic content
TEXTURE	- consists dominantly of silt-sized particles (>50% by wt. in range 10-50μm) - contain fine sand and clay-size particles, the latter as aggregates surrounding the coarser particles - silt and fine sand particles dominantly subangular - texture open, with little granular interlock and high void space (porosity 30-60%) - material usually friable, but some calcite cement may be present
COMPOSITION	- quartz predominates (50% +); feldspar subordinate (20%); other minerals dependent on source area - clay-sized fraction may consist of both clay minerals (e.g. illite, montmorillonite) and non-clay minerals (quartz and feldspar) - calcite cement often present (but secondary in origin) - principal organic remains are shells of terrestrial snails
STRUCTURE	- stands vertically in cut faces if dry - displays vertical (polgonal) fracture patterns resulting from desiccation and shrinkage - may contain tubular (root?) structures to depths of 10m (+) - carbonate encrustations common on fracture faces - carbonate and iron concretions may occur in some horizons - massive, compact layer ("fragipan") often developed within soil profile
TOPOGRAPHIC FORM	- blankets underlying topography to variable depth - often displays intricate drainage patterns (both surface and subsurface) - chimneys and tunnels may form as a result of subsurface erosion and surface collapse - creep "terracettes" common, especially toward base of slopes - aprons of reworked (water deposited) loess common at base of slopes

2.3.3 Banks Peninsula Loess

Loess Deposits

Loess accumulated gradually on Banks Peninsula in a series of extended jumps across the fans and plains adjacent to the aggrading rivers of the Canterbury region (Ives, 1973). Raeside (1964) suggests that during the sea-level recessions of the Pleistocene (max. 100m below present sea level), the continental shelf was a likely additional source region for the Banks Peninsula loess (see figure 2.4).

Cegla (1969) suggests that loess size particles accumulate in places where the capillary water fringe rises to the ground-air interface. Hence the presence of moisture in the ground is of primary importance for the accumulation of loess. Cegla emphasises the ability of loess to transmit water by capillary action, and that a capillary rise of some 20m is obtainable in loess deposits (possibly the controlling factor in deposit thickness).

Figure 2.5 shows those Pleistocene loess deposits thicker than 30cm and the approximate extension of the Pleistocene land surface around the South Island. Raeside has suggested that during the last glaciation, the present shoreline was extended by approximately 50km in South Canterbury and Pegasus Bay. Therefore,

the toes of the great Pleistocene alluvial fans, of which only the heads are exposed on the Canterbury Plains today, would have been an abundant source of fine detritus (Raeside, 1964).

The thickest and coarsest loess deposits occur on the northwest side of the Peninsula which, according to Griffiths (1973), indicates transport by prevailing north-westerly winds from the nearby floodplain and fan of the Waimakariri River.

Four episodes of loess deposition marked by periods of non-deposition and hence soil formation have been recognised in the most complete loess sections on Banks Peninsula (Griffiths, 1973). Attempts to date the depositional episodes have been reviewed by McDowell (1989), who suggests they relate to four glacial/interglacial cycles. This is supported by work conducted by Brown and Wilson (1988) on four gravel (glacial) and four, fine sediment (interglacial) sequences.

Two distinct facies of loess have been recognised on the Peninsula, and are named after their type locations, Birdlings Flat and Barry's Bay. They tend to be found in different areas on Banks Peninsula (see figure 2.6, Griffiths p659), although some intermingling of loess sheets is evident on the inner wall of the eroded Lyttelton crater (Griffiths, 1973). Barry's Bay loess is found in the area researched in this thesis.

Barrys Bay loess is non-calcareous and fine, with a silt loam texture. It is prevalent around the heads of inlets and on ridge tops in the eastern segment of Banks Peninsula. Both loesses are different facies of the same loess, from the same source and deposited during the same periods.

Birdlings Flat loess is calcareous and coarse, with a fine sandy loam texture. It is thickest at lower elevations and on north facing slopes. Salts (calcium sulphate, calcium chloride, and sodium sulphate and chloride) are found in the loess at the extremities of ridges at lower elevations. Calcium carbonate is found at higher elevations only, as it is the first salt to precipitate out of the loess. Sparsely distributed hard calcareous concretions are found throughout the strata, or concentrated in seperate horizons (Griffiths, 1973).

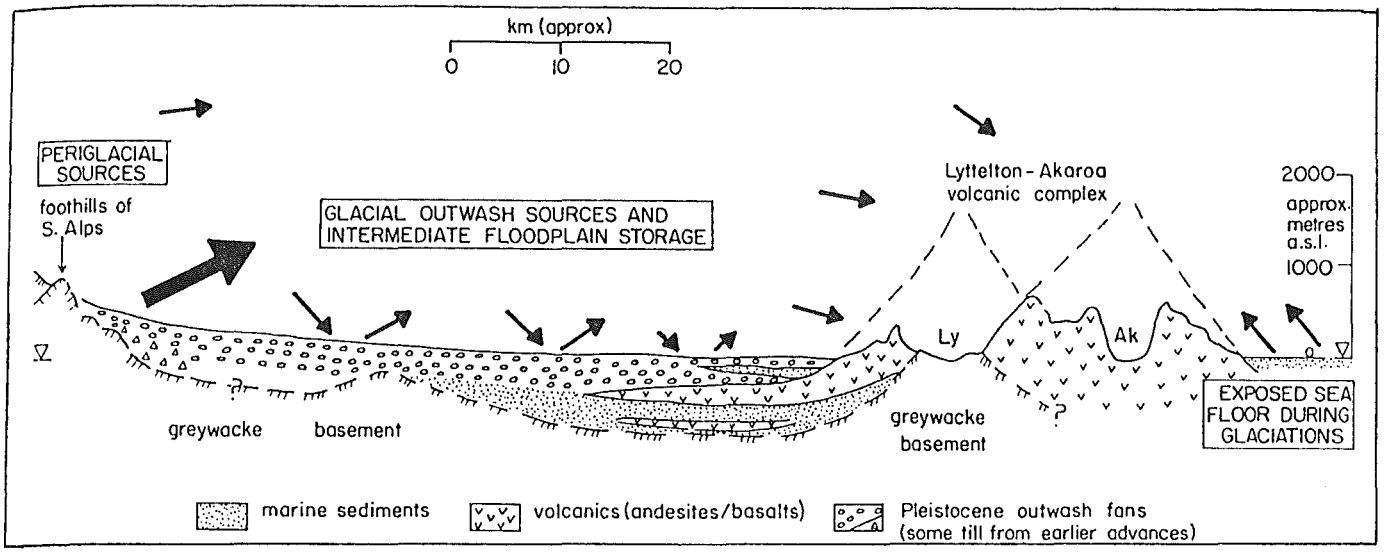

Figure 2.4 Schematic Representation Showing Origin for Banks Peninsula Loess Deposits (after Bell, 1978)

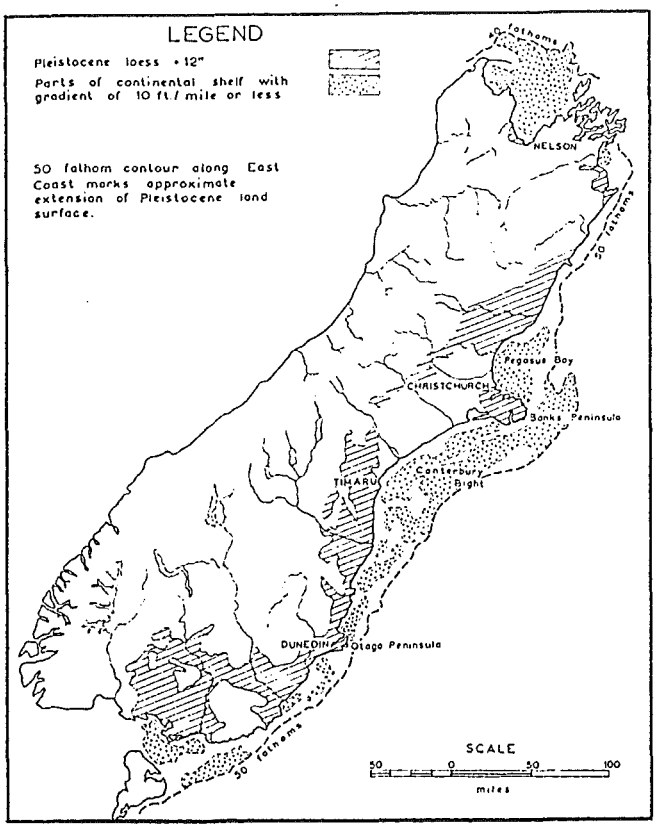

Figure 2.5 Loess Deposits of the South Island Thicker than 30cm (after Raeside, 1964)

The distribution of loessial soils on Banks Peninsula today, reflects the topographic relief at the time of primary airfall deposition, and the subsequent reworking by slope processes during the Quaternary to form secondary deposits (Bell et al., 1986).

Ives (1973) divides loess into two categories based on collation of overseas information. These are:

1) Primary loess- initial deposits derived from either fluvio-glacial or continental sources;
2) Secondary loess- derived from primary loess by being altered in place (soil horizon formation), or reworked and redeposited.

Pye (1984) separates loess into three categories:

1) Primary loess- wind deposited;
2) Weathered loess- primary loess whose sedimentary characteristics have been markedly modified by weathering, soil formation and diagenesis;
3) Reworked loess- consisting of material eroded from primary and weathered loess, and redeposited by running water and slope processes.

Bell and Trangmar (1987) categorize the loessial deposits on the Peninsula as:

1) In situ (primary airfall) loess;
2) Loess-colluvium (reworked in situ loess).

For the purposes of this study, the categorisation used by Bell and Trangmar (1987) is adopted because, on Banks Peninsula, Ives' and Pye's *Primary* loess is indistingishable from Pye's *Weathered* loess. As there is no primary loess exposed at the surface, it is superfluous as a mapping term.

Pedogenic Layering

Figure 2.7 shows the pedogenic layering that has developed in Banks Peninsula loess, and the terminology used to describe the layering.

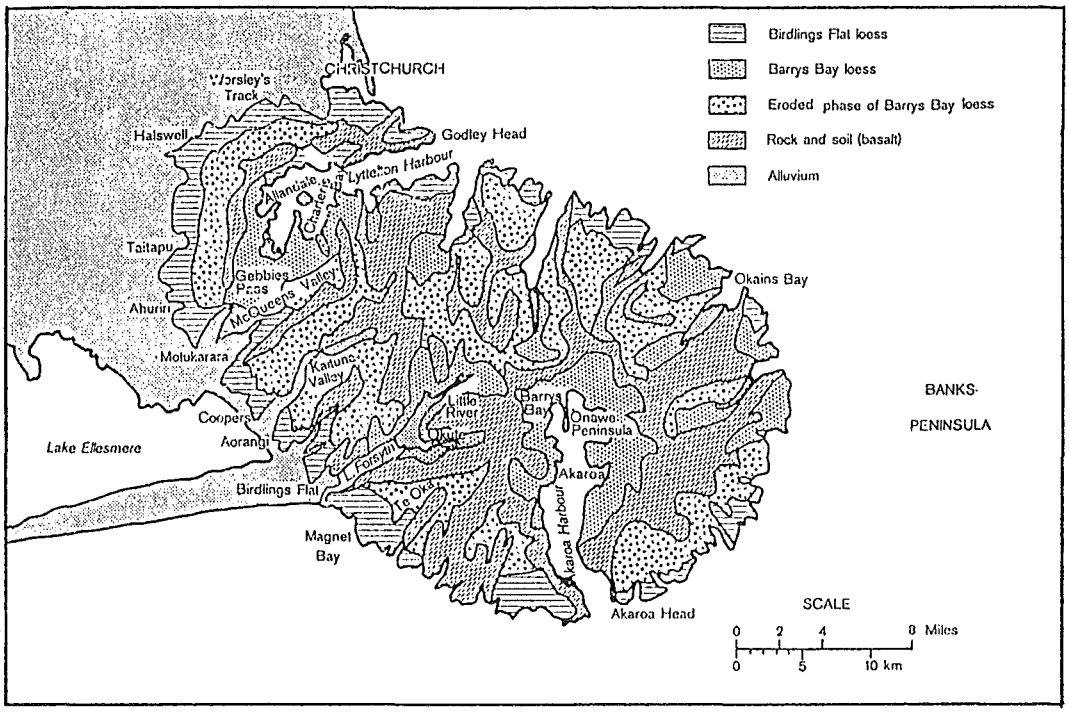

Figure 2.6 Distribution of Loess on Banks Peninsula (after Griffiths, 1973)

This non-generic terminology was introduced by Hughes (1970) and has subsequently been adopted by engineers and engineering geologists (Evans, 1977a; Evans and Bell, 1981; Bell, 1978; Bell et al., 1986). However, a more recent publication by Bell and Trangmar (1987) uses pedological nomenclature to describe the loess layering, similar to that used by Griffiths (1973).

The surface (S) layer consists of top soil that grades into a moderately weathered sandy silt. Underlying the surface layer is the compact (C) layer, generally plastic, mottled clayey silt (relatively higher clay content than S and P layer loess). The compact layer typically exhibits vertical joints with associated gammation and mottling zones (Griffiths, 1973). Selby (1976) calls the compact layer the fragipan, and suggests that it originates from seasonal drying, which causes cracking of the subsoil and subsequent infilling by loose material. The following wet season causes the loess to swell and compact the soil. Underlying the compact layer is the parent (P) material which, in contrast to the overlying layers, is a non-plastic homogeneous silt.

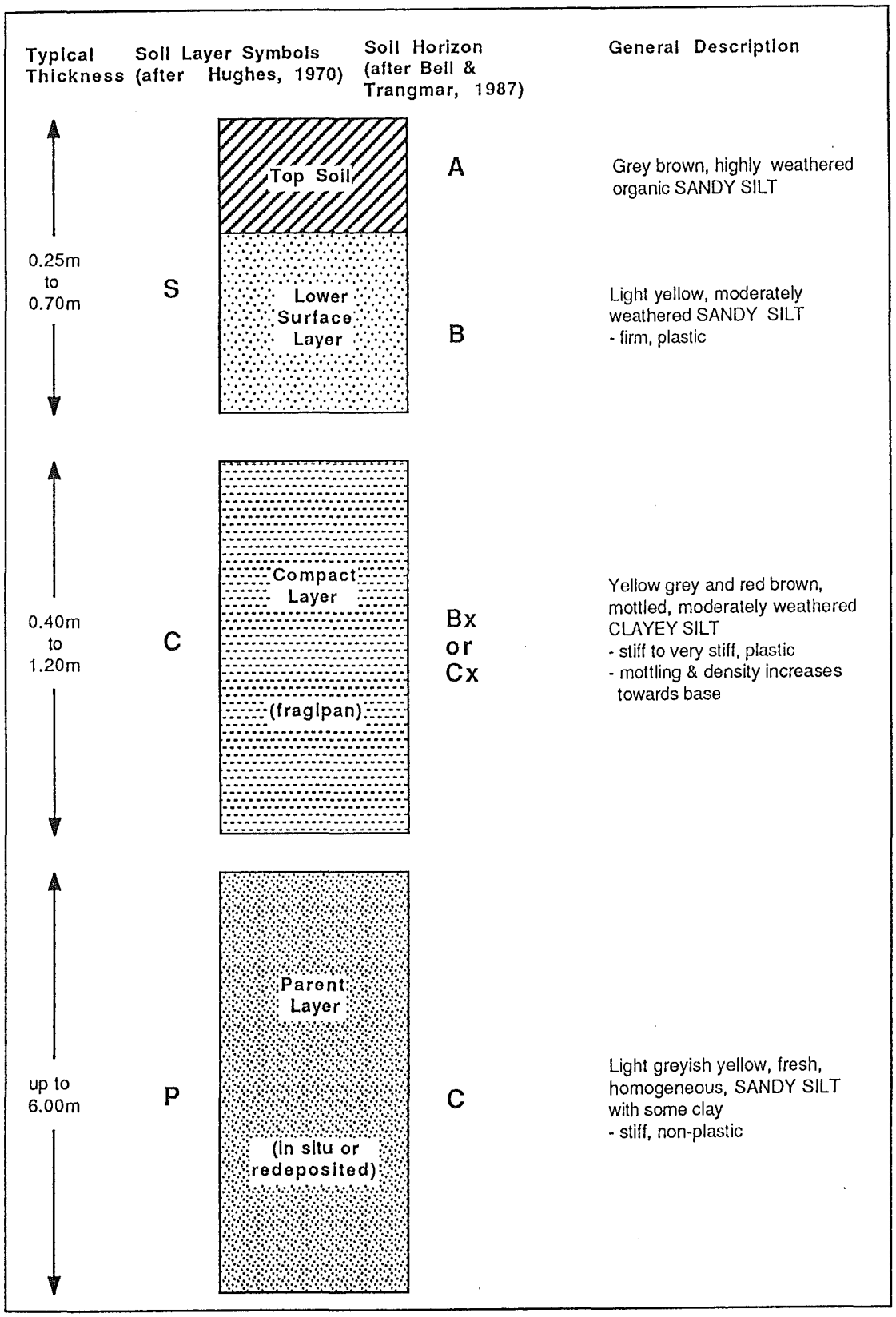

Figure 2.7 Pedogenic Layering that Develops in Banks Peninsula Loess

Table 2.3 Geotechnical Properties of Banks Peninsula Loess

Parameter	Typical Range of Values	Source Reference
POROSITY	30 - 40%	Birrel & Packard (1953)
VOID RATIO	0.4 - 0.7	Birrel & Packard (1953) Miller (1971)
ATTERBERG LIMITS	LL 18 - 33 PL 17 - 22 (C layer) PI < 12	Alley (1966) Hughes (1985) Crampton (1985) Yetton (1986)
GRAIN SIZE	(Silt range > 0.002mm & < 0.06mm) Sand ≈ 10% Silt 65 - 80%, Clay 11 - 25%	Alley (1966) Hughes (1985) Crampton (1985) Yetton (1986)
DRY DENSITY	S layer average = 1.54t/m^3 (1.39 - 1.62t/m^3 range) C layer average = 1.64t/m^3 (1.51 - 1.88t/m^3 range) P layer average = 1.55t/m^3 (1.32 - 1.71t/m^3 range)	Evans (1977) Crampton (1985) Yetton (1986)
LINEAR SHRINKAGE	0 - 2% in lower S and P layers > 5% in C layer	Alley (1966) Yetton (1986)
PERMEABILITY	1.5 * 10^{-7} m/s (undisturbed) ≈1*10^{-7}m/s (In-situ test)	Birrel & Packard (1953) Sanders (1986)
INTERNAL ANGLE OF FRICTION	35 - 37° (Residual, Ring shear) 30° (Peak, Triaxial (total)) 30° (Peak, Triaxial (total)) 15 - 25° (Peak, Triaxial (effective))	Salt (1983) Mackwell (1986) McDowell (1989) Alley (1966)
COHESION	0 kPa (effective) 85 - 112kPa (apparent) 0 - 180 kPa (apparent)	Alley (1966) Macwell (1986) McDowell (1989)
COMPRESSION INDEX	Cc = 0.17 (1.7% vol. change dry to saturated)	Birrel & Packard (1953)
Ph	Acidic - 5(S layer) to 7(P layer)	Miller (1971)
SOLUBLE SALT CONCENTRATION	Incr. with depth, from 1meg/l to 60meg/l in P layer	Miller (1971)
EXCHANGEABLE SODIUM %	0.9 in S layer to41 deep in P layer	Hughes (1970)
SEISMIC VELOCITY	250 - 400m/s	Crampton (1985) Yetton (1986) McDowell (1989)
RESISTIVITY	Varying with depth from 90 ohm/m near surface to <10 ohm/m in P layer	Yetton (1986)
CONDUCTIVITY	From 1.0 *10^{-4} mho/cm to 14 *10^{-4} mho/cm with depth	Birrel & Packard (1953) Yetton (1986)

(Modified from Yetton (1986))

Table 2.4 SOME GEOTECHNICAL PROPERTIES OF INTERNATIONAL LOESS

Parameters	Chinese	Czechoslovakia	USSR	USA (Iowa)	(Vicksburg)	Yugoslavia
Natural water content	9.5 - 20.1%	14.8 - 17.8%	9.0 - 22.0%	9.0 - 20.0%		14.5 - 20.0%
Dry density (t/m^3)	1.29 - 1.55		1.43 - 1.98	1.2 - 1.5	1.49	1.20 - 1.48
Degree of Saturation	55 - 58%	56 - 76%		20 - 60%		
Void ratio	0.76 - 1.10	0.63 - 0.77	0.43 - 1.00		0.81	
Liquid limit Plastic limit	26 - 31 8 - 12	26 - 39 15 - 20			26.5 24.5	
Grain size sand silt clay	 12 - 35% 54 - 70% 8 - 24%				 9%	
Gs					2.71	
w (opt)					16% ($1.62t/m^3$)	
Angle of internal friction (effective) (total) Remoulded (total)	26.1 - 28.4°				20° (w <1%) 15° (w = 16%) 34° (w < 1%) 24° (w = 16%) 27° (w < 1%) 23° (w = 16%)	27 - 62kPa (qu) (w = 14 - 20%)
Cohesion	20 - 24 kPa				303 (kPa) (34°) 76 (kPa) (24°) 207 (kPa) (27°) 21 (kPa) (23°)	
References	Lin & Wang (1988)	Feda (1966)	Lysenko (1971)	Saye et al. (1988)	Matalucci (1970)	Milovic (1988)

Geotechnical Properties

Tables 2.3 and 2.4 summarise the general geotechnical properties of Banks Peninsula loess and some international loess. There are large gaps in the international material, which is largely due to poor reporting of these properties. These tables are included for interest only, as in many cases the methods for determining these properties are unknown.

2.4 General Slope Stability

2.4.1 Introduction

This study concentrates on a particular slope failure within loess on Banks Peninsula. This section presents a general review of literature relevant to the analysis of the slope failure investigated.

Slope movement is essentially a geological phenomenon resulting from either natural processes or human actions (or both), which involve the displacement of soils, rocks, or combinations of both. Although the causes of slope movements tend to be complex and varied, geological factors are generally the fundamental cause of slope failure in natural ground (Hancox, 1974).

The largely qualitative descriptive approach to slope movement by geologists differs considerably from the quantitative approach of engineers. Today, slope stability also falls into the domain of the engineering geologist. Hancox (1974) describes the qualitative and quantitative information with respect to geology, hydrology, and material mechanics, on which engineering calculations can be soundly based. This requires a close liason and understanding between the engineering geologist and the engineer.

2.4.2 Slope Stability Classification

Slope movement classification is an attempt to reduce a multitude of different but related slope processes, to a few easily recognisable and meaningful groups on the basis of common properties. By definition, a good classification system must have consistent terminology to avoid ambiguity, accommodate new findings with minimal change, be universally applicable and allow for reproduction of results.

Publications by Hansen (1984) and Crozier (1986) review the published literature on slope movement classification systems. However the generalised descriptive classification system of Varnes (1978) is the most universal, and as such has been adopted for this study. Principal criteria used in his classification are:

1) Mechanism and mode of movement;
2) material properties;
3) failure geometry;
4) geologic, geomorphic, geographic and climatic setting;
5) age and state of activity;
6) causes of movement.

Varnes (1978) classified slope movement into six broad groups which are described in figure 2.8, a pictorial representation of Varne's slope movement classification. Often slope movement cannot be attributed to a single mechanism and so requires a multiple classification, in which case the dominant mechanism is listed last.

2.4.3 Causes of slope movement

Terzaghi (1950) states that there are two ways to initiate slope movement:

1) external causes, resulting in an increased shearing stress along the rupture surface.
2) internal causes, resulting in a decreased shearing resistance of the material.

Table 2.5 outlines the factors that contribute to changes in internal and external conditions which could result in slope movement. Moisture content has been added to the *Internal changes in stability conditions,* as it has been noted by Bell and Trangmar (1987) to reduce shear strength in Banks Peninsula loess. The extent to which this occurs forms a fundamental part of this study.

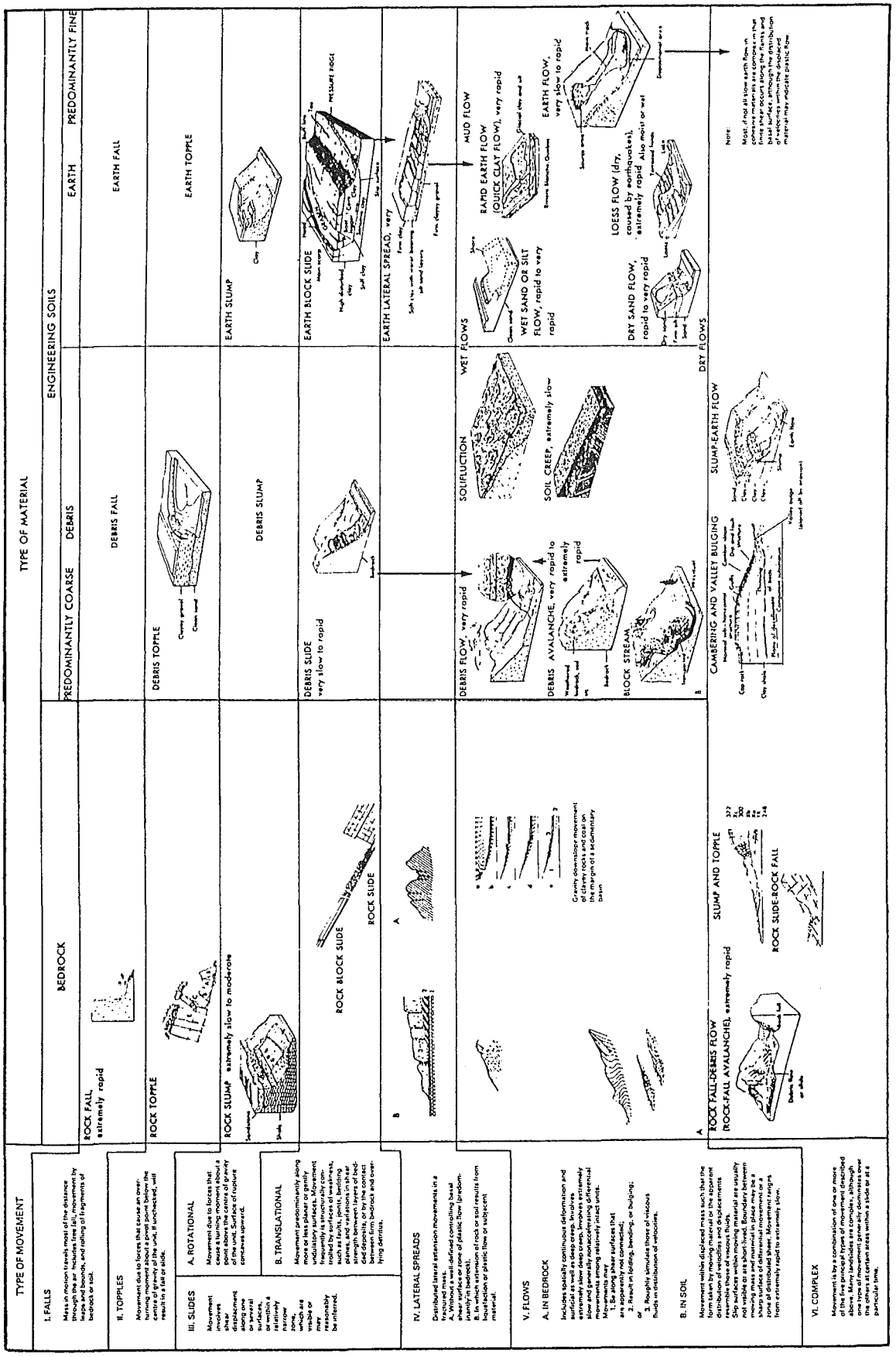

Figure 2.8 Varne's Slope Movement Classification- pictorial (after Varnes, 1978)

Table 2.5 Causes of Mass Movement
(modified after Terzaghi, 1950; Brunsden, 1979; Hansen, 1984)

External changes in stability conditions

1) Geometrical changes (undercutting, erosion, stream incision, artificial excavation leading to changes in slope height, length or steepness)
2) Unloading (erosion, incision, artificial excavation)
3) Loading (addition of material, increase in height, etc.) including undrained loading
4) Shocks and vibrations (artificial, earthquakes, etc.)
   Associated processes:
   a) Liquefaction
   b) Remoulding
   c) Fluidisation
   d) Air lubrication
   e) Cohesionless grain flow
5) Drawdown (lowering of water in lake or reservoir)
6) Changes in water regime (rainfall, increase in weight, pore pressure, reduced apparent cohesion)

Internal changes in stability conditions

1) Progressive failure (following lateral expansion or fissuring and erosion)
2) Weathering (freeze-thaw, desiccation, reduction of cohesion, removal of cement)
3) Seepage erosion (solution, piping etc.)
4) Increased moisture content (reduced apparent cohesion)

2.4.4 Basic Shear Strength Properties

Shear stress and shear strength are fundamental to any quantitative study of slope stability. This section provides a basic introduction to the determination of these parameters.

Effective stress

Terzaghi (1936) developed the principle of effective stress, which is approximately the force per unit area carried by the soil skeleton. It is the effective stress in a soil mass that controls its volume change and strength. The effective stress (σ') within a given element of saturated soil is:

$$\sigma' = \sigma - u \qquad 2.1$$

where σ is the total stress acting in the same direction, and u is the pore water pressure acting in the element. For soils with a single fluid, either water or air in the pore space, equation 2.1 is essentially true (Bishop and Henkel, 1957).

In partially saturated soil, water in the void space is not continuous, but consists of a three-phase system- that is, solid, pore water, and pore air. Based on laboratory test results, Bishop and Henkel (1957) gave the following equation for effective stress in partially saturated soils:

$$\sigma' = \sigma - u_a + X(u_a - u_w) \qquad 2.2$$

where u_a = pore air pressure

u_w = pore water pressure

In equation 2.2, X is an experimentally determined coefficient, which represents the fraction of a unit cross-sectional area of the soil occupied by water. For dry soil X = 0, and for saturated soil X = 1. Bishop and Henkel show that X is primarily dependent on the degree of saturation, though it is influenced by soil structure. The relationship between parameter X and the degree of saturation for a silt is shown in figure 2.9.

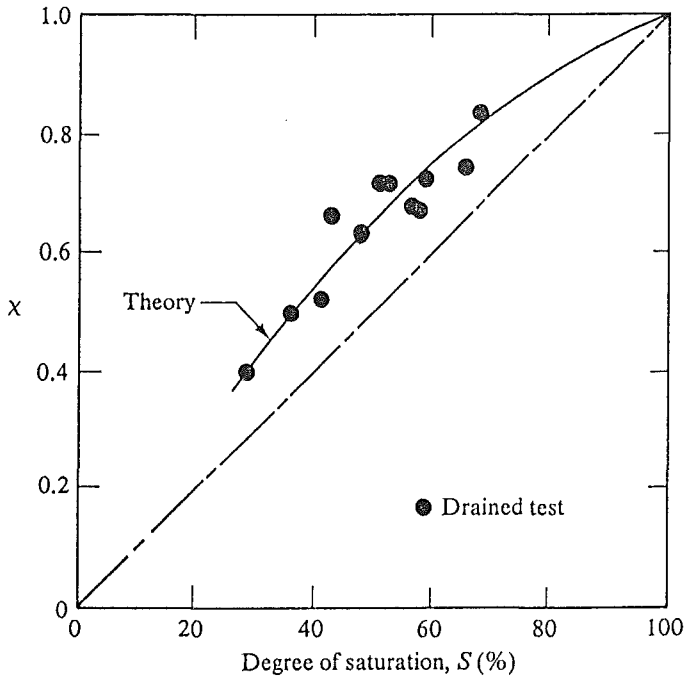

Figure 2.9 Relationship between Partially Saturated Parameter X and the Degree of Saturation S for a Silt (after Bishop & Henkel, 1957)

Peak and Residual Strengths

When a soil is subjected to shear strain, the shear resistance increases. For any applied effective normal stress, the limit to the resistance that the soil can offer is known as the peak shear strength. If the soil is sheared beyond the peak shear strength value, the resistance offered by the clay particles decreases until a constant value is reached, which is known as the residual strength. The decrease in shear strength to its residual value is related to the orientation of clay particles in the sheared zone (Skempton, 1985). For a normally consolidated and an over consolidated clay tested under drained conditions, figure 2.10 shows the typical stress-strain curves and defines the peak and residual strength failure envelopes.

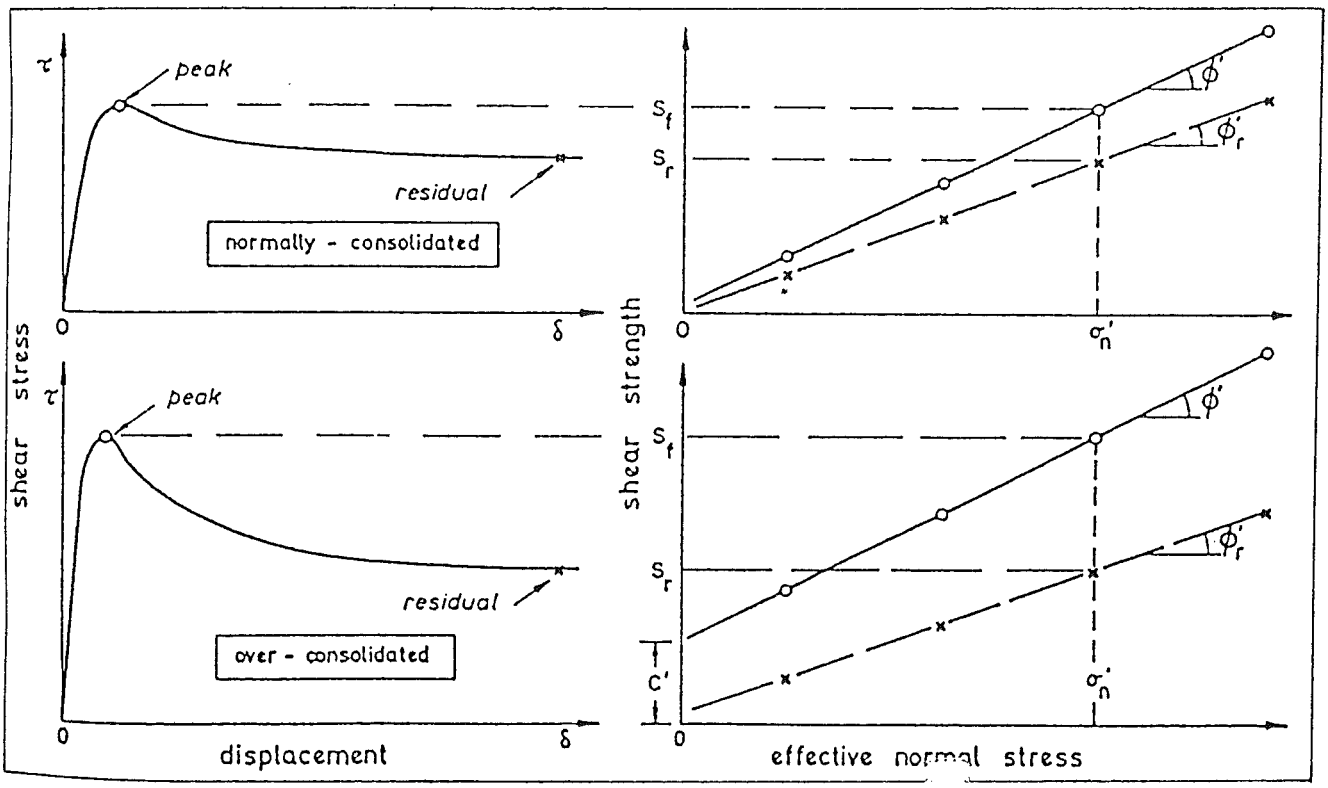

Figure 2.10 Definition of Peak and Residual Stress Envelopes (after Skempton, 1964)

Many laboratory tests will not measure the true residual strength because the test apparatus are limited as to the amount of relative displacement they can apply to a sheared sample. The resulting measured post peak strength is often referred to as the remoulded strength, which falls part way between the peak and residual strengths on the stress-strain curves shown in figure 2.10.

Failure Criterion

Conventional soil strength analysis is based on the Mohr-Coulomb failure criterion and the effective stress theory for saturated soils, given by the following expression:

$$\tau \leq c' + \sigma'_n \tan\phi' \qquad 2.3$$

where shear strength (τ) on any plane in a soil is related to the effective normal stress (σ'_n), and the soil parameters, effective cohesion (c', cohesion intercept, figure 2.10), and the internal angle of friction (ϕ'). Although shown as a linear relationship, this is a simplification, because the true failure envelope is often curved, especially at low normal stresses (Skempton and Hutchinson, 1969). This causes the tangentially defined parameters $c'$and $\phi'$to vary with the applied normal stress level.

Determination of Shear Strength Properties

Soil disturbance is inevitable during sampling for laboratory testing and also occurs with most forms of in situ testing. The effects of disturbance are particularly applicable to sensitive soils and cemented soils. If on remoulding clay particle reorientation substantially decreases the available shearing resistance, the soil is said to be *sensitive* (Terzaghi and Peck, 1967). The effects of pore water pressure on soil strength calculated from in situ or laboratory testing methods will now be considered.

In general, a strength test deforms a soil until the point of failure (peak strength) is attained. The rate at which the deforming load is applied becomes important if the free flow of pore water is too slow for full pore pressure equilibration at all stages of the applied loading, or if free flow is not permitted at the soil boundary.

Excess pore water pressures are then generated. Selecting a rapid strain rate will ensure that failure takes place without significant drainage, while setting a slower rate will have the opposite effect, and drainage will allow excess pore water pressures to dissipate. Shear strength tests can be conducted under drained or undrained conditions, so that an apparatus which permits the control of drainage or measurement of pore water pressures is desirable for the determination of effective stress parameters c' and σ'.

Where pore water pressures can not be measured or calculated, effective stresses can not be used in shear strength calculations, and an alternative method must be used. The conventional approach is to use undrained shear strength, which relates only to conditions where the pore water in the soil can be considered immobile relative to the soil structure. Such conditions only exist in a failing slope when failure is very rapid.

Two common methods of undrained shear strength determination are the *unconfined compression test,* and the *vane shear test.* In both tests the specimen is brought to failure relatively quickly and not allowed to consolidate. The appropriate interpretation of the unconfined compression test is to plot the known total stresses at failure on a Mohr diagram. This produces a horizontal ($\phi_u = 0$) Mohr-Coulomb envelope where the cohesion intercept represents the deviator stress at failure q_f (see figure 2.11). The undrained shear strength s_u from these tests are given by $s_u = \frac{1}{2}q_f$.

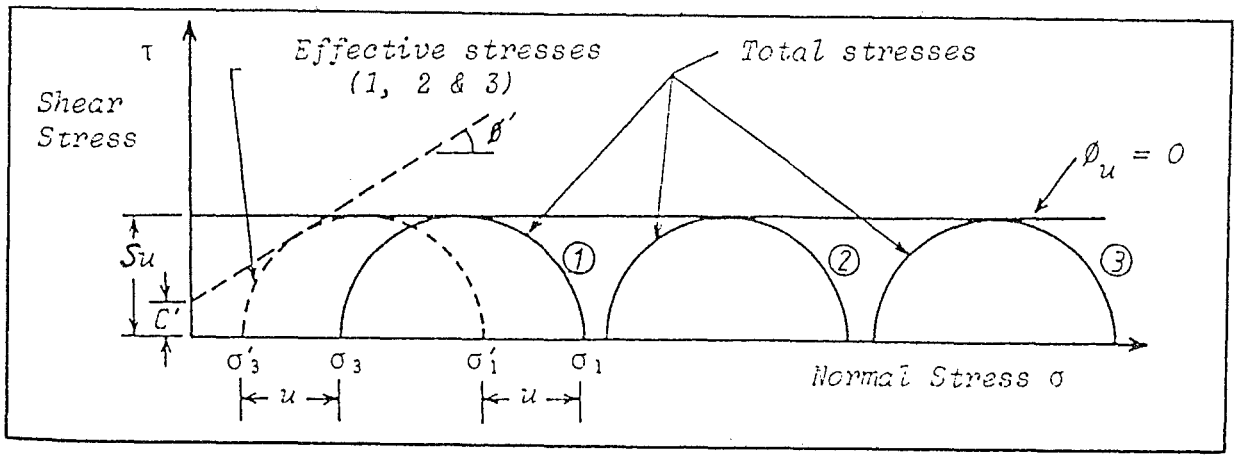

Figure 2.11 Mohr Stress Circles for Undrained Tests on Saturated Cohesive Soil (after Miller, 1982)

Atkinson and Bransby (1978) suggest that the undrained shear strength s_u measured in triaxial compression tests is independent of the applied total stress path, but the pore water pressure at failure is mainly influenced by the applied total stress path. They state:

> In both cases of undrained strength and undrained elastic strain the total stress technique is valid only for the special case when the soil is saturated and undrained so that volumetric strains are zero; in all other cases the total stress analyses are not valid and calculations must be carried out in terms of effective stresses.

Theories covering the mechanical behaviour of soils, methods of determining these, and their effects on slope stability is a diverse topic, beyond the scope of this thesis, but is comprehensively covered by Atkinson and Bransby (1978), Atkinson (1981), and Walker and Fell (1987).

2.4.5 Slope Stability Assessment

Slope stability assessment can generally be divided into three phases: a field investigation phase; a soil parameter determination phase; and a stability analysis phase.

The field investigation phase (engineering geological investigation), essentially involves recognition of five components that contribute to slope failure, these being: topography; geology; groundwater; weather and site history (including past and current movement). Methods of establishing the contribution of each component to slope instability is varied, and often requires different methods and approaches for different situations. These are discussed in detail by Sowers and Royster, 1978; Hansen, 1984; Petley, 1984; and Veder, 1981. Generally the field investigation phase involves literature research, aerial photograph interpretation, engineering geological mapping at a suitable scale, logging of trenches and pits, groundwater monitoring (piezometer installation), and displacement monitoring (surveying and inclinometers).

The soil parameter determination phase usually involves in situ and laboratory strength testing. This has been covered in the previous section, section 2.4.4.

There are essentially three approaches appropriate to slope stability analysis in soils:

1) Limit equilibrium methods
2) Finite element methods
3) Empirical methods

All these methods require an engineering geological investigation to determine the important features of the soil mass, including both geotechnical properties and hydrogeological conditions.

Limit Equilibrium Method

Most of the methods which have traditionally been used to analyse the stability of a slope under static gravity loading, give upper bound solutions based on the principle of limit equilibrium (for example: Skempton, 1948; Bishop, 1955; Bishop and Morgenstern, 1960; Janbu, 1957; Morgenstern and Price, 1965; Spencer, 1967; Sarma, 1973; Sarma, 1979). These methods usually assume a profile of a two or three dimensional surface through the slope (often an inclined plane or circular arc), on which failure is postulated to occur. A *factor of safety* against failure is established, based on the computation and ratio of the available resisting and destablilising forces, acting on the failure surface in an integrated or global sense.

Finite Element Method

The finite element method attempts to obtain a lower bound stress-strain solution for the entire slope which satisfies equilibrium at any point. The stress-strain details are hence free to dictate the failure surface initiation and propagation in a natural way (Mostyn and Small, 1987).

Empirical Methods

The empirical approach to slope stability is qualitative assessment based on engineering geological information, which is used to classify the problem in a behavioural grouping and relate it to similar past failures in the same geological enviroment. Thus stability analysis is based on the previous experience and judgement of the engineering geologist and engineer (Brown, 1975).

These approaches to slope stability analysis and their limitations are discussed in detail by Schuster and Krizek (1978), Brunsden and Prior (1984), Walker and Fell (1987).

2.5 Slope Stability of Loess

2.5.1 Loess Shear Strength Parameters

Introduction

Loess is an unusual soil deposit, in that it exhibits high strengths when partially saturated, forming near vertical cliffs, yet when saturated it is prone to slope failure. This section discusses international and local literature concerned with the shear strength of loess.

International Literature

Many publications during the past 30 years consider the structural collapsibility of loess (for example: Feda, 1966; Minkov et al., 1979; Myslinka, 1986; and much of *Eng. Geol.*, Vol.25, 1988), which does not appear to be a serious problem with New Zealand loess (Birrel and Packard, 1953). Some of this literature gives details of shear strength and related parameters, though much of the literature does not discuss how these parameters were determined, making comparison difficult.

Barden et al. (1973) wrote a general paper on partially saturated soils, suggesting that collapsing soil involves the breakdown of either simple capillary suctions, clay buttresses or chemical cementation. The addition of water to the soil weakens the three forms of cohesion. In the case of capillary suction the drop will be immediate; in clay buttresses it may be slower and in chemical cementing slower still.

Kie (1988) investigated the geotechnical properties of loess from China, and showed that shear strength decreases rapidly with increasing moisture content to 11.5%,

and then more slowly, levelling out at 20% moisture content. Milovic (1988) conducted extensive unconfined compression, moisture content and dry density tests on loess from Yugoslavia, which show unconfined compressive strength decreases with increasing moisture content (range 16-24%)(figure 2.12). He also showed that unconfined compressive strength increases gradually with increasing dry density (with moisture content, 22-24%), until dry density is approximately 1.53t/m^3, where the rate of increase accelerates (figure 2.13). Figure 2.14 shows the additional scatter introduced to the plot with an increased range of moisture content.

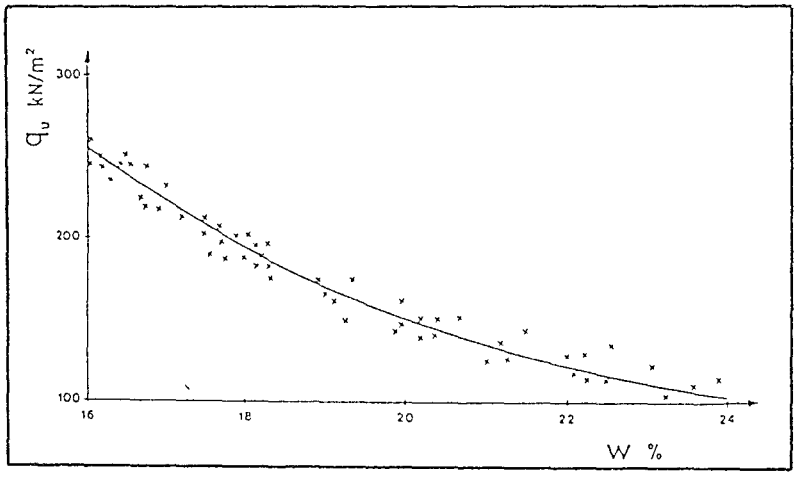

Figure 2.12 Relationship between the Unconfined Compressive Strength q_u and Moisture Content w for Undisturbed Loess Samples from Yugoslavia; ρ_d=1.49-1.51t/m^3 (after Milovic, 1988)

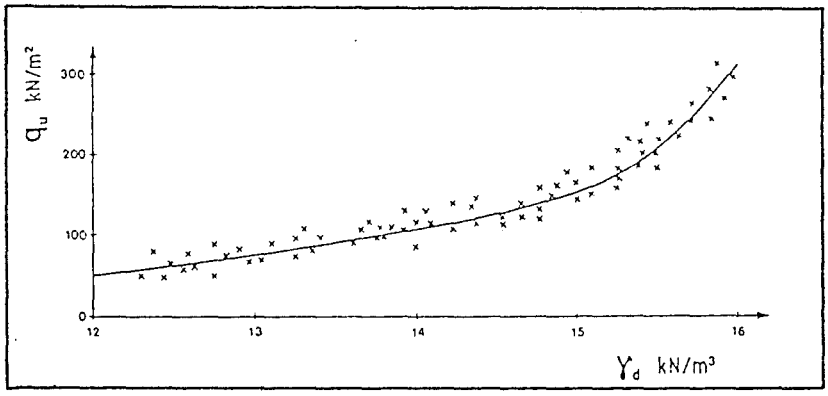

Figure 2.13 Relationship between the Unconfined Compressive Strength q_u and Dry Unit Weight γ_d for Undisturbed Loess Samples from Yugoslavia; w=22-24% (after Milovic, 1988)

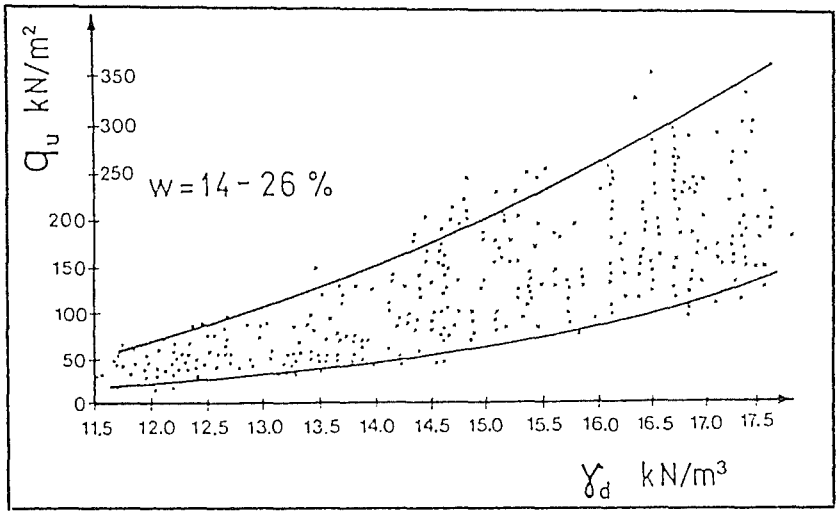

Figure 2.14 Results of Unconfined Compressive Strength q_u and Dry Unit Weight γ_d over a Moisture Content range of w=14-26% (after Milovic, 1988)

Banks Peninsula

It is generally reported in most review papers discussing Banks Peninsula loess, that shear strength reduces with increasing moisture content. However comprehensive laboratory investigations of the strength behaviour of Banks Peninsula loessial soils have not been reported.

Blakeley (1965) conducted California Bearing Ratio Tests (CBR) on 'Heathcote loess' to determine the relationship among dry density, compaction moisture content and CBR strength. Although the CBR test does not directly measure shear strength, it can be considered to be a crude undrained shear strength test. Blakeley showed that the CBR value decreases with increasing moisture content during soaking, with a minimum CBR value at 16% moisture content. He also showed that the rate of water absorbtion by the loess soil follows the same trend. He graphically presented good correlations among dry density, compaction moisture content and CBR as shown in figure 2.15. This is the most thoroughly reported investigation into the shear strength behaviour of Banks Peninsula loess.

Alley (1966) suggested that the angle of internal friction (σ') for loess is between 15° and 25° with a cohesion (c') of zero from drained tests, although he presented no discussion or details of his results.

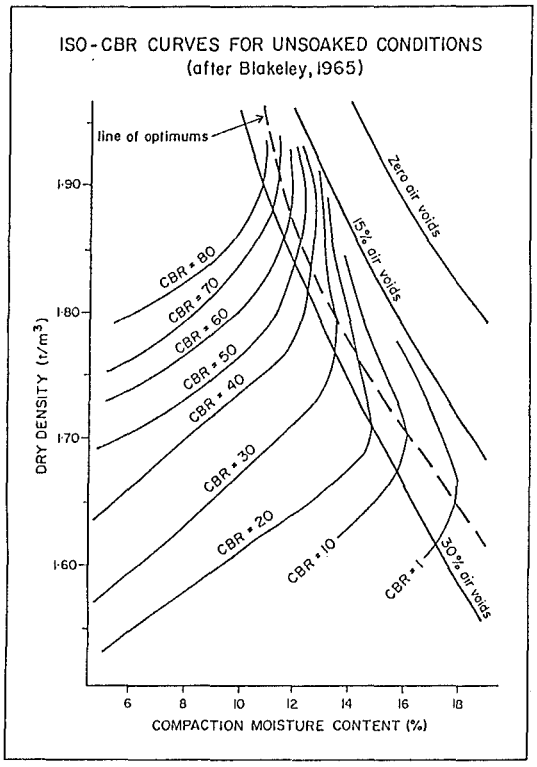

Figure 2.15 Relationship among Dry Density, Compaction Moisture Content and CBR values for Heathcote Loess

Scott (1979) made general comments about shear strength and suggested that high shear strength is due to cohesive bonds (clay flocs, capillary tension and interparticle Van der Waals forces), although with sufficient quantities of water in the loess voids, raised pore water pressures and reduced cohesion causes the metastable structure of loess to collapse.

Evans and Bell (1981), whose work was essentially concerned with chemical stabilisation of Port Hills loess, gave results of unconfined compressive tests on untreated loess. They showed a near linear, inverse relationship between unconfined compressive strength and remoulded water content (range 10-20%) for P layer loess. Their results showed that at similar moisture contents ($\approx$12%) the C layer loess (s_u $\approx$ 80kPa) has approximately twice the undrained shear strength of P layer loess (s_u $\approx$ 40kPa). Evans and Bell empirically corrected their unconfined compression data to a height:diameter ratio of 1:1.

Mackwell (1986) conducted a series of unconsolidated undrained triaxial tests on partially saturated loess colluvium. She recognised after testing, that effective stress parameters could not be obtained from the results, and therefore did not use them for stability analysis.

Glassey (1986), who worked primarily on chemical stabilisation of Port Hills loess, reported results of unconfined compression tests on untreated loess. He compared immediately tested samples with 14 day moist cure and 7 day moist cure + 7 day air drying, with no consideration for consequential moisture content variations. No area corrections at large strains were applied, and samples with a height:diameter ratio of 1.1:1 were used.

Bell and Trangmar (1987) noted that with increasing moisture content, loessial soils display a marked reduction in shear strength, with a change from an essentially brittle failure mode to one of plastic deformation at moisture contents greater than 15%, thus providing the mechanism for soil creep.

Tehrani (1988) also investigated chemical stabilisation of loess. Though he did not directly comment on the relationship between unconfined compressive strength and moisture content, his results for untreated P layer loess showed that the same inverse relationship exists between undrained shear strength and moisture content. Tehrani showed no evidence of correcting for area changes at large strains and used samples with a height:diameter ratio of 1.1:1.

Unfortunately no true comparisons can be made among the data reported above in the absence of a consistent test method. Evans and Bell, Glassey and Tehrani have either empirically corrected the sample height:diameter ratio, or introduced experimental error by using a height:diameter ratio less than 2:1 which introduces end friction effects, particularly significant with squat samples (Miller, 1982; Bishop and Henkel, 1957). Furthermore, area corrections become significant at large strains and these do not appear to have been applied in many of the strength tests reported above.

In addition to unconfined compression testing, Tehrani (1988) conducted direct shear tests on untreated P layer loess. He presented no raw data, but reported shear strength parameters with an internal angle of friction ranging from 30° to 39° and a cohesion of 30kPa. The tests were conducted at a fast shearing rate of 1.2mm/minute with no time allowance for sample consolidation under normal loads. It is apparent that his shear strength parameters were based on a quick undrained test and should therefore be interpreted using total stresses. They represent a measure of pore pressure generation in the partially saturated soil, rather than inherent shear strength parameters.

McDowell (1989) conducted unconsolidated, undrained triaxial tests on partially saturated loessial soils, as did Mackwell (1986). He reported a total stress internal angle of friction (ϕ_u) of approximately 30° and cohesion (c_u) varing from 0 to 180kPa, with moisture content decreasing from 19 to 8%. Although McDowell's trends are well defined, they are only valid at the total stress levels tested, which are higher than those common in loess slope failures on Banks Peninsula. These results could be reinterpreted as showing undrained strength reducing with increasing moisture content, since total stress parameters should generally only be used for soils subject to zero volumetric strain (section 2.4.4), which is restricted to the case where soil is fully saturated.

If in situ conditions could be simulated exactly in the laboratory, then total stress analysis on partially saturated soils would be useful. However as previously mentioned, the total stress parameters are influenced by the applied total stress path and the soil strains occurring prior to failure, and hence the applied strain rate. Moisture content and normal stresses can generally be reproduced in the laboratory (ignoring effects of sample disturbance, which can be significant with loessial soils (Miloviv, 1988)), but the applied strains are difficult to reproduce and therefore the total stress parameters are not an accurate measure of in situ soil strengths.

Despite these considerations, unconfined compression tests are a means of establishing soil behavioural trends on partially saturated soils, provided shearing strain modes are similar. The inverse relationship between undrained shear strength and moisture content has been noted in most strength testing reported above.

Terminology

Undrained shear strength parameters $\phi_u=0$, and s_u are only valid for specimens which fail with no change in specific volume (Atkinson and Bransby, 1978). Strength tests, such as unconfined compression and vane shear, are generally conducted at strain rates high enough to prevent any significant specific volume change in fine but partially saturated soils (Dr D.M. Elder, pers. comm., 1990). On this basis, the term *undrained shear strength* (s_u) will be adopted in this study to describe strength values obtained from unconfined compression and vane shear testing on partially saturated soils. This is consistant with terminology used by Seed and Chan (1960).

2.5.2 Loess Slope Stability

International Literature

Reference to slope failures in loess (excluding structural collapse) in the international literature is rare. Varnes (1978) refers to the 1920 earthquake in Kansu Province, China, which resulted in a dry loess flow that killed about 100,000 people. Varnes's 1958 classification of failures involving loess showed a block glide of loess material on a planar surface of glacial clay (failure appears to have little to do with loess material). This is not included in Varnes's 1978 classification, although the Kansu Province loess flow has been classified. Varnes (1978) also referred to loess falls along bluffs of the lower Mississipi River Valley and extensive loess flows associated with the July 1949 earthquake in Tadzhikistan, south-central Asia. Rid and Liang (1978) refer to the unmistakable identity of loess deposits in aerial photographs, which are highlighted by vertical-sided gullies, evenly spaced along wide, flat-bottomed tributaries showing a featherlike drainage pattern. Slope features include earthflows and minor slumps. Sharpe (1968) referred to the lower Mississippi Valley loess bluffs and the formation of 'cat steps' (terracettes) in deep loess deposits of western Iowa. Lohnes and Handy (1968) studied the same loessial bluffs of western Iowa with regard to predicting their instability, which they successfully modelled as sliding-wedge failures. Terzaghi (1950) referred to the effects of earthquakes on loess deposits, citing the 1920 Kansu Province loess flow and the 1811 New Madrid loess flows. He also refers to the effects of water, in removing calcium carbonate from loess and thus substantially reducing cohesion,

making the loess deposit akin to supersaturated rock flour which flows like molasses. Calcium carbonate is not present in any effective quantity in Banks Peninsula loess (Raeside, 1964).

Although the international literature does make reference to slope movement involving loess deposits, no reference has been found which gives a detailed account of a slope failure of similar proportions, and loessial properties similar to those investigated in this study. The only exception to this is an interesting paper by Lutenegger and Hallberg (1988) which described slope failures in loess, appearing to result not from simple shear failure (although they suggest it is undoubtedly part of the process), but from structural collapse of the loess to form mud-flows.
These mud-flow like forms occur on hillslopes in areas where the loess is moderately thick (4-6m). During wet periods a perched water table forms above low permeability material, and eventually forms seepage zones at the groundsurface on the hillslope. Under these conditions a variety of mud-flows and slabslides (a slope movement with apparently coherent upper increment, which has flowed on a soft, or liquid lower increment) occur. These leave "pipe" like scars which extend back into the failed hillslope.

Lutenegger and Hallberg suggested that zones of unstable loess (nearly liquid) occur naturally in otherwise stable loess profiles. They noted that in situ zones of "liquid loess" exhibit the same properties as collapsible loess and are recognisable where the in situ moisture content is at the soil liquid limit.

Banks Peninsula Literature

Much of the slope stability research conducted on Banks Peninsula to date has been biased towards a qualitative descriptive approach. Some present a relatively simplistic analysis of slope failure initiation. For example, Hutchinson (1975) discussed the effects of a heavy rain storm in August 20 - 22 1975 which deposited up to 400mm of rain on Banks Peninsula, resulting in widespread slope failures. He suggested the widespread slipping, slumping and earthflows were due to the subsoil becoming completely saturated, thus providing the additional mass required to induce movement.

Harvey (1976) analysed the effects of the same heavy rain storm on 519 soil slips that occurred on the Port Hills. Harvey suggested that there was little or no soil moisture deficit prior to the storm, with the storm rapidly saturating the soils leading to high positive pore water pressures, and providing the trigger mechanism for the slope failures, which all occur on well defined hydraulic discontinuities (above the fragipan and soil-bedrock interface). Harvey concluded that east and south facing slopes of between 25° and 31°, composed of loess, and mixed loess and basalt colluvium, are most prone to failure as the result of prolonged low intensity rain storms. These are essentially the same conclusions drawn by Evans (1977b), Evans and Trangmar (1977), Scott 1979), Bell (1978), and Bell and Trangmar (1987), although Bell and Trangmar suggest that high intensity rainstorms are often precursors to mass movement.

Hill (1978) investigated a slope failure at the La Clare subdivision, Akaroa, which resulted from the burial of ephemeral springs beneath the construction of a large road embankment. The embankment was constructed with re-worked loess, which Hill suggested was inherently weak and prone to failure when excessively wet. He described the failure as being a rotational failure, with the main movement apparently a translational block-slide, with movement changing from sliding to flowage in the toe region. Analysis of seasonal (three-monthly moving mean) rainfall indicated that whenever the summer 'deficit' was substantially exceeded by a following winter 'surplus', major slope movement ensued.

Scott (1979) suggested the single most imortant factor causing the instability of loess slopes is water, which enters the void space in sufficient quantity to raise pore water pressures and reduce the cohesion between quartz grains so that the metastable structure of loess collapses. He suggested that poor drainage results in rotational and translational failures within the P layer and that slopes with a southerly aspect are more prone to slope movement.

Mackwell (1986) investigated what she described as two 'slide-avalanche-flow' complexes at Akaroa Harbour. These followed high rainfall winters and high intensity rainstorm events, which saturated subsoil layers and perched groundwater above less permeable colluvium or bedrock, promoting failure. Mackwell suggested

the predominant failure mechanism was translational sliding, and that rapid 'avalanching' features were preserved in the form of low angle, fan-like flow lobes.

Papers by Bell (1978), and Bell and Trangmar (1987) present the most extensive review of erosion forms on Banks Peninsula. They recognised slide-avalanche-flow mass movements and reported that this form of slope movement is initiated by positive pore water pressures developed in a saturated zone immediately above a zone of low permeability, suggesting four possible zones:

1) The upper surface of a high bulk density, very low permeability fragipan 0.6 to 0.9m below the ground surface;
2) A contact between different layers of colluvium and at depths between about 0.9 and 2.0m;
3) The contact between younger colluvium and an underlying erosion surface (often a truncated fragipan) in buried loess, at depths between 1.2 and 2.5m; or
4) A contact between colluvium and volcanic bedrock at depths between 1.0 and 1.9m, with or without a saporlite zone of clay loam texture present in the top 0.2m of the weathered volcanics.

They further suggested that as the volcanic-colluvium component increases, so too does the clay mineral content, resulting in a change of the shear strength parameters controlling stability. However, they did not say whether or not the increased clay content improves or weakens the stability of the slope, although Harvey (1976) suggested it reduces shear strength.

2.5.3 Summary

In terms of quantitative and qualitative research, the following conclusions can be drawn from what has been termed the slide-avalanche-flow on Banks Peninsula.

1) Water from both high intensity and long duration rainstorms are the principal agents of slope failure;
2) Slope movement is initiated within four possible saturated zones that overlie lower permeability zones, as a result of raised pore water pressures;
3) Water causes a reduction in the apparent cohesion of loessial soils and hence a reduction in shear stength;
4) Increased clay content reduces shear strength.

5) Slopes of between 25° and 31°, and facing east and south are most prone to slope failure.

Although much of the research to date has provided very useful qualitative descriptive information about the slide-avalanche-flow on Banks Peninsula, no work has been done on the effects of water and loess soil properties and their effect on shear strength. The necessity to quantify slope stability on Banks Peninsula (noted in chapter 1) requires further work in the following general areas, to determine in particular:

1) The influence of water, density, clay minerology, and chemical cementation on the shear strength of the loessial soils of Banks Peninsula;
2) The geohydrology of loessial soil layering (permeability and infiltration variability);

This study adopts 1) and 2) above as it's main objectives and attempts to qualify and quantify the influence of water on the shear strength of in situ loess from one site at Allandale. It is also hoped that this research will further understanding of typical slope failures in loess.

Chapter 3
SITE INVESTIGATION

3.1 Introduction

The purpose of this chapter is to: 1) identify the nature of the slope instability at Allandale; 2) obtain an understanding of the processes which contributed to the formation of observed morphological features; and 3) to discuss the factors which contribute to slope instability. To achieve this, information has been gathered by engineering geological mapping, aerial photographic interpretation, logging of pits, piezometric and displacement monitoring, and the study of relevant literature.

3.2 Setting

The investigated site is approximately 50m by 100m in area, and is located at grid reference 43°39'S, 172°39'E. The site forms part of a pasture covered hillslope (approximately 0.5km^2 in area), located between Bamfords and Teddington Roads, Allandale (figure 3.1). The arcuate hillslope (sloping 18° - 22°; figure 3.1) faces southeast, has a maximum elevation of 118m above mean sea level, and a minimum elevation of 10m above mean sea level. At the toe of the slope is a 3m to 4m high oversteepened sea cliff, associated with the 6000 year old sea level maximum, which is separated from tidal mudflats by some 250m of lowlying pasture and Teddington Road.

Figure 3.1 Vertical Aerial Photograph Showing Investigated Site and Adjacent Area

The hillslope can be divided into three sections facing; north-northeast, east-southeast, and southeast. These three aspects are separated by two converging entrenched ephemeral streams, with native manuka growth in their lower reaches. The eastern most portion of the southeast facing hillslope forms the basis of this investigation.

3.3 Site History

3.3.1 Land Usage

The east - southeast and southeast facing portions (figure 3.1) of the hillslope were cultivated for the production of early market potatoes and turnips for winter sheep feed on an eight year rotation (1 year cultivated, 7 years pasture). The hillslope was cultivated in the early 1920's through to 1950 by a horse drawn, single furrow reversible plough. Turnips were grown on the steeper parts of the hillslope and potatoes on the less steep parts (B. Gebbie, pers. comm., 1989).

3.3.2 Slope Failures

Slope movement occurred in the early 1920's shortly after the first cultivation. Notable slope movements included: the winters of 1945, when 25 farm fences were demolished by slips; 1968, when there was substantial movement on the southeast facing slope; and 1978 where there was substantial movement on the east-southeast facing slope (B. Gebbie, pers. comm., 1989). For a more detailed discussion on the development of the hillslope failures see section 3.4.

3.3.3 Rainfall Data

Monthly rainfall data (appendix A3.1) recorded at Allandale and Living Springs show a good correlation between maximum rainfall events and dates of slope failures noted above. May 1945 had the highest ever recorded monthly total (403mm) and April 1968 had the second highest ever recorded monthly total (375mm). Unfortunately, 1974 saw the close of Allandale rain station and Living Springs did not open until November 1978. December 1978, however, remains the

highest December rainfall total on record (242mm). For comparison, the average monthly rainfall over the period 1951-80 for April, May and December are 87, 99, and 61mm respectively (table 3.1).

Table 3.1 **Monthly Rainfall Normals 1951-1980 (mm)** (Modified from N.Z. Met. Misc. Pub. 185)

STATION	Jan	Feb	Mar	Apr	May	Jun	Jul	Aug	Sep	Oct	Nov	Dec	Year
Allandale	67	53	73	87	99	90	115	89	58	63	60	61	915
Lyttelton	50	52	49	60	71	60	69	59	35	39	36	42	602

The storm of August 19-25, 1975 produced 217mm of rainfall at Living Springs (Harvey, 1976) and caused some 627 slips on the Port Hills. Although 217mm of rainfall in 7 days is considerably higher than the monthly average of 89mm, it is not known what effect this storm had on the area being investigated.

Monthly rainfall totals (appendix A3.1) indicate that the months in which the failures reported by Gebbie have occurred (see above) are preceded by at least two months of below or average rainfall. This does not necessarily mean the slope failures are a result of high intensity rainstorms. Monthly rainfall data does not differentiate between a month of persistant daily rainfall and a month with one or more high intensity rainfall events, that would otherwise show a below-average total.

3.4 Aerial Photography Interpretation

3.4.1 Introduction

Four aerial photographs, covering a period of 43 years (1941-84) record the progression of slope failure development. Figures 3.2 (a,b,c,d) show sketches based on vertical aerial photograph runs 135/10-11 (1941), 3155/57-58 (1963), SN2634 K/52-53 (1973) and SN8389 J/14-15 (1984) respectively.

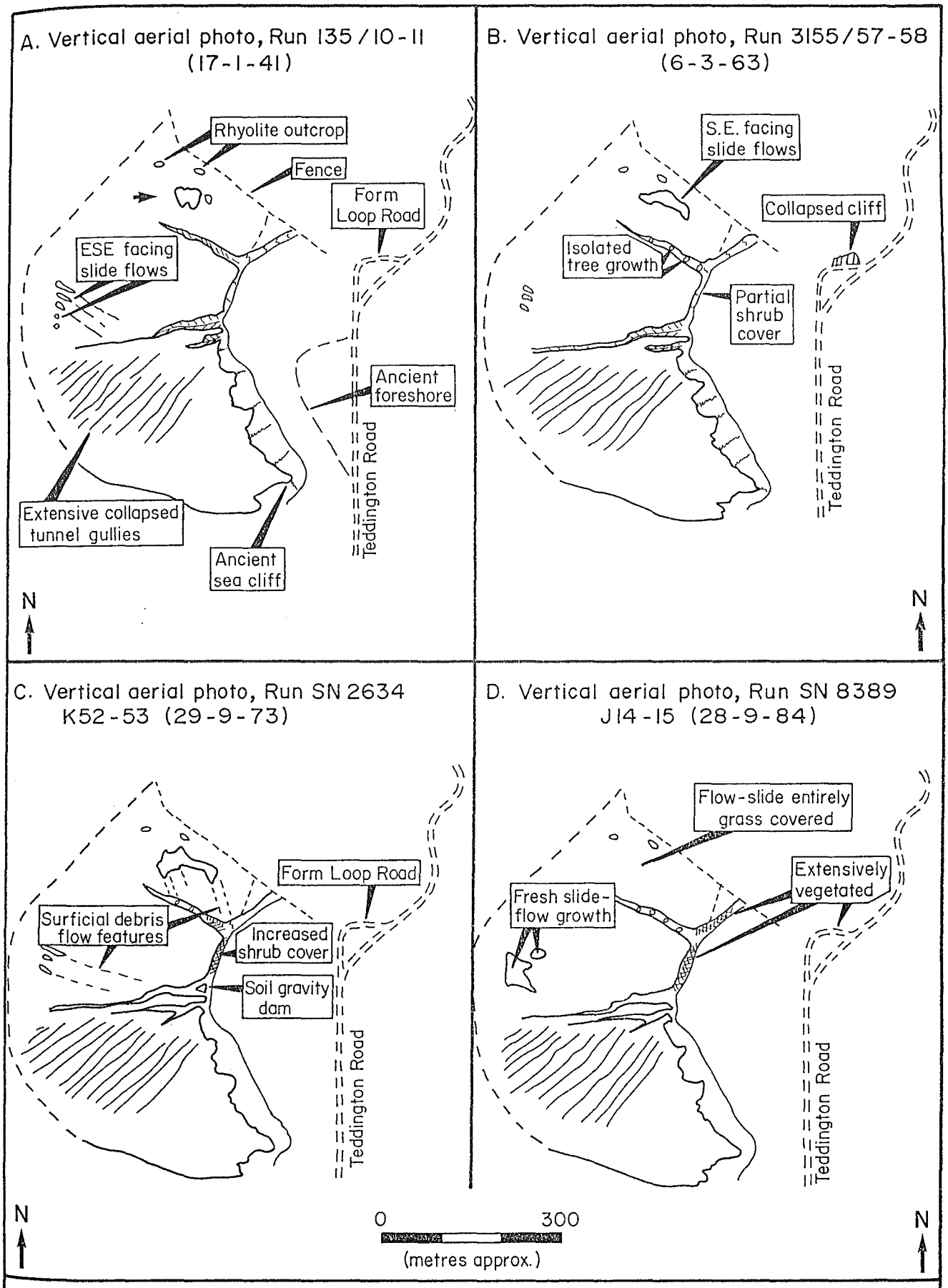

Fig 3·2: Aerial photograph interpretations showing development of site and adjacent areas

3.4.2 Failure Complex Development

1941 (figure 3.2a)

Extensive collapsed tunnel gullies and the east-southeast facing and southeast facing slope movements all existed prior to January 1941. The east-southeast facing slope movements consisted of five individual failures which had little or no vegetation cover, whereas the southeast facing slope movements were partially covered with pasture.

1963 (figure 3.2b)

The southeast facing slope movement had spread laterally in an eastward direction, but was entirely pasture covered. This may imply that prior to 1963 there had been no slope failure for some time. The 1963 aerial photograph indicates that the two southern most slope failures on the east-southeast portion had become inactive and were obscured by vegetation. The three other failures show signs of minor activity, probably erosional. Some partial shrub cover had established on the ancient sea cliff and in the ephemeral streams between 1941 and 1963. The sea cliff above the farm loop road had failed and covered the road.

1973 (figure 3.2c)

Renewed surficial flow deposit features had developed, trailing from both slope movement complexes. Substantial enlargement of the failure to the west of the southeast facing failure complex can be seen. Also apparent is fresh material in the heads of the east-southeast facing sectors. Vegetation growth had increased on the ancient sea cliff and in the ephemeral streams. The farm loop road had been restored.

1984 (figure 3.2d)

The southeast facing failure complex was entirely pasture covered, indicating no recent failure activity. The three east-southeast facing slope failures had spread laterally both north and south to form a larger complex.

3.4.3 Discussion

Observations from the aerial photographs show that both pasture quality and slope stability deteriorated from 1941 to the present day. These interpretations are consistent with the site history as given by Gebbie (section 3.3).

3.5 Engineering Geological Investigations

3.5.1 Introduction

An engineering geology plan and cross-section of the investigated site and adjacent area were prepared at scales of 1:500 and 1:250 respectively, utilising a topographic base map. This was based on topographic surveying (section 3.6.2), low-level vertical aerial photographs, auger holes and hand dug pits. Engineering geological mapping was initiated on the 3/4/89, prior to and concurrent with, subsurface investigations and surveying.

The main objectives of the engineering geological mapping were to identify and obtain an understanding of the development and nature of:

1) the lithology
2) the slope morphology
3) the slope hydrogeology
4) the slope failure.

3.5.2 Geological Observations

Only one rock unit (Allandale Rhyolite) was identified in the field area. It is exposed at two outcrops on the crest of the hillslope and was found in auger holes 1, 2 and 8.

The rhyolite is slightly weathered (completely weathered in auger holes) creamy white to light brown, and porphyritic with black bipyramidal smoky quartz

phenocrysts (Sewell, 1988). Steeply dipping columnar joints and a major low angle dip joint set are present (see figures 3.3 and 3.4, map pocket).

Charteris Bay Sandstone is exposed in failed ground of the central east-southeast slope portion (not recorded on the most recent geological map (Sewell, 1988)), and at one outcrop at the base of the old sea cliff (both outside the field area).

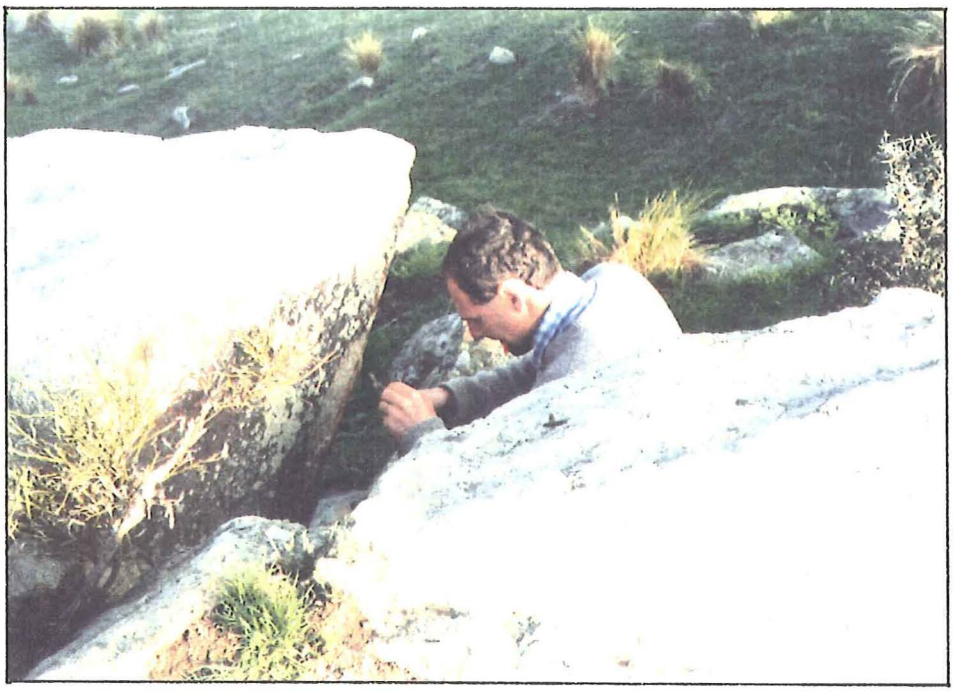

Figure 3.3 Columnar Jointed Rhyolite- Outcroping at Crest of Hillslope

3.5.3 Geomorphology

a) Features Adjacent to the Failure Complex

Three morphologic features are distinguishable adjacent to the slope failure complex investigated (see figure 3.4 and 3.5): 1) break in slope angle; 2) slope deposits, trailing from failed ground; and 3) soil creep.

Break in Slope

The slope is approximately 22° from the crest of the hillslope to just below the failed ground, where it changes to approximately 18° (see figure 3.4).

Slope Deposits

The down slope orientated slope deposits (figure 3.4) trailing from the flanks of the failed ground are best described as thin bands of hummocky ground, orientated perpendicular to the slope contours (figure 3.5). Figure 3.6 shows similar slope deposits trailing from the western extreme of the failed ground on the southeast facing hillslope. These appear to be more recent examples of the same slope feature and consist of blocks of displaced top-soil (up to 1m in size) on the same downslope path.

Soil Creep

Soil creep is active over most of the hillslope in the form of rolling hummocks that create contour-like parallel features on the slope (figure 3.4 and 3.5). These features are accentuated by stock movements. Bell and Trangmar (1987) present a detailed discussion of the processes involved in the formation of Banks Peninsula soil creep.

b) Failure Complex

The area investigated in detail consists of six elongated channels up to 1.5m deep and 5m wide that converge downslope (figure 3.4 and figure 3.5). Between each channel is a downslope orientated row of "terracette" like slump features, often with head scarps up to 0.4m high (figure 3.9).

Two slump blocks and associated minor scarps are evident at the top of the main failure (figures 3.10 and 3.11). From the surface, the failures appear to be back tilted slumps.

c) Surface Erosion

Many of the slope features at the investigated site are likely to pre-date 1941 (see figure 3.2a). Some of the earliest slope features are likely to have been obliterated, covered over, reworked or eroded by wind and water over the years.

Figures 3.6 and 3.7 show the effects of erosion on the flow deposits that have come to rest on the hillslope. The smooth hummocky appearance of the older eastern-most flow deposits (figure 3.6), contrast considerably with the angular appearance of the younger western most flow deposits. The erosional action of water through time is the most probable cause of this. Figure 3.12 shows the smoothed slope features and the incised drainage channels within the failure complex resulting from the erosional action of surface runoff water.

Figure 3.5 Vertical Aerial Photograph of Southeast Facing Slope Failure Complex

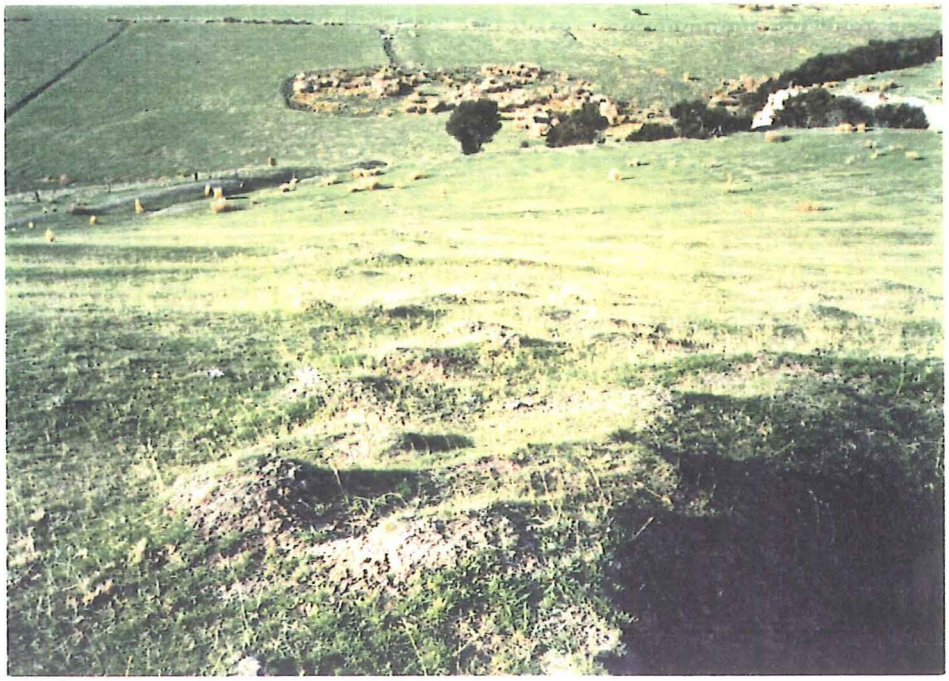

Figure 3.6 Slope Deposit Trailing from Flanks of Failed Ground- photograph taken from the downslope portion of the eastern flank of the investigated failed ground complex.

Figure 3.7 Slope Deposits below Western Portion of Failed Ground Complex- looking upslope towards western extreme of failed ground complex.

Figure 3.9 Terracette like Slump Features within Investigated Failed Ground- looking upslope.

Figure 3.10 Slump Block- upper western corner of investigated failed ground. Note soil creep features in top left hand corner of photograph.

Figure 3.11 Slump Block with Associated Head Scarp- upper eastern part of investigated failed ground. Note: Pit 1 was dug across this slump feature.

Figure 3.12 Drainage Channels in Investigated Failed Ground Complex. Note smoothing of slope features, resulting from the erosional action of surface runoff water.

3.5.4 Subsurface Data

a) Auger Holes

Introduction

Ten hand augered holes up to 6m deep were bored between 7/4/89 and 18/5/89, in and adjacent to the slope movement investigated (locations shown on figure 3.8, map pocket). There had been no significant rainfall at the site for at least four months prior to commencing the hand auguring. The disturbed soil samples were retrieved using the auger bit illistrated in figure 3.13; the auger logs are presented in figure 3.14 (map pocket).

Lithological Descriptions

S LAYER LOESS

Two layers constitute the S layer loess. Moist, soft, greyish brown, organic SILT, 0.01-0.4m thick is the upper most layer recognised on all auger logs except auger hole 4, which was not covered by vegetation. Auger holes 6 and 7 had very thin organic silt (0.01m) layers at the surface, while auger hole 7 had a organic silt (0.3m thick) layer 0.1m below the surface.

Underlying the organic silt layer is a generally moist, soft, reddish brown speckled light yellow, massive, SILT usually 0.15-0.25m thick, though this was not identified in auger holes 1, 2, 5, 7 and 8. It is likely that this material was present, but the disturbing action of the hand auger probably mixed it with the overlying top soil.

C LAYER LOESS

Underlying the S layer is a moist to wet, soft, reddish brown mottled whitish yellow CLAYEY SILT with intermittent reddish brown speckles (concentrations of iron oxide) up to 5mm in diameter. This layer varies in thickness from 0.6 to 1.2m and is totally absent from auger log 4. The moisture content would appear to increase with depth and the soil was usually wet in the lower 0.05 to 0.10m of the layer.

P LAYER LOESS

Underlying the C layer is a dry to wet, soft to firm, yellowish brown, homogeneous SILT with intermittent reddish brown speckles (concentrations of iron oxide), up to 3mm in diameter. This material has wet zones which do not appear to be related to depth or soil boundaries. Rhyolite clasts were encounted in auger holes 1, 2, and 8, which are probably due to the deposition of the in situ loess rather than reworking by slope processes. Bedrock (Rhyolite) was encounted in auger hole 1 at a depth of 4.0m and a possible cavity was located in auger hole 4 at a depth of 2.0m (the hand auger dropped 0.3m with little force). The P layer material increased in thickness moving down slope as inferred by cross-section A-A (figure 3.14).

Figure 3.13 Auger Bit used for Retrieving Disturbed Auger Samples

Figure 3.15 Photograph showing the development of a large belly, resulting from resting on shovel instead of digging pits.

b) Pits

Introduction

Five pits were hand dug (figure 3.15) on the 26/7/89 in and adjacent to the slope failure investigated. Locations were selected on the basis of auger holes and completed engineering geological mapping, and are shown on figure 3.8 (map pocket). Bulk, undisturbed and tube samples were collected from Pits 1 and 2 for laboratory investigations. Figures 3.16, 3.17, 3.18, 3.19, and 3.20 show the face logs of Pits 1, 2, 3, and 4, and 5 respectively.

Descriptions

Pit 1 (figure 3.16)

Pit 1 was dug across a minor scarp upslope of the eastern extreme of the slope failure. Logging of the pit revealed the three layers (S, C, & P) similar to those designated by Hughes (1970). Below the scarp a tension crack infilled with a super saturated spongy clayey silt with inclusions of organic silt, had formed. A wet zone extended from this material down to the base of the pit. Seepage waters exited from

the pit face via the tension crack material (and the associated wet zone) and the C-P layer interface. Particle size distribution, moisture contents, densities and Atterberg limits for the loess layers are presented in chapter 4.

Pit 2 (figure 3.17)

Pit 2 was dug within the failed zone just below a head scarp in an attempt to visually locate the failure surface. Logging of the pit revealed two organic silt horizons (top soil), of which the lower one had been disturbed, containing large inclusions of lower S layer horizon. The original C layer material (Pit 1 for reference) appeared to be entirely removed, although a new C layer would appear to be forming (weathering process). The P layer (lighter coloured material than Pit 1 P layer) material revealed features that would appear to be infilled dessication cracks. It would appear to have been subjected to a weathering process, discussed later in chapter 4.

Pits 3 and 4 (figures 3.18 & 3.19)

Pits 3 and 4 were dug in the toe and the left flank of the failed ground respectively. Both faces were logged parallel to the slope. Pit 3 had two organic silt horizons, the lower of which displayed flame structures which incorporated the loessial horizons above and below it. Pit 4 also had two organic silt horizons, the lower horizon exhibited minor flame structures involving the upper loessial layer and considerable bioturbation associated with the lower loessial horizon.

Trench 5 (figure 3.20)

Trench 5 was dug perpendicular to the slope incline to investigate the slope deposit below the failed ground. Logging of the trench showed that it consists predominantly of top soil overlying a thin sandy silt zone that overlies in situ top soil. Of note is the considerable amount of bioturbation associated with the lower loessial horizon and the single source seepage zone that resulted in ponding at the base of the trench.

3.5.5 Discussion

Pit 1 was dug across the back tilted slump feature and the associated infilled tension crack shown in figure 3.11. Logging of pit 1 revealed a super saturated spongy soil zone infill in the tension crack. On the down-slope side of the tension crack the lower S layer loess is lens-like and considerably thinner than the same soil on the up-slope side of the tension crack (figure 3.16). It would appear that the lower S layer loess down-slope from the tension crack has structurally collapsed, decreased in volume and flowed into the void space associated with the tension crack. This suggests that the slump blocks are only associated with the top 0.5m of loess-the S layer loess. It also suggests that a continuous failure surface from the tension crack to the toe of the block (through the C layer loess) is unlikely. It is more probable that the tension crack formed at the same time the lower S layer loess structurally collapsed, and that failure is associated with the plastic deformation of the lower S layer loess.

Fig 3·16: Pit I: East facing cut, date logged 26/7/89

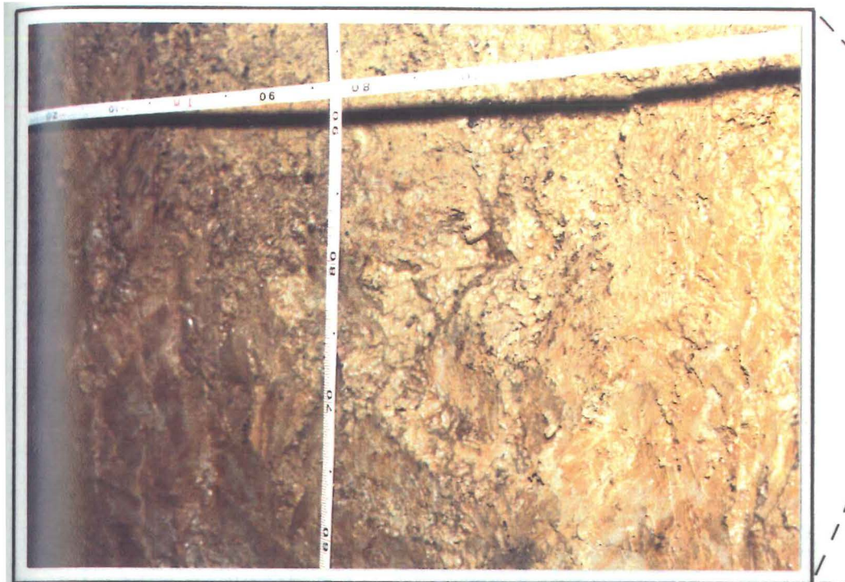

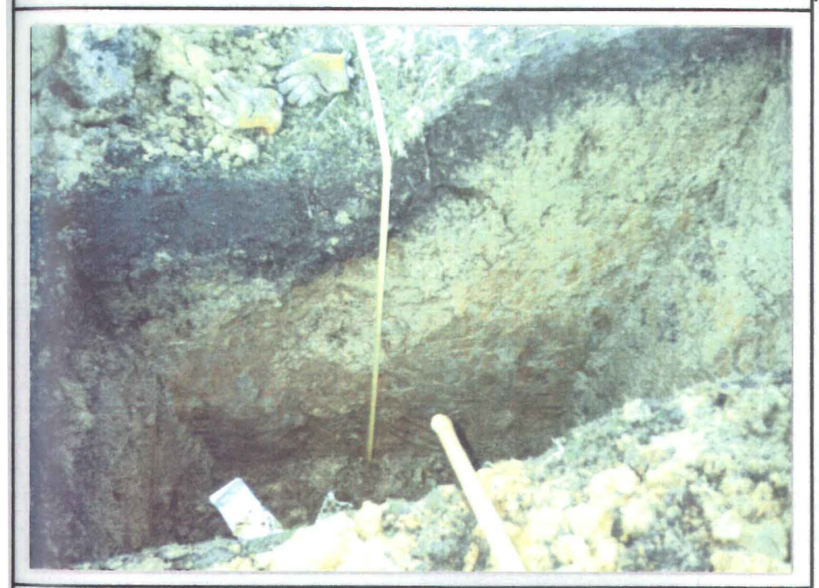

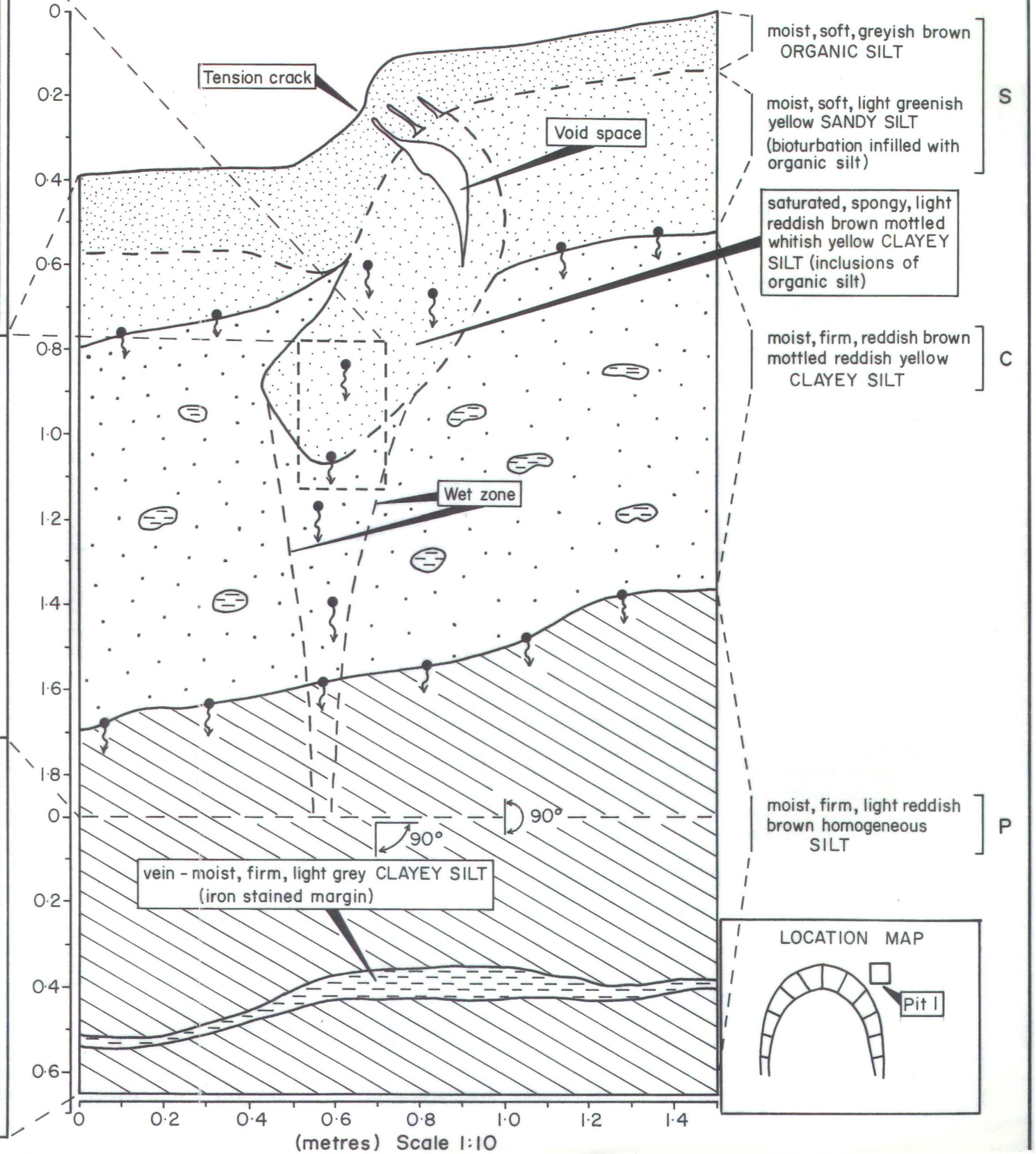

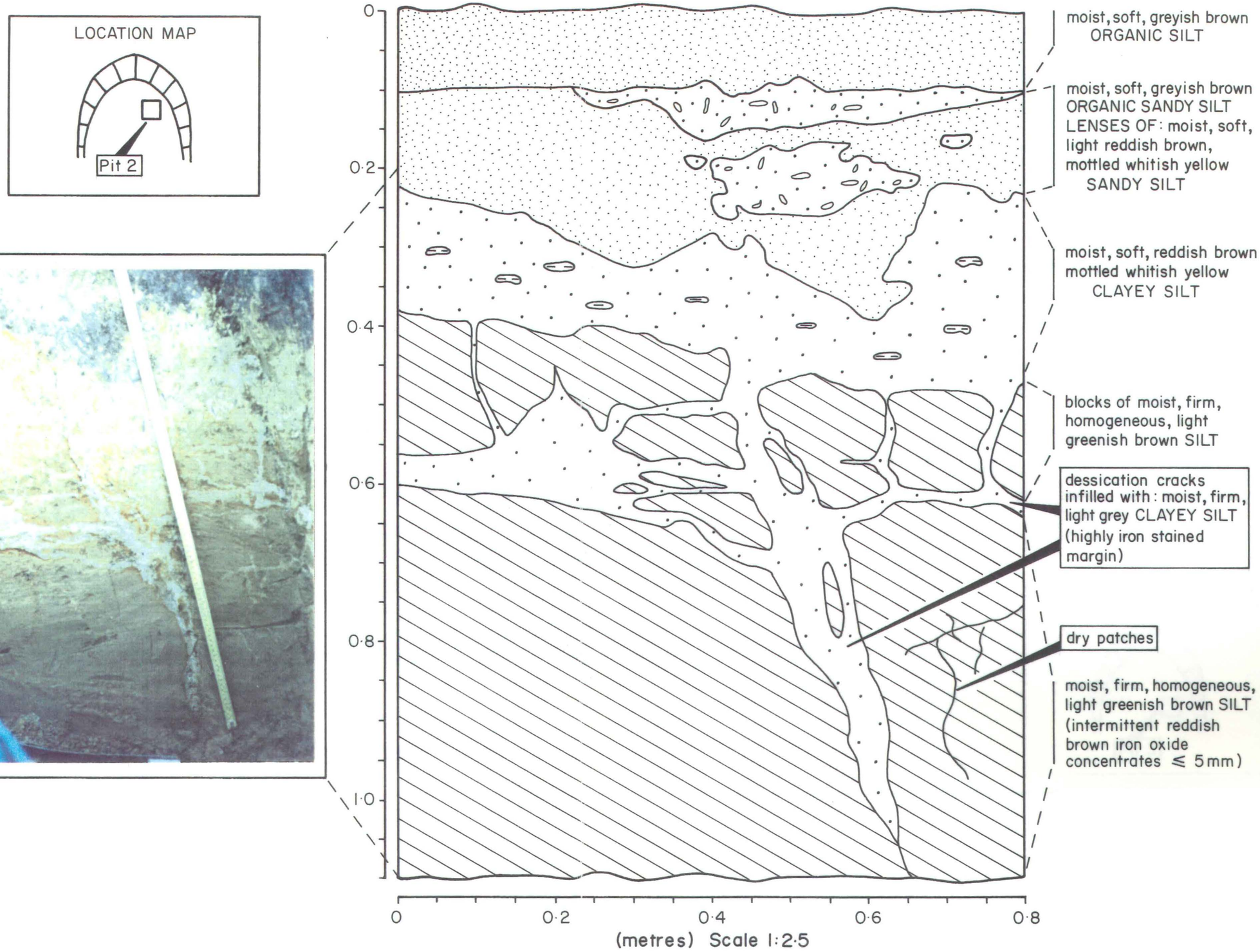

Fig 3·17: Pit 2: South east facing cut, date logged 26/7/89

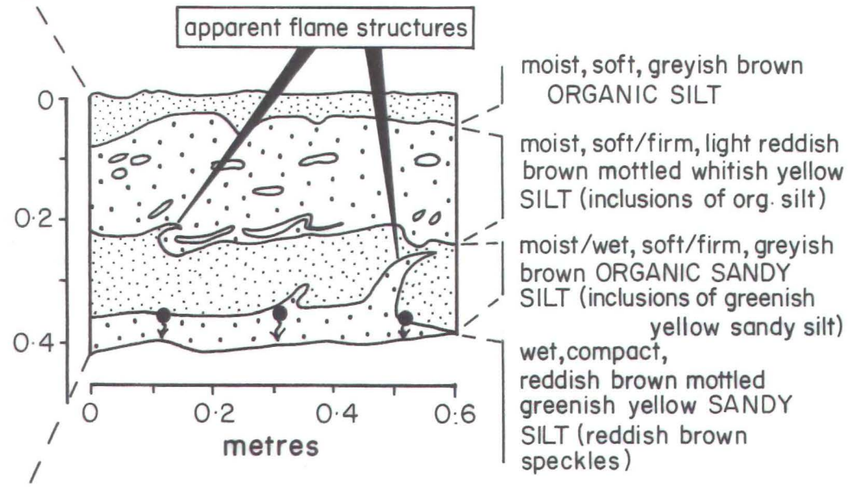

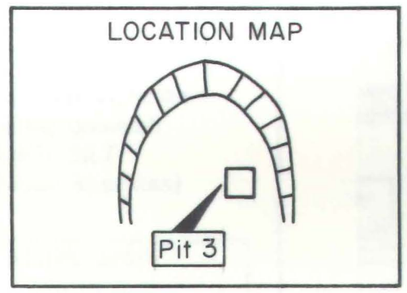

Fig 3·18 : Pit 3: South west facing cut, date logged 26/7/89

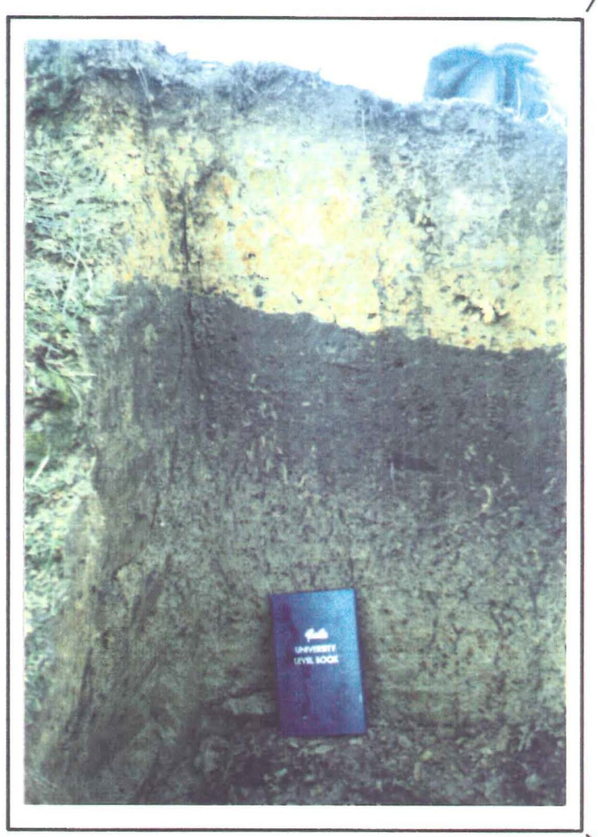

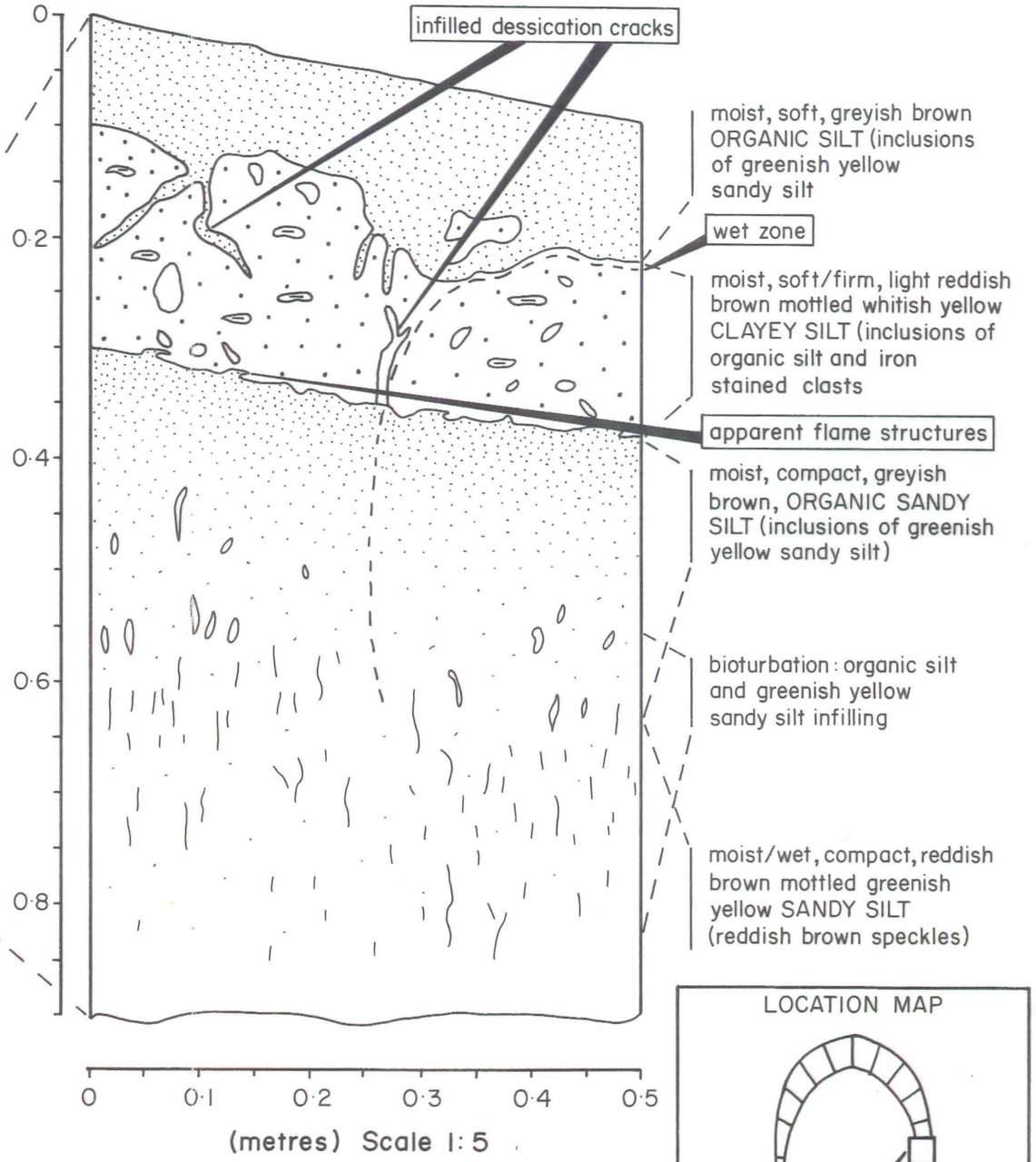

Fig 3·19: Pit 4: South west facing cut, date logged 26/7/89

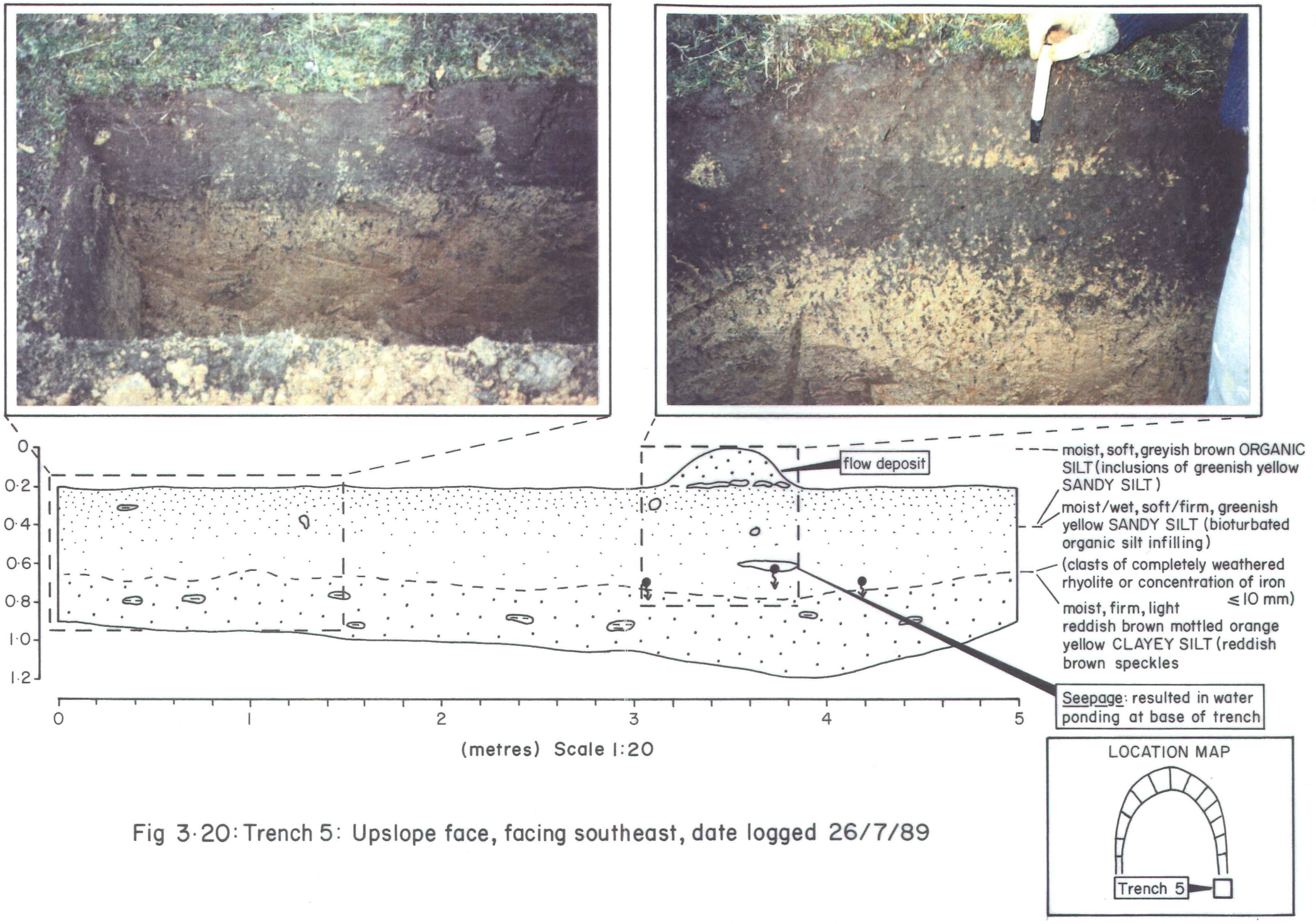

Fig 3·20: Trench 5: Upslope face, facing southeast, date logged 26/7/89

The face log of pit 1 shows that the super saturated spongy soil extends down into the C layer loess. The super saturated spongy soil appears to be infilling a tension crack that is working its way through the C layer loess at an angle inclined downslope to the vertical. It is likely that the tension crack will propogate through to the base of the C layer loess over time.

On the 14/9/89 a "turfmat slide" took place in the S layer loess at the upslope end of the western portion of the failed ground. Figure 3.21 shows the "turfmat slide" that buried piezometer 4. The slope movement consists of a coherent upper increment (essentially top-soil, upper S layer loess), which has flowed on a soft, or liquid lower increment (lower S layer loess). The coherent upper increment was a triangular shaped block, approximately $1m^2$ in area. Figure 3.22 shows the saturated lower S layer loess which oozed (flowed) out from under the coherent block of top-soil. The photographs were taken three days after the slope movement. Despite no rainfall, the footprints almost completely filled with water (figure 3.22), indicating the soil was still highly saturated. Figure 3.23 shows that a coherent block of upper S layer loess appears saturated in only the bottom 6cm, while the still attached coherent portion of the lower S layer loess is entirely saturated.

Raised ground (above the normal hillslope surface) on the left and right flanks (figure 3.24) of the failed ground complex was investigated by digging pit 4. Figure 3.10 shows some 0.25m of loess overlying the original top soil. Of particular interest are flame structures involving the original (bioturbation zone present) top-soil and the overlying soil deposit. This suggests the soil overlying the original top-soil was fluidised at the time of deposition (flow deposit). The flow deposit is more consistent with C layer loess than with lower S layer loess described in pit 1, suggesting a slope movement of larger proportions than a "turfmat slide", and involving fluidised flow of C layer loess.

Figure 3.21 Turfmat Slide that occured on the 14/9/89

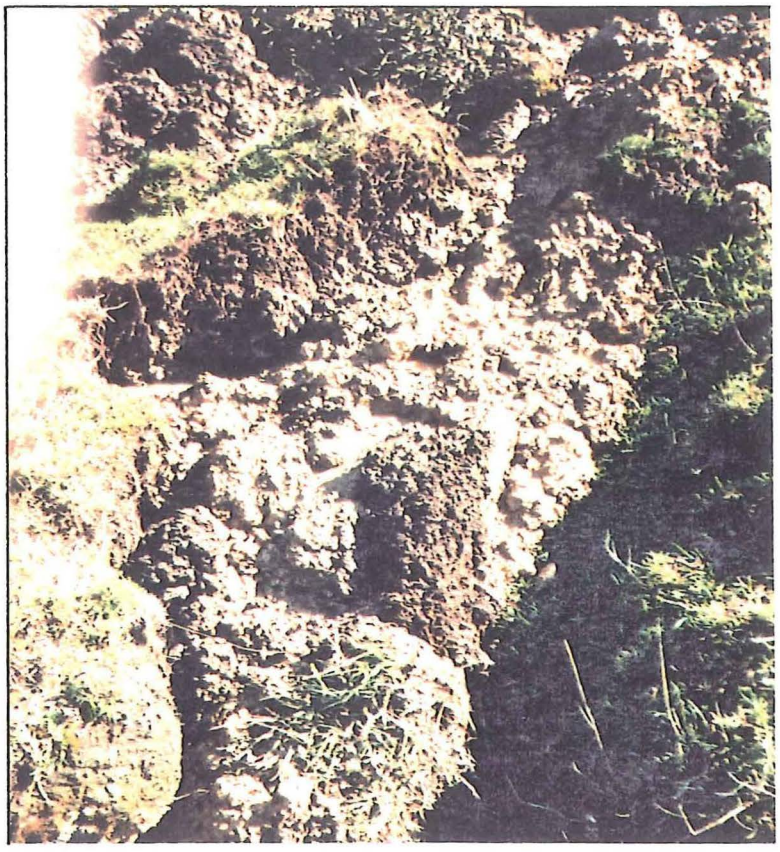

Figure 3.22 Saturated Lower S Layer Loess which oozed from under the Coherent Block of Upper S Layer Loess. Note the water filled footprints in upper-centre part of photograph.

Figure 3.23 Section through Coherent Block of Failed Soil

Figure 3.24 Raised Ground Forming Lower Right Flank of the Investigated Failure Complex. Note: A similar slope feature was evident on the lower left flank of the investigated failure complex.

Pit 2 (figure 3.17) was located in the centre of the eastern portion of the failure complex. The face log of pit 2 indicates that the C layer loess (based on pit 1 C layer loess) is almost completely absent from the soil profile. It appears that a soil similar to C layer loess is presently forming on the slightly weathered P layer loess. The latter is dissected by infilled dessication cracks, suggesting that it may have been exposed at the surface at some stage. The P layer loess is overlain by at least one deposit from an upslope failure, probably a "turfmat slide".

Pit 3 (figure 3.18) was dug at the toe of the eastern side of the failure complex. Flame structures were documented within the lower paleosol and the loess layers above and below. This appears to indicate the presence of at least two separate fluidised flow deposits.

3.6 Surveying

3.6.1 Introduction

Two control stations (S1 and S2) shown on figure 3.8 (map pocket) were established on ryholite bedrock outcropping upslope of the failure complex. The control stations were fixed permanently by pop-riveting webbing onto the bedrock surface (figure 3.25). The control stations were used as reference points for:

1) topographic surveying;
2) locating auger holes, pits, trenches and piezometers;
3) base control and false origin (S1) for displacement network; and
4) accurately determining slope features for engineering geological mapping.

Figure 3.25 Survey Control Station (S1)- position fixed permanently by pop-riverting webbing to bedrock surface.

3.6.2 Topographic, Feature Location, and Displacement

Appendix A1 describes the equipment, method and accuracy of survey used to produce topographic contours, locate piezometers, locate pits, and locate many of the slope features. Results of the surveying were used in the construction of all maps in section 3.5 (Engineering geological mapping). Reduced data for the eleven months of displacement monitoring are presented in appendix A1.4.2 and A1.4.3.

3.6.3 Discussion

There was no significant movement trend for any of the displacement points over the survey period. All horizontal movement (x and y directions) can be explained by instrument and operator errors. The one exception is a trend for the vertical component to increasre over the wetter months, then decrease during the dryer months, indicating a minor seasonal swell/shrink characteristic of the slope.

3.7 Site Hydrogeology

3.7.1 Piezometers

Introduction

Features and uses of various types of piezometers are discussed by Stanley and Mikkelsen (1978); Hunt (1984) and Hana (1985). The Casagrande type, open-tube piezometer (Singleton, 1984) was chosen for this investigation due to simplicity of operation and its cost effectiveness. Basic theory, equipment and method of installation are discussed in appendix A2.

Piezometer groups were installed at eight different locations in and adjacent to the slope failure, to monitor groundwater pressure variations within the different pedological horizons of the loessial soil mass during the study period. Installation was implemented in May 1989 and the piezometers were monitored until Febuary 1990.

Each piezometer group was located either in, or adjacent to, pre-existing auger holes (figure 3.8), and therefore the depth (soil horizon) to be monitored was determined from the auger hole logs (figure 3.14, map pocket). Identification of each piezometer is based on the auger hole number (group) and the monitored depth.

Results

Reduced piezometer data are presented in appendix A2.4. Figure 3.26 shows a graphical presentation of pore water pressures and daily rainfall over time. Monitoring was conducted on an occasional basis, usually after a period of rain. Two

periods of continuous daily monitoring were conducted- 12/9/89 to 29/9/89 and 18/10/89 to 27/10/89. Piezometers 1/2.0, 3/2.7, and 8/2.0 (not shown on figure 3.26), show no pore pressure generation over the entire monitoring period. These were located in the P layer. On 24/9/89 the three piezometers were recharged with tap water. Within a 3 day period all three standpipes were dry.

Piezometers 1/1.3, 2/1.4 and 3/1.16 showed roughly the same pore water pressure response to daily rainfall, with peak pore water pressures lagging 1 to 4 days behind peak rainfall data. During periods of peak rainfall, pore water pressures were marginally greater the further up slope the piezometer was located. All three piezometers were located in the C layer material (moist, soft, reddish brown mottled whitish yellow CLAYEY SILT).

Piezometers 1/0.5 and 7/0.4 showed roughly the same pore water pressure reponses to daily rainfall, with pore water pressure peaks lagging 1 to 2 days behind peak rainfall data. Piezometer 7/0.4 apparently produced artesian pressure (although unlikely to be significant) during periods of peak rainfall, because the piezometer cap was forced off on two occasions (14/9/89 and 23/10/89). Piezometer 1/0.5 was located near the S-C layer interface above the failure. Piezometer 7/0.4 was located within the organic rich top soil below the failure.

Piezometers 1/4.2 and 2/2.68 showed minimal response to daily rainfall fluctuations. Piezometer 1/4.2 was located within highly weathered rhyolite basement, while piezometer 2/2.68 was located within the P layer. Piezometers 1/4.2 and 4/6.0 show a response that goes against the trend of all other piezometers. On about the 18/8/89 both piezometers responded to what is believed to be the ground water table, and lagged some 6 days behind the rainfall peaks.

Piezometer 7/2.3 located in P layer material showed the most extreme fluctuations to rainfall. This may be due to a combination of water table effects, and the soil mass permeability at this location. Piezometer 8/1.28 also shows large extreme responses to rainfall, though the peak pore water pressures lag some 3 days behind rainfall peaks. The ground surface adjacent to piezometer 8/1.28 dried out days before all other piezometer locations. This is probably because its location on a

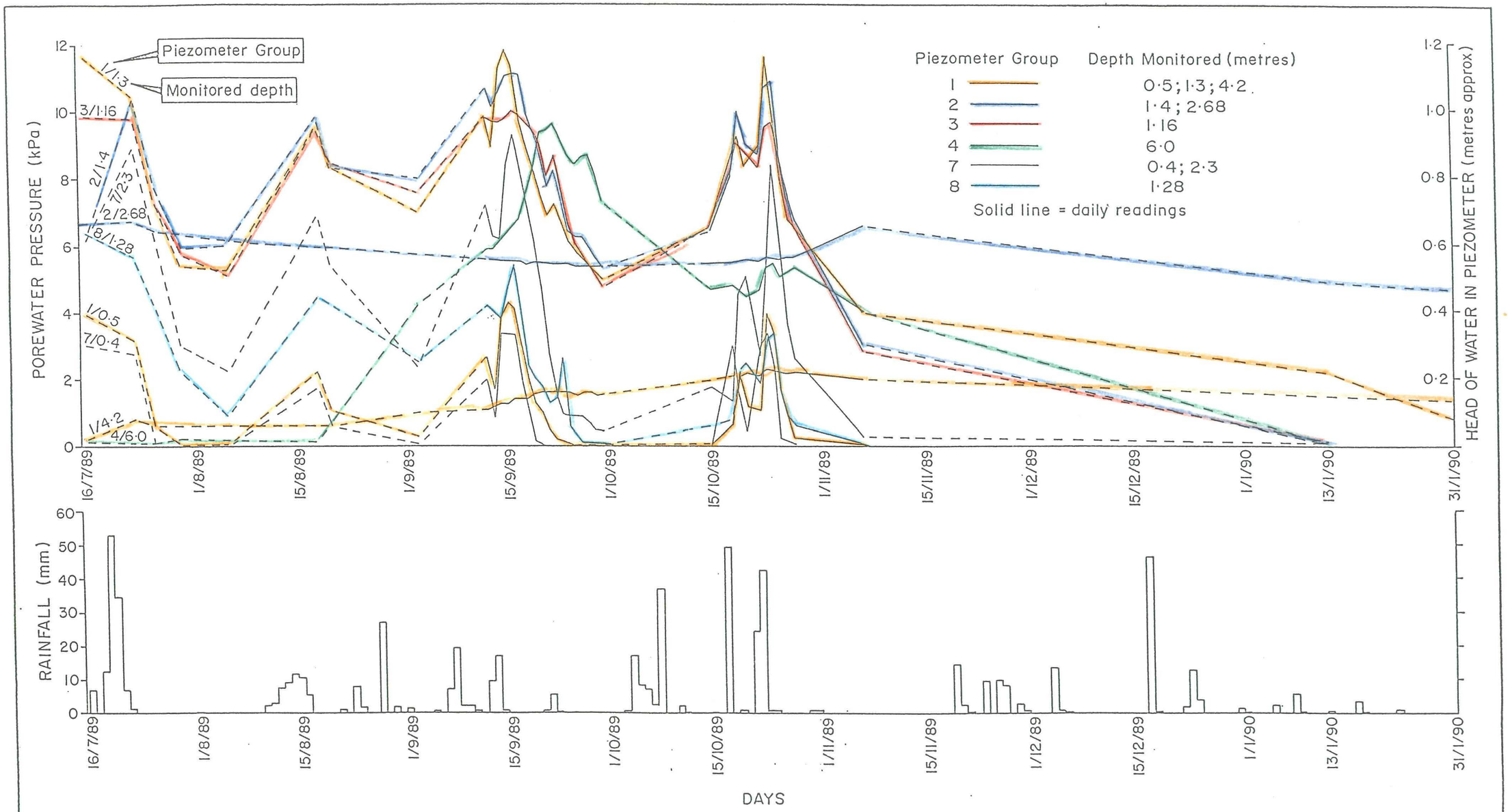

Figure 3·26: Graphical presentation of slope monitored pore water pressures with time, and daily rainfall data from Living Springs (Grid reference: 43 39S 172 38E) Daily rainfall data given in Appendix A3-2

ridge, and is exposed to the predominant easterly and southerly winds (discussed later). This dehydration may also be influenced by diverging drainage (ie. located on top of a ridge).

Discussion

It appears that all piezometers display a storm response, but some show a greater response than others. Piezometers 1/4.2 and 2/2.68 show a predominantly seasonal response. Piezometers 1/4.2 and 4/6.0 appear to respond to ground water table fluctuations. Ground mass permeability within the P layer is considerably variable. In some places no pore water pressure is generated, while in others pore pressures as high as 9.5kPa are generated (e.g. top of P layer, below failed ground, 7/2.3). The base of the C layer appears to consistently generate the highest pore water pressures, with a maximum of 11.8kPa being recorded during the monitoring period.

3.7.2 Effects of Site Orientation

Harvey (1976) showed that east and south facing loessial soil slopes on the Port Hills, were most prone to slope movement during the storm of 19-25 August 1975. He related the slope failures to the slope aspect (sunny and shady slope faces). His results show that 42% of the total slope failures occurred on east facing slopes, and 25% on south facing slopes. Harvey infered that the reduced sunshine hours on the shaded south and east facing slopes, leaves the soil with a high moisture content and therefore more prone to failure. He suggested that the large number of movements on slopes with an easterly aspect and a sunny face, are due to the dispersive nature of the soils, which promotes instability. This appears to contradict the effects of shade in promoting instability on the south and east facing slopes.

The predominant winds recorded at Lyttelton Harbour and Christchurch Airport are from the northeasterly and southwesterly quarters (figure 3.27). Figures 3.27 and 3.28 illustrate the strong influence of local topography in channelling the wind flow and hence influencing wind speed and direction. Floods and periods of heavy rainfall affecting Banks Peninsula, occur predominantly with easterly and southerly winds, and are associated with the weather patterns shown in figures 3.29 and 3.30, along with the indicated rainfall distributions.

The question of whether slope exposure to rain bearing winds is a more significant factor than exposure to the sun in initiating slope failure is debatable. Observations during this study suggest that the easterly and southerly winds act to evaporate slope moisture.

After a period of rainfall, the ridge east of the failed ground (where piezometer group 8 was located) appeared to dry out more quickly on cloudy, windy days than it did on windless sunny days. Auger hole logs also show that the top 1.4m of the soil profile was drier on the ridge (auger hole 8) than elsewhere on the site. Ground within and immediately adjacent to the failed ground was substantially wetter than the ridge irrespective of the weather conditions. Based on observations, it appears the drying effects observed on the ridge are influenced more by the wind and topography (drainage) than by sunshine.

Site topography (figure 3.4, map pocket) shows the slope movements have occurred in a topographic depression. The depression results in a convergent surface drainage pattern, thus concentrating water in this zone. It is therefore likely that subsurface flow within the loessial horizons also converge in the topographic depression.

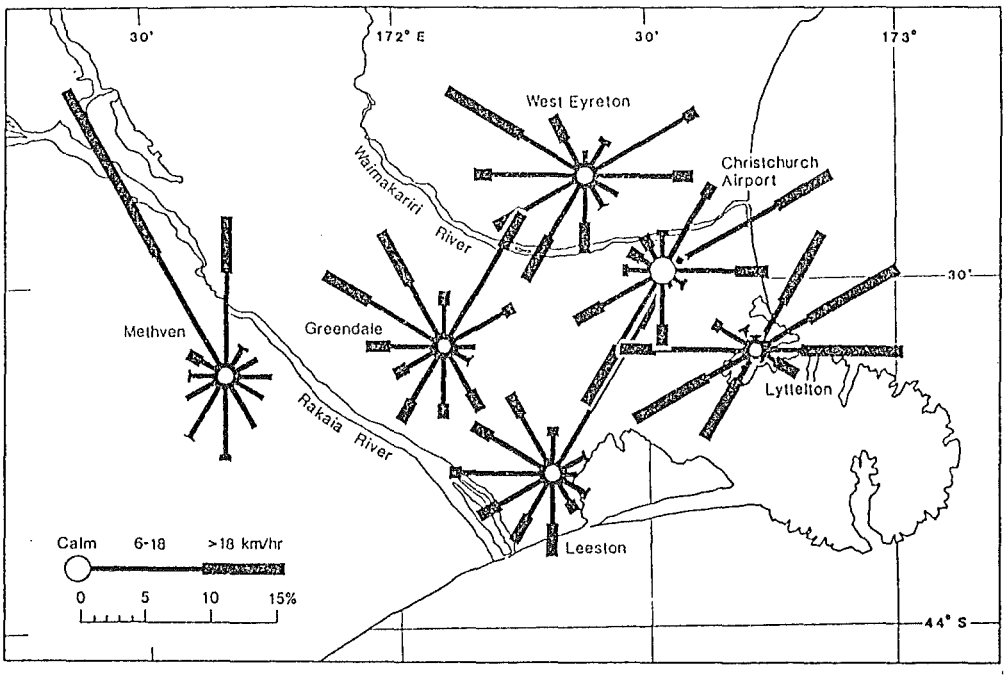

Figure 3.27 Wind Roses divided by 12 to Show the Predominance of Northeasterly Winds (after Ryan, 1987).

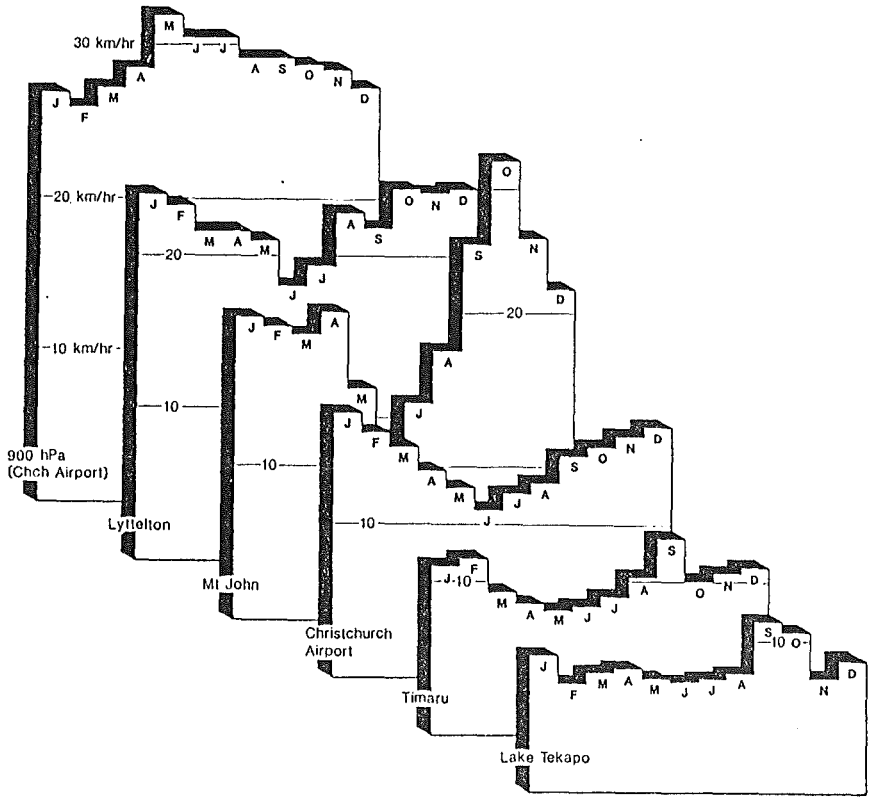

Figure 3.28 Mean Monthly Surface Wind Seed for Selected Locations (after Ryan, 1987).

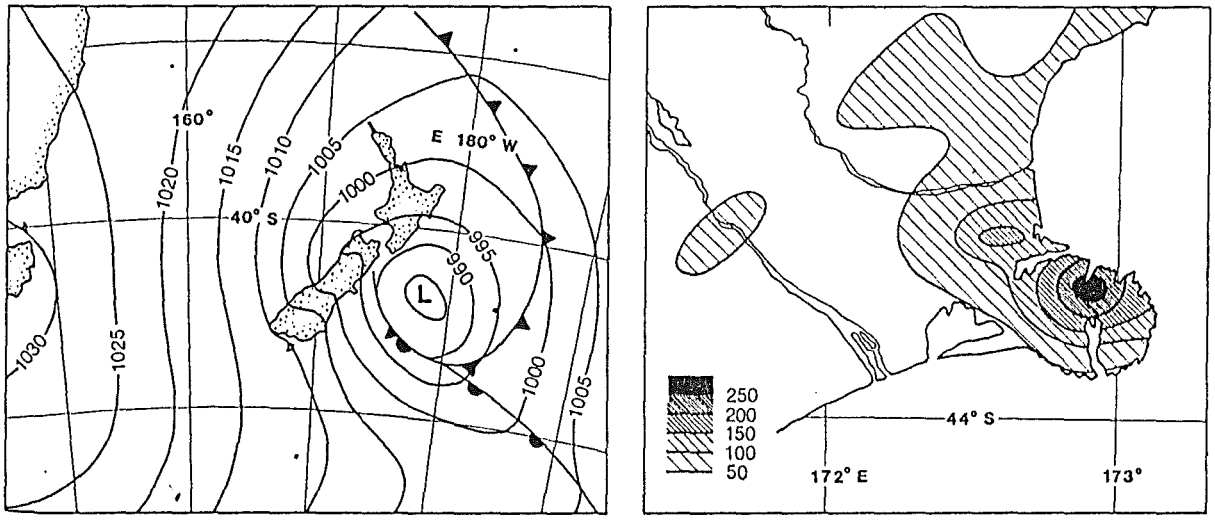

Figure 3.29 Weather Situation at Midnight 20/12/63 and 24 hour Rainfall (mm) Distribution at 9a.m. 21/12/63 (after Ryan, 1987).

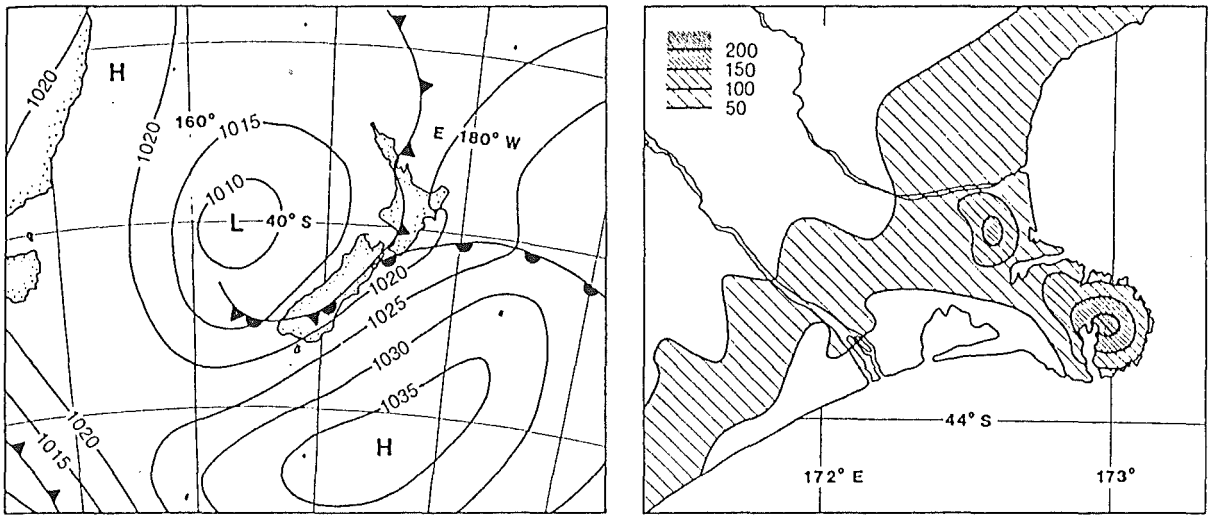

Figure 3.30 Weather Situation at Midnight 15/4/74 and 24 hour Rainfall (mm) Distribution at 9a.m. 17/4/74 (after Ryan, 1987).

3.7.3 Weathering

Three general forms of chemical weathering have been identified from the pit face logs:

1) iron staining at the boundaries of dessication cracks;
2) clasts of iron oxide; and,
3) mottling of soil horizons.

Selby (1982) describes chemical weathering processes that affect soil profiles, and suggests that the formation of iron (ferric) oxide requires the percolation of water and air. Iron oxidises quite readily from the ferrous to the ferric state, forming iron stains on the surfaces of dessication cracks. The accumulation of iron oxide to form clasts takes place where ferrous iron links silica tetrahedra in a silicate structure and then reacts with oxygen to form ferric oxide. The silicate structure then falls apart (Selby, 1982). This chemical weathering process appears to be active in lower S layer loess, and some P layer loess.

Mottling in soil is the result of an alternating oxidising and reducing environment. This is produced by seasonal fluctuations in the water table, that is, fluctuating between a saturated (reducing) and a partially saturated (oxidising) state (Selby, 1982). This chemical weathering process appears to be active in C layer loess.

The water effects and the resulting chemical weathering processes on the soil horizons at the site are generally in agreement with the proposed geohydrological model (section 3.7.5).

3.7.4 Hydrogeology

Introduction

To appreciate the proposed geohydrological model for the southeast facing Allandale site, a general explanation of some key geohydrological processes is required.

Infiltration

Infiltration is defined as the movement of water from the ground surface into the soil via the pore spaces and defects of the soil mass (Brand, 1984). The infiltration rate is affected by:

1) The amount of water at the soil surface;
2) The nature of the soil surface (vegetation cover);
3) The ability of the soil to absorb water from the soil surface, and;
4) The state of the soil moisture deficit (a saturated soil has a zero soil moisture deficit).

The ability of a soil to absorb water depends on the size, number and interconnection of voids and their potential change in size due to swelling of clay minerals on wetting. Generally, the rate of surface infiltration is an inverse function of the volume of capillary moisture in the soil column. That is, a relatively dry soil will have a higher initial infiltration capacity than the same soil with a higher moisture content, primarily because saturation of the soil causes a reduction in the hydraulic gradient near the surface (Chorley, 1978; Knapp, 1978). However, some

pre-existing soil moisture is important, as many dry soils exhibit an initial resistance to wetting (Selby, 1982). For some loessial soils, the pre-existing soil moisture content may need to be reasonably large to initiate a high infiltration rate (for example: P layer loess).

Permeability

The permeability (the ability of a soil to transmit water) of an unsaturated soil is dependant upon its texture and particle geometry. The permeability of an unsaturated soil is related to soil moisture content and may be orders of magnitude less than under saturated conditions. Essentially, as the water content of a partially saturated soil decreases, the largest pores are drained first, due to the greater water potential. Therefore, as a soil becomes drier, and the remaining water is held in progressively smaller pores with progressively lower potentials, the total conductive volume reduces and the interconnecting pathways become fewer and more tortuous. The permeability of the soil decreases very rapidly as it becomes drier, dependant upon size distribution, shape and interconnection of the pores (Wellings and Bell, 1982).

Boundary Effects

Whipkey and Kirkby (1978) show that variations in particle size distribution between two soils in a partially saturated state, will result in different boundary flow effects, dependant on the moisture conditions (dry or wet). They show how a fine particle sized soil (such as C layer loess), overlying a relatively coarser particle sized soil (such as P layer loess), can generate an apparent impermeable boundary between the two soil layers under partially saturated conditions.

3.7.5 Hydrogeological Model

The proposed hydrological site model is based on piezometer data, pit and trench logs, and personal observations during the period of site investigation. Figure 3.31 shows a generalised schematic drawing of the site geohydrology for immediate post rainstorm conditions. During periods of rainfall, a large proportion of water runs off the slope as surface flow, while a proportion of the water infiltrates the soil. The exposed bedrock (being relatively small in area, with only joint derived permeability), is a relatively insignificant water catchment zone.

"Quasi-impermeable" boundaries form at the S-C layer and C-P layer interfaces. The "quasi-impermeable" boundaries have been informally named because when the soil mass is in a partially-saturated state there appears to be significant water flow variation between the soil layers. It is inferred here that, when fully saturated, the permeability variations are relatively insignificant. (P and S layers may be slightly more permeable than the C layer). These boundaries form largely as a result of particle-size variations, and the degree of saturation which control the inter-particle water meniscus tension in the partially saturated soils.

Water that infiltrates the slope enters the S layer, saturating it from the base upwards. Some of the water infiltrates the lower C layer while the rest travels down slope within the S layer, which acts as a leaky perched unconfined aquifer.

Similarly, the C and P layers form leaky, unconfined aquifers from the infiltrating water supplied by their respective overlying soil layers. Saturation starts at the base of the respective layers and progresses upwards. Results from the piezometer monitoring (section 3.7.1) showed that the largest pore water pressures generated were at the base of the C layer. The P layer-bedrock interface intercepts the ground water table, reflected in the largely seasonal response in piezometers 1/4.2, 4/6.0 and 2/2.68.

Figure 3·31 : Generalised schematic model of site hydrogeology

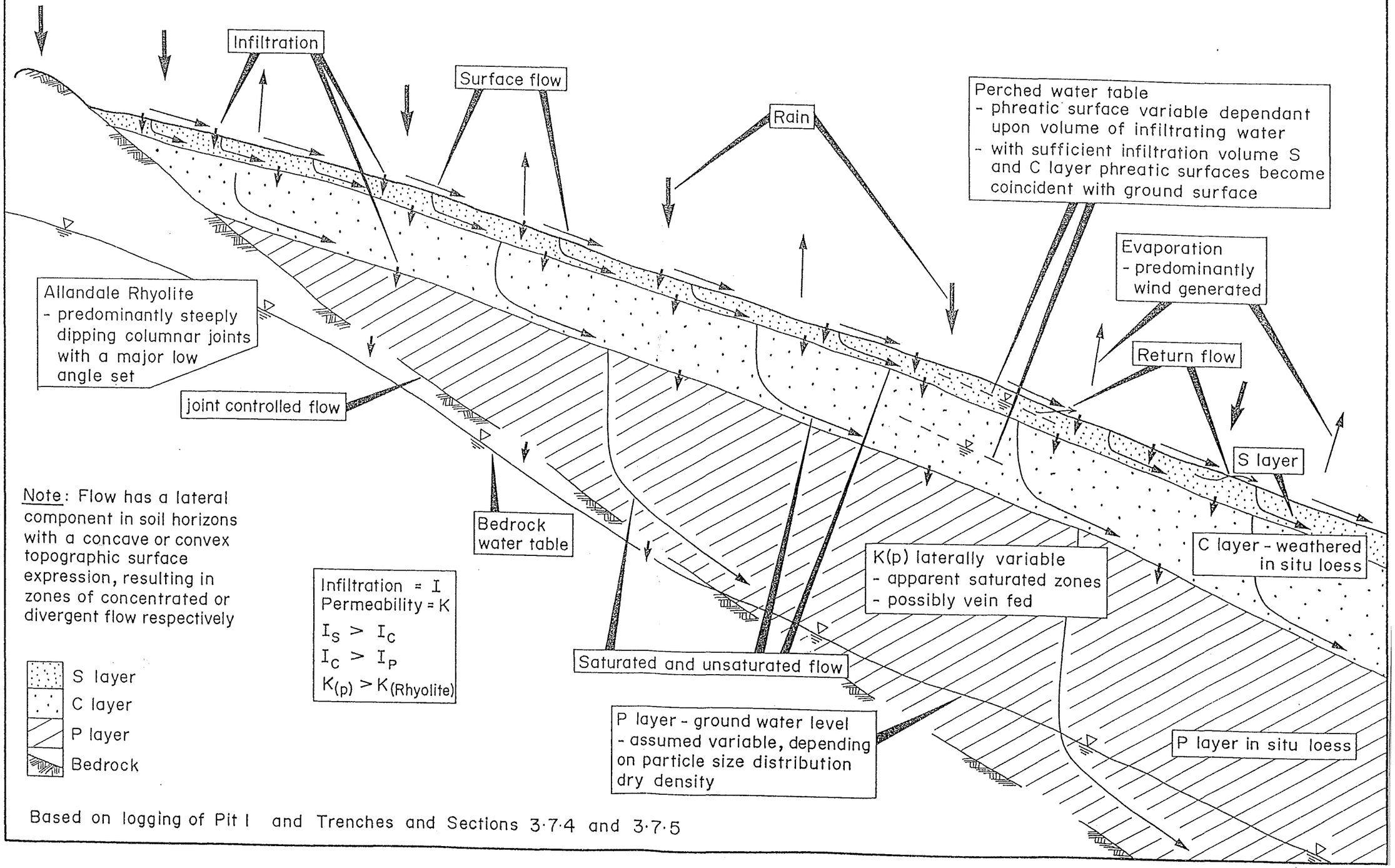

Based on logging of Pit I and Trenches and Sections 3·7·4 and 3·7·5

The dessication and tension cracks feed water directly into the layers which they penetrate. This is probably the cause of saturated zones within the P layer. To produce significantly large pore water pressures at the base of soil layers, saturation of the layer must be more rapid than infiltration into the lower layer. Conversely, if rainfall is of low intensity and long duration, that is, infiltration at the surface is at the same rate as infiltration across the C-P layer interface, then saturation is likely to start at the base of the P layer. This will generate the greatest pore water pressures at the P layer-bedrock interface.

Some time after the rainstorm, when evaporation and drainage volumes exceed the infiltration volume the hydrological model reverses. That is, seepage flow ceases in the S layer before ceasing within the C layer, which in turn ceases flow before the P layer. This is essentially due to the layers proximity to the surface, thickness and porosity.

Summary

It appears that to generate the largest pore water pressures at the S-C and C-P interfaces, the underlying layer should have a large as possible soil moisture deficit (though not dry), and incident rainfall should be of high enough intensity to allow the overlying layer to become fully saturated before the underlying layer. This means the S layer will initially generate the highest pore water pressures, assuming there are insignificant differences in the permeability of the soil layers and ignoring seepage forces. As the C layer becomes more saturated, its basal pore water pressures will increase, reaching a maximum when the S and C layers are fully saturated and thus hydraulically connected.

Further Work

This generalised site hydrology model is based on piezometer monitoring data, pit logging and some assumptions regarding permeability. Further work is required to confirm the assumptions, which is beyond the scope of this thesis. Specific areas requiring further research include the quantification of pedogenic differences in saturated and partially saturated permeability, infiltration rates and soil suction effects.

3.8 Classification of Slope Failure

3.8.1 Introduction

A complete hillslope failure model is presented in chapter 6. For the purpose of classifying the slope failure in this chapter, a brief morphological description of the failed and adjacent ground is included. In addition, eye witness accounts are used to classify the slope failures in accordance with Varnes 1978 classification.

3.8.2 Failure Processes

Gebbie (Pers. comm., 1989) suggested that the slope failures he had observed, take the form of a slow moving flow. The speed of the advancing flow is similar to a walking pace, although there are considerably faster moving boulders bouncing down the hillslope ahead of the flow. The flow forms a hard crusted, fan shaped deposit at the base of the hill, although 7-14 days later a tractor sunk up to its axles in the super-saturated, puggy loess below the hard crust. This eyewitness account indicates a significant amount of loessial soil flowed down the hillslope and indicates the involvement of C layer loess. Varnes's 1978 classification would classify the movement rate of the flow as *very rapid*.

Although no actual failure surface was identified in the failed ground, observations from pits 1 to 5 (section 3.5.5) show failure deposits which involve fluidised flow of C layer loess. Observations from pit logging show some of the fluidised C layer loess remained in the slide area, while Gebbie's eyewitness account suggests that the majority of the failed C layer loess flowed a considerable distance, to produce a fan-like deposit at the foot of the slope. Coherent blocks of top soil came to rest on the slope as they slid off the back of the flowing fluidised C layer and lower S layer loess.

Each down slope orientated trail of top soil blocks represents separate slope failure episodes. The investigated failed ground therefore represents relict scarps of at least six separate failures involving fluidised flow of C layer loess. The form of the relict scarps suggests a translational sliding failure mode (failure plane at base of C layer or within C layer), with a failure geometry of at least 10m long, possibly up to 40m

long, 3m to 5m wide and its depth somewhere within the C layer.

3.8.3 Classification

The slope failure depicted above is best described as an earth flow according to the Varnes 1978 classification. This type of failure has been generally classified as a "slide-avalanche-flow" on Banks Peninsula. Varnes 1978 only uses the word avalanche in conjunction with debris (for example; debris avalanche), and defines debris as a generally surficial engineering soil with a significant (20-80%) proportion of coarse (>2mm) material. Soil that could be classified as debris does not exist in the hillslope investigated. The earth flow classification is adopted in this study.

The "turfmat slide" (referred to in section 3.5.5), which is in common usage in Banks Peninsula literature is not included in Varnes 1978 classification scheme. According to Varnes's classification the "turfmat slide" would be best described as an earth lateral spread, where movement involves fracturing and extension of coherent soil, owing to liquefaction or plastic flow of subjacent soil. The mechanism of failure may initially involve simple shear translational sliding, but spontaneously transforms into a very rapid plastic flow. However, the local classification of Bell and Trangmar (1987), ("Turfmat slide") better describes the slope movement observed on Banks Peninsula, and therefore is adopted in this study.

Chapter 4

Laboratory Investigations

4.1 Introduction

This chapter presents the results of the laboratory investigations and provides a brief discussion of those results. Geotechnical classification tests are discussed fully, while only a brief discussion of strength test results is presented. A more detailed discussion of strength testing is presented in chapter 5.

4.2 Geotechnical Classification

4.2.1 Intoduction

Geotechnical classification tests, which include grain-size analysis, Atterberg limits (liquid and plastic limits), moisture content and densities, are used to characterise soil behaviour.

Sampling for classification tests on the soils in this study was conducted during the excavation and logging of the pits (chapter 3). Bulk and tube samples were obtained from the S,C, and P layers in specific pits.

4.2.2 Particle-size Analysis

Particle-size analyses were conducted using the sieve and pipette method in accordance with N.Z.S. 4402:1986, test 2.8.3. Samples analysed were taken from pits 1 and 2, trench 5 and remoulded material at the completion of unconfined compression testing. Results from the analysis are given in table 4.1, and particle-size distribution curves are given in appendix A4.1.

Table 4.1 Particle-Size Data

Sample		Cumulative Weight Percent		
Pit/Trench	**Layer**	**Clay (%)**	**Silt (%)**	**Sand (%)**
1	Tension Crack	25.3	68.4	6.25
1	Tension Crack	25.1	68.5	6.36
1	C	26.1	66.7	7.18
2	C	25.1	67.3	7.52
5	C	24.3	68.0	7.74
1	P	14.6	75.9	9.45
1	P	14.3	77.1	8.62
Remoulded	C	31.2	63.2	5.64
Remoulded	P	20.6	71.9	7.42
2	P	20.4	71.3	8.30

This shows that the 'tension crack', C layer, remoulded C and P, and P (pit 2) layer to be predominately CLAYEY SILT with minor sand, and P (pit 1) layer to be a SILT with some clay and minor sand.

Table 4.1 shows that the C layer loess in pit 1, 2 and 3 have essentially the same particle size distribution. The tension crack soil in pit 1 has a little less clay and sand, with slightly more silt than the C layer loess. This is probably because it originated from S layer loess which was not analysed. Pit 2 P layer loess has approximately 6% (of total soil) more clay, approximately 5% (of total soil) less silt and similar amounts of sand as Pit 1 P layer loess. Pit 2 P layer loess is more akin to pit 1 P layer loess that has been subjected to mechanical remoulding (Remoulded P).

The effect of mechanical remoulding on pit 1 C and P layer loess is to reduce the relative sand content substantially (C layer -27%, P layer -21%), marginally reduce the relative silt content (C layer -6%, P layer -6%), and substantially increase the relative clay content (C layer +19%, P layer +42%). While both layers of loess have similar reductions in relative silt and sand contents, mechanical remoulding produces a substantial gain in clay size content with remoulded P layer loess.

4.2.3 Atterberg Limits

Determination of the liquid limit, plastic limit and plasticity index were conducted in accordance with N.Z.S. 4402:1986, tests 2.2, 2.3, and 2.4. Samples analysed were obtained from pits 1 and 2, trench 5, and remoulded material at the completion of unconfined compression and vane shear testing.

Averaged results from the testing are given in table 4.2, while full results are presented in appendix A4.2. Table 4.2 shows that P layer material from pit 1 had no liquid limit, yet P layer material from pit 2 had Atterberg limits which are similar to the C layer Atterberg limits. Pit 1 P layer material had measurable Atterberg limits after mechanical remoulding.

Table 4.2 Atterberg Limits (averaged)

Sample		Field moisture	Liquid	Plastic	Plasticity Index		
Pit/Trench	**Layer**	**content *w* (%)**	**Limit**	**Limit**	**mean**	**max**	**min**
1	T/crack	24.7	28.5	19.1	9.4	10.2	8.6
1	C	16.8	24.4	17.1	7.3	8.0	6.5
2	C	20.1	28.2	19.2	9.1	9.2	8.9
2	C	20.1	26.0	19.9	6.2	6.3	5.9
5	C	23.7	30.2	19.1	11.1		
1	P	19.5	N/A				
2	P		26.1	19.0	7.2		
Remoulded	C		25.0	16.4	8.6		
Remoulded	P		22.0	16.2	5.8		

4.2.4 Insitu Moisture Content and Densities

Determination of in situ moisture content and bulk density was conducted in accordance with N.Z.S. 4402:1986, test 4.1.2. All samples were retrieved from pits 1 and 2 using thin walled sampling tubes. Dry density (ρ_d), porosity (n), saturation ratio (S_r) and void ratio (e) were calculated from laboratory data. Example calculations and total data are presented in appendix A4.3.

Table 4.3 shows the averaged results for each layer, while figures 4.1 and 4.2 show bulk density, moisture content and sampling positions on the appropriate face logs.

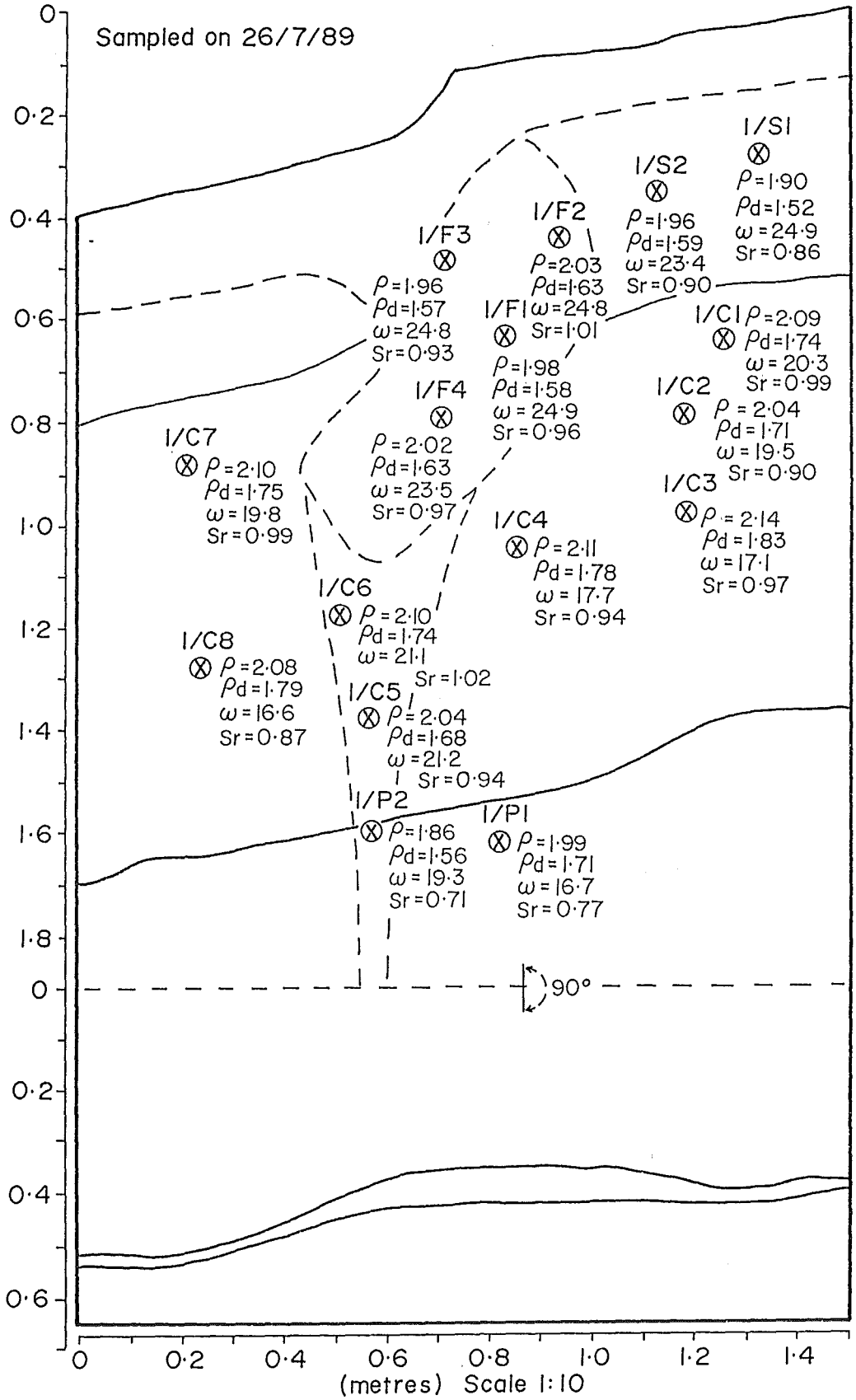

Figure 4·1: Face log of Pit I showing bulk density (ρ,t/m^3), dry density (ρd, t/m^3), moisture content (ω,%) and saturation ratio (Sr) relative to sampling positions

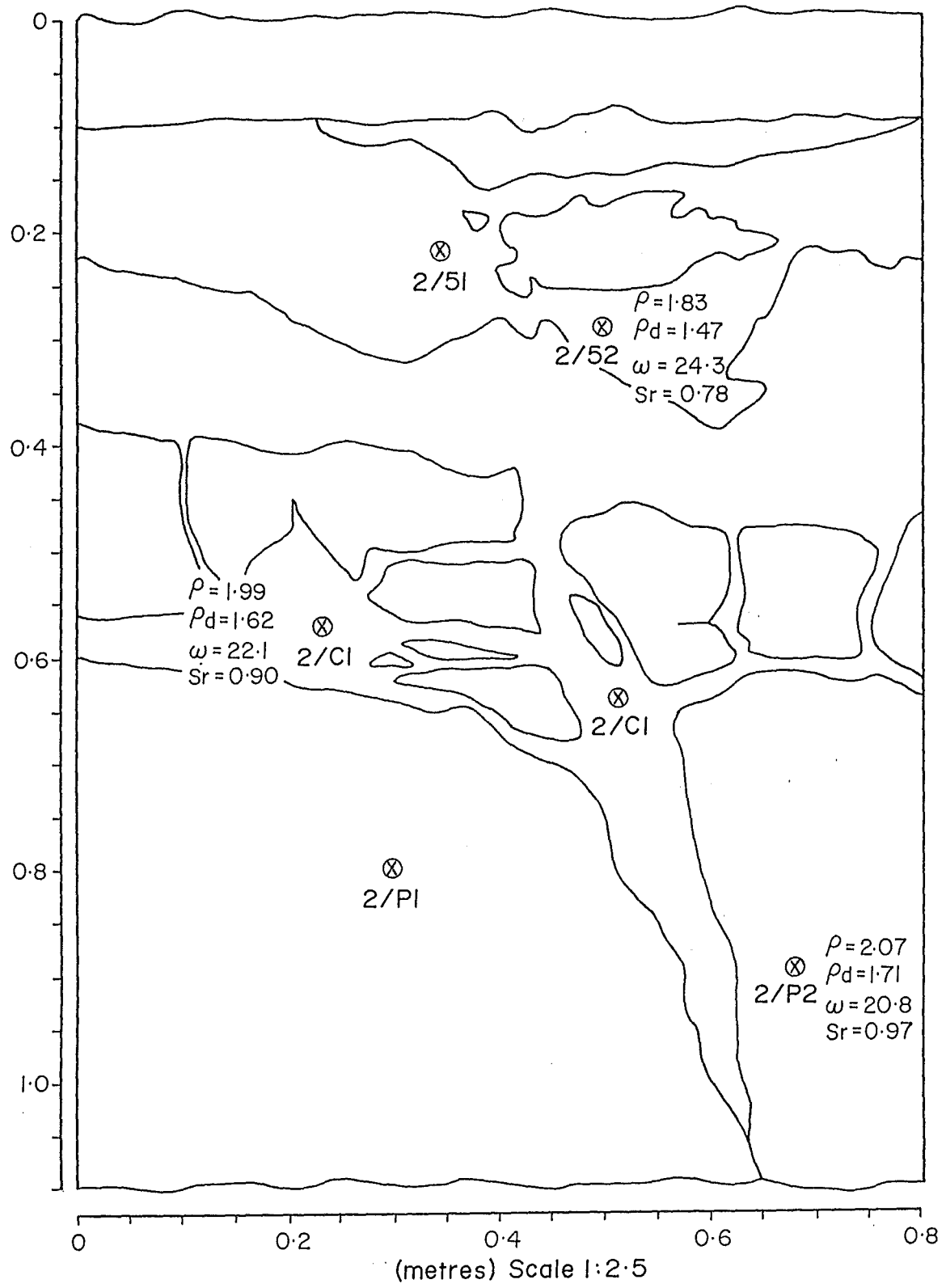

Figure 4·2: Face log of Pit 2 showing bulk density (ρ, t/m^3), dry density (ρd, t/m^3), moisture content (ω, %) and saturation ratio (Sr) relative to sampling positions. (refer to face log figure 3·17 for location and lithology)

Figure 4.1 shows the S and C layers are either saturated or near saturation, while the P layer is only partially saturated (83%). C layer material has the highest dry density followed by the P layer and tension crack soil, while the lower S layer has the lowest dry density. Moisture content is greatest in the lower S layer and tension crack soil, and reduces with depth and distance from the tension crack and its associated wet zone. Figure 4.2 shows dry density increases with depth, while moisture content reduces with depth, though the degree of saturation increases with depth.

Table 4.3 Averaged Insitu densities, water contents, void ratios and saturation ratios for each layer.(sampled 26/7/89)

Pit	Sample Layer	Density Bulk(t/m^3)	Density Dry(t/m^3)	Moisture Cont.(%)	Void Ratio	Saturation Ratio
1	T/crack	2.00	1.60	24.5	0.69	0.96
1	S	1.93	1.56	24.1	0.74	0.88
1	C	2.09	1.75	19.2	0.55	0.95
1	P	2.00	1.70	18.0	0.59	0.83
2	S	1.82	1.47	24.3	0.84	0.78
2	C	1.98	1.62	22.1	0.67	0.89
2	P	2.07	1.71	20.7	0.58	0.97

Determination of the solid density (specific gravity) was completed in accordance with N.Z.S.4402:1986, test 2.7.2. Bulk samples from pit 1, C and P layers were used for testing. Specific gravity varied insignificantly between the P and C layers, yielding an averaged specific gravity of 2.71. Results of testing are presented in appendix A4.3.3.

4.2.5 Discussion

It has been shown that the geotechnical properties of the loessial soils from the site investigated, vary laterally and with depth. In particular it has been shown that mechanical remoulding alters the particle size distribution and Atterberg limits of the loessial soils examined.

Comparison of particle size distribution with other reports shows there is a significant variation with depth and laterally on Banks Peninsula, hence generalising between loessial layers is difficult. Evans (1977a) conducted extensive investigations into particle size distribution of Banks Peninsula loessial soils laterally and with depth. He reports ranges in clay size, silt size and sand size particles of 8-30%, 51-76% and 8-26% respectively. Results from this study generally fall into the same range of particle size distributions with the exception of the sand content which is as low as 6% in the tension crack soil.

Though a lot of particle size information has been reported for Banks Peninsula loessial soils (for example: Evans, 1977a; Evans and Bell, 1981; Mackwell, 1986; Yetton, 1986; McDowell, 1989), it is difficult to compare specific results as different determination methods and different sand/silt boundaries have often been used. Coates and Hulse (1985) suggest that the pipette and hydrometer method compare well and produce excellent reproducibility, however they show a 5% cumulative weight percentage difference at 2μm between the two methods with P layer loess. This is significant when considering that the difference between C and P layer loess clay content is often only 5% (cumulative weight percent). Selection of the definition of the silt/sand boundary is significant, as all particle size distribution curves of Banks Peninsula loessial soils show this region to be a steep portion of the curve. Hence if 62μm is chosen as the boundary (for example: Evans and Bell, 1981; Yetton, 1986), this will alter the silt/sand fraction significantly when comparing with other workers (engineers and engineering geologists) who use 60μm as the silt/sand boundary.

It can be concluded that all in situ loessial layers examined follow the same general particle - size trend reported by other research on Banks Peninsula loessial soils.

As discussed previously the most significant difference between the Atterberg limits involves P layer loess soil from pit 1 (in situ and after mechanical remoulding) and pit 2. The Atterberg limits are generally comparable with those reported by Yetton, 1986 and McDowell, 1989 (liquid limit 21-31; plastic limit 16-21) and the liquid limits are considerably lower than those reported by Mackwell, 1986 (liquid limit 30-44). The plasticity chart (Terzaghi and Peck, 1967) classifies all the loessial soil

tested (except pit 1 P layer) as cohesionless soils and inorganic silts of low compressibility.

The dry density range is consistant with that reported by Evans (1977a), who reports ranges of 1.39-1.62t/m^3, 1.51-1.88t/m^3 and 1.32-1.71t/m^3 for the S, C and P layer respectively.

In situ moisture contents encounted from the loessial soils investigated are generally on the high side of those reported from other work on Banks Peninsula loessial soils. Yetton (1986) reports in situ moisture contents between 10 and 16%, while McDowell (1989) reports in situ moisture contents between 5 and 21%. Mackwell (1986) reports the highest in situ moisture contents, which are as high as 28.4%.

An average specific gravity of 2.71 for loessial soils would appear to be on the high side considering that quartz particles are the dominant (50%+) mineral (Bell, 1978), and have a specific gravity of 2.65 (Hurlbut and Klein, 1977). Miller (1971) reported specific gravity changed with depth, these changes being 900mm = 2.68, 1350mm = 2.68 and 2400mm = 2.71. These results are consistantly higher than the quoted specific gravity of quartz. The possibility that clay minerals provide the additional specific gravity is unlikely due to their relative small contribution to the soil mass and this study showed no evidence of consistent variation (range 2.67-2.73, see appendix A4.3.3) between C and P layer loess soils.

In summary it can be concluded that:

1) The geotechnical classification tests confirm that pit 2 P layer loess is a slightly weathered version of pit 1 P layer loess as discussed in chapter 3.
2) Mechanical remoulding significantly alters the geotechnical description of loessial soils.
3) Loessial soils encounted at the site investigated are generally consistent with those loessial soils reported by other work on Banks Peninsula loessial soils.

4.3 Undrained Strength Tests

4.3.1 Introduction

The aim of this section of testing was to determine the relationship between dry density, water content and undrained shear strength for the loessial C and P layers. This involved unconfined compression, shear vane and compaction testing. All testing for this section was in the Civil Engineering department laboratory of Canterbury University. Material was obtained from pit 1 bulk samples of layers C and P. Soil was air dried to the lowest desired water content in large trays. Distilled water was added in known quantities to bring the material up to successively higher water contents. It was then thoroughly mixed in the soil mixer (figure 4.3), and stored in air-tight plastic bags in the fog room (100% humidity) for a curing period of 24 hours, to further allow the water content to equilibrate through the sample.

The laboratory programme was modified to recycle material as much as possible. The farm manager of Living Springs Trust requested minimal damage to his property. To achieve the desired laboratory program with fresh soil would have required nearly $0.5m^3$ (1 tonne) of soil, which would have left a large hole in the farmers paddock, as well as being difficult to transport. It was thus decided to collect 75kg of soil from each of the C and P layers which was remoulded several times to conduct the large number of tests. The possible consequences of this are discussed in chapter 5.

4.3.2 Unconfined Compression Testing

A laboratory program was set up to determine the undrained shear strength of remoulded loessial layers C and P over a wide range of dry densities and water contents. This involved compacting the remoulded soil in three layers, in a standard proctor mould, using a kneading compactor (figure 4.4). The kneading machine had a load controllable hydraulic ram with variable tamp control. Dry density and water content were determined in accordance with N.Z.S. 4402:1986, test 4.1.1, except that only a central strip of soil (from top to bottom of mould) was used for the determination of water content, instead of the entire mould contents. Three thin

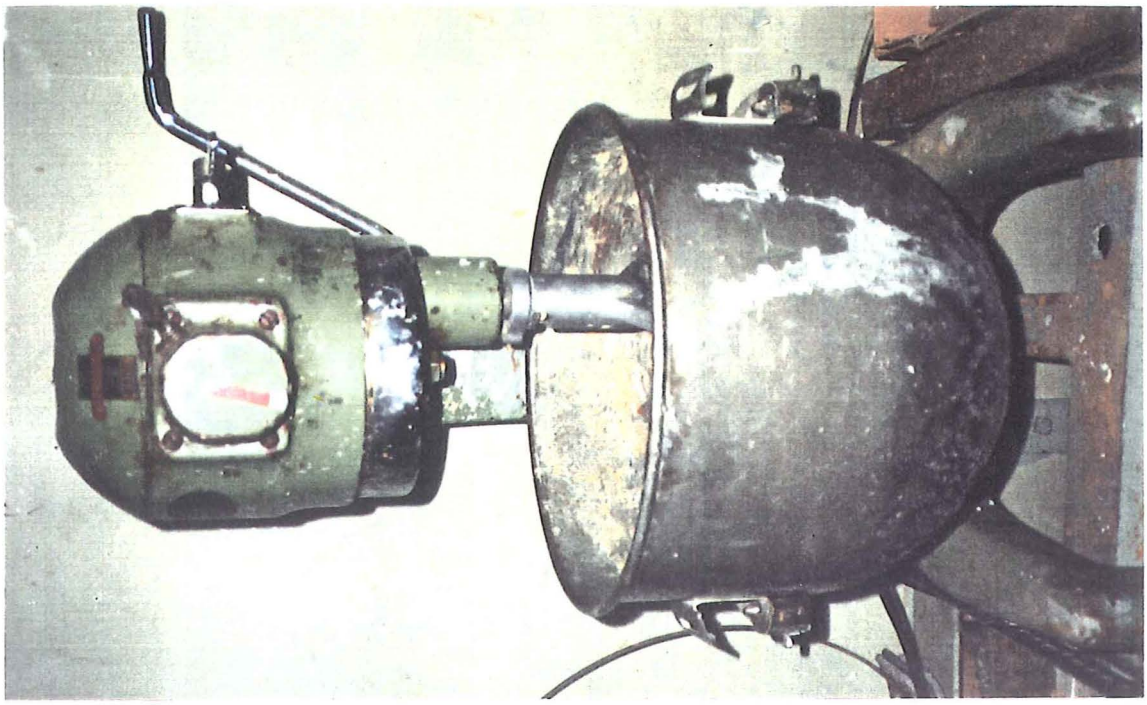

Figure 4.3 Soil Mixer- used to mix remoulded samples

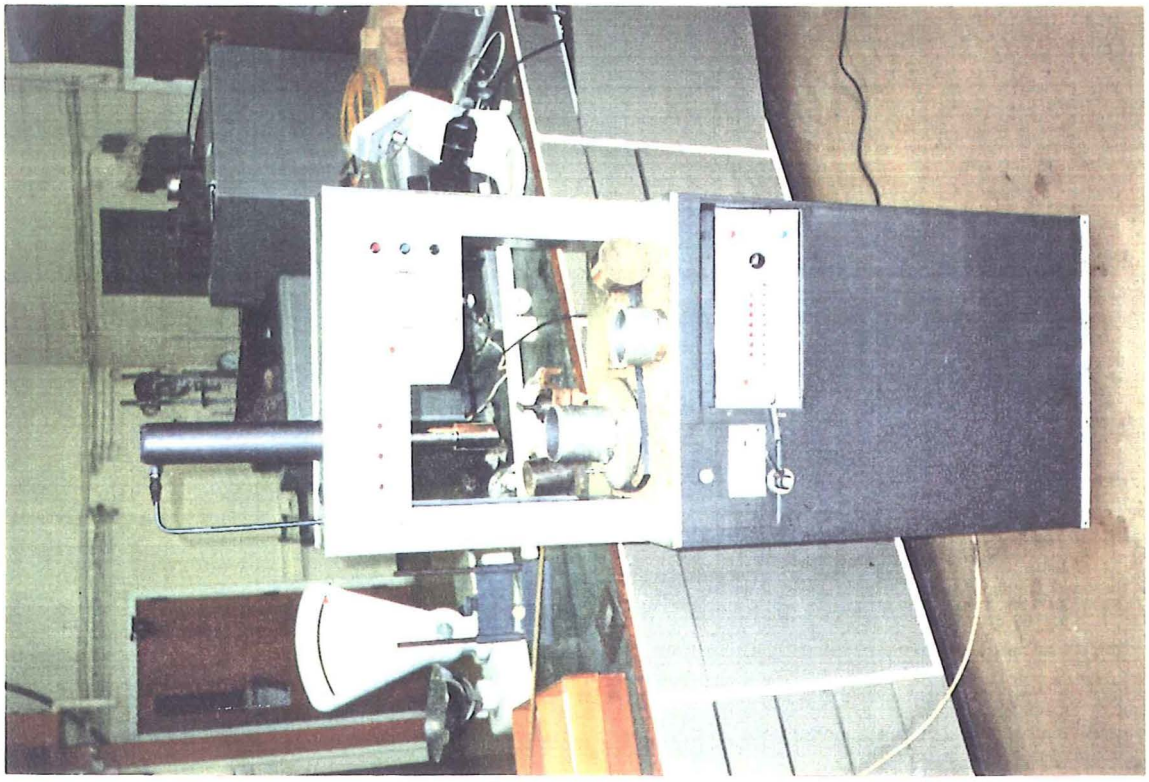

Figure 4.4 Hydraulic Kneading Compactor

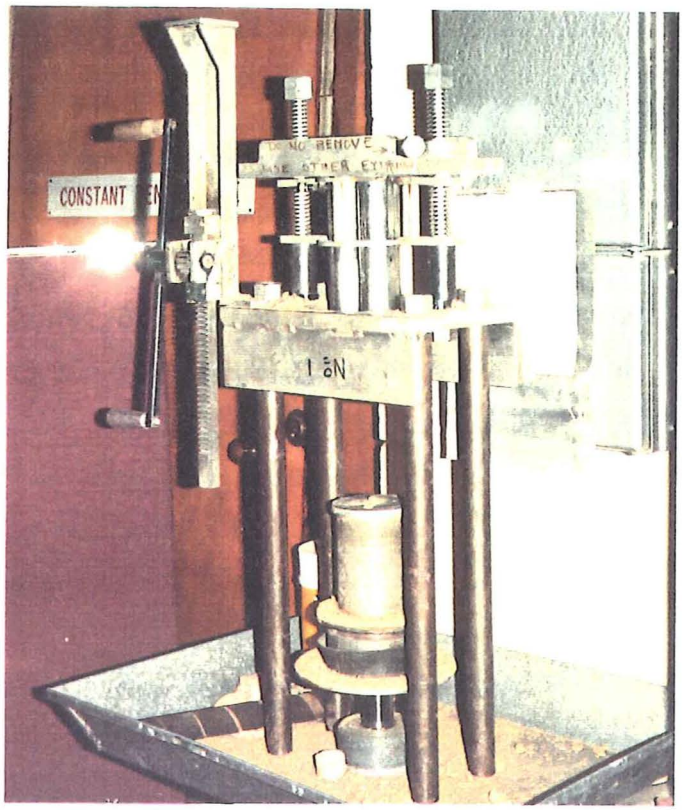

Figure 4.5 Hydraulic Proctor Mould Extruder

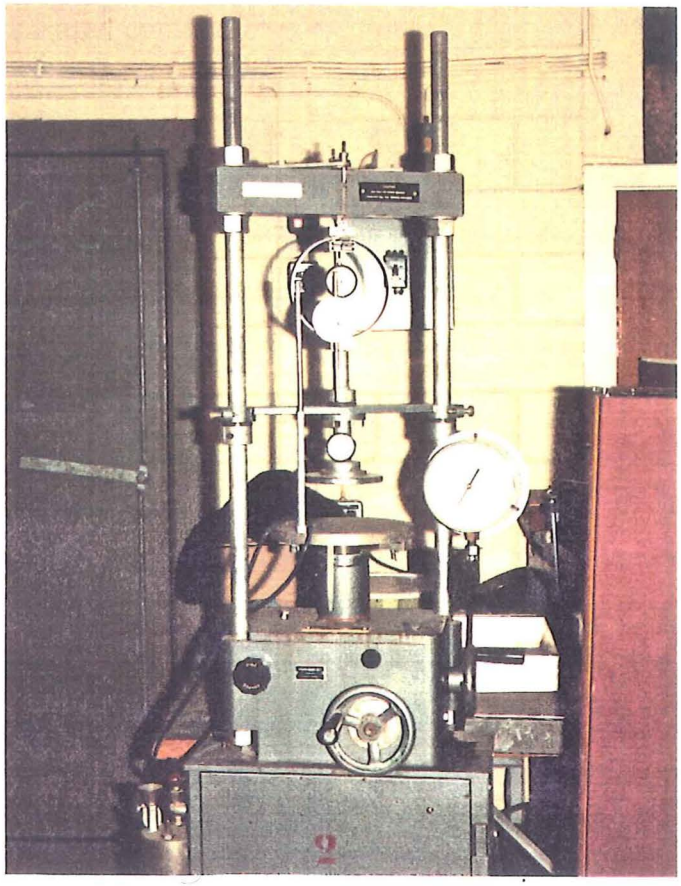

Figure 4.6 Wykeham Farrance Unconfined Compression Machine

walled sampling tubes were forced into the compacted material as it was extruded from the proctor mould. Figure 4.5 shows the hydraulic extruding machine used. Two of the three samples were then sealed with hot wax and air-tight plastic bags and placed in the fog room (99% humidity and 20°c temperature), then tested in the unconfined compression machine at 10 and 100 days to determine effects of cure time on the undrained shear strength of the remoulded soil. The other sample was extruded from the sample tube, prepared and tested immediately in the Wykeham and Farrance (Machine 2) unconfined compression machine (figure 4.6), in accordance with N.Z.S. 4402:1986, test 6.3.1. All samples were tested at a rate of axial compression of 1mm/minute.

Figures 4.7 and 4.8 show the results of undrained shear strength plotted against failure moisture content for the remoulded C and P layers respectively. Both plots show a large scatter in undrained shear strength at failure moisture contents below 15% with C layer soil and at all moisture contents with P layer soil. The C layer plot (figure 4.7) suggets a possible inverse relationship between undrained shear strength and failure moisture content greater than 14.5%. This same relationship is not obvious with the P layer soil (figure 4.8).

Figures 4.9 and 4.10 show plots of curing sensitivity against cure time. Curing sensitivity was determined by dividing the undrained shear strength of the non-cured samples by the undrained shear strength of the cured samples, at the same initial moisture content and dry density. The data is presented this way because plots of undrained shear strength against cure time produced to much scatter (due to the experimental scatter with undrained shear strengths), making a trend impossible to determine. Figures 4.9 and 4.10 show a definite trend of strength increase with increased cure time (up to 100 days) for the C and P layers respectively.

Specimen condition at failure are shown in figure 4.11, for the C and P layers. Example P layer specimens are stacked on top of example C layer specimens, with moisture content (range from 9-18%) at failure, increasing from left to right. Processed data in accordance with N.Z.S. are presented in appendix A4.4.1 and A4.4.2.

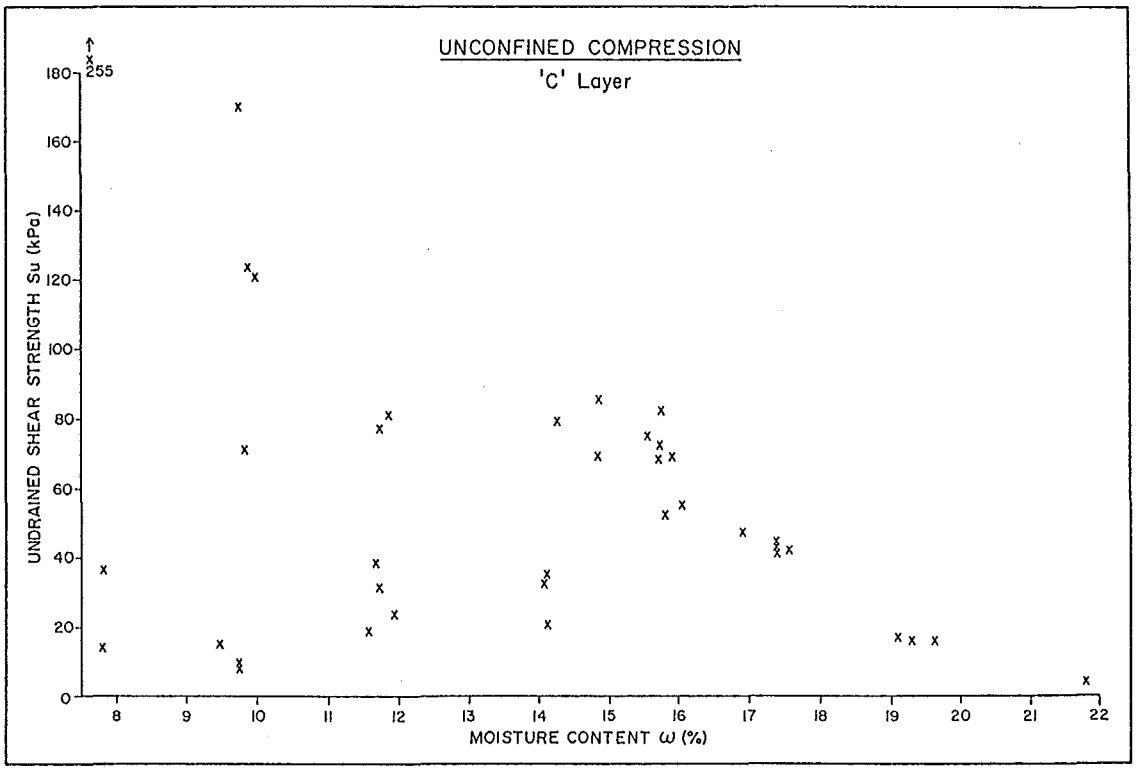

Figure 4.7 Results of Unconfined Compression Tests- remoulded C layer

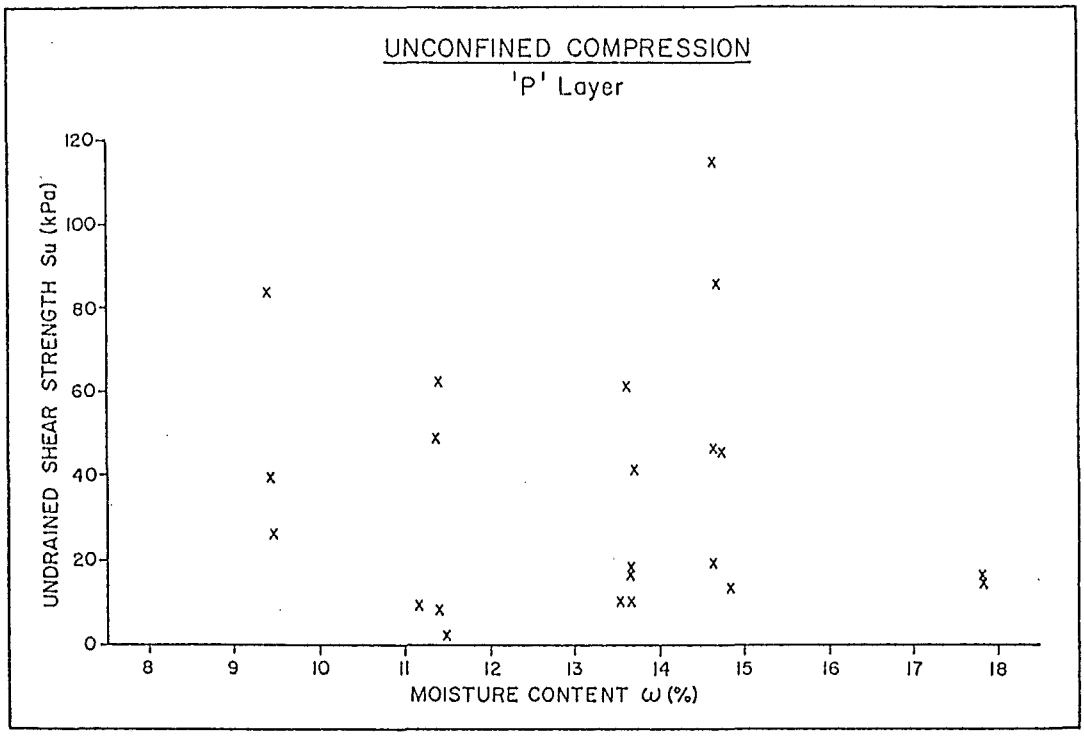

Figure 4.8 Results of Unconfined Compression Tests- remoulded P layer

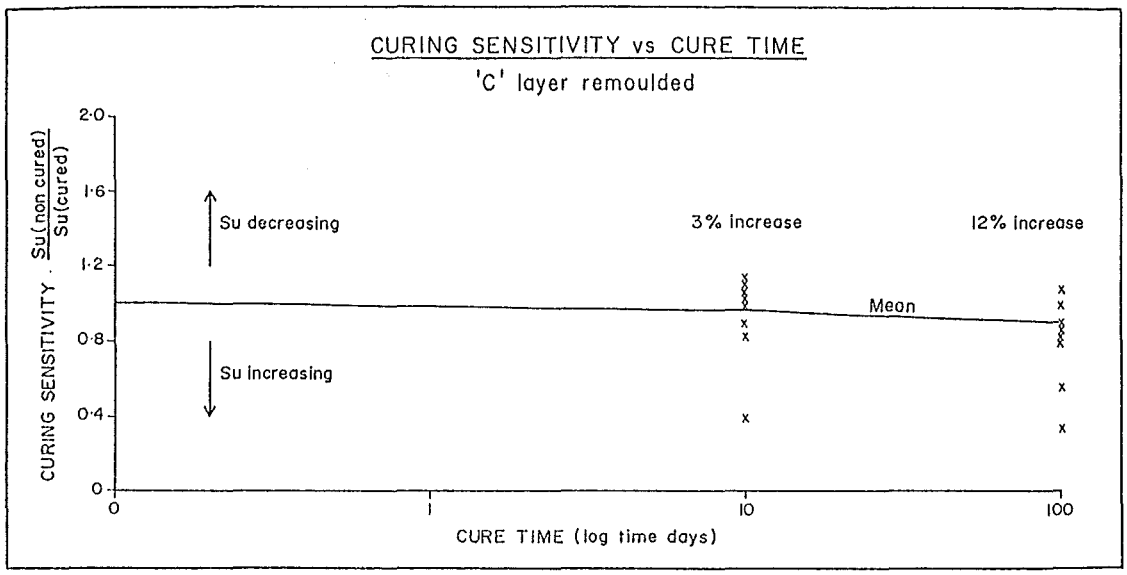

Figure 4.9 Results of Curing Sensitivity- remoulded C layer

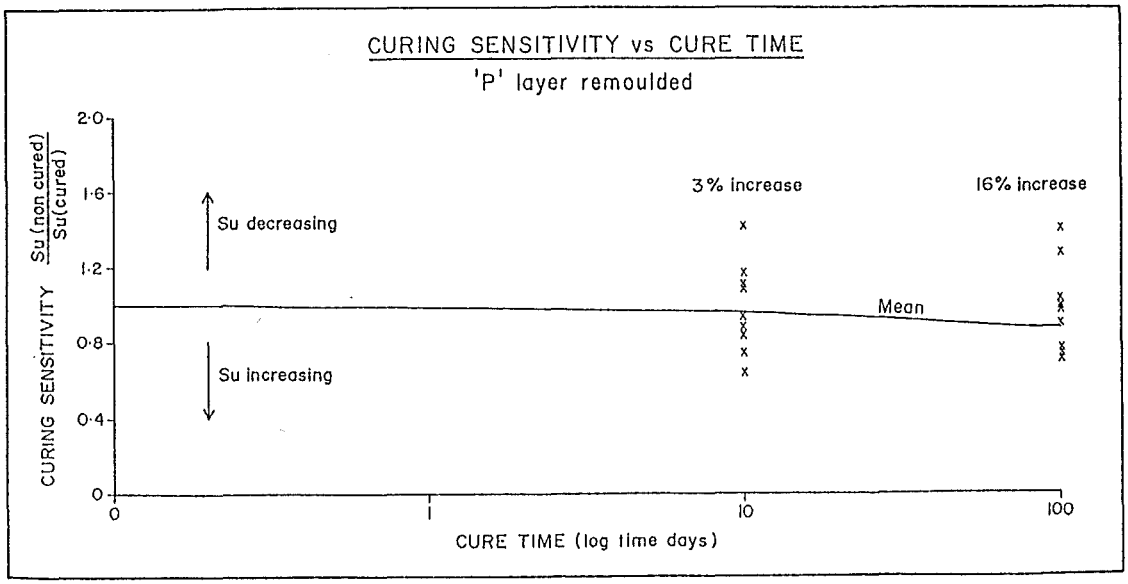

Figure 4.10 Results of Curing Sensitivity- remoulded P layer

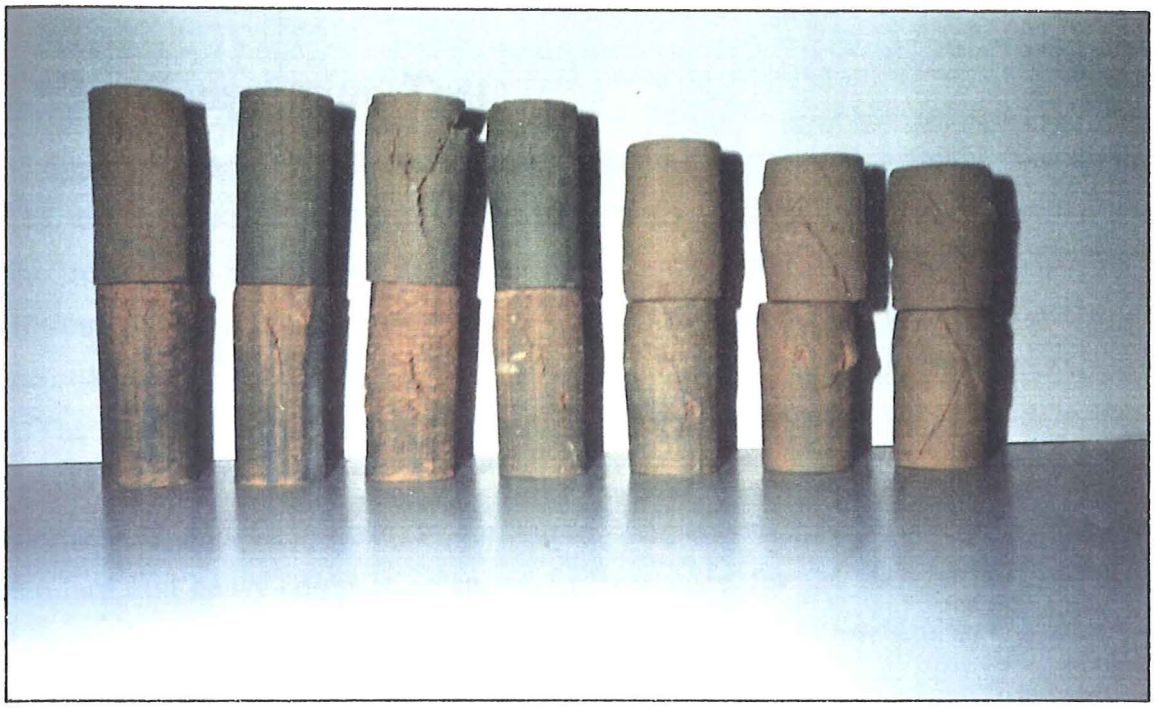

Figure 4.11 Test Specimen Condition at Failure- remoulded C & P layer

Possible Errors

Specimens that were failed at low water contents, and dry densities (figure 4.11) produced failure surfaces that were near vertical and at the top of the sample. This was due to additional compaction at one end, produced by the thin walled sample tube extruder. Though attempts were made to remove the effected portion from the specimen, this was seldomly accomplished. The effect was noted on most extruded samples up to a water content of 14%, which produced large scatter between test samples of similar dry density and moisture content, see appendix A4.4.1 and A4.4.2. Milovic (1988) reported similar problems with loessial soils from Yugoslavia and discusses the influence of sampling technique on unconfined compressive strength. Samples taken from the same place by thin-walled sampling tubes and by hand carved blocks show significantly different undrained shear strength responses which results from mechanical disruption (additional compaction) to the piston samples causing an increase in the dry density.

The increase in dry density was not accounted for in this testing program as dry density was calculated from the original compacted soil in the proctor mould. This means some test specimens actually had higher dry densities than those recorded, particularly those tested at relatively low dry density and moisture content.

4.3.3 Compaction Tests

Compactive effort was calculated from all compaction tests undertaken in sections 4.3.2 and 4.3.5 based on the product of compactive load and the number of tamps. The results of these tests are presented in appendix A4.4.1 and A4.4.2. For reference, New Zealand standard and heavy compaction tests were conducted in accordance with N:Z.S. 4402:1986, tests 4.1.1 and 4.1.2 for both loessial layers C and P. The results of these tests are presented in appendix A4.4.3.

Figures 4.12 and 4.13 show the contoured compaction curves with New Zealand standard and heavy compaction curves for reference, for the loessial layers C and P respectively. All compaction curves (and dry densities) follow similar trends with scatter reducing as moisture content increases.

4.3.4 Four Day Soak Test

The soak test was conducted to assess the effects of soaking on dry density, moisture content and undrained shear strength. Blakeley (1965) reported tests on 'Heathcote loess', and showed that the 4 day soak test used in C.B.R. testing gave adequate time for samples to become approximately 95% saturated.

Specimens of remoulded loessial layers C and P were compacted as in section 4.3.2 at different dry densities and water contents. The specimens were then placed in a constant level water tank (figure 4.14), in their proctor moulds with free draining bases and tops. Dial gauges were installed to monitor swelling during the 4 days of soaking.

Dry densities and water contents were calculated before and after soaking as in section 4.3.2, with the exception of initial water content which was determined from excess sample after compaction. Undrained shear strengths were determined as in sections 4.3.2 and 4.3.3 for all specimens after 4 days soaking. Results of these tests are tabled in appendix A4.4.4.

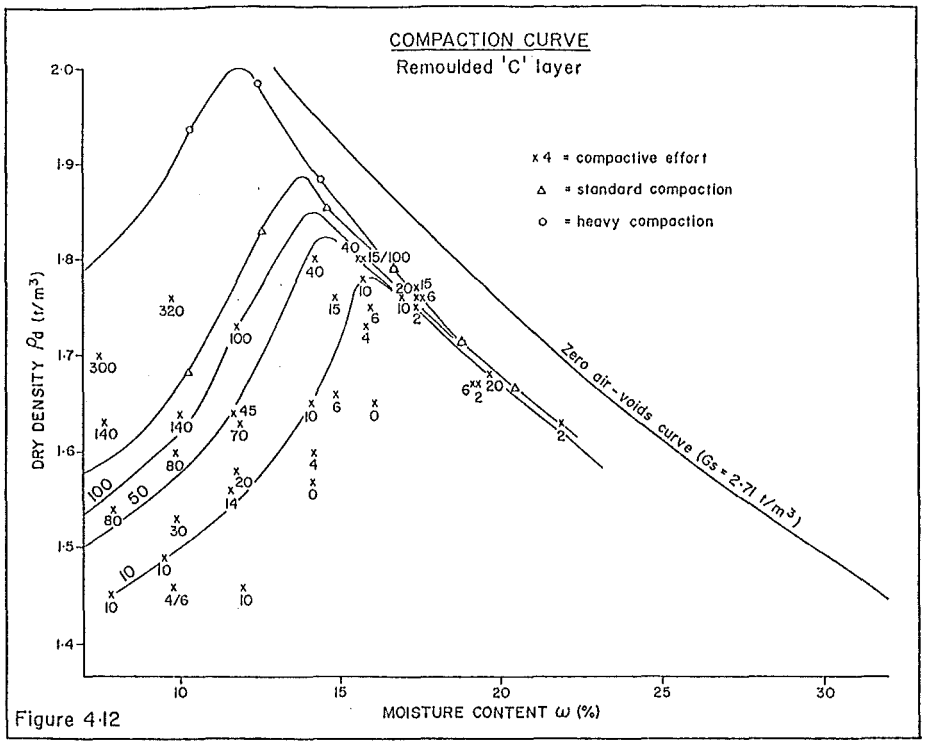

Figure 4.12 Compaction Curve- remoulded C layer

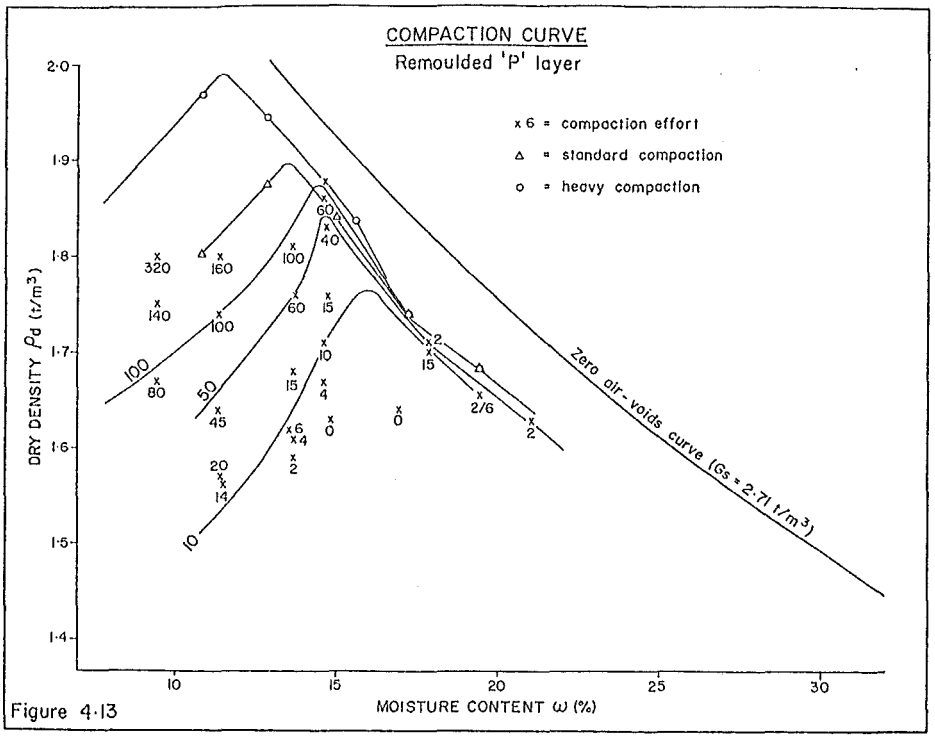

Figure 4.13 Compaction Curve- remoulded P layer

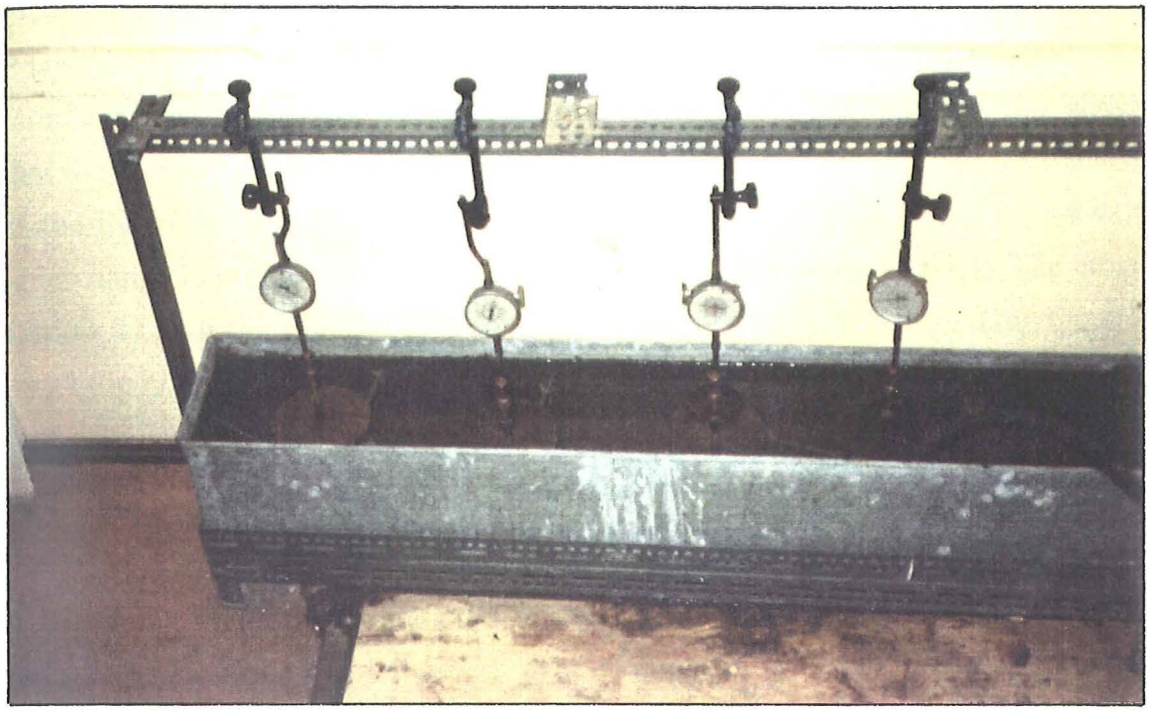

Figure 4.14 Constant Water Level Tank- for Four Day Soak Test

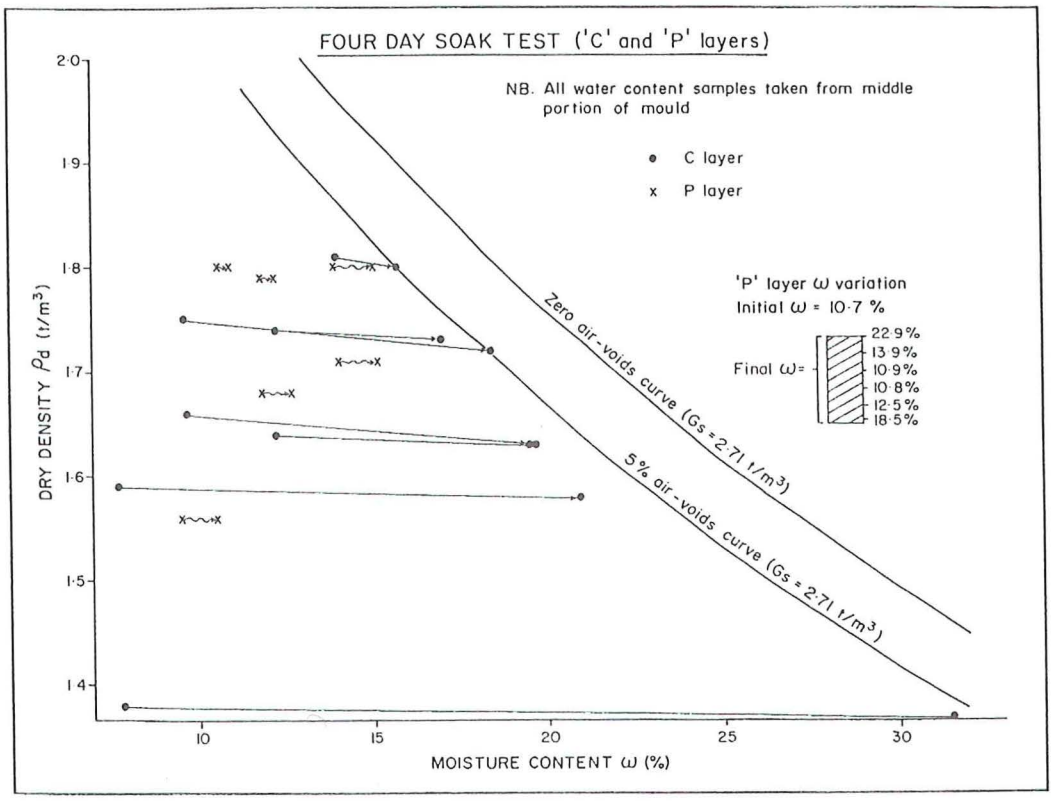

Figure 4.15 Results of Four Day Soak Test- remoulded C and P layer

Figure 4.15 shows the results of the 4 day soak tests on remoulded loessial C and P layers. Also included in this figure is a cross-section through a P layer soak tested sample, showing the water content variation through the specimen. The plot shows that the C layer soil nearly always attains a degree of saturation of 95% irrespective of the initial dry density and moisture content. However, P layer soil shows very little change in moisture content (generally < 1%) after 4 days soaking. The cross-section through the P layer soaked sample shows that after 4 days soaking there is very little change in the moisture content at the centre of the sample.

4.3.5 Vane Shear Test

A laboratory program was initiated to determine the undrained shear strength of remoulded loessial C and P layers over a range of dry densities and moisture contents, to compare with results obtained from unconfined compression tests (section 4.3.2) and insitu vane shear tests.

A Pilcon direct reading hand vane tester (figure 4.16) was used to determine all undrained shear strength values. The Pilcon direct reading hand vane (shear vane) gives a direct dial reading in kPa units, based on empirical correlation with triaxial shear strengths over a wide range of saturated clays (Serota and Jangle, 1972). However for the purposes of this testing program, the shear vane was calibrated to formula (vane dimensions and applied torque) according to B.S. 1377:1975. All tests were conducted at or near to a revolution rate of 360°/minute, with the vane tip forced 70mm into the sample, as recommended by Serota and Jangle.

Remoulded Testing

Specimens for vane shear testing were obtained by compacting remoulded loessial C and P layers by the same method and at the same dry densities and moisture contents as for unconfined compression testing, described in section 4.3.2. Specimens were tested with the shear vane while the protor mould was clamped in place during shear vane rotation.

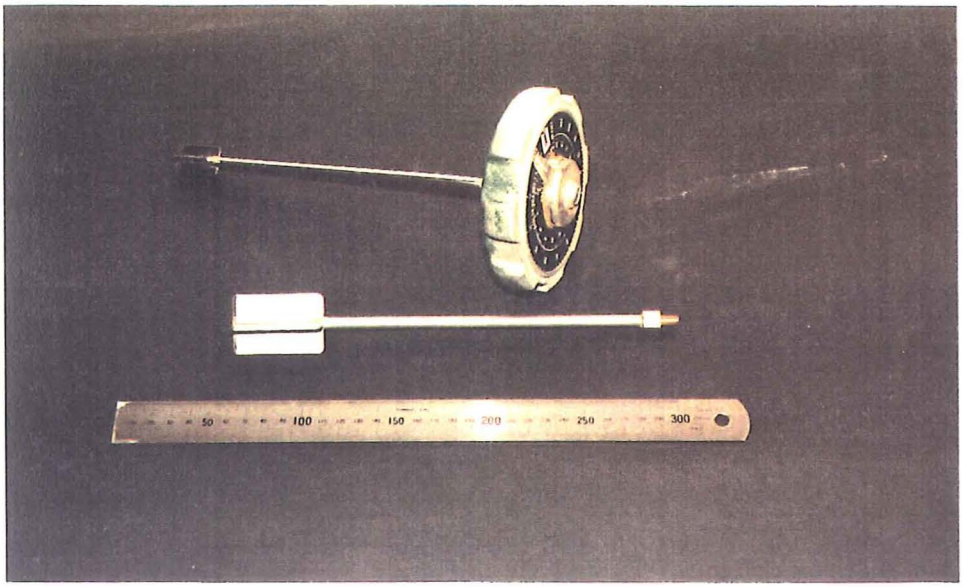

Figure 4.16 Pilcon Direct Reading Vane Tester

Figures 4.17 and 4.18 show the results of undrained shear strength plotted against compaction moisture content for remoulded C and P layer respectively. Both graphs show a trend between undrained shear strength and compaction moisture content. Both graphs show a large scatter in undrained shear strength at low compaction moisture contents. There would appear to be a greater scatter in the P layer soil, with the scatter being significantly reduced at compaction moisture contents greater than 15%. The C layer scatter would appear to reduce uniformally with increasing compaction moisture content, with an apparent change in the plot tend at 19% compaction moisture content. Processed data are presented in appendix A4.4.1 and A4.4.2.

Insitu Testing

Insitu vane shear testing was undertaken on Pit 1 loessial layers S, C, P, and in a vein and a tension crack. Soil samples at each test position were sealed in tins and air-tight plastic bags, and analysed for water content. Processed data are presented in appendix A4.4.5.

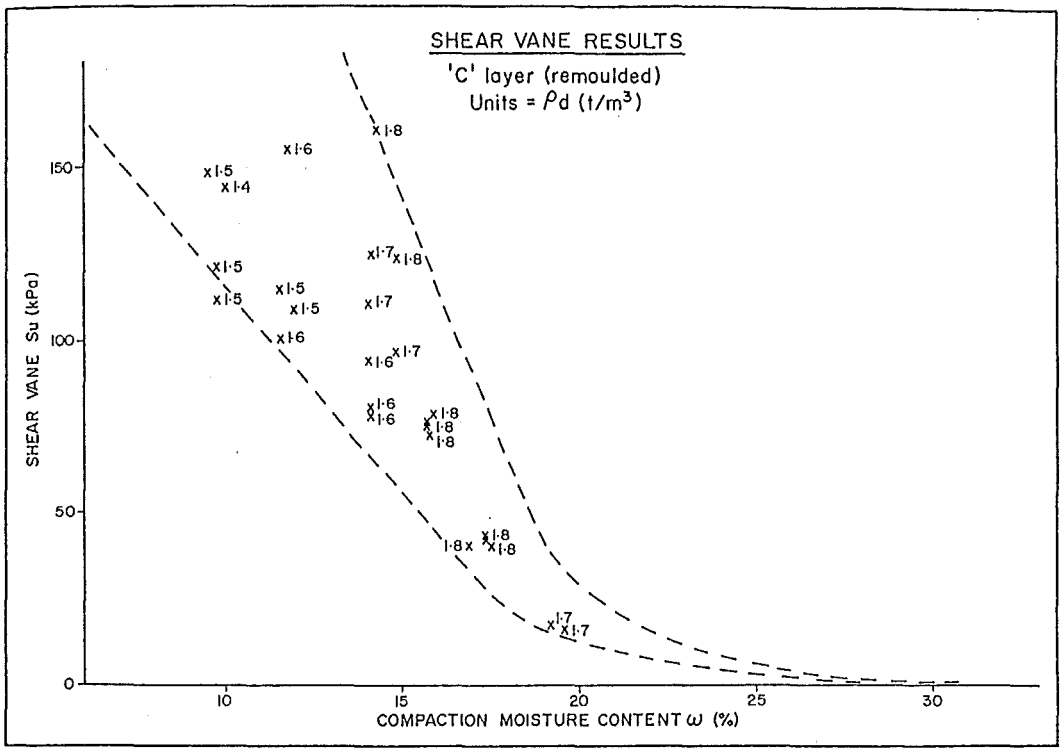

Figure 4.17 Results of Shear Vane Testing- remoulded C layer

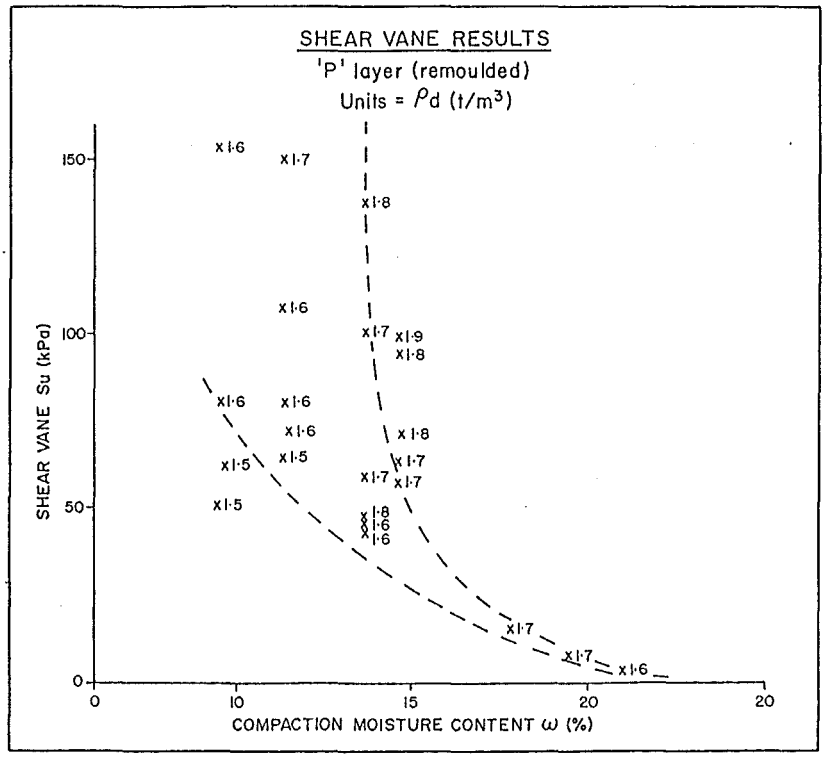

Figure 4.18 Results of Shear Vane Testing- remoulded P layer

Figure 4.19 shows a face log of Pit 1 with the location of sample positions, undrained shear strength and in situ moisture content.

Figure 4.20 shows the relationship between undrained shear strength and in situ moisture content for the loessial layers tested. The plot shows that the P layer soil produces greater in situ undrained shear strengths than the S layer which in turn produces greater undrained shear strengths than the C layer at similar in situ moisture contents. The plot shows an apparent change in trend at 24% in situ moisture content, with increasing scatter in undrained shear strength as in situ moisture content reduces. The vein soil would appear to be a continuation of the C layer soil, suggesting localised weathering processes.

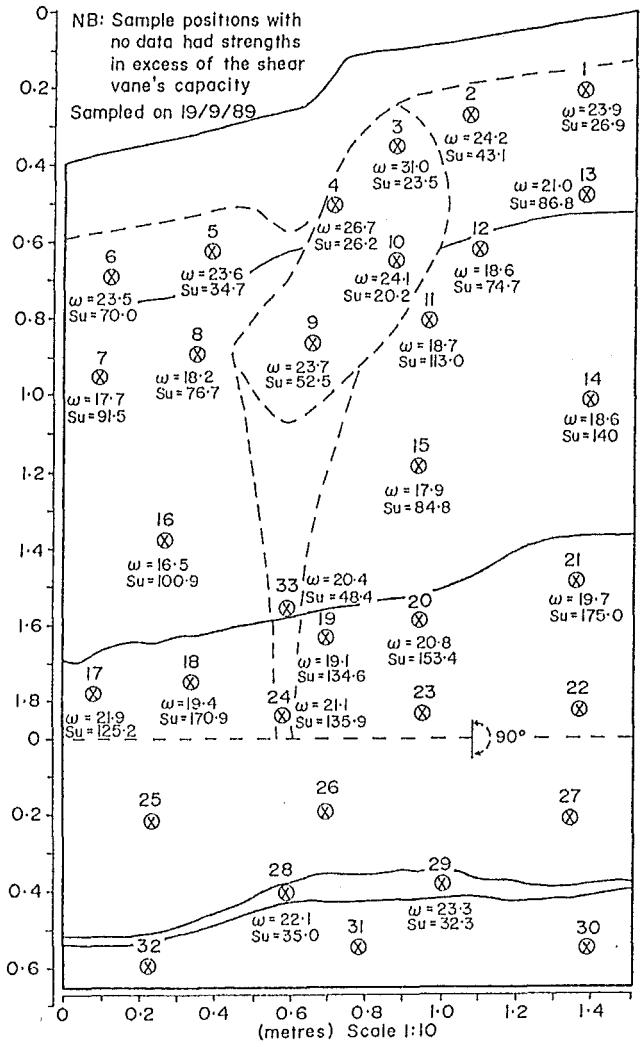

Figure 4·19: Face log of Pit 1 showing undrained shear strength (Su, kPa) and in situ moisture content (ω, %) relative to sampling positions (refer to face log Fig. 3·16 for location and lithology)

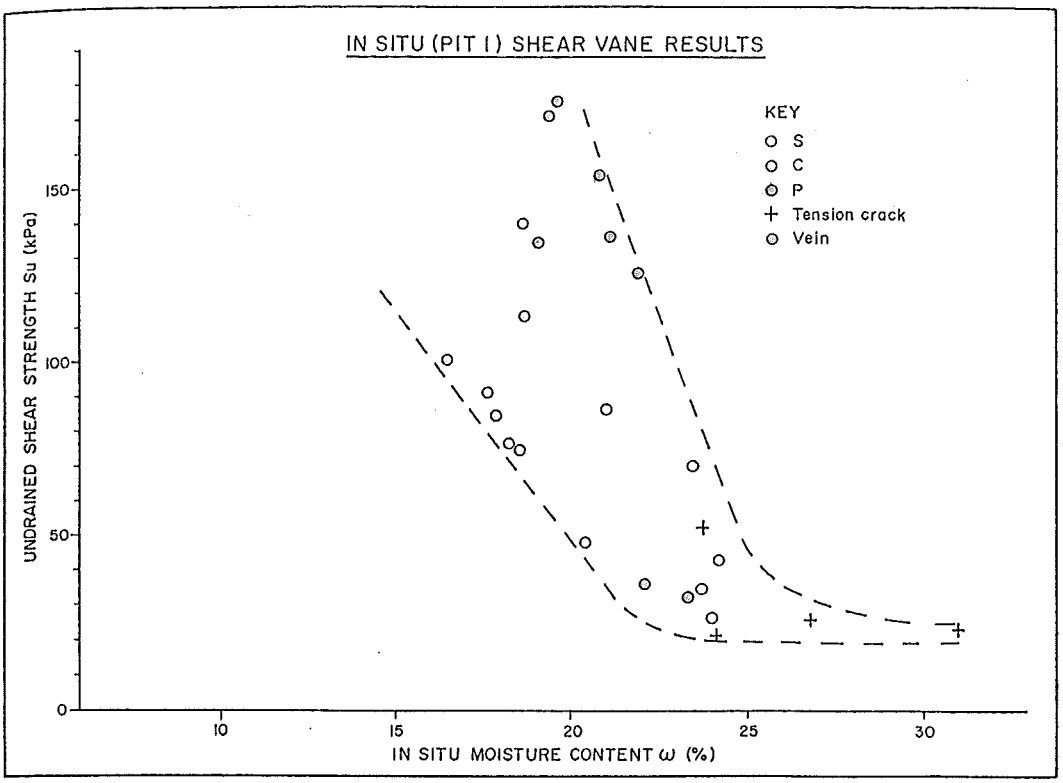

Figure 4.20 In Situ Shear Vane Results- Pit 1

4.4 Drained Strength Test

4.4.1 Introduction

Though the direct shear (shear box) apparatus is in common use by practicing engineers and researchers world wide, there is no New Zealand standard test procedure. The test procedure standardised in this work is described in appendix A4.5.1. Testing was carried out in the Engineering Geology laboratory at Canterbury University.

4.4.2 Rate Effects

The Wykeham Farrance shear box booklet provides a method for determining strain rate, which is the same as that recommended by Bishop and Henkel (1957). This predicts the time to failure allowing for 95% dissapation of pore water pressure. This method requires an estimate of the relative shear displacements at failure. A

series of tests were run at different strain rates to observe the rate effects. Five remoulded P layer samples were tested at strain rates of 1.2, 0.12, 0.012mm/minute, and two at 0.08mm/minute, with a confining stress of 400kPa. Remoulded P layer soil was used for these tests, since it had been noted in previous work in this study (section 4 day soak test) that the P layer loess absorbed and lost water more slowly than the C layer loess, suggesting a lower partially saturated permeability for P layer loess, which controls shear and water dissipation rate. This was verified from the consolidation curves (A4.5.3 and A4.5.4) that show the C layer loess achieves maximum settlement much earlier than the P layer loess. This effect was more marked with the remoulded soil than with undisturbed soil.

Results of rate effect tests (table 4.4) show an apparent increase in shear strength with a reduction in strain rate. This was unexpected as it is contrary to findings for most soils which show increasing strain rate typically increases the shear strength of soils, due to pore pressure generation, when drained conditions are not met.

Two tests conducted at a strain rate of 0.08mm/minute produced a 7.0% difference in peak shear strength and no real difference in residual strength. Assuming the 7.0% difference to be within the bounds of experimental repeatability, then the difference of 5.8% between peak shear strengths and 4.2% between residual strengths at strain rates of 0.12 and 0.012mm/minute (factor of 10 increase in strain rate) must also be considered to be within the bounds of experimental repeatability.

A strain rate of 0.08mm/minute was selected for all testing, for convenience, as there is no significant rate effect for strain rates from 0.12 and 0.012mm/minute. Shear load/displacement graphs are presented in appendix A4.5.2.

Table 4.4 Results of Rate Effects

Shear Rate (mm/minute)	Shear Strengths (kPa) (area corrected)	
	Peak	**Remoulded**
1.2	226.7	237.3
0.12	260.4	289.1
0.012	275.6	277.3
0.08	272.3	272.0
0.08	254.6	272.0

Note: The apparent increase in shear strength from peak to remoulded is due to the area corrections applied. That is, the remoulded strengths are subjected to large area corrections as they failed at large displacements. These area corrections must also be applied to the normal loads. Hence the greater remoulded shear strength when compared to the peak shear strength is due to the difference in normal stress being applied to the sample at large displacements.

4.4.3 Reversing Effects

Reversal of the shear box during the shearing stage produced results which suggest a continual increase in residual shearing load with additional shearing displacement as shown in figure 4.21. This effect was noted on all samples subjected to reversal. During shearing a portion of the sample was abraded away, getting trapped between the box halves. The abraded soil appeared to consist of predominantly coarse fraction particle size loess. It is possible that the effect noted above is due to increased friction between abraded sand and the box halves, as the amount of abraded sand increased with increasing reversals.

Figure 4.21 also shows a different shear load - displacement characteristic between the tension and compression cycles. The non-peak load-displacement curve on the compression cycle is difficult to explain, as the load cell was calibrated both in tension and compression and any effects due to particle reorientation or relocation of the shear plane should also be evident on the reversed tension cycle. This difference is possibly due to variable rotation of the principle stresses or increased friction caused by rotation of the sample and or tilting of the box halves upon reversal. Corne (1973) suggests this to be a potential source of error with reversable direct shear apparatus, which results from apparatus alignments. Although with his own results he reports the same effect and suggests it is due to shear surface irregularities. Cullen and Donald (1971) recommend that the shear box travel be modified so that it offsets an equal amount in both directions from a central start position and all the end play be removed. The shear box apparatus used in this investigation offsets only in one direction and has considerable end play.

All data used in the following sections are based on their initial shearing run and therefore reversal effects are not considered further.

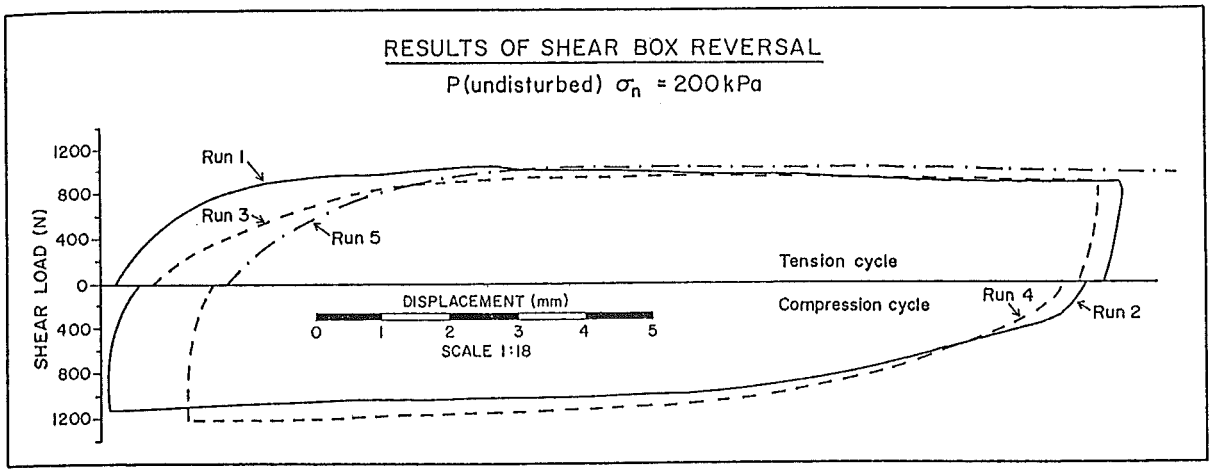

Figure 4.21 Results of Shear Box Reversals

4.4.4 Remoulded and Undisturbed Direct Shear Tests

Consolidated drained direct shear tests were conducted on loessial material for remoulded and undisturbed C and P layers, at normal stresses of 100, 200 and 400kPa (except $P_{undisturbed}$ which was tested at 50, 100 and 200kPa). It should be noted that the original intention was to test at normal stresses of 25, 50 and 100kPa, however, a mis-calculation of sample area resulted in normal stresses being four times greater than originally intended.

It is not known whether or not this is significant, but as discussed in chapter 2, the Mohr failure envelope is not neccessarily linear over all applied normal stresses. Anayi et al. (1990) show from work with Lias clay, that at normal stresses below 150kPa, the failure envelope for this clay changes from linear to a convex Mohr-Coulomb failure envelope. Although the testing stresses are considerably greater than those expected in a typical loess earth flow, the curvature of the Mohr envelope is unlikely to be significant for a low plasticity soil such as loess.

All direct shear tests on remoulded and undisturbed samples were conducted in accordance with the test procedure outlined in appendix A4.5.1.

Remoulded Tests

Remoulded loessial C and P layer material was obtained from the remoulded material used in tests in section 4.3, which had been mixed at approximately 20% moisture content and stored in air-tight plastic bags for two weeks. Shear box samples were retrieved from extruded proctor mould samples (using the 20mm high sampler shown in figure A4.2 {appendix A4.5.1}) which had been compacted in accordance with N.Z.S. 4402:1986, test 4.1.1 (standard compaction).

Table 4.5 shows the results from the tests, while figures 4.22 and 4.23 show graphs of shear stress versus normal stress for the C and P layers respectively, giving effective peak and remoulded angles of friction (ϕ') and cohesion (c'). Appendix A4.5.3 presents the raw data.

Table 4.5 Direct Shear Test Results

PARAMETER	SAMPLE											
	C	(remoulded)		P	(remoulded)		C	(undisturbed)		P	(undisturbed)	
Normal Stress (kPa)	100	200	400	100	200	400	100	200	400	50	100	200
Shear Stress (kPa)												
(Peak)	57.4	110.6	227.6	58.5	123.3	244.6	67.2	117.8	238.2	48.9	76.6	133.1
(Remoulded)	55.3	108.5	214.8	54.2	106.3	219.1	60.4	113.1	221.2	31.9	61.7	114.8
Strain failure (mm)	8.2	9.4	8.3	6.2	3.9	7.2	6.3	8.8	9.3	4.2	5.5	5.2
Moisture Content (%)												
Inital	20.8	20.7	21.3	19.3	19.5	19.2	19.7	19.7	20.4	18.3	18.2	18.3
Final	17.8	15.3	14.3	18.4	15.9	12.7	19.1	17.2	16.4	19.9	20.4	18.5
Dry Density (t/m^3)												
Initial	1.68	1.67	1.66	1.71	1.69	1.71	1.56	1.56	1.53	1.65	1.64	1.65
Final	1.80	1.90	1.95	1.79	1.87	1.91	1.80	1.83	1.88	1.72	1.74	1.68
Settlement (mm)												
Consolidation phase	2.27	2.45	2.65	2.40	2.79	3.12	1.60	2.24	3.41	2.18	1.54	1.64
Shear phase	0.27	0.33	0.35	0.14	0.28	0.32	0.77	0.72	0.61	-0.38	0.22	0.45
Void Ratio	0.49	0.41	0.38	0.50	0.43	0.28	0.51	0.47	0.44	0.56	0.55	0.51
Saturation Ratio	0.98	1.01	1.02	0.99	1.01	1.23	1.02	0.99	1.01	0.97	1.00	0.98

The results show there is no cohesion in either the C or P layer with remoulded loess. There is no significant difference between the remoulded angle of internal friction for the C and P layers. P layer loess produced a peak angle of internal friction 2° higher than the C layer loess.

Undisturbed Tests

Undisturbed bulk samples of loessial layers C and P were obtained from pit 1. Shear box samples were retrieved from the undisturbed bulk samples using the 20mm high

ring sampler shown in figure A4.2 (appendix A4.5.1). However, the P layer bulk sample partially collapsed upon the application of the sampler, which left the samples with multiple randomly orientated partings, loose soil and hence disturbed. These samples will be refered to as undisturbed for ease of grouping only. Samples were orientated such that a failure plane expected in situ would be coincident with that formed in the test samples. After attaining the peak strength, samples were sheared further to reach the remoulded state.

Table 4.5 shows the results from the tests, while figures 4.24 and 4.25 show graphs of shear stress versus normal stress for the C and P layers respectively, giving effective peak and remoulded angles of internal friction (ϕ') and effective cohesion (c'). Appendix A4.5.4 presents the raw data.

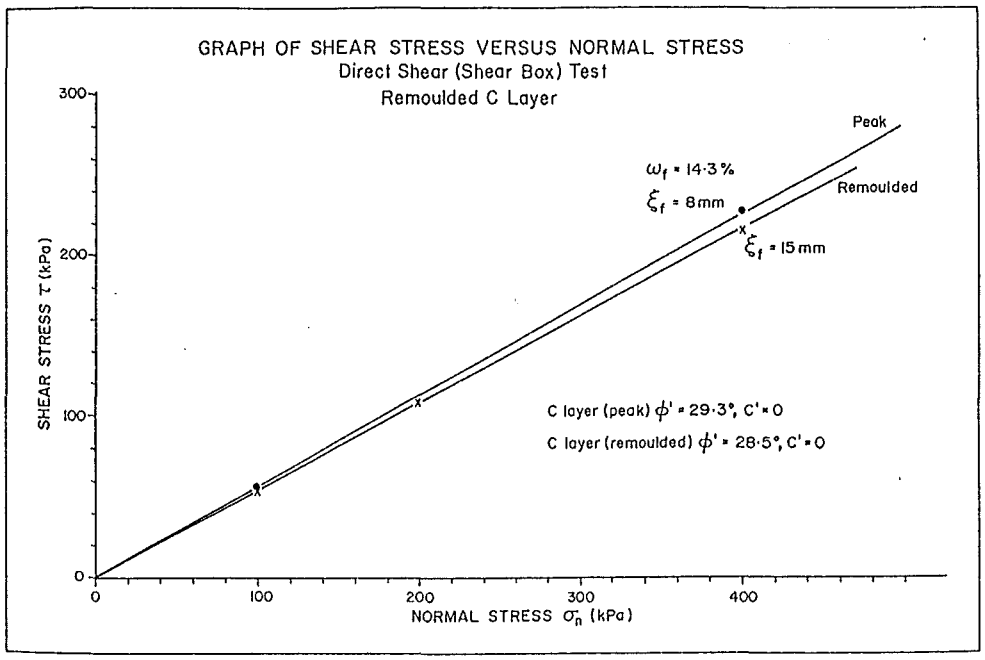

Figure 4.22 Direct Shear Results- remoulded C layer

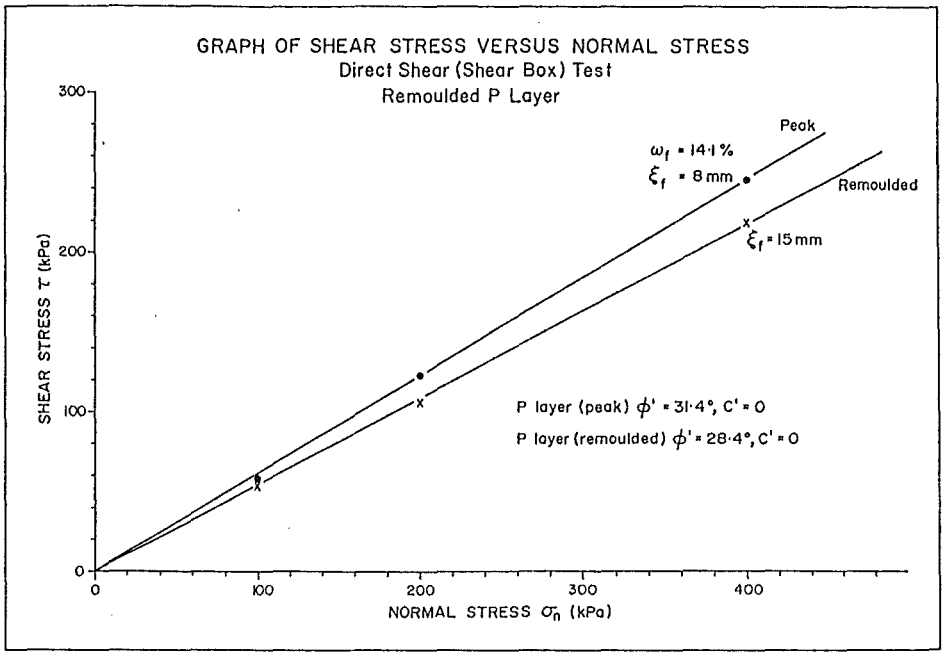

Figure 4.23 Direct Shear Results- remoulded P layer

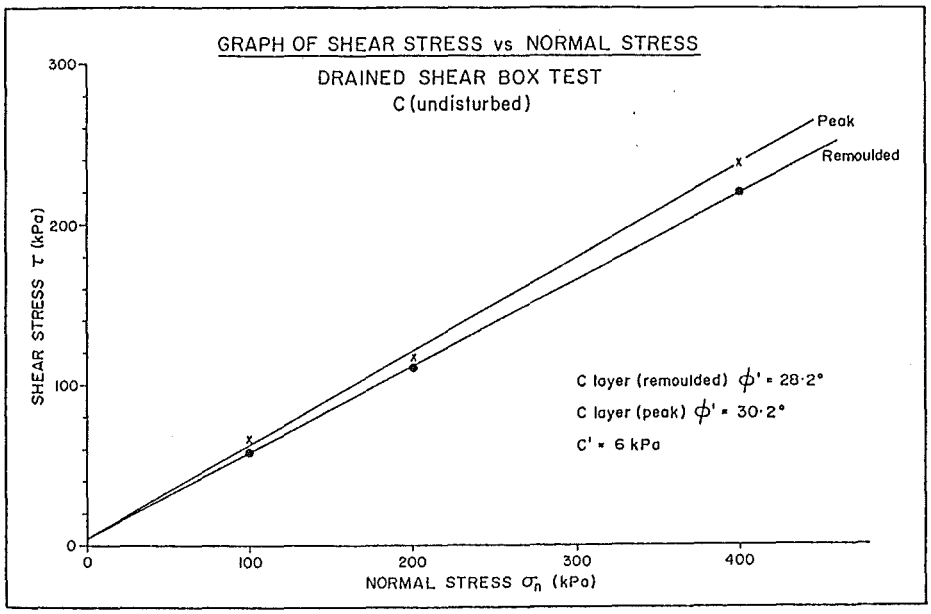

Figure 4.24 Direct Shear Results- undisturbed C layer

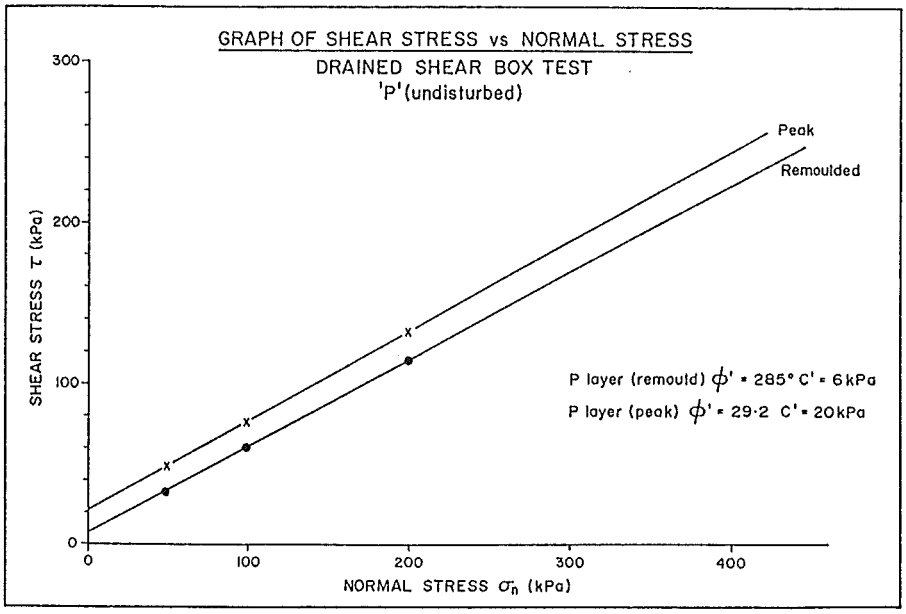

Figure 4.25 Direct Shear Results- undisturbed P layer

Figure 4.24 shows that cohesion (c' = 6kPa) was the same for peak and remoulded C layer samples while the remoulded angle of friction at large displacement (σ'_R = 28.2°) was 2° lower than the peak angle of internal friction (σ'_P = 30.2°). Figure 4.25 shows that cohesion differed by 14kPa between the peak cohesion (c'_P = 20kPa) and the remoulded cohesion (c'_R = 6kPa). There is only a small difference (0.7°) between the remoulded angle of friction (σ'_R = 28.5°) and the peak angle of friction (σ'_P = 29.2°), and the remoulded value is consistent with that observed in tests where soil was initially in the remoulded state before shearing.

4.5 Summary

The following trends can be drawn from the laboratory investigations completed in this chapter:

1) There is a difference between particle size distribution in the C and P layers investigated.
2) Mechanical remoulding affects the particle size distribution in the C and P layers.
3) Atterberg limits vary between the C and P layers.

4) There is no obvious difference in specific gravity between C and P layer loess.
5) For both C and P layer loess in a partially saturated state there is an inverse trend between undrained shear strength and moisture content.
6) There is a significant scatter in dry density contours at moisture content below their respective (contour) optimum moisture content for both C and P layer loess.
7) Four day soak test shows a significant difference in the ability to absorb water by the C and P layers.
8) There is little difference between remoulded angle of internal friction (0.3°) between C and P layer loess in the undisturbed and remoulded states. The remoulded angle of friction is about 28.4°.
9) There is no effective cohesion for remoulded samples of C and P layer loess.
10) Undisturbed C layer loess showed no significant drop in cohesion from peak to and remoulded strengths. This cohesion was equal to that for undisturbed P layer material at the remoulded state. Undisturbed P layer material at peak strength possesses the highest cohesion.
11) All peak angles of internal friction are within 2.2° for the C and P layer loess in the undisturbed and remoulded states.

Chapter 5
Analysis of Strength Behaviour

5.1 Introduction

In chapter 4 it is shown that undrained shear strength is sensitive to dry density and moisture content. Milovic (1988) reported similar trends with loessial soils in Yugoslavia, while Evans and Bell (1981), Glassey (1986), Tehrani (1988) and McDowell (1989) all reported an inverse trend between undrained shear strength and moisture content. These are discussed in chapter 2.

Probably the most extensive general study of the strength behaviour of partially saturated compacted clays was that conducted by Seed and Chan (1960 a and b), who reported a relationship among moisture content, dry density, undrained shear strength and CBR values for partially saturated clays. They found a good correlation among dry density, moisture content, degree of saturation, and CBR values or undrained shear strength for partially saturated clays.

Blakeley (1965) reported results of CBR tests on 'Heathcote loess', as discussed in chapter 2. Once again the most significant finding was the correlation among dry density, moisture content, degree of saturation and CBR values for partially saturated loessial soil.

This chapter discusses in detail the results of the laboratory strength testing presented in chapter 4 and considers the implications with respect to these earlier studies.

5.2 Undrained Strength Tests

5.2.1 Remoulded Samples

a) Unconfined Compression Testing

Undrained shear strength, moisture content and dry density results from unconfined compression testing of remoulded C and P layer loess have been presented on plots of dry density versus moisture content. Strengths measured in each test are noted (refer figure 5.1 and 5.2 respectively).

In both figures contours of undrained strength have been constructed by eye. It is apparent that there is considerable scatter in the undrained shear strength data, particularly at low dry density and moisture content. This is discussed in section 4.3.2.

However the plots do show trends among the three determined soil parameters. Results for remoulded C layer loess (figure 5.1) show that undrained shear strength increases approximately linearly with increasing dry density and reducing moisture content. This suggests that undrained shear strength is not strongly affected by the degree of saturation, which is reflected on the plot by the strength contours being mutually subparallel, and nearly perpendicular to the air-void curves.

Testing of remoulded P layer loess (figure 5.2) show that undrained shear strength increases significantly with increasing dry density, but only show a minor reduction in undrained shear strength associated with increasing moisture content. This is reflected on the plot by the near linearity of the strength contours, which are subparallel to the horizontal (moisture content) axis.

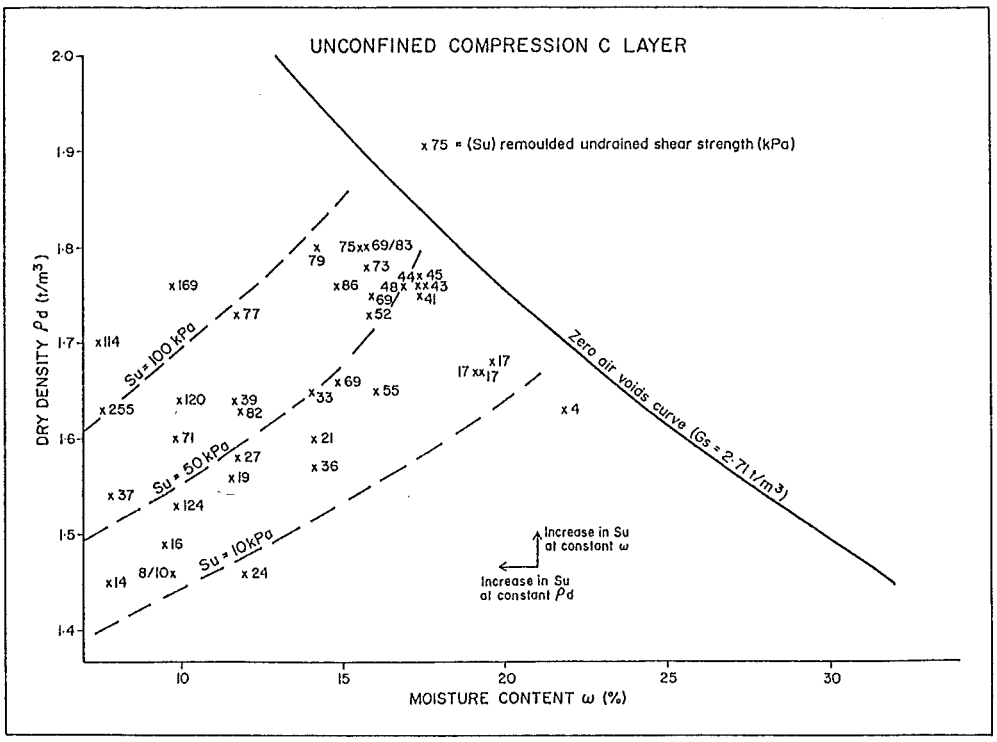

Figure 5.1 Unconfined Compression Test Results- remoulded C layer

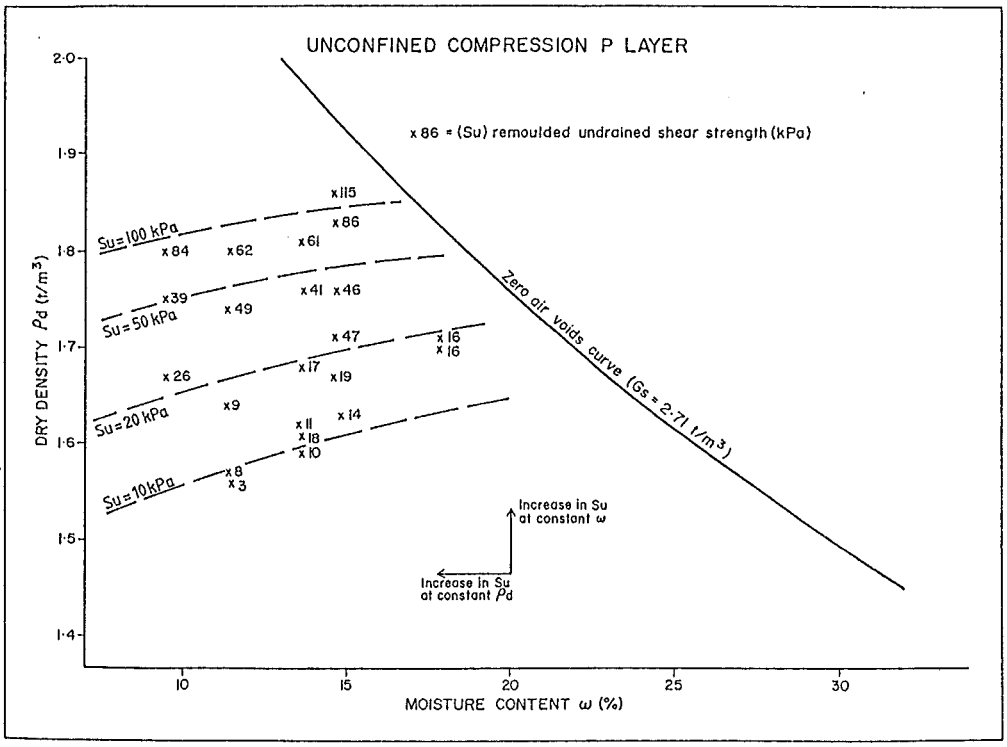

Figure 5.2 Unconfined Compression Test Results- remoulded P layer

Comparison of the strength contours obtained for the C and P layer loess shows that at similar low dry densities and moisture contents, the C layer loess produces significantly higher undrained shear strengths than the P layer loess. For example, at 10% moisture content and dry density of 1.55t/m^3, the C layer and P layer strengths are about 50kPa and 10kPa respectively. The C layer loess, therefore has a shear strength approximately 5 times higher than P layer loess. As both soils approach saturation their respective strengths are similar at the same moisture contents and dry densities. This may indicate that there is little difference in undrained shear strength between the two loess layers close to saturation. However, in light of the errors (section 4.3.2) associated with the unconfined compression testing at low degrees of saturation (which appear to be significant), these results should be treated with some caution.

b) Cure Time Effects

In chapter 4 graphs of curing sensitivity versus log(cure time) are presented to highlight the effects of curing time on strength of remoulded loessial soils. Both figure 4.9 and 4.10 show a concentration of data points above and below a curing sensitivity of 1. By ignoring the small number of extreme data points (attributing these to experimental error due to differential compaction, sensitivity <0.8 and >1.2) and averaging the remainder data points, a curing trend was approximated.

Both remoulded C and P layer loess show an average 3% increase in undrained shear strength after 10 days curing. Remoulded C layer loess shows an average increase of 12% in undrained shear strength after 100 days curing, while remoulded P layer loess shows an average increase of 16% for the same curing period. Once again, the potential error observed with unconfined compression testing means these results should be treated with caution.

c) Four Day Soak Test

The original intention in conducting four day soak tests was to assess the effects of soaking on dry density, moisture content and undrained shear strength. However insufficient tests were conducted to assess general trends associated with soaking for undrained shear strength.

The results of the four day soak tests are presented in figure 4.15. These show a significant difference in the moisture absorption behaviour between remoulded C and P layer loess. The plot suggests that remoulded C layer loess has a significantly higher infiltration rate than remoulded P layer loess. Particle size variations (table 4.1) show that remoulded C layer loess is a (relatively) finer soil than P layer loess, and hence would be expected to have a lower permeability value.

The reason for the infiltration rate difference in remoulded samples, and the existence or otherwise of this phenomenon in undisturbed samples, is beyond the scope of this thesis. However, the result is significant and requires further research.

d) Vane Shear Testing

Results from vane shear testing on remoulded C and P layer loess in chapter 4 have been plotted in the same manner as the unconfined compression results above (refer fgures 5.3 and 5.4).

Both figure 5.3 (remoulded C layer loess) and figure 5.4 (remoulded P layer loess) indicate less experimental scatter of undrained strength from the vane shear test than do unconfined compression test results shown in figures 5.1 and 5.2.

Strength contours constructed in figures 5.3 and 5.4 follow similar trends, but actual values of strength differ. In both plots the strength contours are curved, indicating a non-linear relationship among dry density, moisture content and the degree of saturation. At low moisture contents and dry densities, strength contours are roughly parallel, and close to perpendicular to the air-void curves, hence undrained shear strength is nearly independent of the degree of saturation.

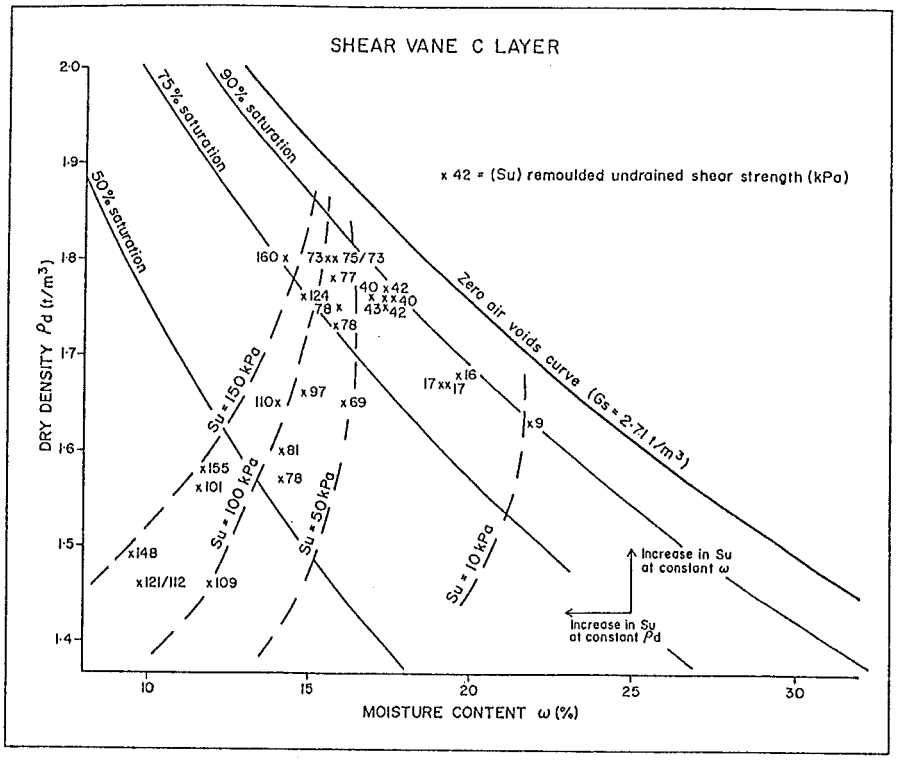

Figure 5.3 Vane Shear Test Results- remoulded C layer

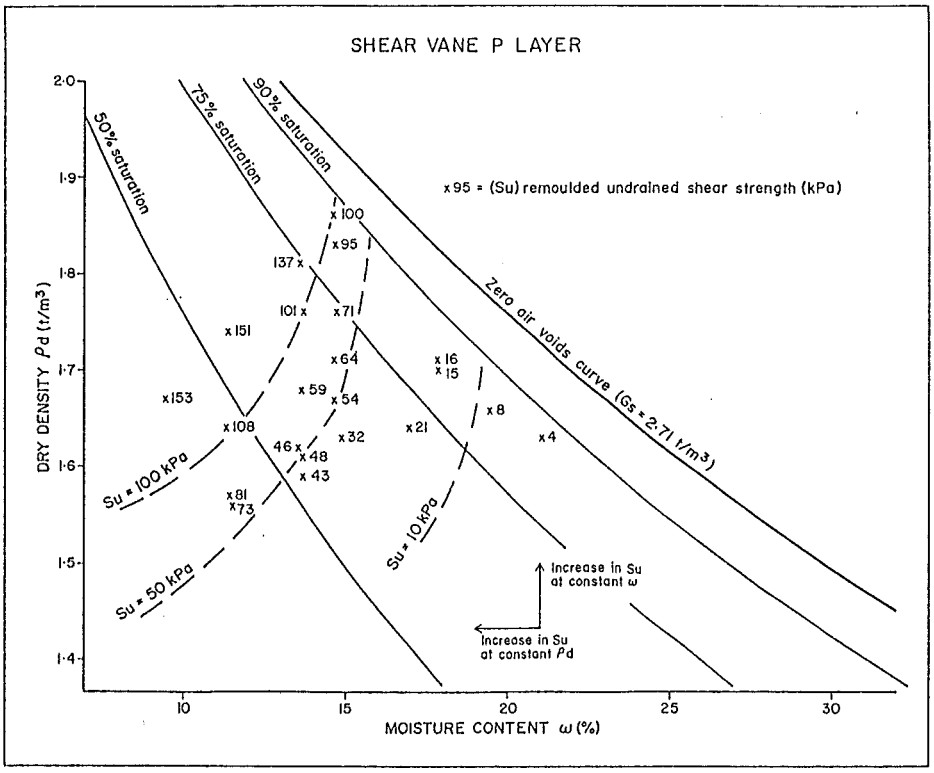

Figure 5.4 Vane Shear Test Results- remoulded P layer

Along a constant strength contour, as dry densities and moisture content increases the strength contours curve upwards. The influence of dry density decreases whereas the influence of moisture content increases.

Where the strength contours are perpendicular to the air-void curves, the degree of saturation has no influence on undrained shear strength. As the strength contours deviate from this perpendicularity, the influence of the degree of saturation upon undrained shear strength increases.

Both figures 5.3 and 5.4 show similar trends. Dry density and moisture content have similar influences on undrained shear strength at low dry densities and moisture contents. Undrained shear strength increases with increasing dry density and reducing moisture content. At higher dry densities and moisture contents approaching saturation, strength contours on each plot coverge (ignoring s_u = 10kPa contour which is based on limited data), and moisture content has a greater influence on undrained shear strength than does dry density.

To aid the interpretation of figures 5.3 and 5.4, a separate idealised plot of undrained vane shear strength versus moisture content with contours of constant dry density (figure 5.5) is presented. This figure is calculated from the smoothed strength contours presented in figures 5.3 and 5.4. Several major trends are apparent.

The contours of constant dry density in figure 5.5 show a near linear inverse relationship between vane shear strength and increasing moisture content below 16% moisture content. At higher moisture contents the dry density contours are curved. The rate of strength reduction with increasing moisture content decreases markedly.

The vane shear strength of remoulded C layer loess is significantly higher than that of remoulded P layer loess, at the same dry density. At all moisture contents the ratio of remoulded C layer strength to remoulded P layer strength is close to 2:1. It is useful to examine, for soil at constant dry density, the rate of strength reduction with increasing moisture content, since under wetting conditions in the field this will show which soil suffers most rapid strength reduction.

The rate of strength change with moisture content in the near linear portion of these contours may be determined uniquely as a function of the dry density and the soil type. Figure 5.5 indicates that at higher dry density the rate of strength reduction with increase in moisture content increases. Similarly, remoulded C layer loess at the same dry density as remoulded P layer loess, has a greater rate of strength reduction with increasing moisture content.

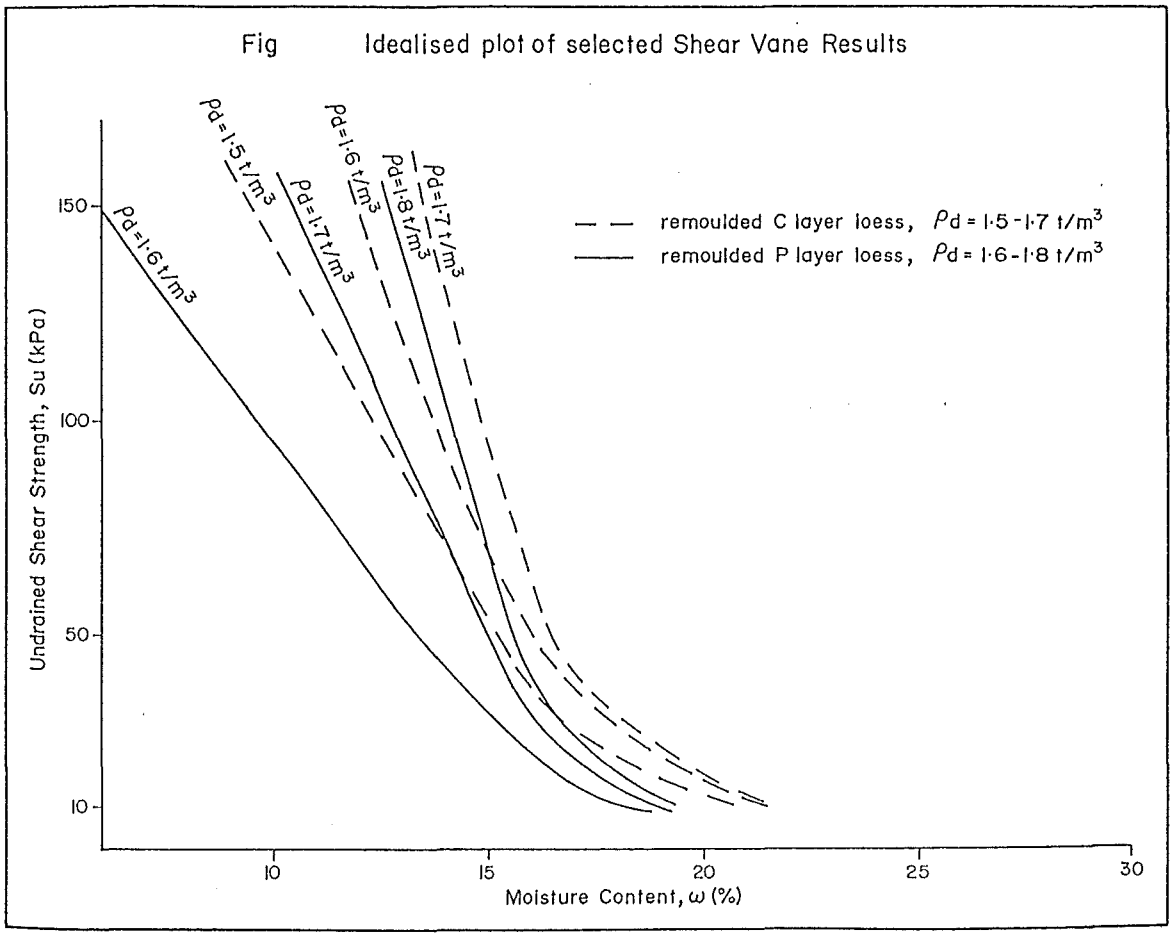

Figure 5.5 Idealised Plot of Undrained Shear Strength and Moisture Content with selected Dry Density Contours- C & P layer

5.2.2 In Situ Vane Shear Testing

As no detailed density determination was conducted in association with the in situ vane shear testing, averaged density values obtained from the tube sampling of pit 1 are used in determining strength trends.

Assuming an average dry density (table 4.3) of 1.75t/m^3 for the C layer and 1.70t/m^3 for the P layer loess and using a specific gravity of 2.71, the range of moisture contents encounted during vane shear testing (figure 4.20) gives a range in the degree of saturation of 81-101% for the C layer and 89-100% for the P layer loess. This is likely to be realistic and confirms the validity of the assumed dry density values.

The undrained shear strength of the C layer falls from 140kPa to 48kPa as the degree of saturation increases from 81% to 101%, while the undrained shear strength of the P layer falls from 175kPa to 125kPa as the degree of saturation increases from 89% to 100%. Both in situ C and P layer loess show a decrease in undrained shear strength with increasing degree of saturation, even at high degrees of saturation.

In situ vane shear testing (figure 4.20) shows that the P layer loess has higher vane shear strength than does C layer loess at similar moisture contents. For example at 20% moisture content, C layer loess has an undrained shear strength of 55kPa (S=98.9%) while P layer loess has an undrained shear strength of 170kPa (S=91.2%), a difference of 115kPa. However P layer loess at the same degree of saturation as C layer loess (S=98.8%) has an undrained shear strength of 126kPa, a difference of 71kPa.

Figure 5.6 also presents the idealised contours of laboratory determined remoulded undrained shear strengths at similar constant dry densities to the in situ soils, for comparison with the peak undrained shear strengths measured in situ. As previously discussed, it can be seen from figure 5.6 that the C layer loess has considerably higher remoulded strengths than P layer loess, at similar degrees of saturation. However peak strength results do not show this trend. In fact peak C layer strengths

in situ are considerably lower than peak P layer strengths.

Specific interpretation of this plot is difficult, but the obvious trend presented on the graph is that P layer loess is considerably more sensitive to remoulding than the C layer loess. The most probable cause of this phenomenon is structural collapse of the more porous P layer upon remoulding. This dramatic loss of strength with porous loess is noted in international literature concerned with the structural collapse of loess.

Lutenegger and Hallberg (1988) suggested that loess has the potential to structurally collapse if the loess can attain in situ moisture contents equal to, or greater than, its liquid limit. The liquid limit for the P layer (LL = 22°) is less than that in the other loess layers and comparable to the in situ saturation moisture content (w=22°). Structural collapse of the P layer loess upon remoulding is a very likely cause of the recorded high sensitivity.

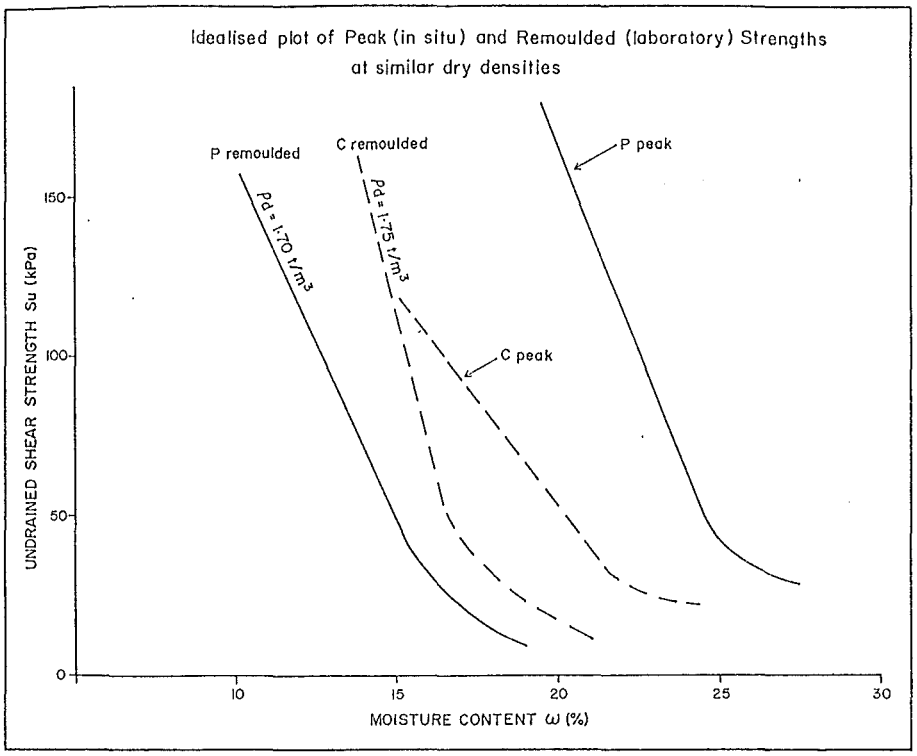

Figure 5.6 Idealised Plot of Selected Laboratory and In Situ Undrained Shear Strength Results

In section 4.2 it is suggested that mechanical remoulding increased the percentage of clay size particles in the C layer loess by 19% and the P layer loess by 42%. The increase may subject the remoulded results to introduced errors which are difficult to quantify. The exact determination of the sensitivity of the two loess layers is therefore impossible. It is not known from this study whether remoulding in situ would produce an equivalent increase in clay size particles.

5.3 Drained Strength Tests

The results obtained from direct shear testing in chapter 4 on both remoulded and undisturbed C and P layer loess are tabulated (table 5.1) for comparison.

Table 5.1 Results of Drained Direct Shear Results

Sample	Strength	Cohesion	Angle of friction
Remoulded C layer	Peak	0	29.3°
	Remoulded	0	28.5°
Remoulded P layer	Peak	0	31.4°
	Remoulded	0	28.4°
Undisturbed C layer	Peak	6kPa	30.2°
	Remoulded	6kPa	28.2°
Undisturbed P layer	Peak	20kPa	29.2°
	Remoulded	6kPa	28.5°

As recorded previously in chapter 4, the remoulded angle of friction is constant (ϕ' = 28.2° to 28.5°) for remoulded and undisturbed C and P layer loess. It should be noted that peak angles of friction were also recorded for samples of remoulded C and P layer loess despite the thorough remoulding before testing. This behaviour was probably due to either:

1) insufficient pore pressure equilibration in the samples prior to formation of the failure plane; or
2) dilation prior to reaching the constant shearing volume state due to the coarse silt and fine sand fraction (this accounts for > 50% of the particle size distribution, see appendix A4.1).

Dilation is the most probable explanation as no significant rate effects were encounted during testing (section 4.4.2). Cohesion evident in undisturbed samples is also probably due to dilation effects, as the differences between the peak internal angles of friction are similar.

Skempton (1985) reported that residual strength is dependent almost entirely on sliding friction of the clay particles. For fine particle soils with a clay fraction less than approximately 25%, frictional strength is controlled largely by the sand and silt particles. Skempton showed that silty and sandy clays with low clay fractions (<25%) exhibit the classical "critical state" type behaviour in which the frictional strength is seldom less than the normally consolidated or remoulded value, even at large displacements. The expected little difference in peak and remoulded angles of friction was observed in the drained test results.

No remoulded samples exhibited cohesion, while undisturbed samples had a minimum cohesion of 6kPa, confirming that with sufficient mechanical remoulding, cohesion can be reduced to zero, but this was not fully achieved in the direct shear tests. This suggests that both C and P layer loess have true cohesion due to some combination of clay mineral electrostatic attractions and cementation which is broken down during mechanical remoulding. The nominally undisturbed P layer loess (somewhat disturbed, refer section 4.4.4) exhibited a peak cohesion of 20kPa. As the P layer samples were all somewhat disturbed, this cohesion value can only represent a minimum value. The drained testing was limited and a more extensive investigation is desirable to check reproducability and ensure a greater degree of confidence in the results.

5.4 Discussion

5.4.1 Summary of Results

Comparison between undrained shear strength determined by unconfined compression and vane shear testing, shows vane shear testing produces less experimental scatter and therefore more reproducible results.

Results of in situ (peak strength) and laboratory (remoulded strength) vane shear testing on C and P layer loess show the following trends.

1) Both C and P layer loess in a partially saturated state show a reduction in undrained strength with increasing degree of saturation.

2) The undrained strength of partially saturated remoulded C and P layer loess can be defined by any two of dry density, moisture content and degree of saturation.
3) Undisturbed P layer loess has significantly higher peak undrained strength than does C layer loess at similar degrees of saturation.
4) Remoulded C layer loess has significantly higher remoulded undrained strength than does remoulded P layer loess at similar degrees of saturation.
5) P layer loess is significantly more sensitive to remoulding than C layer loess.

The behavioural difference of remoulded C and P layer loess in a partially saturated state is significant. Remoulded C layer loess has about twice the undrained shear strength of P layer loess at a similar degree of saturation. The infiltration rate in remoulded C layer loess appears considerably greater than the infiltration rate in remoulded P layer loess. Both these behaviourial differences are probably due to different capillary water surface tension responses, resulting from the respective difference in particle size distributions between C and P layer loess.

Drained testing shows there is no significant difference in the angle of friction ($\phi' =$ 28.4°) for C and P layer loess. This suggests the internal angle of friction is controlled by the fine sand and coarse silt sized particles. This is consistent with the particle size distribution curves (appendix A4.1) which show these fractions to be similar for the two loess layers and account for ≥50% of the particle size distributions. Since the clay contents for both layers are less than 25%, it is likely that strength decrease to a residual state at large shear displacements will be very slight. However this has not been investigated in this study.

The sensitivity observed during undrained testing is less evident in drained testing. This can be explained by the fact that no truly undisturbed P layer sample was tested, although the disturbed P layer sample (c'=20kPa) tested did produce significantly greater cohesion than the mechanically remoulded P layer sample (c'=0).

5.4.2 Significance of Results

Effective Stress Analysis versus Total Stress Analysis

McDowell (1989) reported total stress shear strength parameters of $\phi_u \approx 30°$ and c_u varying from 0 to 180kPa, with moisture content decreasing from 19 to 8% (chapter 2). This implies that loess at 19% moisture content and at the ground surface (zero normal stress) would have zero shear strength. Clearly this is not the case in the field.

By using the effective stress relationship for partially saturated soils (equation 2.1, chapter 2):

$$\sigma' = \sigma - u_a + X(u_a - u_w)$$

and calculating the effective stress at the ground surface, where the total normal stress $\sigma = 0$ and pore air pressure $u_a = 0$, the effective stress relationship can be rewritten as:

$$\sigma' = -Xu_w$$

For example, if it is assumed that the maximum capillary rise in a 10 meter thick loessial soil deposit is coincident with the ground surface (as suggested by Cegla (1969)), then the pore water pressure (u_w) is negative and equal to -98kPa ($\gamma_w h$, where γ_w is the unit weight of water and h is the capillary head). The experimentally determined coefficient X is related to the degree of saturation and is approximately comparable in magnitude (Bishop and Henkel, 1957). Assuming a degree of saturation of 70%, typical of P layer loess at 19% moisture content, then X is likely to be about 0.7.

The effective stress at the ground surface is then:

$$\sigma' = - Xu_w$$
$$= -(0.7)(-98)$$
$$= 68.6\text{kPa}$$

Ignoring the true cohesion recorded for loess and using $\phi' = 28.4°$, the apparent cohesion (c_a) component at the surface caused by pore water tension alone can be considered equal to the effective shear strength at the surface. Thus:

$$c_a = \tau = \sigma' \tan\phi' = 68.6 \tan 28.4° = 37\text{kPa}$$

Including the minimum true cohesion of P layer loess measured in this study, $c' =$ 20kPa, the total cohesion is at least 57kPa in freshly exposed P layer loess. This is considerably greater than the zero shear strength implied by total stress strength parameters reported for loess with moisture content 19% at the ground surface.

It can be seen from this analysis that in partially saturated loess, even where total stresses are negligible, high strengths can occur which can be attributed to effective stress friction effects and true cohesion.

Implications For Likely Location Of Landslide Failure Surface

It is suggested by the drained direct shear tests carried out to date that P layer loess develops considerably higher true cohesion than C layer loess (i.e. 20kPa compared to 6kPa). Since the angles of friction are the same for each ($\phi' = 28.4°$), failure is most likely to occur in the C layer. The undrained tests support this finding, however this applies only if the P layer loess is undisturbed. In addition typical hydrogeological factors must also be considered. The formation of a perched water table above and within the C layer reduces the apparent cohesion in the C layer by increasing the moisture content to give it a positive pore water pressure and reduce the effective stress. This confirms that, in undisturbed loess, a failure surface is more likely to form in the C layer than in the P layer loess.

Chapter 6

Slope Stability

6.1 Introduction

In chapter 3 it is shown that in the particular loess landslide studied, topsoil blocks were the only coherent failed mass. Failure deposits of the C layer and lower S layer loess apparently involved fluidised flow. Although no readily apparent shear failure surface was identified at the site, shear failure by translational sliding is undoubtedly part of the initial failure process. Mathematical models of slope movement assume that slope failure occurs by simple shear sliding along a clearly defined failure surface.

Slope stability assessment of the failed ground investigated at Allandale, based on the site investigation and computer back analysis, is described in this chapter.

6.2 Computer Modelling

6.2.1 Introduction

The shallow translational slide investigated in this study is most suited to analysis by slope stability modelling which considers planar failure surfaces. Both the infinite slope equation and an adapted version of non-circular failure surface analysis derived by Sarma (1979) have been used. Both can be used to model planar failure and are limit equilibrium methods. Considering these briefly in more detail:

1) Infinite Slope Equation

The term *infinite slope* refers to a uniform slope, of sufficiently large extent that a typical element can be considered representative of the slope as a

whole. Irregularities at the toe and the crest of the slide are ignored. The soil properties and pore water pressures at any given distance below the ground surface are assumed constant.

When the failure surface is parallel to the ground surface, the equation for factor of safety against sliding is:

$$FS = \frac{c'}{\rho g h \sin\delta \cos\delta} + \frac{\rho - \rho_w}{\rho} \frac{\tan\phi'}{\tan\delta}$$

where
- FS = Factor of Safety
- c' = cohesion
- ϕ' = angle of friction
- δ = slope angle
- ρ = bulk density of soil
- ρ_w = density of water

2) Sarma (1979)

Hoek (1983) formulated a general two-dimensional slope stability computer program based on the slope stability theory of Sarma (1979). The computer program used here (supplied by Soils and Foundations Ltd.) allows for the stability determination of complex failure profiles with circular, non-circular, or planar sliding surfaces or or any combination of these. Hence the program can consider end effects on a block failing by translational sliding. These end effects are not considered by the infinite slope equation. For comparison, both the Sarma and the infinite slope analysis have been used in the following computer modelling and back analysis.

No failure surface was identified at the site. The only input parameter known is therefore the angle of the hillslope. For a drained analysis this means the failure block geometry, the piezometric surface, the angle of friction and the cohesion are potentially all variables. A preliminary parameter study was carried out to determine which of these had most effect when varied. Those to which the analysis results were insensitive were held constant in later analysis.

6.2.2 Determination of the Failure Geometry

Failure Surface

Different failure wedges (figure 6.1) were modelled to determine the effect of ß, the down slope exit failure surface angle relative to the slope angle. Values of ß from 5° to 30° were investigated, for maximum depths to the failure surface of 0.50, 0.75, 1.00, 1.25 and 1.50m. In addition, variable length blocks (2, 4 and 40m long) of uniform depth attached to the failure wedges were also modelled. (The above variables were only selected to observe trends.) The piezometric surface (ground level) and the strength parameters (c'=6kPa; ϕ'=28.4°) were kept constant through out this parameter study. Cross-sections of the modelled failure geometries are presented under the input data for each case in appendix 5.

The factors of safety for each case have been plotted against relative failure surface angle ß in figures 6.2 to 6.6, for failure surface depths of 0.50, 0.75, 1.00, 1.25 and 1.50m respectively. For all failure depths, and for all realistic slide lengths the factor of safety is independent of the exit wedge angle (ß). The factor of safety is lower for deeper failure surfaces.

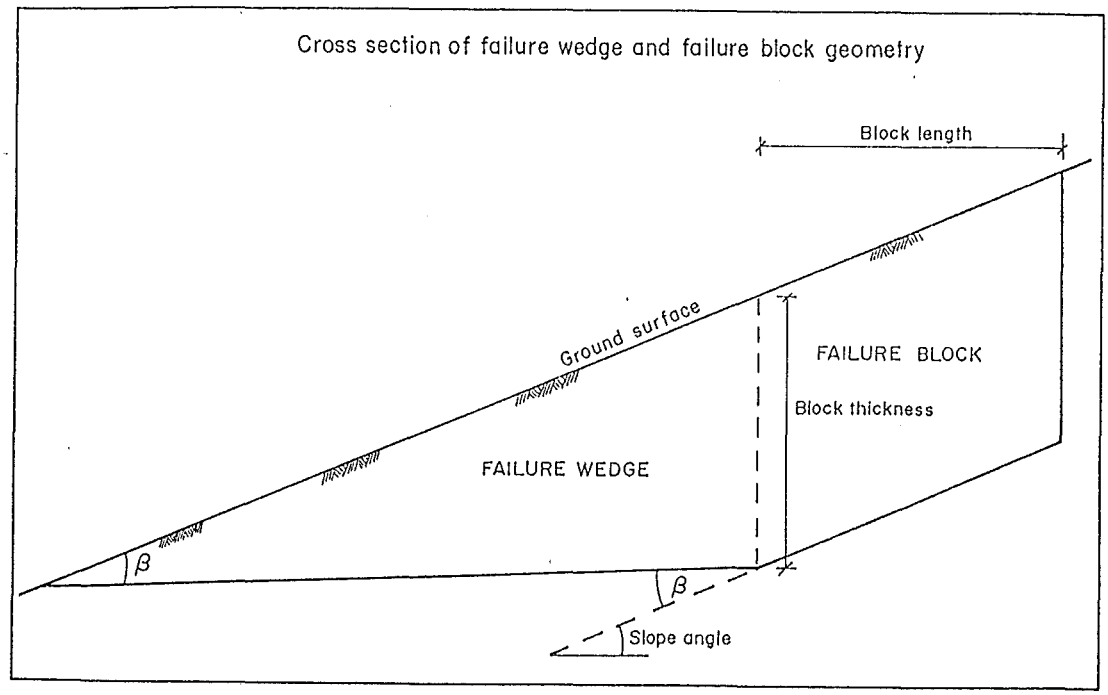

Figure 6.1 Cross-Section of Modelled Failure Wedge and Block

Comparison with Infinite Slope Equation

Factors of safety obtained from the infinite slope equation and from modelling a semi-infinite (100m long) slope using the Sarma computer analysis are compared in figure 6.7. The factor of safety decreases with increasing depth in both analyses. The infinite slope theory predicts a higher factor of safety for the same block thickness and is therefore slightly less conservative.

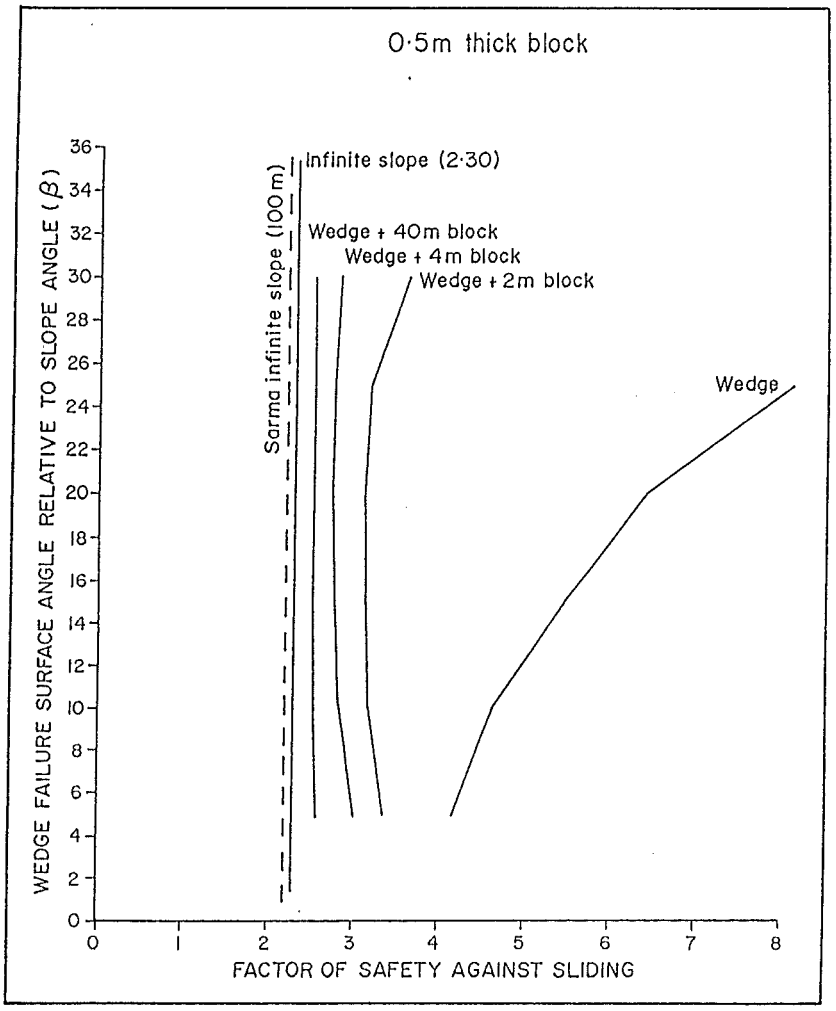

Figure 6.2 Results of Computer Modelled Failure Geometry- 0.5m thick block

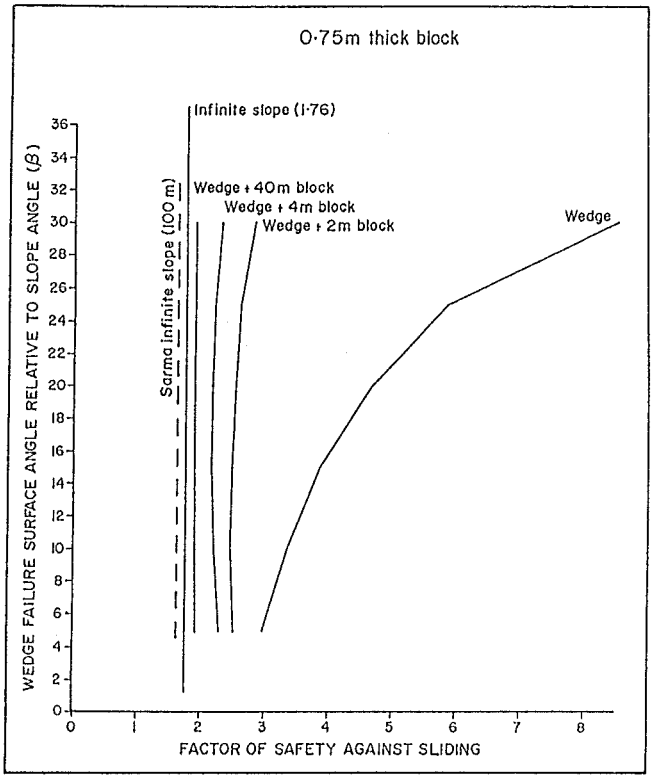

Figure 6.3 Results of Computer Modelled Failure Geometry- 0.75m thick block

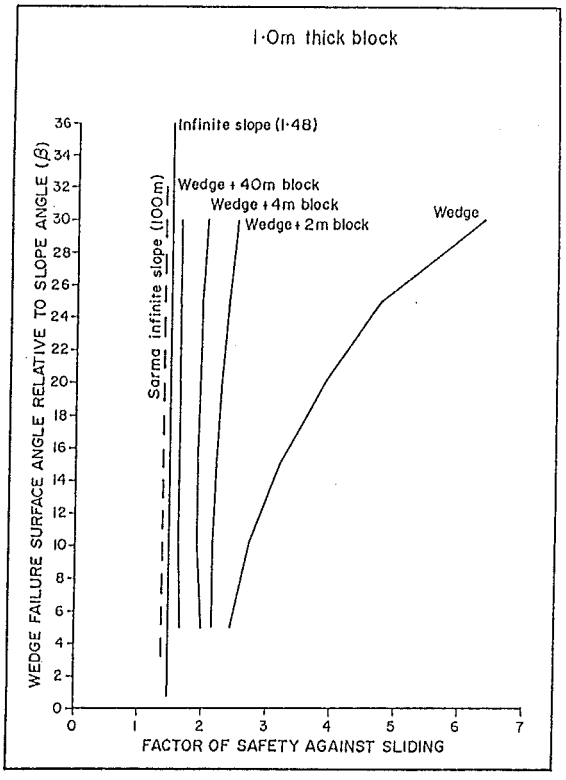

Figure 6.4 Results of Computer Modelled Failure Geometry- 1.0m thick block

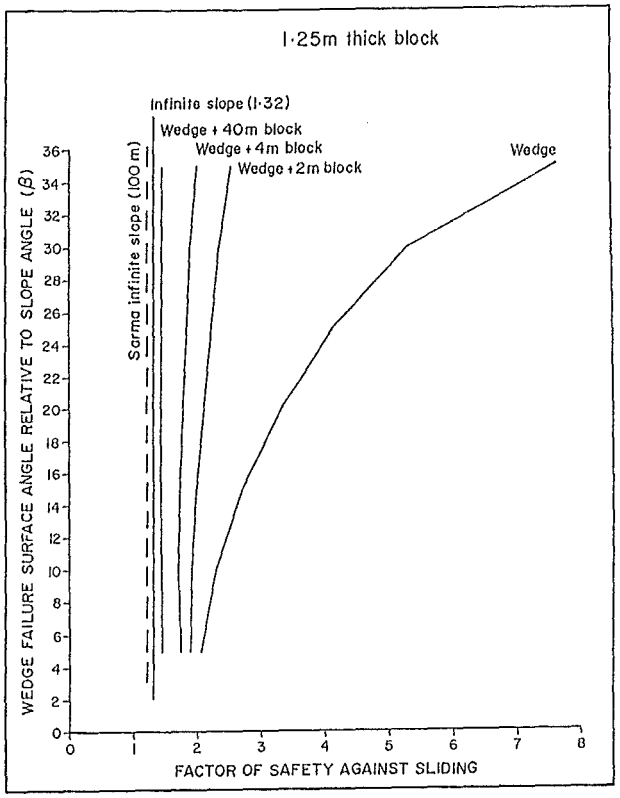

Figure 6.5 Results of Computer Modelled Failure Geometry- 1.25m thick block

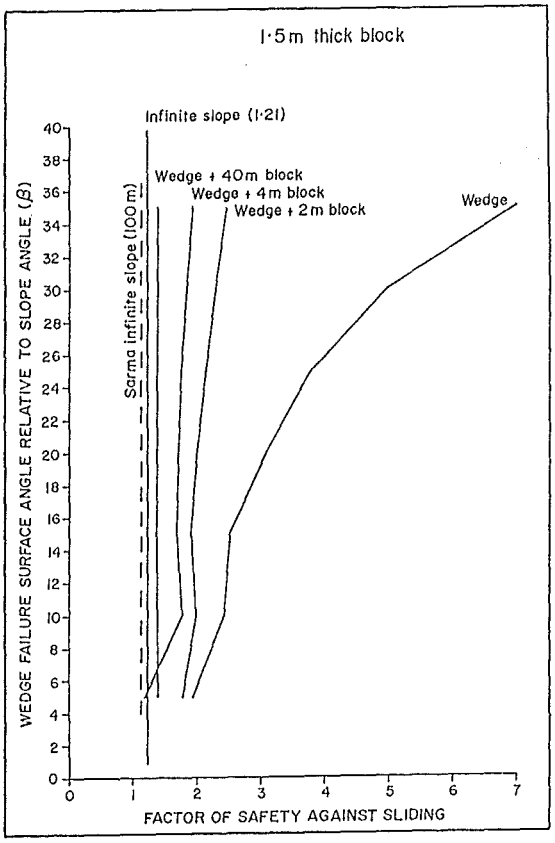

Figure 6.6 Results of Computer Modelled Failure Geometry- 1.5m thick block

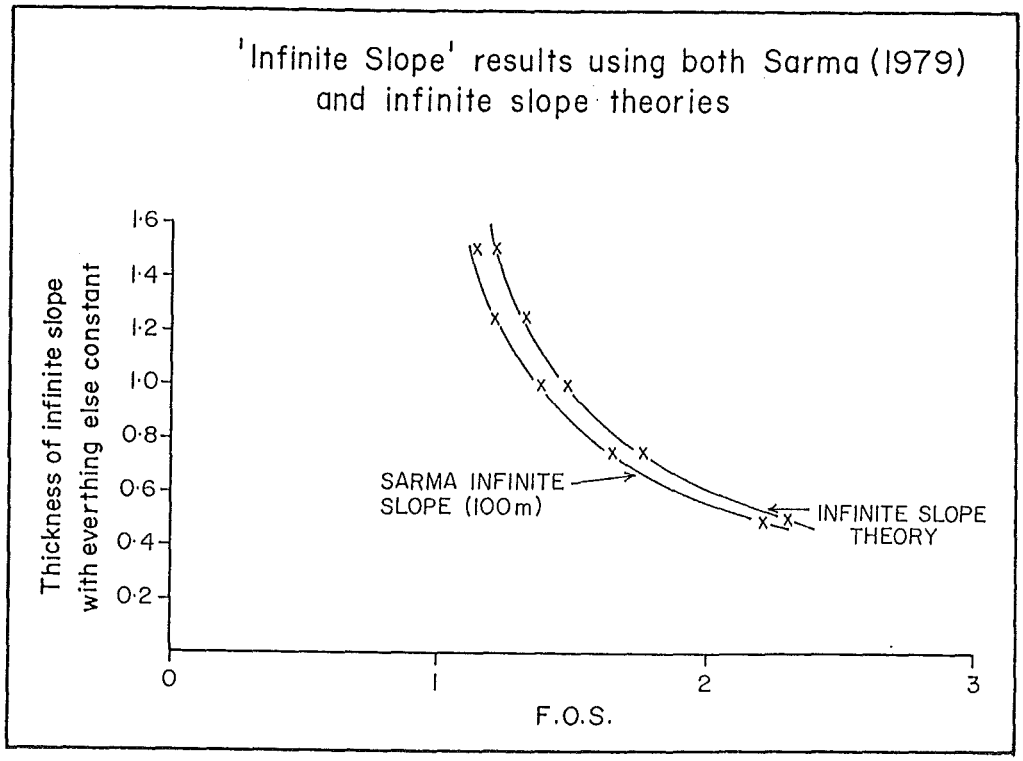

Figure 6.7 Comparison of Sarma (1979) and Infinite Slope Theories

Synthesis

Three general conclusions can be drawn from this parameter study:

1) The effect of varying the assumed relative exit angle, ß, is minor for slide lengths greater than 2 meters and insignificant for lengths greater than about 5 - 10m.
2) The factor of safety is lower for deeper failure surfaces.
3) The factor of safety decreases for longer slides if end wedges are included, but infinite slope theory predicts slightly higher factors of safety than the finite slide model used.

6.2.3 Back Analysis

Computer modelling demonstrates that in a homogeneous soil deeper seated failures are more likely than shallow failures. However, the site investigation (chapter 3) shows this is not the case in the field as only shallow 'turfmat slides' and a deeper translational slide were observed. Soil horizons are therefore the controlling factor. This is further supported by piezometer monitoring which identified perched water

tables within the S and C layer loess.

For the purposes of back analysing the slope failures at the investigated site, two failure depths corresponding to the depths of the S-C and C-P soil layer boundaries have been chosen. An angle ß of 15° and a block length of 10m have been selected, as computer modelling shows there will be little significant error between a 40m and a 4m long block with an angle ß of 15°. Piezometric levels at the base of the failure block, the mid-height, and at the ground surface have been used to analyse the effect of soil saturation. Drained testing (chapter 5) showed no significant variations in the internal angle of friction for the loess layers tested, and the constant value ϕ' = 28.4° has been used for the drained analysis. Back analysis for the two failure geometries and the three piezometric levels was carried out. In the drained strength analysis with ϕ'=28.4° the cohesion, c, to produce a factor of safety FS = 1 was calculated.

Table 6.1 Results of Back Analysis - cohesion or strength required for FS=1

Sarma 1979 Theory						
Depth to failure surface	*0.53m (S-C boundary)*			*1.40m (C-P boundary)*		
Piezometric level in slide	Base	Midheight	Surface	Base	Midheight	Surface
Undrained analysis: s_u (kPa)	3.15	3.17	3.25	7.39	7.57	8.03
Drained analysis (ϕ'=28.4°): c'(kPa)	FS>1 for all c'		1.28	FS>1 for all c'		2.71

Infinite Slope Theory						
Depth to failure surface	*0.53m (S-C boundary)*			*1.40m (C-P boundary)*		
Piezometric level	Base	Midheight	Surface	Base	Midheight	Surface
Undrained analysis: s_u (kPa)	3.62	3.62	3.62	9.54	9.54	9.54
Drained analysis (ϕ'=28.4°): c'(kPa)	FS>1 for all c'		1.20	FS>1 for all c'		3.15

Back analysis was completed using the Sarma and infinite slope theories for comparison. The results (table 6.1) show that the infinite slope theory indicates higher factors of safety so that this method is less conservative. However considering the difficulties in mathematically modelling a shallow failure (discussed later) in natural slopes, the differences are not significant. In the discussion below, the mean of the two values for each of these cases is used. As expected both stability theories show that to induce failure, cohesion (drained case) or undrained shear strength (undrained case) have to be reduced significantly as the piezometric level drops from the surface to the base of the failure block.

6.2.4 Discussion

Determined Strengths

Strength testing (chapter 5) produced effective strength parameters from drained (direct shear) tests which ranged from $c'=0$, $\phi'=28.4°$ for remoulded C layer loess to $c'=6$kPa, $\phi'=28.4°$ for undisturbed C layer loess. Undrained (vane shear) tests produced shear strengths (saturated samples) which ranged from $s_u=9$kPa for remoulded (laboratory) C layer loess to $s_u=48$kPa for undisturbed (in situ) C layer loess. Only peak undrained shear strengths were obtained for the lower S layer loess, which makes comparison with the back analysed determined strengths impossible. (The lowest undrained shear strength measured in laboratory testing was $s_u=4$kPa, obtained for saturated remoulded P layer loess.)

Failure at S-C layer Boundary (Depth 0.53 meters)

Back analysis summarised in table 6.1 shows that undrained failure will initiate at the S-C loess layer boundary (approximate depth, 0.5m) ("turfmat slide"), if the piezometric level is at the ground surface (worst case), when the undrained shear strength is less than about $s_u=3.4$kPa. The lowest undrained shear strength obtained for C layer loess during testing, $s_u=9$kPa, at moisture content 22% (close to full saturation), would not be low enough to initiate undrained failure. This mode of failure is therefore unlikely.

For drained failure with an angle of friction $\phi'=28.4°$, failure will occur if the water level is at the slope surface and the cohesion is less than about $c'=1.2$kPa. A

cohesion of c=1.2kPa falls in the range of C layer values determined from laboratory strength testing (c′=0, remoulded to 6kPa, undisturbed), and is towards the lower end of the range, suggesting that this drained failure mode at the S-C interface is reasonable, if some in situ strength reduction occurs (eg. during progressive failure). Back analysis shows that drained failure would not occur if the piezometric level were deeper than the midheight of the slide, since no cohesion (c′=0) is needed to produce a factor of safety >=1 for this mode of failure.

Failure at C-P Layer Boundary (Depth 1.4 meters)

Back analysis summarised in table 6.1 shows that undrained failure will initiate at the C-P loess layer boundary (approximate depth 1.4m) if the undrained strength is less than about s_u=8kPa. Although remoulded strengths of s_u=9kPa (C layer) and 4kPa (P layer) were measured in laboratory tests at very high degrees of saturation and moisture content, peak strengths were considerably higher. It is unlikely that failure at the C-P loess layer boundary would involve remoulded strengths, as no in situ evidence was observed of remoulded in situ C layer loess. Undrained failure is therefore an unlikely failure mode.

Drained failure (with an angle of friction ϕ'=28.4°) is predicted if the cohesion is less than about c′≈3kPa, for the water level at the ground surface. This falls in the middle of the range of laboratory determined remoulded to undisturbed cohesions (c′=0 to 6kPa). If the piezometric level is below the ground surface, drained failure is unlikely.

Even with the piezometric level at the ground surface, the back analysed cohesion (c′≈3kPa) is below the laboratory determined peak cohesion (c′=6kPa) for undisturbed C layer loess. The formation of a tension crack (discussed in chapter 3) may reduce this difference in cohesion, but the difference is more likely to be due either to local variations within the loess, laboratory errors, or the inherent errors involved in mathematically modelling shallow failures in natural slopes.

Accuracy of Mathematical Models

Mathematically modelling shallow failures in natural slopes is usually difficult and often regarded as almost impossible (Fell and Jeffery, 1987). This is because these natural slopes are typically comprised of soils whose effective strength characteristics vary slightly in all directions. This is mainly due to the complex hydrogeology of the surficial soils and the resulting strength variability in partially saturated soils. Added to this is the difficulty in accurately determining the precise failure geometry.

In contrast, for deep seated slope failures slight variations in effective strength properties and the determination of the failure geometry become less significant. However the exercise is very useful in determining the theoretical sensitivity of shallow slopes to the various parameters discussed above.

Synthesis

Having noted problems of accuracy in mathematically modelling shallow slope failures, the following conclusions can be drawn from this work for the slide modelled:

1) For the particular slide modelled, and for many similar slides in Port Hills loess, infinite slope analysis is sufficiently accurate, although slightly less conservative than analyses which allow for variable boundary conditions.
2) Slope failure by translational sliding could occur at the S-C and C-P loess layer boundaries.
3) Failure at the S-C loess layer boundary is likely to involve lower S layer drained shear strengths approaching remoulded values, with the piezometric level at or near the ground surface.
4) Failure at the C-P loess layer boundary is likely to involve C layer loess drained shear strengths closer to peak values with the piezometric level at the ground surface.
5) Slope failure for the geometry studied is very unlikely (even if remoulded strengths are developed) when the piezometric level is close to or below midheight in a potential slide, unless artesian pressures are acting.
6) The strength values obtained from laboratory and field investigations in this study are consistent with the approximate theoretical strengths suggested by stability modelling.

6.3 Hillslope Failure Model

6.3.1 Introduction

The proposed hillslope failure model for the investigated earthflow complex is based on information presented in this chapter and the previous chapters. A schematic representation of the evolution of one of the earthflows from the earthflow complex is presented, from its initiation to its present form.

6.3.2 Suggested Failure Model

Figure 6.8a shows a schematic representation of the formation of a tension crack. It is inferred that the formation of the tension crack is associated with slope creep in the lower S layer loess. When the available resistance to movement offered by the overlying top soil (upper S layer) is exceeded, the top soil fractures, forming a tension crack roughly parallel to the slope contour. Once the tension crack is initiated, it propogates down through the C layer loess, driven by seasonal swell/shrink characteristics of the C layer loess. Tension crack formation of this nature was observed in pit1 and is believed to be actively forming at the western end of the southeast facing failure complex (expressed at the surface as a minor scarp) (see figure 3.4, map pocket).

Figure 6.8b shows the tension crack which has been infilled by lower S layer (plastic deformation) and some topsoil. The tension crack infill offers little or no shear resistance, thus reducing the total available resistance against failure. The slope has a piezometric level coinsident with the ground surface (as indicated by computer modeling). High pore water pressure acting at the base of the C layer are sufficient to initiate the failure of a saturated block of C layer loess and the overlying S layer loess. The block of loess fails by translational sliding at the C-P loess layer boundary. Based on site morphology and computer modelling, the failed block leaves a scarp at least 10m long and may be as long as 40m, with a width of approximately 5m.

Upon failure (figure 6.8c), the failed block of C layer loess collapses and flows downslope, depositing coherent blocks of upper S layer loess (top soil) on the slope. Some C layer loess is deposited on the toe region of the failure surface.

Figure 6·8a: Schematic representation of tension crack development during seasonal and annual climatic fluctuations

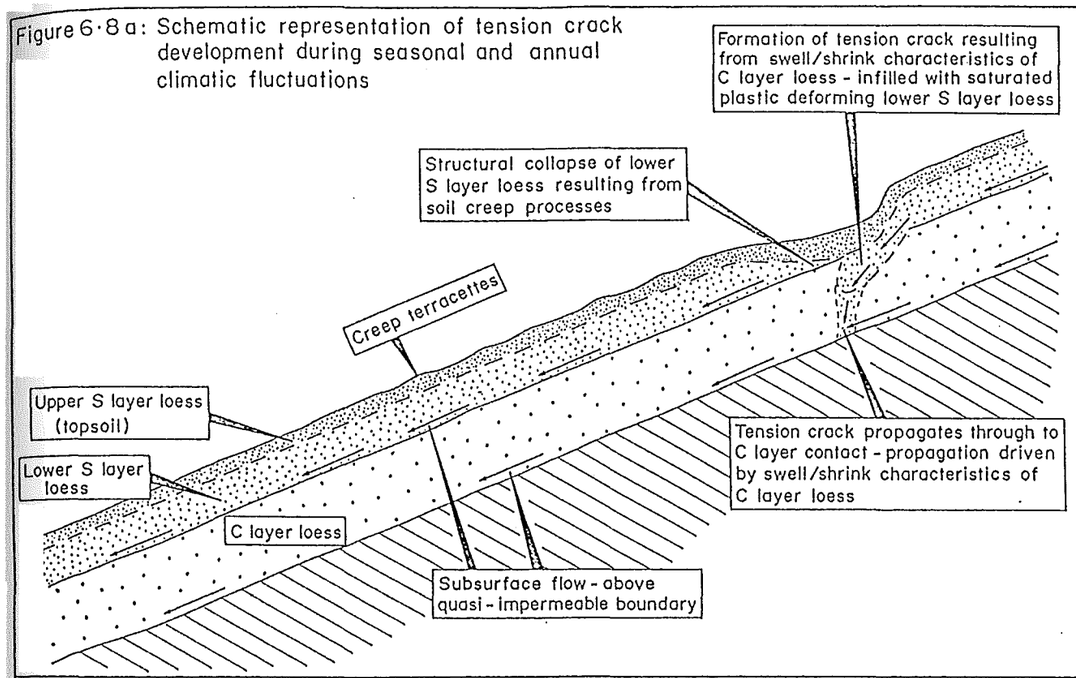

Figure 6·8b: Schematic representation of failure surface development during period of intense rainfall

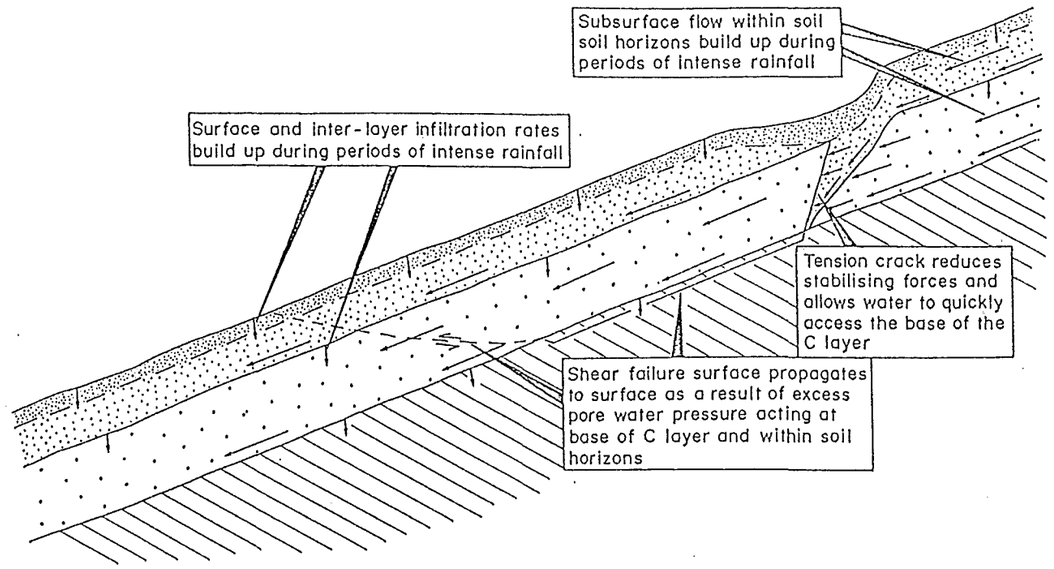

Figure 6·8c: Schematic representation of failed ground post slope failure

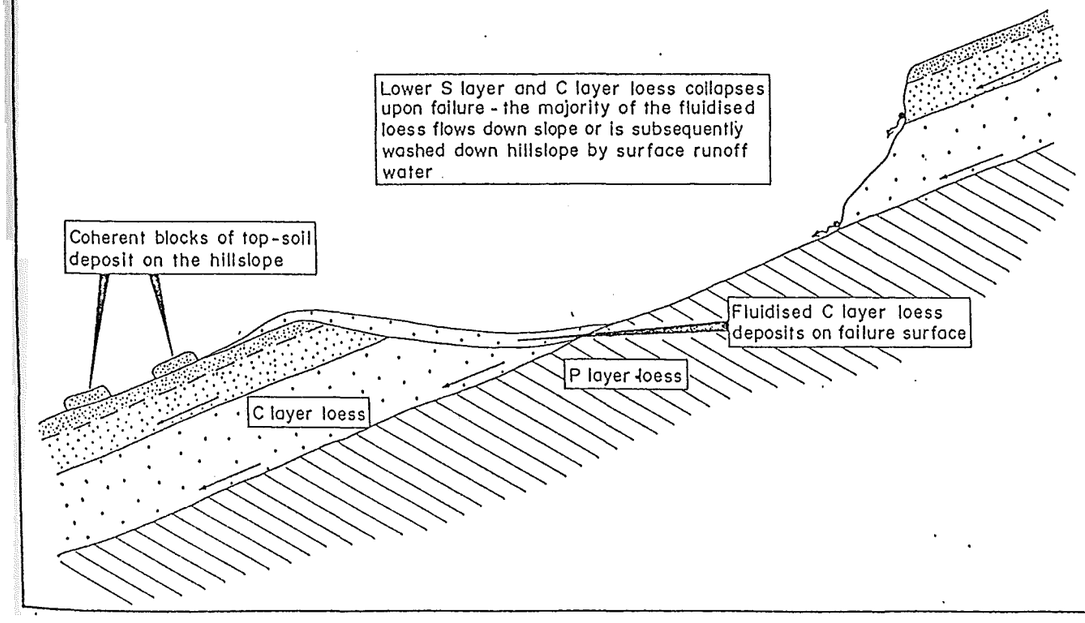

Figure 6·8d: Schematic representation of cross section through site

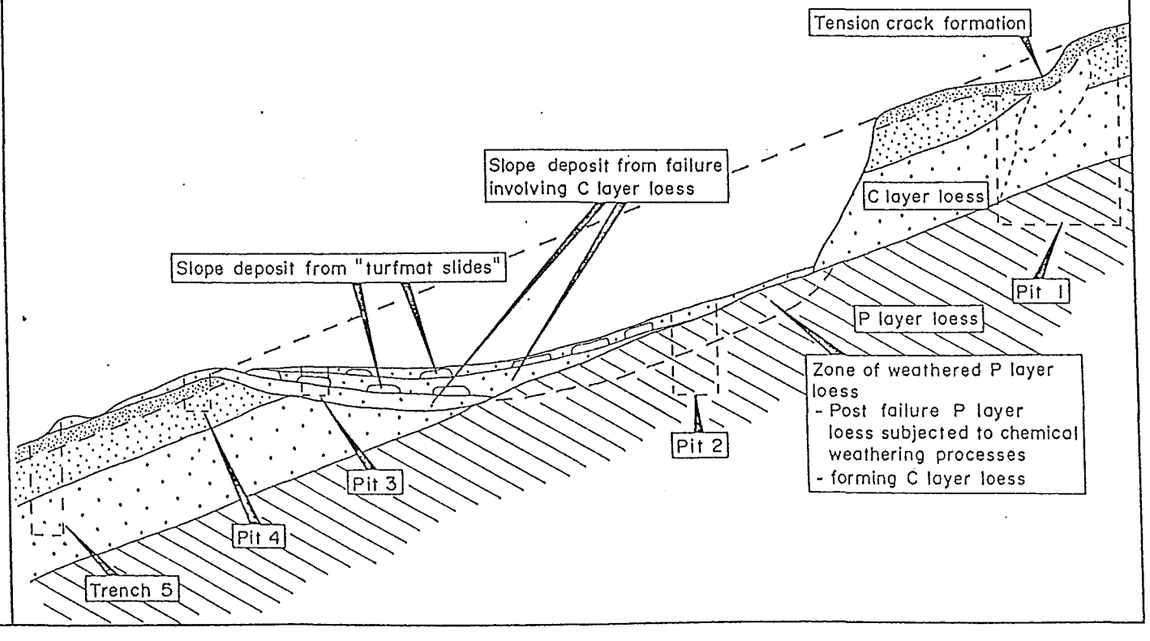

It is believed that the original earth flow involved a block of soil approximately 10m in length, and that the present day scarp length (approximately 40m) is the result of retrogressive behaviour of the back scarp upslope of the original failure. The ground behind the backscarp has no toe support from the ground surface to the base of the C layer loess, allowing two failure mechanisms to act on the ground upslope of the original slope failure. These mechanisms are a function of the rainfall conditions on the slope and the presence of upslope tension cracks. With sufficiently intense rainfall, saturated flow is initiated in the lower S layer loess, which may initiate a "turfmat slide" similar to that observed during the site investigation. It is likely that the underlying C layer loess will be gradually eroded away through time by surface runoff. If the rainstorm is of high enough intensity and of sufficient time duration, a failure similar to the original failure may initiate in the C layer loess. The tension crack need not extend to the base of the C layer as the reduced toe support would reduce the resisting forces sufficiently. It was not possible to model the destabilising influence of the tension crack using the available computer program.

Figure 6.8d shows a schematic cross-section representation of the failed ground today. Information gathered from logging of the pits is consistent with the proposed failure model. The failed ground today represents a slope failure complex which consists of the development of many individual earth flows and "turfmat slide" events since the original slope failure depicted in figure 6.8c.

The location and geometry of the failed ground investigated, the adjacent failed ground and the failed ground on the central east-southeast facing hillslope all suggest that the original slope failures occurred more or less at the same distance downslope from the crest of the hillslopes. This suggests that the soil creep at this slope position is severe enough to break the surface, forming tension cracks.

The initial slope failures occur laterally on the same contour with subsequent retrogressive failures up slope during times of intense rainfall.

Chapter 7

Conclusions

7.1Summary

7.1.1 Allandale Site

Hydrogeology

1) The S and C loess layers both behave as leaky unconfined aquifers which are recharged by infiltrating surface incident precipitation.
2) The hydrogeology of P layer loess is extremely variable in all directions.

Displacement

1) No horizontal surface displacements were recorded during the period of monitoring.
2) A minor (<10mm) vertical surface displacement trend was recognised during the period of monitoring. This is probably associated with seasonal shrink/swell soil characteristics.

Slope Morphology

1) Surface creep is active on the steeper (>22°) portions of the hillslope and particularly in the failed ground where terracettes are formed.
2) Blocks of top soil trailing down slope from failed ground represent slope deposits from a single earth flow event.
3) Relatively minor deposits of fluidised C layer loess from earth flow activity are preserved in the failed ground.

4) The surface expression of minor scarps (generally <0.2m high) adjacent to failed ground may represent tension crack formation in the C layer loess.
5) Two kinds of slope failure have been recognised as forming the present day failed ground:
    a) earth flows involving the C layer; and
    b) "turfmat slides" involving the S layer.

7.1.2 Laboratory Results

Classification Tests

Particle size distributions, density variations and Atterberg limits for all loess layers tested fall into the same general ranges reported for Banks Peninsula loessial soils.

Unconfined Compression Tests

1) Unconfined compression testing on remoulded specimens of C and P layer loess produced significant error, particularly at relatively low moisture contents (<14%).
2) Error can be attributed to differential compaction associated with the insertion of thin-walled sampling tubes and extraction of the specimens from the thin-walled sampling tubes.

Vane Shear Tests

1) Vane shear testing on remoulded C and P layer loess showed the following trends:
    a) Both C and P layer loess in a partially saturated state display a significant reduction in undrained shear strength with an increasing degree of saturation. The strength reduction can be attributed to the decrease in pore water tension associated with capillary suction, as the degree of saturation increases.

b) The undrained shear strength of remoulded C and P layer loess in a partially saturated state can be defined by any two of three parameters: i.e. dry density, moisture content and degree of saturation.

c) Remoulded C layer loess at low degrees of saturation (<50%) produces significantly higher undrained shear strength than remoulded P layer loess at similar degrees of saturation.

2) Vane shear testing on in situ C and P layer loess showed the following trends:

a) Both C and P layer loess in a partially saturated state display a significant reduction in undrained shear strength with increasing degree of saturation.

b) In situ P layer loess at all degrees of saturation produces significantly higher peak undrained shear strengths than in situ C layer loess.

c) The limited drained tests carried out to date suggest the significant difference in the peak undrained shear strength recorded between P and C layer loess at saturation can be attributed to a significantly higher true cohesion in P layer loess than C layer loess.

d) Comparing C and P layer loess remoulded strengths / peak strengths shows the P layer to be significantly more sensitive to remoulding than the C layer.

Direct Shear Tests

1) Drained direct shear tests on mechanically remoulded C and P layer loess showed that the remoulded shear strength parameters are identical for both layers ($c'=0$, $\phi'=28.4°$).

2) Drained direct shear tests on undisturbed C layer loess showed no difference between the peak and remoulded shear strength parameters ($c'=6$kPa, $\phi'=28.4°$).

3) Drained direct shear tests on disturbed P layer loess gave peak shear strength parameters of c'=20kPa, ϕ'=28.4° and remoulded shear strength parameters of c'=6kPa, ϕ'=28.4°.

Four Day Soak Test

The four day soak test showed that mechanically remoulded C layer loess has a significantly greater infiltration rate than mechanically remoulded P layer loess.

7.1.3 Slope Stability Analysis

Computer Modelling

1) "Turfmat slides" can be modelled as essentially translational slides which require remoulded drained shear strengths to initiate failure at the base of the S layer loess. The piezometric level has to be approaching the ground surface to initiate failure.
2) Earth flows can be modelled as essentally translational slides which require peak drained shear strengths and a tension crack in the head region to initiate failure at the base of the C layer loess. The piezometric level has to be close to the ground surface to initiate failure.

7.2 Recommendations for Further Work

The following recommendations are made for further research:

1) Further drained direct shear testing of loessial soils from elsewhere on Banks Peninsula for comparison with results from this study.
2) A detailed study into in situ undrained shear strength variations among other loessial soils elsewhere on Banks Peninsula for comparison with results from this study.

3) Research into the hydrogeology of loess soil horizons, in particular to quantify the differences in the infiltration rate and permeability of all three soil layers.
4) Detailed study of tension crack formation and propagation from the surface into the C layer loess.
5) Research into the structural collapsibility of P and lower S layer loess.

Acknowledgements

I wish to thank the following people for their assistance and support during the preperation of this thesis:

Jarg Pettinga for introducing me to Don Elder and Mark Yetton.

Don Elder and Mark Yetton from Soils and Foundations Ltd. who initated the project and provided perceptive discussion throughout, and for their encouragement, astute supervision and patient editing of thesis drafts.

David Bell for arranging financial support, his supervision and editing of thesis drafts.

John van Dyke and Siale Pasa for the use of their laboratory, equipment and their entertaining, cheerful conversation.

Nick Smith for his constructive suggestions and bad politics.

Rob Davis for pointing me in the right direction.

Ken Mitchell and Todd Warner for their expertise with a spade and their constructive input during the writing up of this thesis.

David Johnston, Tim Coote, Tim McMorran, Richard Little, Dave Barrel, Hugh Cowan (for editing two chapters as well) and any others who put their hands to a spade or helped with surveying.

Michelle Wright for her company and support both generally and on trips to the site.

Arthur Nicholas for making what I wanted, when I wanted it, even if it did cost ½ dozen beer.

Kerry Swanson and Cathrine Conway for their assistance with particle-size analysis.

David Shelley for interesting lunch time conversation and being a true academic.

Jim Cole and Wendy Nuthall for always being helpful.

Calvin Nichol for his aerial photography skills.

Taz Carryer and Tracey Robinson from the Zoology Dept. for their help and expert computing skills.

Last but by no means least, a very special thanks to Bronwen, my daughter Saatchi and my dog Zigi without whose encouragement, financial and emotional support, the project would not have been possible (especially Bronwen for her editorial skills, company on trips to the site, and for going beyond the call of duty and recharging several piezometers).

REFERENCES

ALLEY, P.J. (1966) Cashmere Hills Loes. *N.Z. Engineering*, vol.11, no.10, p424.

ANAYI, G.F., BOYCE, J,R., ROGERS, C.D. (1990) Comparison of Alternative Methods of Measuring the Residual Strength of a Clay. Transportation Research Record 1192, pp16-26.

ATKINSON, J.H. (1981) Foundations and Slopes- An introduction to applications of critical state soil mechanics. McGraw-Hill, pp382.

ATKINSON, J.H. and BRANSBY, P.L. (1978) The Mechanics of Soils- An introduction to critical state soil mechanics. McGraw-Hill, pp375.

BARDEN, L., McGOWAN, A. and COLLINS, K. (1973) The Collapse Mechanism in Partly Saturated Soil. *Eng. Geol.*, Vol.7, pp49-60.

BELL, D.H. (1978) The engineering geology of Banks Peninsula Loess Deposits. Paper presented at a seminar on "Slope Stability and Urban Development", Dept. of Extension Studies, University of Christchurch, 24-25 Feb. 1978, pp1-35.

BELL, D.H. and TRANGMAR, B.B. (1987) Regolith Materials and Erosion Processes on the Port Hills, Christchurch, New Zealand. Proc. 5th Int. Conf. Field Wksp. on Landslides, Christchuch, Aug. 1-12.

BELL, D.H., GLASSEY, D.J., YETTON, M.D. (1986) Chemical stabilisation of dispersive loessial soils, Banks Peninsula, Canterbury, New Zealand. Proc. Fifth IAEG Congress, Buenos Aires, Argentina, Oct 1986, pp1-16.

BIRRELL, K.S. and PACKARD, R.Q. (1953) Some Physical Properties of New Zealand Loess. *N.Z.J. Sci. Tech.*, vol.B35, pp30-35.

BISHOP, A.W. (1955) The Use of the Slip Cicle in the Stability Analysis of Slopes. *Géotechnique*, Vol.5, pp7-17.

BISHOP, A.W. and MORGENSTERN, N.R. (1960) Stability Coefficients for Earth Slopes. *Géotechnique*, Vol.10, pp129-150.

BISHOP, A.W. and HENKEL, D.J. (1957) The measurement of soil properties in the triaxial test., Edward Arnold, pp228.

BLAKELEY, J.P. (1965) The CBR test of Loess- Parts A and B. *Road Research Unit, Bulletin No. 2, National Roads Board,N.Z.*, pp18.

BRADSHAW, J.D., ADAMS, C.J. and ANDREWS, P.B. (1981) Carboniferous to Cretaceous on the Pacific margin of Gondwana: the Rangitata Phase of New Zealand. *In:* Cresswell, M.M. and Vella, P. (Eds), Fifth International Gondwana Symposium, Balkema, Amsterdam, pp217-221.

BRAND, E.W. (ed.) (1984) Geotechnical Manual for Slopes. Government Control Office, Engineering Development Department, Hong Kong, pp295.

B.S. 1377:1975 Methods of test for soils for civil engineering purposes. Test 18.

BROMHEAD, E.N. (1986) The Stability of Slopes. Surrey University Press, 373p.

BROWN, I.R. (1975) The Stability of Slopes in Soft Rocks. Report No.112, University of Auckland, *for* The National Roads Board (N.Z.), pp71.

BROWN, L.J. and WILSON, D.D. (1988) Stratigraphy of the Late Quaternary Deposits of the Northern Canterbury Plains, New Zealand. *N.Z.J. Geol. Geophysics,* Vol. 31, pp305-335.

BROWNE, G.H. AND FIELD, B.D. (1988) A review of Cretaceous - Cenozoic Sedimentation and Tectonics, East Coast, South Island, New Zealand. *In: Sequences, Stratigraphy, Sedimentology: Surface and Subsurface. James, D.P. and Leckie, D.A. (Eds),* Canadian Society of Petroleum Geologists, Memoir 15, pp37-48.

BRUNSDEN, D. (1979) Mass Movement. *In:* Processes in Geomorphology (Embleton, C. and Thornes, J.B. (Eds)), Edward Arnold, pp130-186.

BRUNSDEN, D. and PRIOR, D.B. (1984) Slope Instability. Wiley, pp260.

CEGLA, J. (1969) Influence of Capillary Ground Moisture on Eolian Accumulation of Loess. *Bulletin de L'Academie Polonaise des Science,* Série des sci. géol. et géogr., vol.17, no.1, *Reprinted in:* Loess Letter, no.13, pp3-4.

CHORLEY, R.J. (1978) The Hillslope Hydrological Cycle. *In:* Hillslope Hydrology (Kirkby, M.J. (ed.)), Wiley, pp1-32.

COATES, G.F. and HULSE, C.A. (1985) A comparison of four methods of size analysis of fine-grained sediments. *N.Z.J. Geol. & Geophys.*, Vol.28, pp369-380.

CORNE, C.P. (1973) Progressive Failure in Clay Slopes. Report No.88, School of Engineering, University of Auckland, pp229.

CRAMPTON, N.A. (1985) Engineering Geological Aspects of the Lyttelton-Woolston LPG Pipeline. M.Sc. Thesis (Eng. Geol.), University of Canterbury, 241pp.

CROZIER, M.J. (1986) Landslides: causes, consequences and environment. Croom Helm Ltd., 252p.

CULLEN, R.M. and DONALD, I.B. (1971) Residual Strength Determination in Direct Shear. *Proceedings 1st A.N.Z. Conf. on Geomech., Melbourne, 1971. pp1-10.*

DAS, B.M. (1985) Principles of Geotechnical Engineering. PWS publishers, Boston, Massachusetts, 571p.

ERVIN, M.C. (ed.) (1983) In-Situ Testing for Geotechnical Investigations, Balkema, pp131.

EVANS, G.L. (1977a) Erosion Tests on Loess Silt, Banks Peninsula. Proc. 9th ISSMFE Conf. Tokyo, July 1977, vol.2, pp63-69.

EVANS, G.L. (1977b) Water in Loess Slopes. Paper presented at a seminar on "Slope Stability and Urban Development", Dept. of Extension Studies, University of Christchurch, 24-25 Feb. 1978, pp10.

EVANS, G.L. and TRANGMAR, B.B. (1977) Appendix II: Selected areas of New Zealand No. 5 Christchurch, *In* Taylor et al. "Slope Stability in Urban Development", D.S.I.R. Information Series No. 122, pp65-71.

EVANS, G.L. and BELL, D.H. (1981) Chemical Stabilisation of Loess, New Zealand. Proc. 10th Int. Conf. Soil Mech. and Found. Eng., Stockholm, June 1981, pp649-658.

FEDA, J. (1966) Structural stability of subsident loess soil from Praha-Dejvice. *Eng. Geol.*, 1(3), pp201-219.

GLASSEY, P.J. (1986) Geotechnical properties of lime stabilised loess, Port Hills, Canterbury. Unpub. M.Sc. (Eng. Geol.) thesis, University of Canterbury, Christchurch, 128p.

GRIFFITHS, E. (1973) Loess of Banks Peninsula. *N.Z.J. Geol. Geophys.*, vol.16, no.3 pp657-675.

HANCOX, G.T. (1974) Geological Aspects of Slope Stability. *Proceedings of the Symposium on Stability of Slopes in Natural Ground, N.Z. Geomech. Soc., Nelson, Nov. 1974,* p4.1-4.13.

HANNA, T.H. (1985) Field Instrumentation in Geottechnical Engineering. Trans Tech. Publications, West Germany, 843p.

HANSEN, M.J. (1984) Strategies for classification of landslides. *In:* Slope Stability (Brunsden, D. and Prior, D.B. eds.), John Wiley & Sons, p1-26.

HARVEY, M.D. (1976) An analysis of the soil slips that occurred on the Port Hills, Canterbury, between 19-25 August 1975. Paper presented to the Soil Science Society of New Zealand, Palmerston North, Aug. 1976, pp11.

HILL, J.K. (1978) A Deep-seated Landslide in Loess, La Clare Subdivision, Akaroa. Paper presented at a seminar on "Slope Stability and Urban Development", Dept. of Extension Studies, University of Christchurch, 24-25 Feb. 1978.

HOEK, E. (1983) Strength of Jointed Rock Masses. *Géotechnique*, Vol.33, No.3, pp187-223.

HUGHES, P.J. (1970) Tunnel Erosion in Loess of Banks Peninsula. M.Sc. Thesis (Geog.), University of Canterbury.

HUGHES, P.J. (1972) Slope Aspect and Tunnel Erosion in the Loess of Banks Peninsula, N.Z., *J. Hydrol. N.Z.* vol. 11 no. 2, pp94-98.

HUNT, R.E. (1984) Geotechnical Engineering Investigation Manual. McGraw-Hill, New York, 983p.

HURLBUT, C.S. and KLIEN, C. (1977) Manual of Mineralogy. 19th Ed., John Wiley & sons, p509.

HUTCHINSON, G. (1975) Akaroa Harbour suffers extensive earth movements. *Soil and Water*, Oct. 1975, pp6-7,14.

IVES, D. (1973) Nature and Distribution of Loess in Canterbury, New Zealand. *N.Z.J. Geol. Geophys.*, vol.16, no.3, pp587-610.

JOHNSTON, I.W. (1983) Why in-situ testing? *In:* In-situ Testing for Geotechnical Investigations. (Ervin, M.C. (ed.)), Balkema, pp1-20.

JANBU, N. (1957) Earth Pressures and Bearing Capacity Calculations by Generalised Procedure of Slices. *Proc. 4th Int. Conf. Soil Mech. and Found. Eng., London,* Vol.2, pp207-212.

KENNEY, C. (1984) Properties and Behaviours of Soil Relevant to Slope Instability. *In:* Slope Instability (Brunsden, D. and Prior, D.B. (eds.)), Wiley, pp27-66.

KIE, T.T. (1988) Fundermental Properties of Loess from Northwestern China. *Eng. Geol.*, Vol.25, pp103-122.

KNAPP, B.J. (1978) Infiltration and Storage of Soil Water. *In:* Hillslope Hydrology (Kirkby, M.J. (ed.)), John Wiley & Sons, pp44-72.

KRIGER, N.I. (1985) Lithoecology and Energetics of Loess: Paleogeographic and Genetic Aspects. *Loess Letter*, no.14, pp21-25.

LIN, Z.G. and WANG, S.J. (1988) Collapsibility and deformation characteristics of deep-seated loess in China. Eng. Geol., *vol.25, pp271-282.*

LO, K.Y. (1972) An Approach to the Problem of Progressive Failure. *Canadian Geotechnical Journal,* Vol.9, pp407-429.

LOHNES, R.A. and HANDY, R.L. (1968) Slope Angles in Friable Loess. *Journal of Geology*, Vol. 76, pp247-258.

LUTENEGGER, A.J. and HALLBERG, G.R. (1988) Stability of Loess. *Eng. Geol.,* Vol.25, pp247-261.

LYSENKO, M.P. (1971) Loessial Rocks of the European USSR (Translated from Russian), Keter Press, Jerusalem, 150pp.

MACKWELL, J. (1986) Engineering Geological Investigations Wainui-French Farm Area, Akaroa County, Banks Peninsula. M.Sc. Thesis (Eng. Geol.), University of Canterbury.

McDOWELL, B.J. (1989) Site Investigations for Residential Development on the Port Hills, Christchurch. M.Sc. Thesis (Eng. Geol.), University of Canterbury.

McGANN, R.P. (1983) The Climate of Christchurch. *N.Z. Met. Serv. Misc. Publ.* 167(2), 27p.

McGRAW, J.D. (1975) Quaternary airfall deposits of New Zealand. *In:* Quaternary Studies, Roy. Soc. N.Z. Suggate, R.P. and Cresswell, M.M. (eds) pp35-44.

MATALUCCI, R.V., ABDEL - HADY, M. and SHELTON, J.W. (1970) Influence of microstructure of loess on triaxial shear strength. *Eng. Geol.,4*, pp341-351.

MILLER, D.E.K. (1971) Soil Properties Affecting Tunnel Gully Erosion. M.Agr. Thesis, Lincoln College.

MILLER, P.J. (1982) The triaxial test method. Central Laboratories Report No.2-82/8, MOW Central Lab., Lower Hutt, pp50.

MILOVIC, D. (1988) Stress deformation properties of macroporous loess soils. *Eng. Geol., vol.25, pp283-302.*

MINKOV, M., EVSTATIEV, D., DONCHEV, P., ALEXIEV, A.P., STEFANOFF, G. and KRASTILOV, I. (1979) On the prediction and real behaviour of loess bases. Design parameters in geotech. eng., *B.G.S.*, London, vol.1, pp53-56.

MORGENSTERN, N.R. and PRICE, V.E. (1965) The Analysis of the Stability of General Slip Surfaces. *Géotechnique*, Vol.15, pp79-93.

MORGENSTERN, N.R. and SANGREY, D.A. (1978) Methods of Stability Analysis. *In:*LANDSLIDES: Analysis and Control, (Schuster, R.L. and Krizek, R.J. eds.), Transportation Research Board Special Report 176, National Academy of Sciences, Washington D.C., p155-170.

MOSTYN, G.R. and SMALL, J.C. (1987) Methods of Stability Analysis. *In:* Soil Slope Instability and Stabilisation, (Walker and Fell (eds.)), Balkema, Rotterdam, pp71-120.

MYSLINSKA, E. (1986) Change of a loess microstructure under the influence of water as reasons for its subsidence. 5th International IAEG Congress, Buenos Aires 1986, pp705-708.

N.Z.M.S. 260 M36 (1984) New Zealand Topographical Map 1:50,000, Lincoln, Edition 1, Department of Lands and Survey, N.Z.

N.Z. MET. SERV. (198?) Rainfall Normals for New Zealand 1951 to 1980. *N.Z. Met. Serv. Misc. Publ.* 185, 36p.

N.Z.S. 4402:1986 Methods of testing soils for Civil Engineering purposes. Tests 2.1, 2.2, 2.3, 2.4, 2.8.3, 4.1.2, 2.7.2, 4.1.1, 4.1.2, 6.3.1.

PETLEY, D.J. (1984) Ground Investigation, Sampling and Testing for Studies of Slope Instability. *In:* Slope Instability (Brunsden and Prior (eds.)), pp67-102.

PYE, K. (1984) Loess. *Progress in Physical Geography*, vol8, no.2, *Reprinted in:* Loess Letter, no.12, pp13-17.

RAESIDE, J.D. (1964) Loess deposits of the South Island, New Zealand, and soils formed on them. *N.Z.J. Geol. Geophys.*, no.7, pp811-838.

RIB, H.T. and LIANG, T. (1978) Recognition and Identification. *In:*LANDSLIDES: Analysis and Control, (Schuster, R.L. and Krizek, R.J. eds.), Transportation Research Board Special Report 176, National Academy of Sciences, Washington D.C., p34-80.

RYAN, A.P. (1987) The climate and weather of Canterbury. *N.Z. Met. Serv. Misc. Publ.* 115(17), 66p.

SALT, G. (1983) The use of Residual Strengths of Soils in Geotechnical Design. Paper to IPENZ Conf., 1983, Hamilton, N.Z.

SANDERS, R. (1986) Hydrogeological studies of springs in Akaroa County, Banks Peninsula. M.Sc. Thesis (Eng. Geol.), University of Canterbury.

SARMA, S.K. (1973) Stability Analysis of Embankments and Slopes. *Géotechnique*, Vol.23, No.3, pp423-433.

SARMA, S.K. (1979) Stability Analysis of Embankments and Slopes. *J. Geotech. Engng Div., Am. Soc. Civ. Engrs*, Vol.105, No. GT12, pp1511-1524.

SAYE, S.R.; NASS, K.H.; EASTON, C.N. (1988) Performance of heavy structures founded upon loess at varying moisture conditions. *Eng. Geol.*, vol.25, pp325-339.

SCHUSTER, R.L. (1978) Introduction. *In:*Landslides, Analysis and Control, (Schuster, R.L. and Krizek, R.J. eds.), Transportation Research Board, National Academy of Sciences, Washington, D.C., pp

SCHUSTER, R.L. and KRIZEK, R.J. (eds.) (1978) Landslides, Analysis and Control, Special Report 176, Transport Roads Board, National Academy of Science, Washington, D.C., pp 234.

SCOTT, G.L. (1979) Engineering Geology and Urban Planning: A study near Christchurch. M.Sc. theis (Eng. Geol.), University of Canterbury.

SEED, H.B. and CHAN, C.K. (1960a) Compacted Clays- Structure and Strength Characteristics. *Trans. ASCE,* Paper 3246, pp1344-1384.

SEED, H.B. and CHAN, C.K. (1960b) Compacted Clays- Undrained Strength after Soaking. *Trans. ASCE,* Paper 3246, pp1408-1425.

SELBY, M.J. (1976) Loess. N.Z.J. Geog., *no.61, pp1-18.*

SELBY, M.J. (1979) Slope Stability Studies in New Zealand. *In:* Physical Hydrology: New Zealand Experience (Murray, D.L. and Ackroyd, P. eds.), New Zealand Hydrological Society, p120-134.

SELBY, M.J. (1982) Hillslope materials and Processes. Oxford University Press, pp264.

SEROTA, S. and JANGLE, A. (1972) A direct reading pocket shear vane. *Civil Engineering- American Society of Civil Engineers, Jan. 1972.*

SEWELL, R.J. (1988) LATE Miocene volcanic stratigraphy of central Banks Peninsula, Canterbury, New Zealand. *N.Z.J. Geol. Geophys,* vol.31, pp41-64.

SEWELL, R.J., WEAVER, S.D., THIELE, B.W. (1988) Sheet M36 BD - Lyttelton. Geological map of New Zealand 1:50,000. Map(1 sheet) and notes. Wellington, New Zealand. D.S.I.R..

SHARPE, C.F.S. (1968) Landslides and related phenomena- a study of mass-movements of soil and rock, Cooper Square, pp137.

SHELLEY, D. (1989) Anteconsequent Drainage: an Unusual Example Formed during Constructive Volcanism., *Geomorphology, 2.*, pp363-367.

SINGLETON, P.L. (1984) Installation of PVC piping for soil water table observations. *N.Z. Soil Bureau Scientific Report 61*, 12p.

SKEMPTON, A.W. and HUTCHINSON, J.N. (1969) Stability of natural slopes and embankment foundations. 7th Int. Conf. on Soil Mech. and Found. Eng., State of the Art vol., Mexico, pp291-340.

SKEMPTON, A.W. (1948) The $\phi=0$ Analysis of Stability and its Theoretical Basis. *Proc. 2nd Int. Conf. Soil Mech. & Found. Eng.*, Vol.1, Rotterdam, pp73-78.

SKEMPTON, A.W. and GOLDER, H.Q. (1948) Practical examples of the $\phi=0$ analysis of stability of clays. *Proc. 2nd Int. Conf. Soil Mech. & Found. Eng.*, Vol.2, Rotterdam, pp63-70.

SKEMPTON, A.W. (1985) Residual strength of clays in landslides, folded strata and the laboratory. *Géotechnique*, Vol.35, No.1, pp3-18.

SMALLEY, I.J. (1975) Loess: Lithology and Genesis, Dowden, Hutchinson and Ross Inc., Stroudsburg, Pennsylvania, pp429.

SMALLEY, I.J. (1983) The literature of Loess (Part 1). *Loess Letter*, no.9, pp27-28.

SMALLEY, I.J. and SMALLEY, V. (1983) Loess Material and Loess Deposits: Formation, Distribution and Consequences. *In:* Developments in Sedimentology: Eolian Sediments and Processes, M.E. Brookfield and T.S. Ahlbrandt (Eds), Elsevier, Netherlands, pp51-68.

SOWERS, G.F. and ROYSTER, D.L. (1978) Field Investigation. *In:*Landslides, Analysis and Control, (Schuster, R.L. and Krizek, R.J. eds.), Transportation Research Board, pp81-111.

SPENCER, E. (1967) A Method of Analysis of the Stability of Embankments Assuming Parallel Inter-Slice Forces. *Géotechnique*, Vol.17, pp11-26.

STANLEY, D.W. and MIKKELSEN, P.E. (1978) Field Instrumentation. *In:* Landslides, Analysis and Control. R.L. Schuster and R.J. Krizek (eds), TRB, National Academy of Science, Washington, D.C., pp112-138.

TAYLOR, S.R.; McLENNAN, S.M.; McCULLOCH, M.T. (1983) Geochemistry of Loess, Continental Crustal Composition and Crustal Model Ages. *Geochimica et Cosmochimica Acta*, No.47. *Reprinted In:* Loess Letter, No.11, p25.

TEHRANI, B.H. (1988) Chemical Stabilisation of Whaka Terrace Loess, Christchurch. M.Sc. thesis (Eng. Geol.), University of Canterbury.

TERZAGHI, K. (1936) The shearing resistance of saturated soils. Proc. 1st Int. Conf. Soil Mech. vol.1, pp54-56.

TERZAGHI, K. (1950) Mechanism of Landslides. *Geological Society of America*, Engineering Geology (Berkey) Volume, p83-123.

TERZAGHI, K. and PECK, R.B. (1967) Soil Mechanics in Engineering Practice, 2nd Edition, Wiley, pp729.

THIELE, B. (1983) Basement Geology to the Lyttelton Volcano. Unpublished MSc Thesis, University of Canterbury.

TODD, D.K. (1980) Groundwater Hydrology, John Wiley & Sons, New York, 535p.

VARNES, D.J. (1958) Landslide Types and Processes. *In:* Landslides and Engineering Practice (Eckel, E.B. ed.), HRB, Special Report 29, pp20-47.

VARNES, D.J. (1978) Slope movement and types and processes. *In:*LANDSLIDES: Analysis and Control, (Schuster, R.L. and Krizek, R.J. eds.), Transportation Research Board Special Report 176, National Academy of Sciences, Washington D.C., p11-33.

VAUGHAN, P.R. (1969) A note on Sealing Piezometers in Boreholes. *Géotechnique*, vol.19, p405.

VAUGHAN, P.R. (1973) The measurement of pore pressures with piezometers. Symposium on Field Instrumentation, London, 1973, pp411-422.

VEDER, C. (1981) Landslides and Their Stabilisation. Springer-Verlag, New York, p247.

WALKER, B.F. and FELL, R. (Eds.) (1987) Soil Slope Instability and Stabilisation, Proceedings of an extension course on soil slope instability and stabilisation, Balkema, pp440.

WEAVER, S.D., SEWELL, R.J., DORSEY, C.J. (1985) Extinct Volcanoes: A Guide to the Geology of Banks Peninsula. N.Z. *Geol. Soc. Guidebook 7,* 48pp.

WEAVER, S.D., SMITH, I.E.M., SEWELL, R.J. et al. (1989, in press) New Zealand Intraplate Volcanism. *In:* Cenozoic Intraplate Volcanism in Australasia, R.W. Johnson and S.R. Taylor (Eds), Cambridge University Press.

WELLINGS, S.R. and BELL, J.P. (1982) Physical controls of water movement in the unsaturated zone. *Q.J. Eng. Geol. London*, Vol.15, pp235-241.

WHIPKEY, R.Z. and KIRKBY, M.J. (1978) Flow within the soil. *In:* Hillslope Hydrology (Kirkby, M.J. (ed.)), Wiley, pp121-144.

WILD T1000 Operators Manual.

WYKEHAM and FARRANCE, WF25300 Direct shear box apparatus manual.

YETTON, M.D. (1986) Investigation and Remedial Methods for Subsurface Erosion Control in Banks Peninsula Loess. M.Sc. Thesis (Eng. Geol.), University of Canterbury.

YONG, R.N. and WARKENTIN, B.P. (1975) Soil Properties and Behaviour. *Developments in Geotechnical Engineering,* Vol.5, pp141-195.

YOUNG, D.J. (1964) Stratigraphy and Petrography of North-east Otago Loess. *N.Z.J. Geol Geophys.*, vol.7, pp839-863.

Appendix 1

SURVEYING

A1.1 Equipment

1 * Wild T1000 Electronic Theodolite
1 * Wild DI1000 Distomat
3 * Wild GST20 Tripod
2 * Wild GPH1A Single-prism and Holder
1 * Wild GLS11 Plumbing pole (staff)
1 * Steel Tape Measure

All surveying equipment was from the Geology department, University of Canterbury.

A1.2 Method

A1.2.1 Topographic and Location Surveys

Topographic surveying commenced during March 1989 for the purpose of producing engineering geological plans, sections and to accurately locate auger holes, pits and piezometers. Control points S1 and S2 alternately had a tripod mounted, electronic theodolite with distomat (EDM, see figure A1.1) and prism, which was used as a reference base line (false origin) for opening and closing each survey. Data points for these surveys were located through the use of a prism mounted, hand held staff (see figure A1.2).

A1.2.2 Displacement Surveys

A survey network was established in and adjacent to the investigated slope failure to monitor displacements. The survey network comprising 18 data points, was monitored on an approximately two monthly basis from April 1989 to February 1990. Wooden pegs 45cm long were used as markers for the displacement points (see figure 3.8, map pocket)(DP1, DP2, ..., DP18). All measurements involving the displacement points were taken using a tripod mounted prism (see figure A1.3) and referenced to the S1-S2 (false origin) base line.

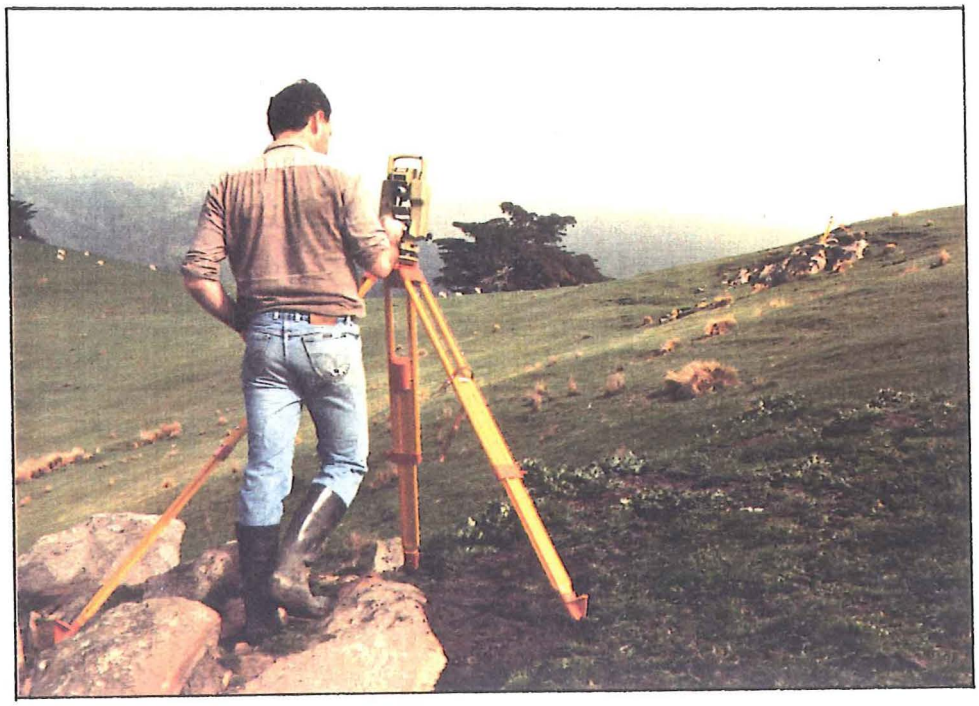

Figure A1.1 Tripod mounted EDM, used for all surveying. Base line (S1-S2) runs between the two rock outcrops.

Figure A1.2 Hand held prism mounted staff.

Figure A1.3 Tripod mounted prism used for displacement surveying.

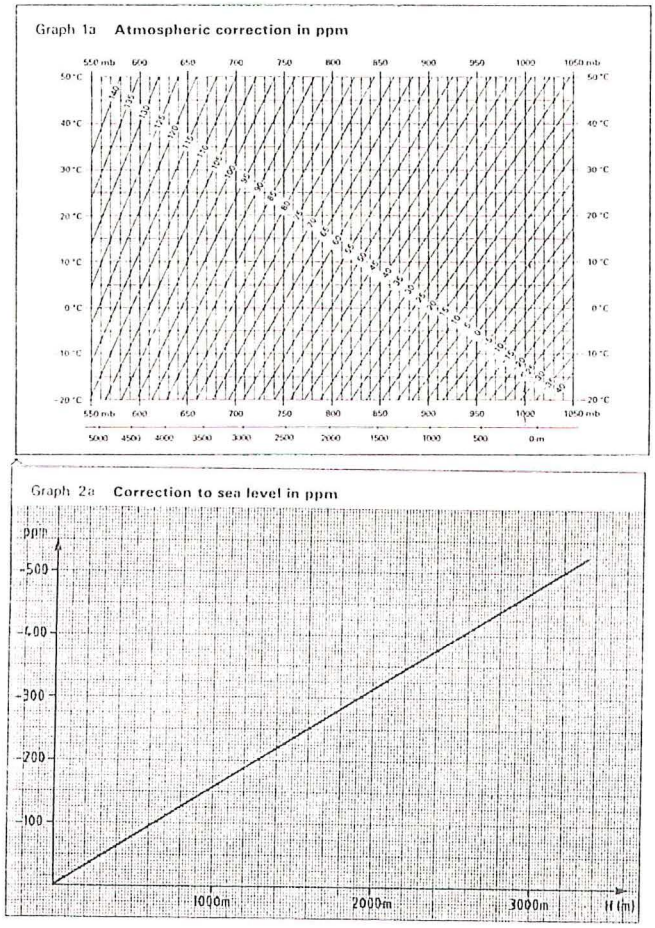

Figure A1.4 & A1.5 Atmospheric correction in ppm (graph 1a) and correction to sea level in ppm (graph 2a).

A1.3 Accuracy

A1.3.1 Instrument Error

The Wild DI1000 Distomat requires a scale correction (Wild DI1000 Operators Manual) in ppm (parts per million) to compensate for the atmospheric conditions at the time of measurement. Using graphs (figures A1.4 & A1.5), a scale correction can be input into the Distomat.

From figure A1.4 the atmospheric correction required for operating the instrument between 25°C and 5°C (expected temperature variation over survey period) is 15ppm and -3ppm respectively at a height of 95m above sea level. The correction to sea level (figure A1.5) at this height is -15ppm. The corrections are summed, hence no scale correction is required when operating the instrument at 25°C, and at 5°C, a scale correction of -18ppm is required, which equates to an error in the distance measurement of -1.8mm at a 100m distance. The instrument has an inherent accuracy of ±5ppm (0.5mm), hence the total potential instrument error over the entire survey period can be expected to be within the range of +0.5mm and -2.3mm for the distance measurements. The potential error in bearing measurements (vertical and horizontal) is negligible as the readings were taken more or less in the same segment of the instrument.

A1.3.2 Operator Error

During the survey period from April 1989 to February 1990, five different people operated the survey equipment. The error associated with each operator can be assumed to be the difference between the opening and closing of each survey, and the average of all opening and closure data. This error affects all bearing and height/distance measurements. Section A1.4.2 details the average and range of survey opening/closure data recorded over the eleven months of surveying.

A1.4 Data

A1.4.1 Calculations of Rectangular coordinates & Actual Height

Data displayed by the EDM are in polar coordinates, being a horizontal distance, a height difference (difference between instrument and staff heights), and a horizontal angle (increasing clockwise). For the purpose of manipulating and plotting data it is more convenient to use rectangular coordinates based on a false origin, hence the following calculations were applied to reduce all raw data.

Reduced Height

The following formula was used to calculate the actual height h, as opposed to the height difference x, which is the height between the instrument h_i and the staff height h_s:

$$h = x + h_i - h_s$$

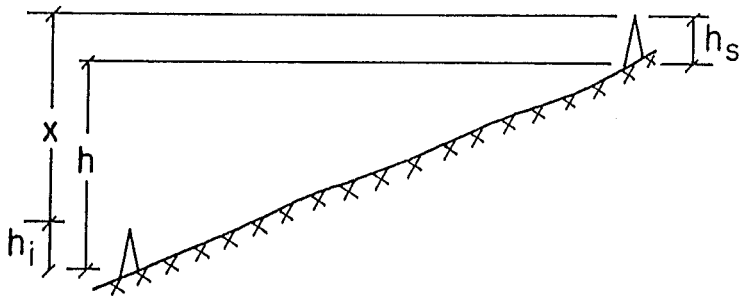

Polar to Rectangular Coordinates

The following formula were used to convert polar coordinates to rectangular coordinates, with S1 being the false origin and the base line coincident with the X-axis:

$$x = (-1)\ d\ cos$$
$$y = d\ sin$$

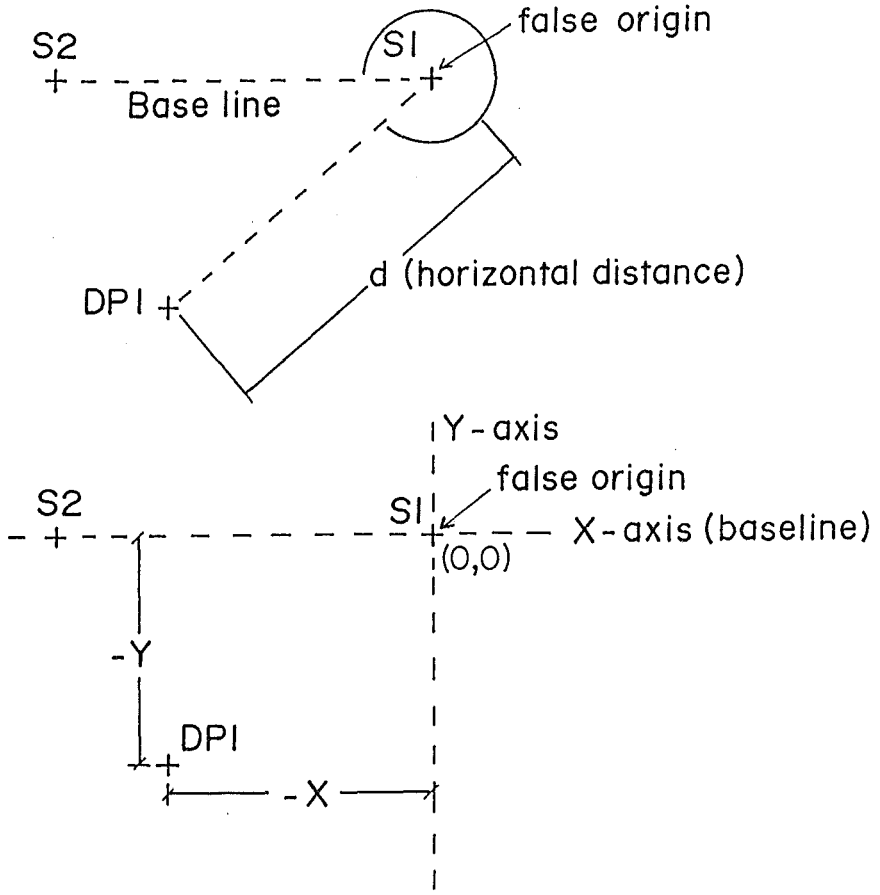

A1.4.2 Reduced Displacement Data

CLOSURE DATA (S1 - S2)

Date of Survey	Reduced Level	X-coord	Y-coord
10/04/89	11.210	-76.258	0
	11.210	-76.257	0
12/04/89	11.211	-76.259	0
	11.214	-76.259	-0.09
14/04/89	11.210	-76.259	0
	11.213	-76.258	-0.004
07/05/89	11.207	-76.257	0
	11.210	-76.257	-0.002
07/06/89	11.209	-76.259	0
	11.211	-76.259	0
19/09/89	11.214	-76.258	0
	11.212	-76.258	0
	11.211	-76.258	0
07/11/89	11.211	-76.257	0
	11.211	-76.254	0
01/02/90	11.213	-76.256	0
	11.213	-76.257	0
	11.214	-76.258	0
AVERAGE	11.211	-76.258	-0.032
RANGE	-0.002,+0.003	-0.004,+0.001	-0.058,+0.032

SURVEY OF DISPLACEMENT POINT 1

Date of Survey	Reduced Level	X-coord	Y-coord
12/04/89	-24.733	37.493	-43.262
07/06/89	-24.726	37.496	-43.262
19/09/89	-24.722	37.499	-43.263
07/11/89	-24.722	37.492	-43.265
01/02/90	-24.724	37.490	-43.253

SURVEY OF DISPLACEMENT POINT 2

Date of Survey	Reduced Level	X-coord	Y-coord
12/04/89	-29.718	38.234	-55.244
07/06/89	-29.710	38.245	-55.242
19/09/89	-29.712	38.247	-55.241
07/11/89	-29.708	38.238	-55.245
01/02/90	-29.715	38.241	-55.239

SURVEY OF DISPLACEMENT POINT 3

Date of Survey	Reduced Level	X-coord	Y-coord
12/04/89	-28.382	44.265	-48.741
07/06/89	-28.375	44.268	-48.734
19/09/89	-28.377	44.272	-48.737
07/11/89	-28.372	44.263	-48.742
01/02/90	-28.377	44.264	-48.738

SURVEY OF DISPLACEMENT POINT 4

Date of Survey	Reduced Level	X-coord	Y-coord
12/04/89	-29.048	50.747	-48.188
07/06/89	-29.037	50.754	-48.183
19/09/89	-29.036	50.757	-48.181
07/11/89	-29.032	50.747	-48.190
01/02/90	-29.034	50.748	-48.185

SURVEY OF DISPLACEMENT POINT 5

Date of Survey	Reduced Level	X-coord	Y-coord
12/04/89	-30.633	50.772	-52.371
07/06/89	-30.619	50.792	-52.368
19/09/89	-30.619	50.794	-52.370
07/11/89	-30.621	50.787	-52.372
01/02/90	-30.622	50.788	-52.367

SURVEY OF DISPLACEMENT POINT 6

Date of Survey	Reduced Level	X-coord	Y-coord
14/04/89	-31.513	62.821	-48.565
07/06/89	-31.502	62.826	-48.563
19/09/89	-31.499	62.828	-48.561
07/11/89	-31.500	62.825	-48.566
01/02/90	-31.508	62.819	-48.563

SURVEY OF DISPLACEMENT POINT 7

Date of Survey	Reduced Level	X-coord	Y-coord
14/04/89	-35.781	76.513	-54.171
07/06/89	-35.773	76.521	-54.170
19/09/89	-35.772	76.521	-54.010
07/11/89	-35.774	76.513	-54.177
01/02/90	-35.777	76.512	-54.170

SURVEY OF DISPLACEMENT POINT 8

Date of Survey	Reduced Level	X-coord	Y-coord
14/04/89	-39.149	77.995	-62.967
07/06/89	-39.148	77.999	-62.968
19/09/89	-39.147	77.999	-62.964
07/11/89	NO READING TAKEN		
01/02/90	-39.145	77.996	-62.964

SURVEY OF DISPLACEMENT POINT 9

Date of Survey	Reduced Level	X-coord	Y-coord
14/04/89	-38.555	73.085	-63.540
07/06/89	-38.557	73.059	-63.552
19/09/89	-38.547	73.063	-63.542
07/11/89	-38.546	73.051	-63.554
01/02/90	-38.554	73.058	-63.545

SURVEY OF DISPLACEMENT POINT 10

Date of Survey	Reduced Level	X-coord	Y-coord
14/04/89	-38.363	64.633	-64.242
07/06/89	-38.359	64.639	-64.242
19/09/89	-38.365	64.639	-64.238
07/11/89	-38.360	64.628	-64.248
01/02/90	-38.365	64.688	-64.186

SURVEY OF DISPLACEMENT POINT 11

Date of Survey	Reduced Level	X-coord	Y-coord
14/04/89	-34.337	51.644	-59.662
07/06/89	-34.325	51.678	-59.661
19/09/89	-34.334	51.650	-59.660
07/11/89	-34.326	51.639	-59.667
01/02/90	-34.334	51.639	-59.663

SURVEY OF DISPLACEMENT POINT 12

Date of Survey	Reduced Level	X-coord	Y-coord
14/04/89	-39.041	53.909	-70.800
07/06/89	-39.035	53.913	-70.803
19/09/89	-39.036	53.916	-70.803
07/11/89	-39.032	53.903	-70.807
01/02/90	-39.043	53.906	-70.802

SURVEY OF DISPLACEMENT POINT 13

Date of Survey	Reduced Level	X-coord	Y-coord
14/04/89	-45.811	68.357	-86.276
07/06/89	-45.800	68.366	-86.274
19/09/89	-45.797	68.365	-86.272
07/11/89	-45.793	68.352	-86.282
01/02/90	-45.808	68.355	-86.277

SURVEY OF DISPLACEMENT POINT 14

Date of Survey	Reduced Level	X-coord	Y-coord
14/04/89	-44.490	74.145	-80.882
07/06/89	-44.483	74.153	-80.882
19/09/89	-44.486	74.154	-80.881
07/11/89	-44.482	74.144	-80.888
01/02/90	-44.488	74.146	-80.881

SURVEY OF DISPLACEMENT POINT 15

Date of Survey	Reduced Level	X-coord	Y-coord
14/04/89	-46.054	81.475	-81.250
07/06/89	-46.050	81.476	-81.252
19/09/89	-46.048	81.484	-81.244
07/11/89	-46.041	81.473	-81.255
01/02/90	-46.052	81.467	-81.246

SURVEY OF DISPLACEMENT POINT 16

Date of Survey	Reduced Level	X-coord	Y-coord
14/04/89	-47.243	91.768	-77.984
07/06/89	-47.235	91.776	-77.979
19/09/89	-47.235	91.782	-77.975
07/11/89	-47.234	91.766	-77.986
01/02/90	-47.243	91.765	-77.978

SURVEY OF DISPLACEMENT POINT 17

Date of Survey	Reduced Level	X-coord	Y-coord
14/04/89	-53.761	94.741	-97.320
07/06/89	-53.746	94.745	-97.322
19/09/89	-53.749	94.745	-97.317
07/11/89	-53.744	94.736	-97.320
01/02/90	-53.755	94.729	-97.318

SURVEY OF DISPLACEMENT POINT 18

Date of Survey	Reduced Level	X-coord	Y-coord
14/04/89	-50.336	77.681	-95.404
07/06/89	-50.326	77.688	-95.408
19/09/89	-50.326	77.697	-95.403
07/11/89	-50.318	77.682	-95.413
01/02/90	-50.331	77.680	-95.408

A1.4.3 Graphical Presentation of Results

Figure A1.6 presents a graphical presentation of the reduced data for all displacement points, showing movement (mm) relative to the initial survey. The data was not corrected for instrument and operator error as horizontal movement (x & y directions) is insignificant and random.

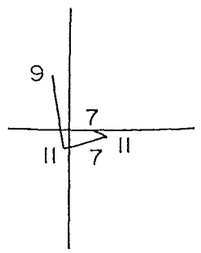

DP 1

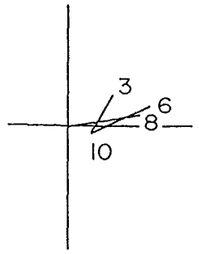

DP 2

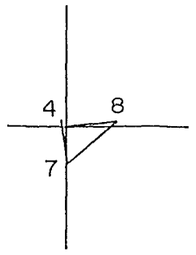

DP 7

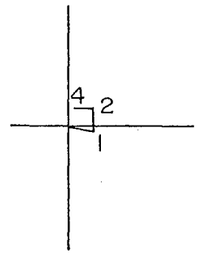

DP8

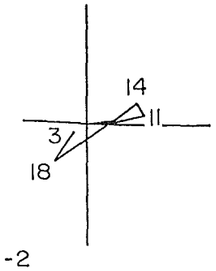

DP 13

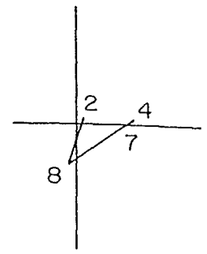

DP 14

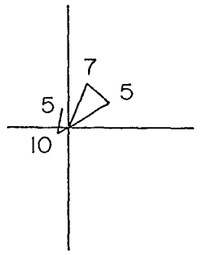

DP 3

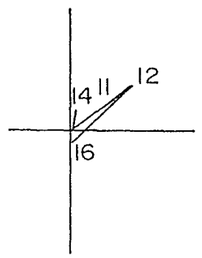

DP 4

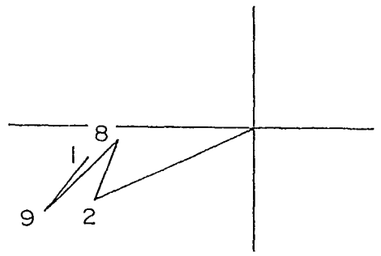

DP 9

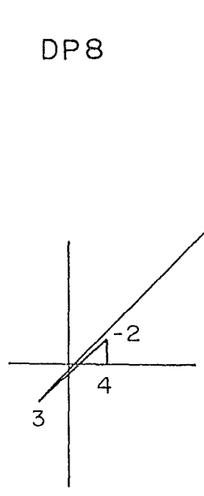

DP 10

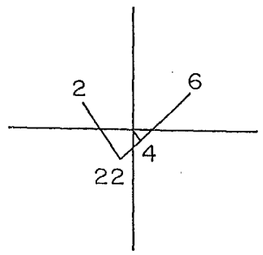

DP 15

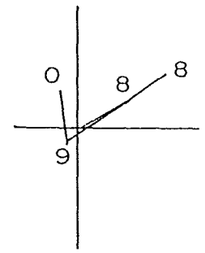

DP 16

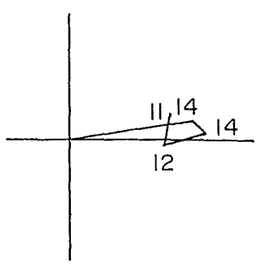

DP 5

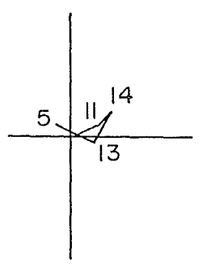

DP 6

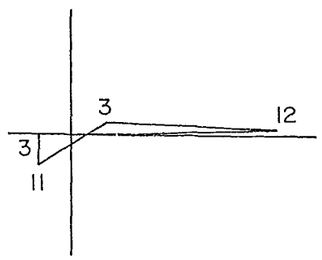

DP 11

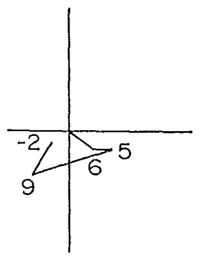

DP 12

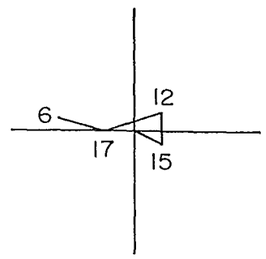

DP 17

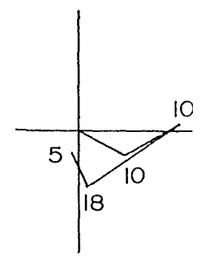

DP 18

Figure A 1·6: Reduced Displacement Survey Data

Note: lines represent horizontal displacement vectors (mm) from from false origin (which was based on initial survey)
numbers represent vertical displacement (mm), negative numbers = downwards

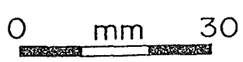

Appendix 2

PIEZOMETERS

A2.1 Theory

An element of soil can be considered to be a three-phase system (see figure A2.1) comprising a solid phase, and a pore phase consisting of liquid and gas phases, usually water and air respectively (Das, 1985). It is the ratios of the volumes of these three phases that are described in soil mechanics terminology as void ratio, porosity and degree of saturation.

When a load (σ) is applied to a saturated element of soil, part is carried by the water (u) in the void spaces (acts with equal intensity in all directions) and part is carried by the solids (σ') at their points of contact. It is the effective stress (σ') in a soil mass that controls its deformation behaviour and strength, and therefore knowledge of the total stress (σ) and the pore water pressure (u) is crucial in soil engineering. These parameters have the following simplified relationship (Das, 1985):

$$\sigma' = \sigma - u$$

Bernoulli's equation describes the energy level of a flowing liquid. Hydraulic head is a measure of energy per unit weight of water and can be expressed as a height. Hydraulic head (H) can be expressed by the (Bernoulli) equation:

$$H = (P/\gamma_w) + (v^2/2g) + z \quad (m)$$

where: v = velocity ($m.s^{-1}$)
g = acceleration due to gravity ($m.s^{-1}$)
P = pressure of a unit weight of water at a given point (Pa)
γ_w = unit weight of water (kg/m^{-3}) ($=\rho g$)
P/γ_w = pressure head (m)
$v^2/2g$ = velocity head (m^{-1})
z = elevation above a reference point (m)

Owing to the very low flow velocities of water in soil, the velocity head can for most practical purposes be ignored (Todd, 1980). The hydraulic head can now be

expressed:

$$H = P/\gamma_w + z$$

Resolving for P (pore water pressure (u)):

$$P = \gamma_w(H - z) \quad \text{(Pa)}$$

A2.2 Construction and Installation

A2.2.1 Materials

19mm diameter PVC pipe
Hacksaw
Geotextile cloth (Bidim U14)
Scissors
Felt pen
Tape measure
19mm diameter caps
Water container
Auger
Bentonite pellets
Masking tape

A2.2.2 Construction

PVC pipe was cut to the desired length and then slots were cut at 1cm intervals to a distance of 0.15m from one end. The slotted portion was then wrapped with geotextile cloth (see figures A2.2) and fixed with masking tape, while air slots were sawn into the other end to maintain atmospheric pressure in the PVC pipe.

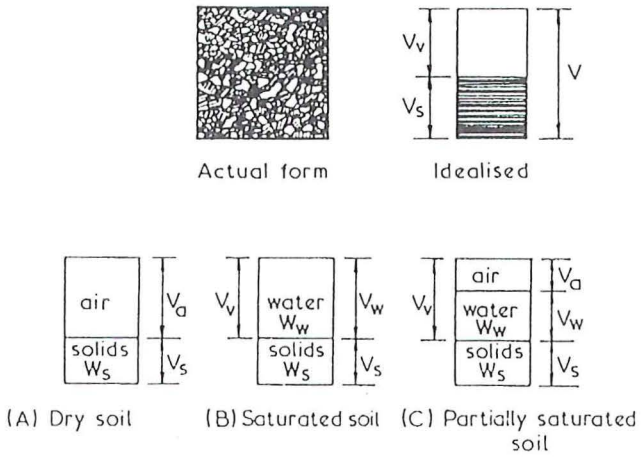

Figure A2.1 The composition of a natural soil (after Hanna, 1985)

Figure A2.2 Slotted end of piezometer wrapped in geotextile

A2.2.3 Installation

Existing auger holes were used to house at least one piezometer in each group of piezometers. Sand was placed in the annular space around the geotextile covered tip as shown in figure A2.3, to prevent clay infiltrating the piezometer. A seal was formed above the sand with rammed bentonite pallets and water, while the remaining void space was back filled with soil.

A2.2.4 Measurement of Piezometeric Level

Measurements of water depths were achieved using a mild steel probe with two well insulated graduated electrical wires fixed to its surface and connected to a multimeter (see figure A2.4). All measurements were referenced to the top of the PVC tubing, while water depths were recorded when the electrical circuit was closed (registered on continuity meter) upon contact with the water.

A2.3 Accuracy

Although the permeability of the fine grained poorly sorted sand filter was not determined, Vaughan (1969) suggests the filter can be in the order of ten times more permeable than the soil before the pore pressure is significantly influenced. Hence the filters are assumed to have negligible effect on measured pore pressures.

Initial equalisation of pore pressures around a borehole piezometer are subject to a time lag known as the initial response time (Vaughan, 1973). Vaughan (1973) shows that the initial response time for a Casagrande type piezometer with a sand filter in clay is approximately 50 days. Although no experimentation was conducted, it is believed that the response time would be somewhat less in silt.

If pore water pressures are to be monitored with the Casagrande-type piezometer, the pressures must be above atmospheric. In partly saturated soils with negative pore water pressures, the Casagrande-type piezometer is useless. However, in partly saturated soils with positive pore pressures and the sand filter equalised to the pore

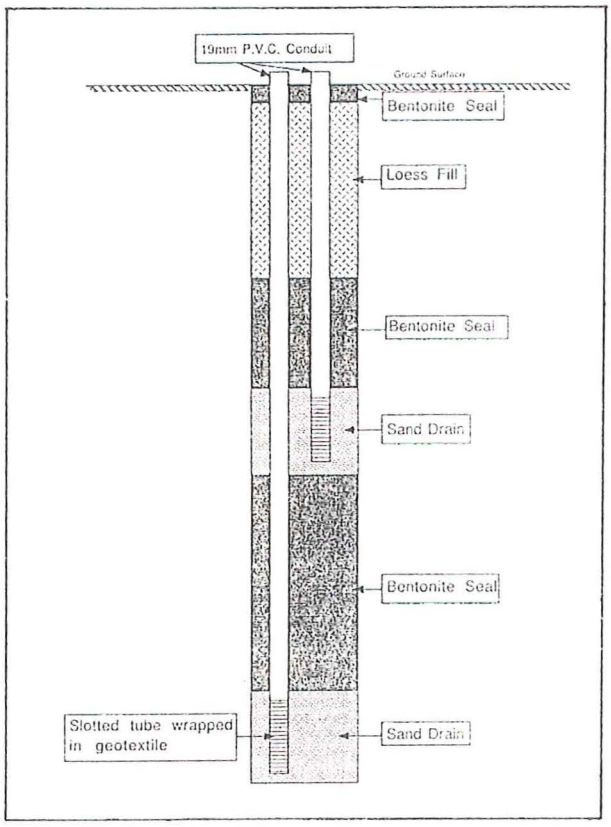

Figure A2.3 Schematic drawing of piezometer installation

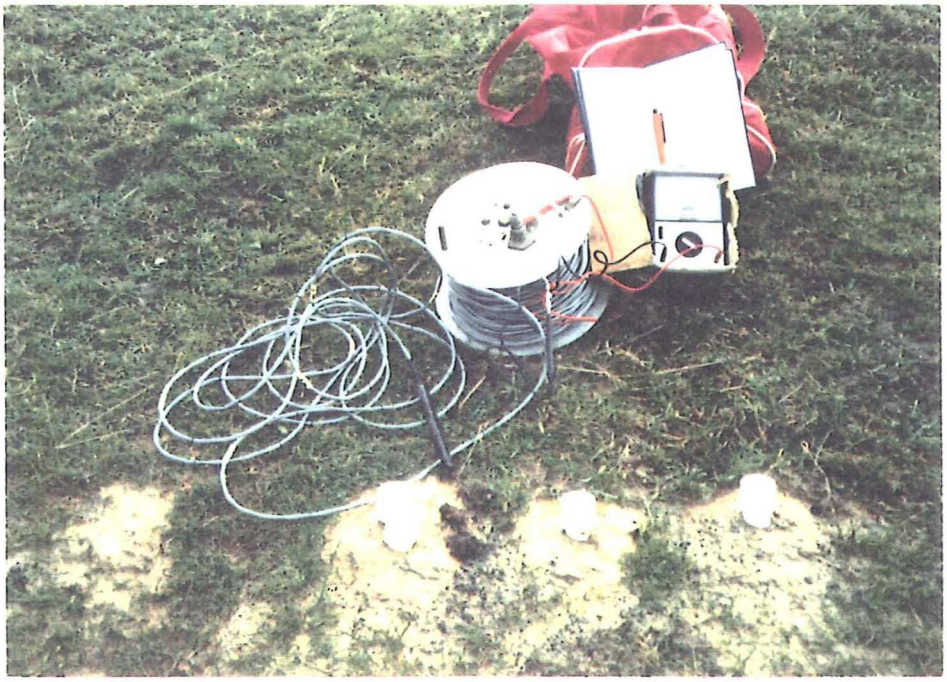

Figure A2.4 Electrical equipment used to measure water level. Multimeter wired to a normally open switch. Switch closes when in contact with water.

water pressure and with suitable de-airing of the sand filter, pore water pressures may be measured. Vaughan (1973) suggests that with a clean open standpipe of sufficient diameter (12mm or greater), the system is self de-airing. On this basis, it was felt that the positive pore water pressures have been monitored accurately by the Casagrande-type piezometer.

Reading accuracy of the graduated electrical wire probe was considered to be in the order of ±3mm when accounting for slight displacements in marking depth and reflex delays between marking depth and noting deflection on the continuity meter. This inaccuracy amounts to a fixed error of ±14.7 Pa, which would effect the accuracy of shorter hydraulic heads more than large heads.

A2.4 Results

Piezometer Group 1

(Pore water pressure = kPa)

Date	2.0	1.3	0.5	4.2
Actual depth	(1.99m)	(1.27m)	(0.47m)	(4.16m)
14/06/89			(FILLED)	
16/07/89	0	11.527	3.924	0.196
23/07/89	0	10.399	3.139	0.785
26/07/89	0	7.357	0.588	0.588
30/07/89	0	5.405	0	0.588
06/08/89	0	5.278	0	0.549
18/08/89	0	9.467	2.178	0.588
20/08/89	0	8.289	1.030	0.559
03/09/89	0	6.965	0.245	0.981
12/09/89	0	9.790	2.639	1.069
13/09/89	0	8.878	1.677	1.128
14/09/89	0	11.174	3.767	1.207
15/09/89	0	11.791	4.306	1.207
16/09/89	0	11.252	4.091	1.373
17/09/89	0	9.673	2.963	1.383
18/09/89	0	8.839	1.913	1.383
19/09/89	0	8.289	1.226	1.521
20/09/89	0	7.465	0.932	1.589
21/09/89	0	6.867	0.422	1.569
22/09/89	0	7.220	0.186	1.560
24/09/89	Filled	6.072	0	1.560
25/09/89	2.237	5.768	0	1.471
26/09/89	1.177	5.523	0	1.550
27/09/89	0	5.395	0	1.540
28/09/89	0	5.199	0	1.481
29/09/89	0	4.983	0	1.501
15/10/89	0	6.504	0	1.952
18/10/89	0	8.584	0.657	2.050
19/10/89	0	9.202	2.079	2.050
20/10/89	0	8.319	1.157	2.138
22/10/89	0	8.927	1.050	2.060
23/10/89	0	11.566	3.944	2.237
24/10/89	0	10.536	3.394	2.227
25/10/89	0	7.917	1.854	2.129
26/10/89	0	6.798	0.853	2.119
27/10/89	0	6.435	0.206	2.138
07/11/89	0	3.983	0	1.942
13/01/90	0	2.148	0	1.461
31/01/90	0	0.775	0	1.295

Piezometer Group 2

(Pore water pressure = kPa)

Date	1.4	2.68
Actual depth	1.4m	2.65m
14/06/89	Filled	
16/07/89	6.180	6.671
23/07/89	10.349	6.720
26/07/89	7.877	6.474
30/07/89	5.984	6.376
06/08/89	6.043	6.190
18/08/89	9.800	5.925
20/08/89	8.279	5.935
03/09/89	7.975	5.729
12/09/89	10.585	5.592
13/09/89	10.026	5.572
14/09/89	10.506	5.503
15/09/89	10.997	5.533
16/09/89	11.046	5.533
17/09/89	11.017	5.513
18/09/89	9.839	5.454
19/09/89	9.388	5.493
20/09/89	8.672	5.493
21/09/89	7.730	5.454
22/09/89	8.191	5.454
24/09/89	6.435	5.454
25/09/89	6.278	5.395
26/09/89	6.209	5.395
27/09/89	5.945	5.395
28/09/89	5.592	5.366
29/09/89	5.317	6.357
15/10/89	6.396	5.493
18/10/89	7.995	5.493
19/10/89	9.957	5.513
20/10/89	9.025	5.543
22/10/89	8.623	5.503
23/10/89	10.673	5.650
24/10/89	10.840	5.601
25/10/89	8.633	5.582
26/10/89	7.465	5.621
27/10/89	6.720	5.611
07/11/89	3.012	6.543
13/01/90	0	4.895
31/01/90	0	4.630

Piezometer Group 3

(Pore water pressure = kPa)

Date	1.16	2.7
Actual depth	1.14m	2.69m
14/06/89	Filled	
16/07/89	9.81	0
23/07/89	9.731	0
26/07/89	7.377	0
30/07/89	5.778	0
06/08/89	5.101	0
18/08/89	9.408	0
20/08/89	8.417	0
03/09/89	7.534	0
12/09/89	9.800	0
13/09/89	9.663	0
14/09/89	9.604	0
15/09/89	9.702	0
16/09/89	9.947	0
17/09/89	9.800	0
18/09/89	9.604	0
19/09/89	9.349	0
20/09/89	8.947	0
21/09/89	8.015	0
22/09/89	8.623	0
24/09/89	6.612	Filled
25/09/89	6.023	1.844
26/09/89	5.680	1.079
27/09/89	5.376	0
28/09/89	5.042	0
29/09/89	4.738	0
15/10/89	6.504	0
18/10/89	8.230	0
19/10/89	9.064	0
20/10/89	8.691	0
22/10/89	8.279	0
23/10/89	9.496	0
24/10/89	9.623	0
25/10/89	8.701	0
26/10/89	7.328	0
27/10/89	6.602	0
07/11/89	2.825	0
13/01/90	0.098	0
31/01/90	0	0

Piezometer Group 4
(Pore water pressure = kPa)

Date	6.0
Actual depth	6.0m
14/06/89	Filled
16/07/89	0.883
23/07/89	0.637
26/07/89	0.637
30/07/89	1.746
06/08/89	1.128
18/08/89	0.736
20/08/89	0.726
03/09/89	4.169
12/09/89	5.954
13/09/89	5.827
14/09/89	5.817
15/09/89	Buried
16/09/89	Buried
17/09/89	6.769
18/09/89	7.554
19/09/89	8.319
20/09/89	9.290
21/09/89	9.339
22/09/89	9.535
24/09/89	8.652
25/09/89	8.368
26/09/89	8.535
27/09/89	8.603
28/09/89	8.073
29/09/89	7.259
15/10/89	4.659
18/10/89	4.748
19/10/89	4.669
20/10/89	4.414
22/10/89	4.659
23/10/89	5.297
24/10/89	5.435
25/10/89	5.042
26/10/89	5.179
27/10/89	5.307
07/11/89	3.953
13/01/90	0
31/01/90	0

Piezometer Group 7
(Pore water pressure = kPa)

Date	0.4	2.3
Actual depth	0.36m	2.28m
14/06/89	Filled	
16/07/89	2.992	6.180
23/07/89	2.678	8.878
26/07/89	0	6.229
30/07/89	0	2.992
06/08/89	0	2.197
18/08/89	1.746	6.867
20/08/89	0.598	5.376
03/09/89	0	2.354
12/09/89	1.923	7.151
13/09/89	0.873	6.239
14/09/89	3.335	6.190
15/09/89	3.325	8.387
16/09/89	3.276	9.250
17/09/89	2.021	8.142
18/09/89	0.922	6.916
19/09/89	0.118	6.062
20/09/89	0	4.493
21/09/89	0	2.737
22/09/89	0	1.540
24/09/89	0	0.942
25/09/89	0	0.883
26/09/89	0	0.873
27/09/89	0	0.824
28/09/89	0	0.657
29/09/89	0	0.422
15/10/89	0	1.717
18/10/89	2.943	1.344
19/10/89	1.422	4.552
20/10/89	0.402	5.081
22/10/89	2.992	2.698
23/10/89	3.394	5.748
24/10/89	2.315	8.338
25/10/89	0.186	5.856
26/10/89	0	3.600
27/10/89	0	2.541
07/11/89	0	0.225
13/01/90	0	0
31/01/90	0	0

Piezometer Group 8

(Pore water pressure = kPa)

Date	1.28	2.00
Actual depth	1.25m	1.96m
14/06/89	Filled	
16/07/89	6.376	0
23/07/89	5.660	0
26/07/89	4.198	0
30/07/89	2.178	0
06/08/89	0.853	0
18/08/89	4.404	0
20/08/89	4.218	0
03/09/89	2.452	0
12/09/89	4.159	0
13/09/89	3.747	0
14/09/89	4.709	0
15/09/89	5.405	0
16/09/89	3.924	0
17/09/89	2.364	0
18/09/89	1.972	0
19/09/89	1.736	0
20/09/89	1.216	0
21/09/89	1.373	0
22/09/89	2.560	0
24/09/89	0.569	Filled
25/09/89	0.284	0
26/09/89	0.059	0
27/09/89	0.049	0
28/09/89	0.039	0
29/09/89	0	0
15/10/89	0.569	0
18/10/89	0.785	0
19/10/89	2.286	0
20/10/89	2.433	0
22/10/89	1.815	0
23/10/89	3.188	0
24/10/89	3.345	0
25/10/89	1.687	0
26/10/89	0.853	0
27/10/89	0.549	0
07/11/89	0	0
13/01/90	0	0
31/01/90	0	0

Appendix 3
Rain Fall Data

A3.1 Monthly totals (1940 - 1988)

Allandale Rain Station

(mm)

	Jan	Feb	Mar	Apr	May	Jun	Jul	Aug	Sep	Oct	Nov	Dec	YR
1940:	152	33	22	100	345	40	95	62	140	30	93	16	1128
1941:	34	47	174	115	47	202	34	325	62	57	35	98	1230
1942:	54	66	35	18	253	10	148	23	71	40	47	53	818
1943:	100	82	34	20	58	170	96	117	131	110	14	4	936
1944:	28	135	92	155	151	93	88	47	101	60	99	185	1234
1945:	52	180	75	47	403	153	163	147	45	73	18	105	1461
1946:	37	22	44	45	143	124	71	75	196	119	122	100	1098
1947:	63	87	77	57	51	216	29	65	72	162	11	26	916
1948:	102	76	26	99	90	48	55	15	48	35	105	11	710
1949:	61	19	101	38	56	85	85	38	10	18	22	61	594
1950:	86	114	74	49	38	67	119	106	9	197	48	111	1018
1951:	166	168	141	227	176	88	110	59	23	148	25	141	1472
1952:	55	29	27	25	105	74	28	164	67	120	141	44	879
1953:	157	60	82	97	101	76	112	94	52	152	31	78	1092
1954:	13	47	58	57	89	56	145	125	25	14	49	41	719
1955:	27	85	15	25	94	176	169	25	33	23	30	14	716
1956:	47	19	68	50	196	40	149	52	113	59	81	67	941
1957:	28	25	108	49	252	47	138	40	84	71	61	82	985
1958:	69	39	38	120	57	52	28	51	15	33	26	34	562
1959:	39	50	46	126	264	10	45	12	7	43	14	52	708
1960:	37	26	171	22	14	141	50	43	32	71	37	171	815
1961:	148	55	55	26	90	49	174	145	104	2	45	17	910
1962:	41	119	70	114	86	110	47	93	26	37	102	57	902
1963:	55	134	60	122	36	80	186	78	53	25	78	116	1023
1964:	8	22	48	52	70	18	139	112	58	31	70	27	655
1965:	60	33	156	70	80	114	142	96	83	67	157	14	1072
1966:	42	38	74	58	80	62	40	67	33	26	113	60	693
1967:	103	34	35	40	105	38	25	46	115	41	108	34	724
1968:	67	53	43	375	65	83	130	55	58	45	70	60	1104
1969:	72	10	4	67	108	74	60	42	34	55	15	51	592
1970:	60	30	152	33	148	118	142	55	66	66	36	19	925
1971:	65	17	27	20	80	111	106	39	47	73	41	20	646
1972:	65	31	41	64	89	104	74	68	26	114	29	44	749
1973:	40	26	31	29	60	38	76	175	45	34	40	31	625
1974:	23	96	68	188	CLOSED								

Living Springs Rain Station

(mm)

	Jan	Feb	Mar	Apr	May	Jun	Jul	Aug	Sep	Oct	Nov	Dec	YR
1978:											47	242	
1979:	33	48	186	24	113	24	197	215	97	145	52	41	1175
1980:	214	129	127	73	16	98	78	115	5	14	89	70	1028
1981:	39	12	59	67	48	147	88	209	30	88	53	26	866
1982:	28	39	26	77	42	82	115	40	45	178	52	115	839
1983:	32	25	22	168	198	98	273	83	165	62	39	98	1263
1984:	111	70	123	34	83	24	141	28	93	44	103	85	939
1985:	12	96											
1986:									42	144	210	28	
1987:	9	160	77	51	76	87	45	21	30	63	61	57	737
1988:	35	51	52	24	59	58	41	64	11	11			

A3.2 Daily Rain Fall Data (Feb 1989 - Jan 1990)

Living Springs Rain Station

(mm)

Date	Feb	Mar	Apr	May	Jun	Jul	Aug	Sep	Oct	Nov	Dec	Jan
1		0.3		3.0	1.0	0.5	0.2	1.1				0.1
2				0.3	16.0							
3	7.0			13.3	7.0				0.4			
4	3.3	3.2		22.8	5.5				17.1		13.5	
5	22.5							0.3	8.2		0.2	2.1
6	0.2					0.5			7.1		0.1	
7	0.3			3.3				7.1	2.5			
8			0.4	12.1	0.2			19.5	36.9			5.6
9				0.1	0.8			2.0				0.1
10		6.6	26.5		1.0		2.2	2.1				
11		7.2	14.6		0.5	1.4	2.9	0.7	2.1			
12	0.2	0.1	0.1		9.0	16.2	7.5	0.2	0.2			
13		0.5			6.0	0.3	9.2	9.7				0.3
14		0.1				3.4	11.5	17.1				
15	1.2		6.2	0.4		3.4	10.5	0.3	0.1			
16		0.3	0.1		5.0	6.7	5.5					
17	3.6	0.2		17.8					49.5		46.5	3.4
18				0.1		12.3			0.1		0.1	0.1
19					2.0	52.8			0.6	14.6		
20		6.1		5.8	5.0	34.4		0.6		2.2		
21	3.0	0.1		8.4	11.5	6.6	1.0	5.6	24.6	0.2		
22	0.5			7.1	15.5	1.0	0.2	0.1	42.6		1.6	
23	2.9	2.0					7.9		0.5	9.5	12.9	0.9
24				1.0	6.0		1.4		0.6		3.9	
25				2.5	1.5					9.8		
26				10.2	2.0					8.0		
27	6.8			21.6			27.1			2.6		
28	3.9	5.8		20.2	5.0		0.6			0.6		
29	-	7.0	20.0	23.2	4.5		1.4		0.9			
30	-	1.8	3.0	0.3					0.9			
31	-	0.3	-	0.1	-		1.1	-		-	1.1	
MONTHLY TOTALS												
	55	42	71	174	105	140	90	66	195	40	80	18

Appendix 4

LABORATORY TESTING

A4.1 Particle size distribution curves

PARTICLE SIZE DISTRIBUTION — SEMI LOG PLOT

PROJECT ..... SAMPLE NO ...2/CA..... SAMPLED BY ..... ANALYSED BY .....

..... LOCATION ..... DATE ..... DATE .....

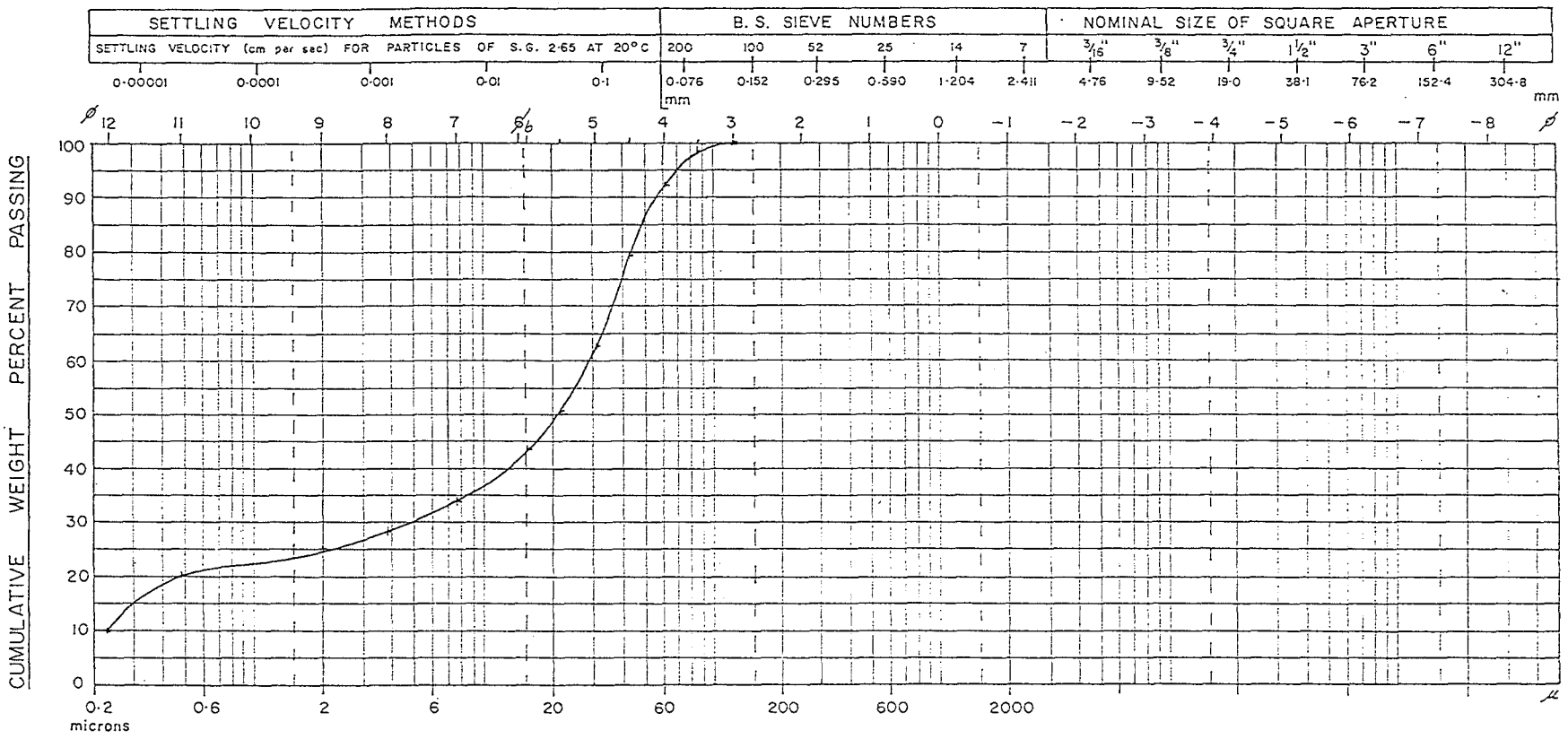

PARTICLE SIZE AND CLASSIFICATION

PARTICLE SIZE DISTRIBUTION — SEMI LOG PLOT

PROJECT ..... SAMPLE NO 1/P2 ..... SAMPLED BY ..... ANALYSED BY .....

..... LOCATION ..... DATE ..... DATE .....

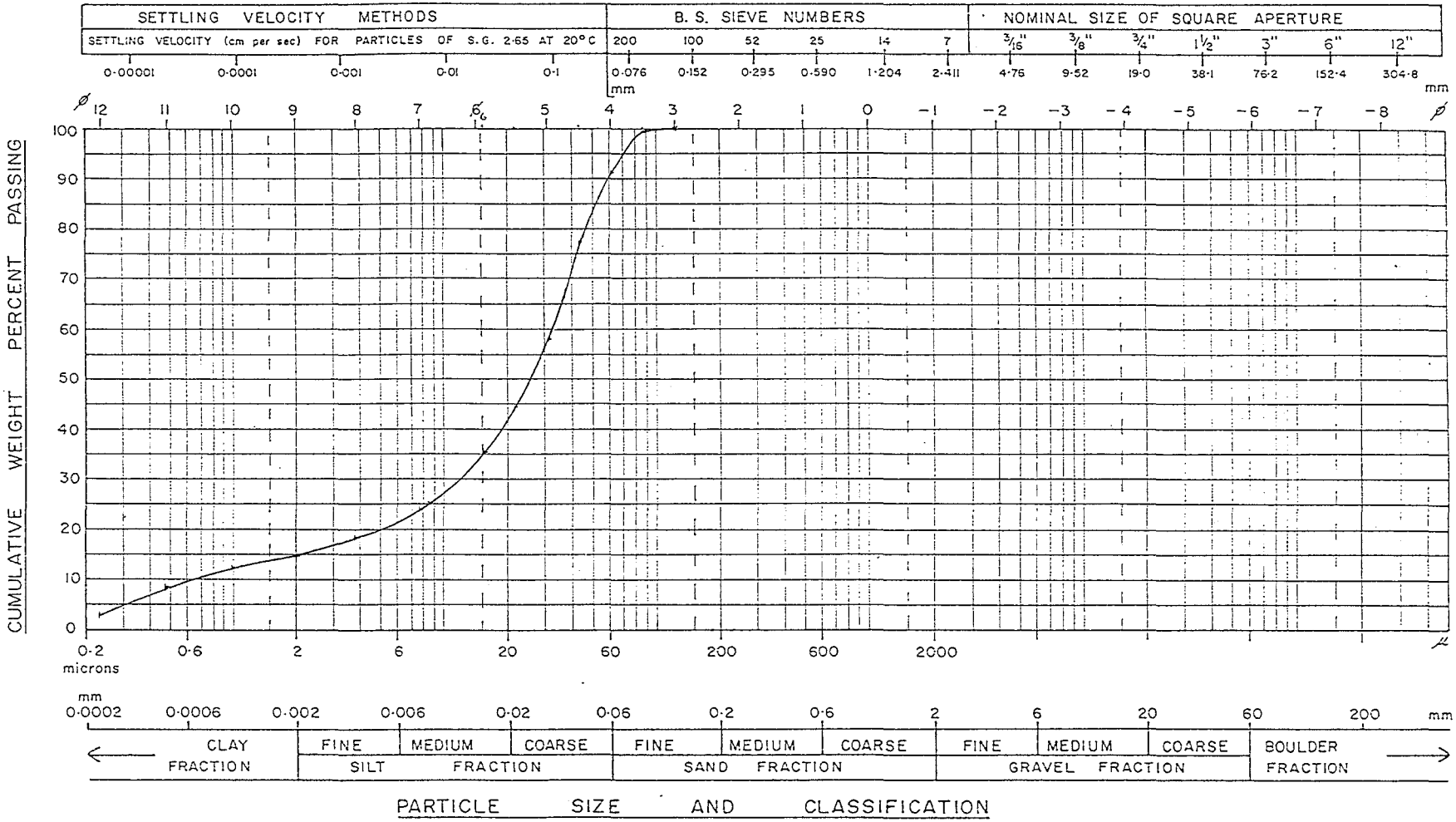

PARTICLE SIZE AND CLASSIFICATION

PARTICLE SIZE DISTRIBUTION — SEMI LOG PLOT

PROJECT ..... SAMPLE NO P remoulded ..... SAMPLED BY ..... ANALYSED BY .....

..... LOCATION ..... DATE ..... DATE .....

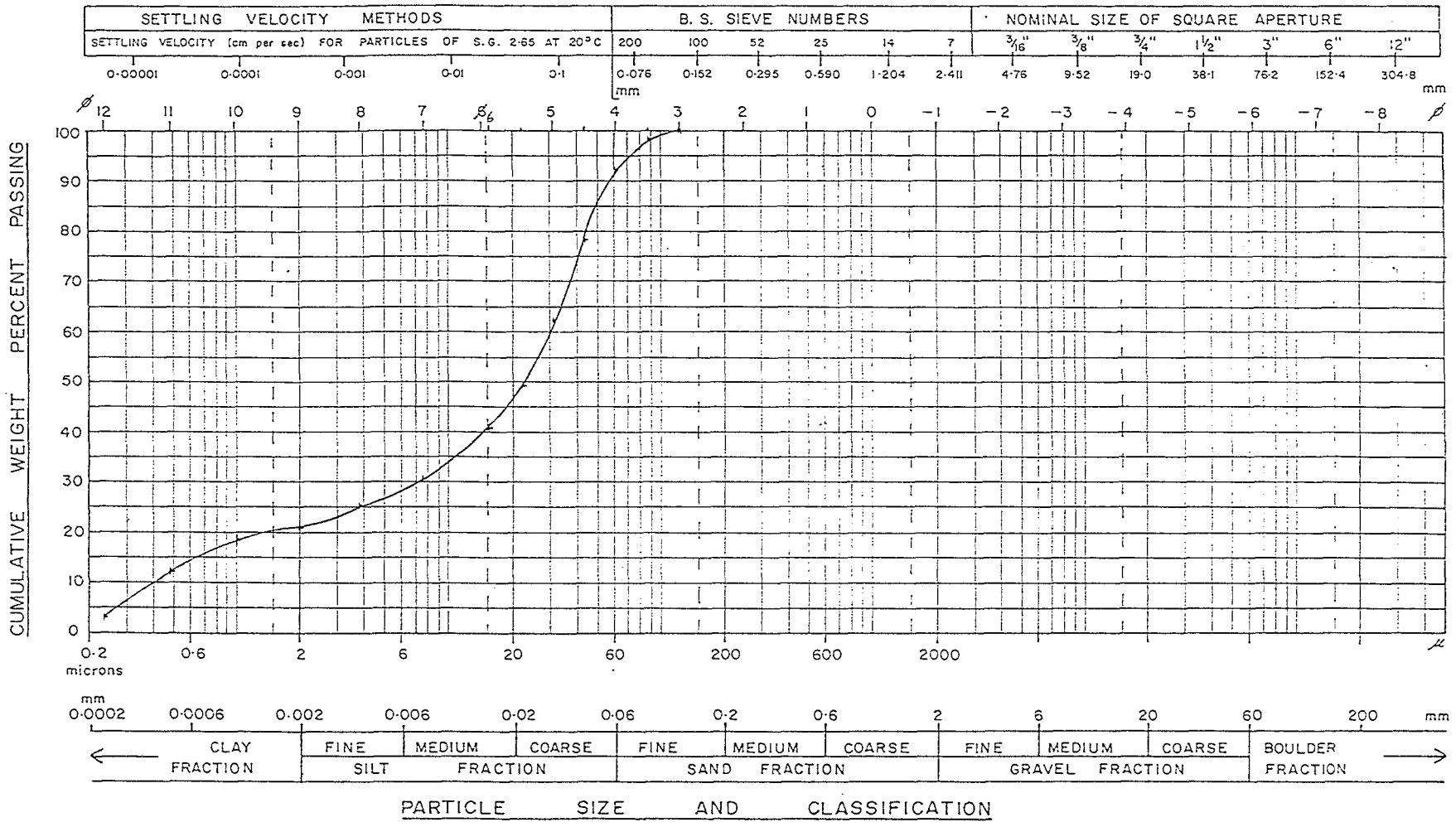

PARTICLE SIZE AND CLASSIFICATION

PARTICLE SIZE DISTRIBUTION — SEMI LOG PLOT

PROJECT ..... SAMPLE NO 1/P1 ..... SAMPLED BY ..... ANALYSED BY .....

..... LOCATION ..... DATE ..... DATE .....

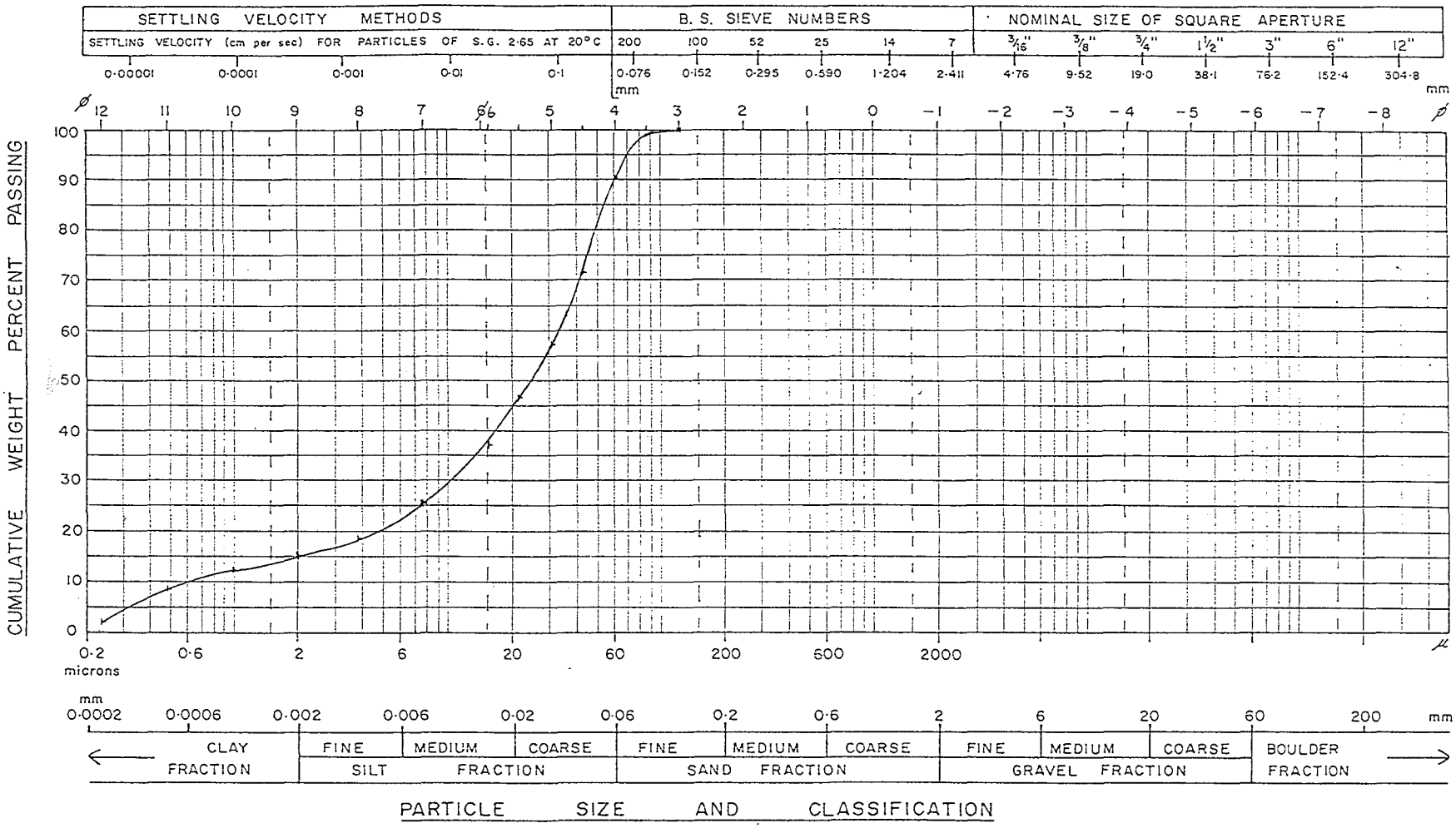

PARTICLE SIZE AND CLASSIFICATION

PARTICLE SIZE DISTRIBUTION — SEMI LOG PLOT

PROJECT ..... SAMPLE NO 1/C.B. ..... SAMPLED BY ..... ANALYSED BY .....

..... LOCATION ..... DATE ..... DATE .....

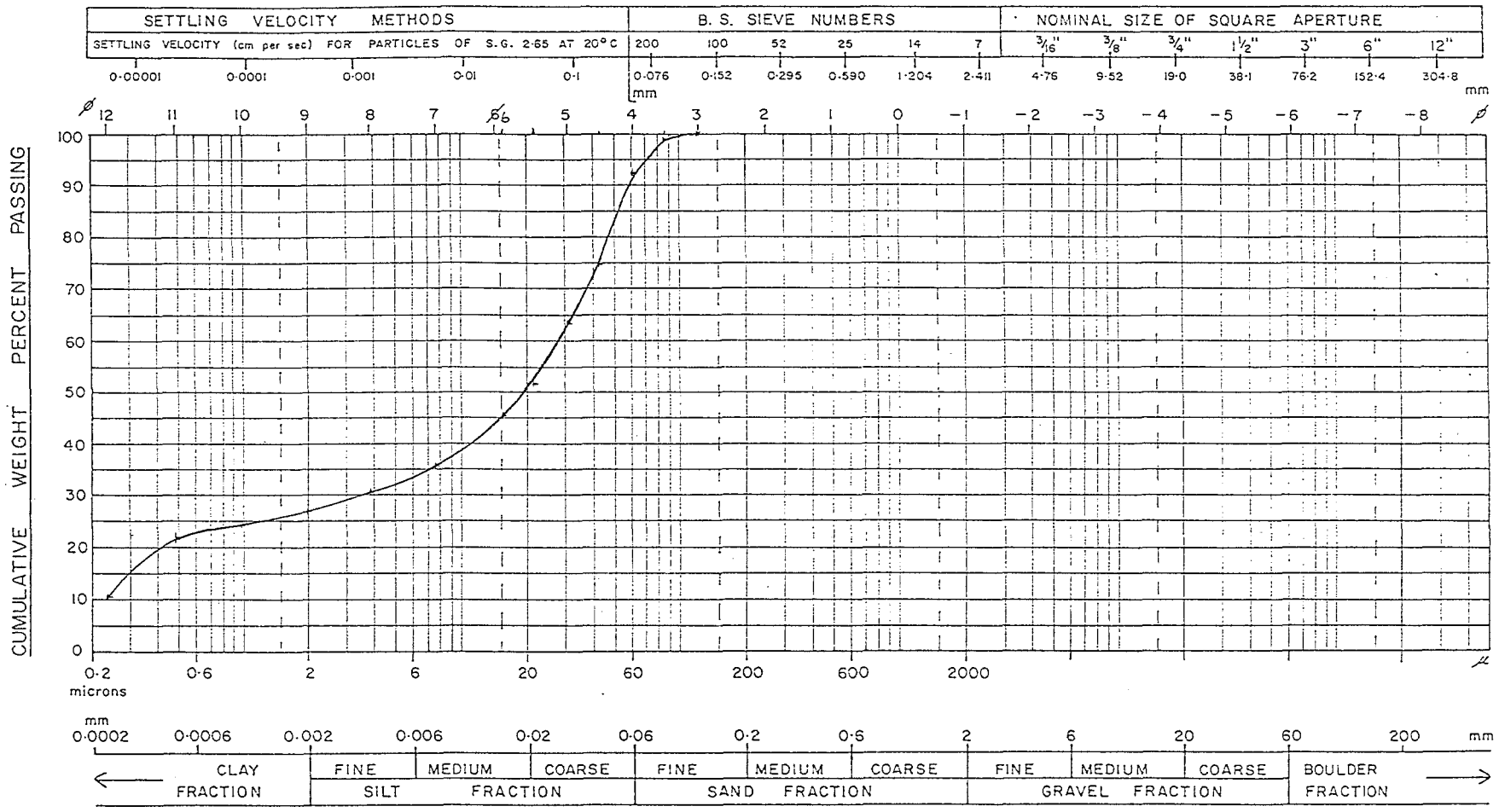

PARTICLE SIZE AND CLASSIFICATION

PARTICLE SIZE DISTRIBUTION — SEMI LOG PLOT

PROJECT ..... SAMPLE NO C. remoulded ..... SAMPLED BY ..... ANALYSED BY .....

..... LOCATION ..... DATE ..... DATE .....

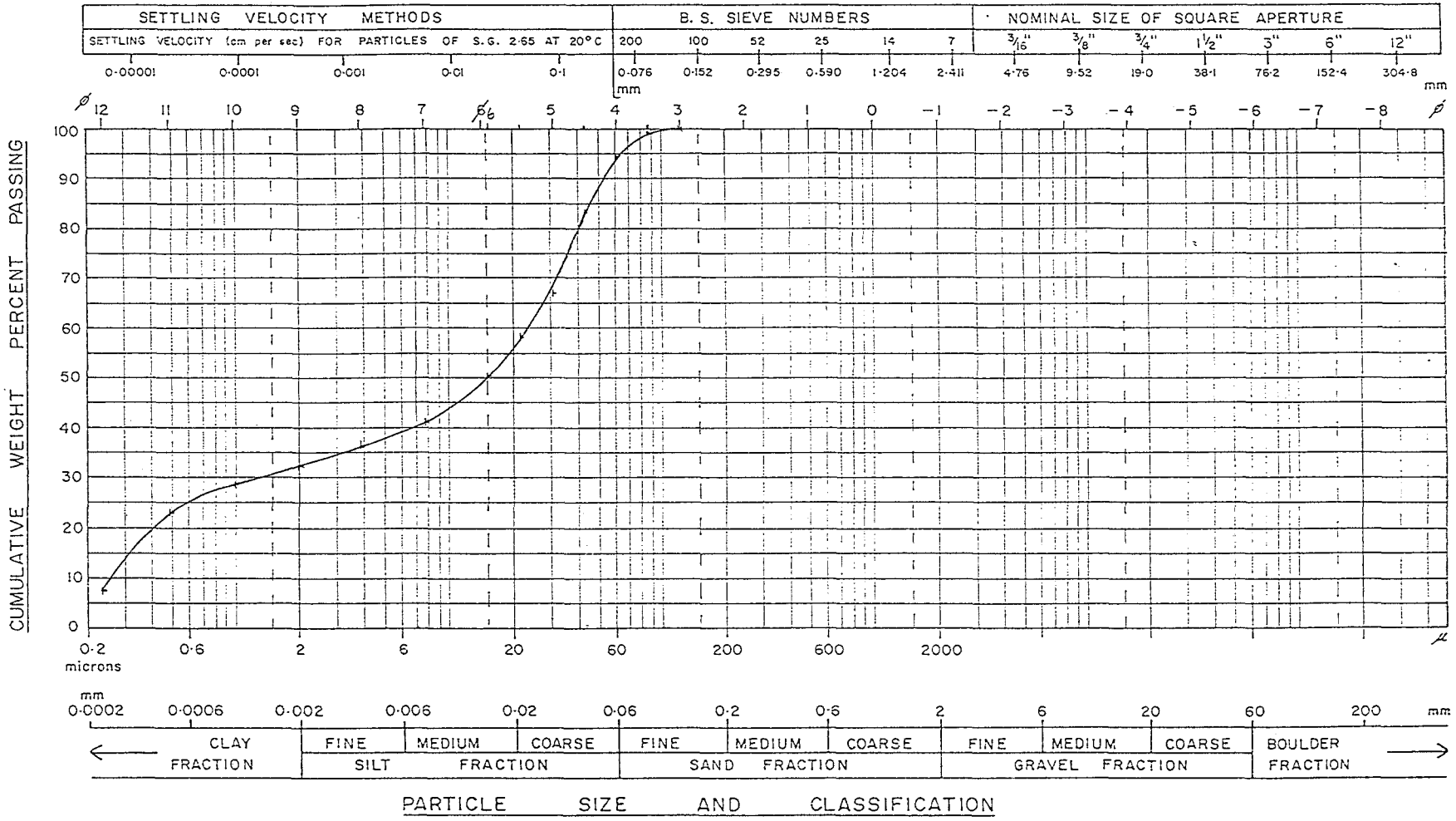

PARTICLE SIZE AND CLASSIFICATION

PARTICLE SIZE DISTRIBUTION — SEMI LOG PLOT

PROJECT ..... SAMPLE NO. 5/C ..... SAMPLED BY ..... ANALYSED BY .....

..... LOCATION ..... DATE ..... DATE .....

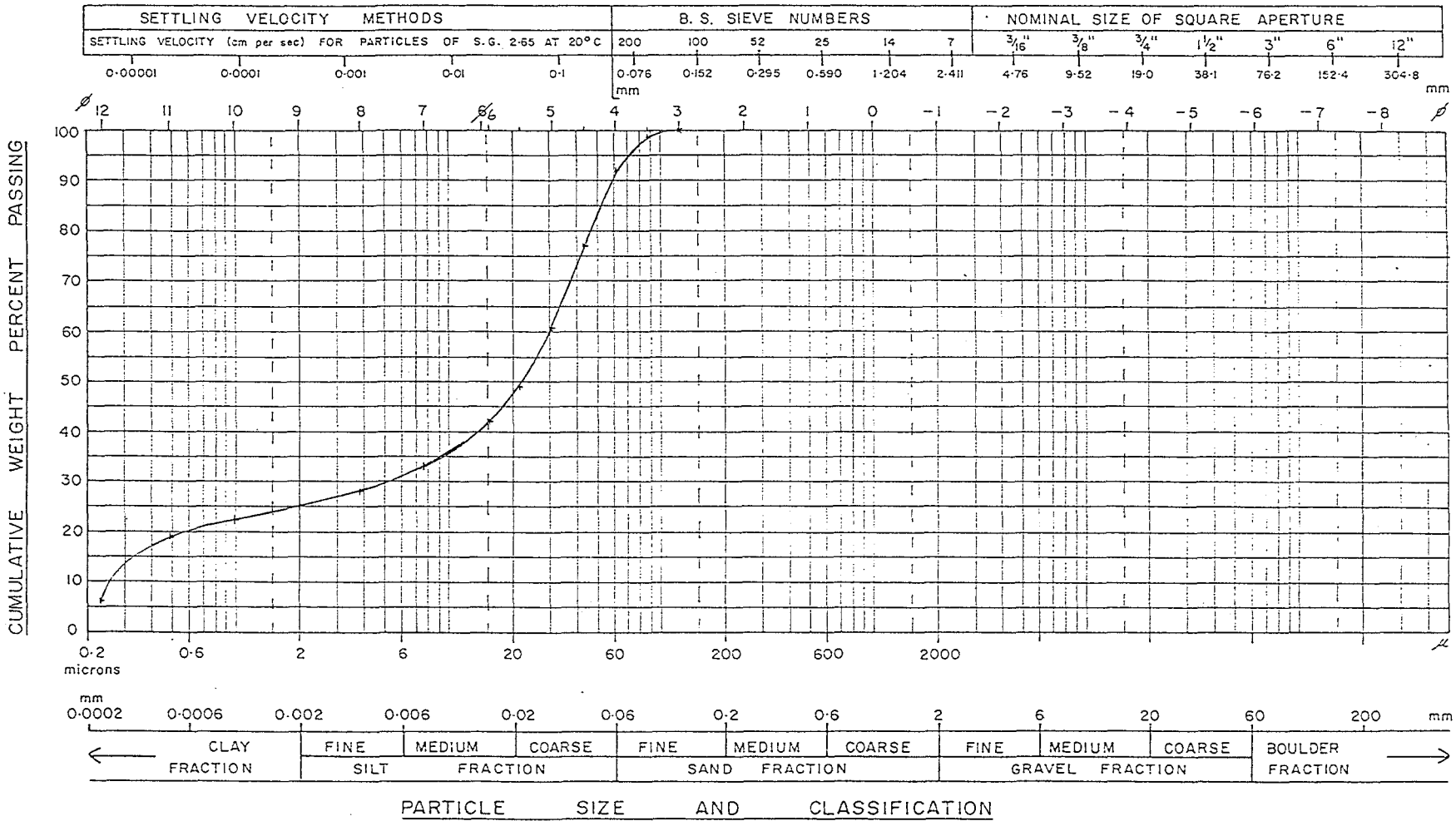

PARTICLE SIZE AND CLASSIFICATION

PARTICLE SIZE DISTRIBUTION — SEMI LOG PLOT

PROJECT ..... SAMPLE NO 1/Tension Crack B... SAMPLED BY ..... ANALYSED BY .....

..... LOCATION ..... DATE ..... DATE .....

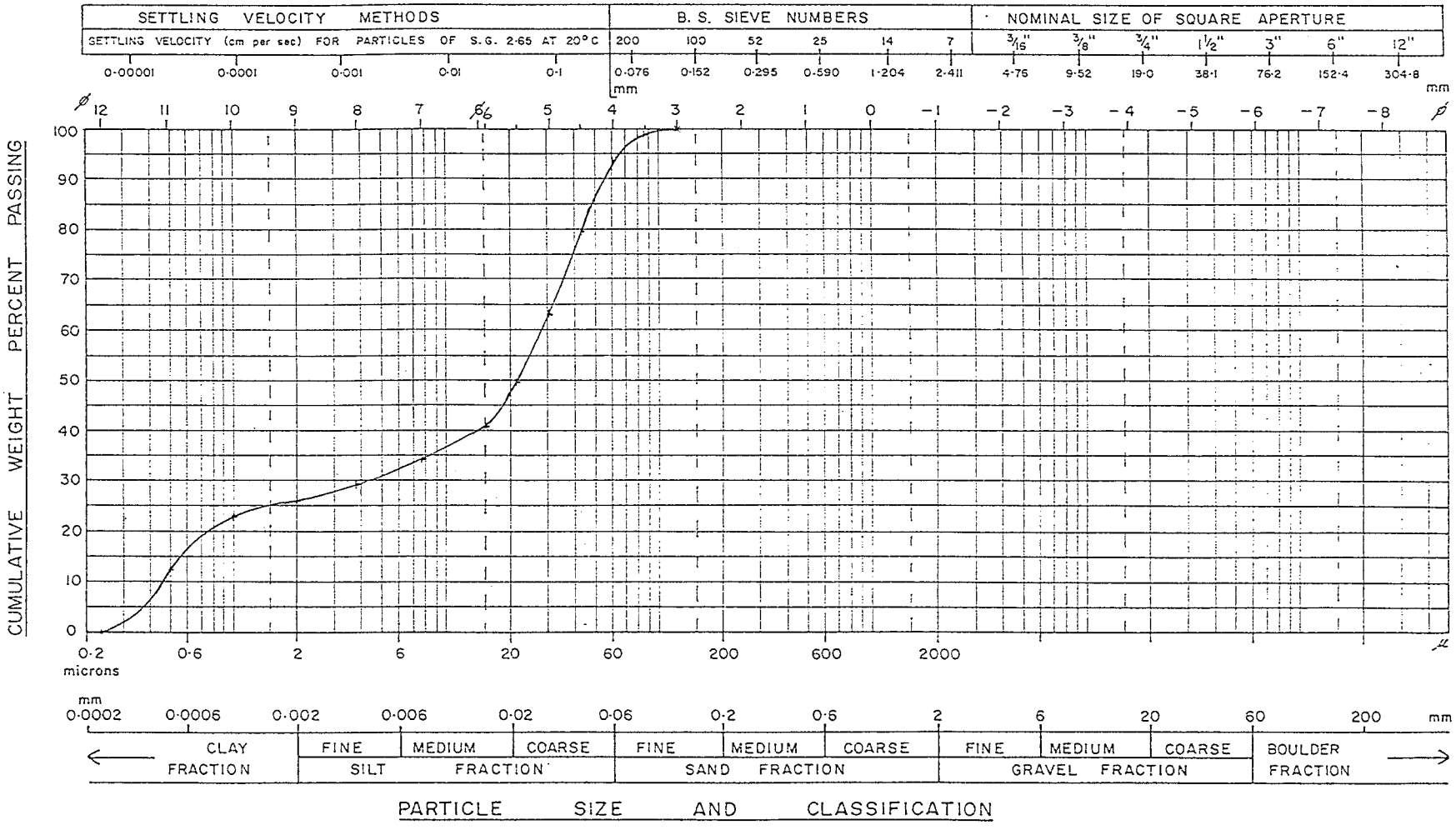

PARTICLE SIZE AND CLASSIFICATION

PARTICLE SIZE DISTRIBUTION — SEMI LOG PLOT

PROJECT ..... SAMPLE NO 1/Tension Crack A. SAMPLED BY ..... ANALYSED BY .....

..... LOCATION ..... DATE ..... DATE .....

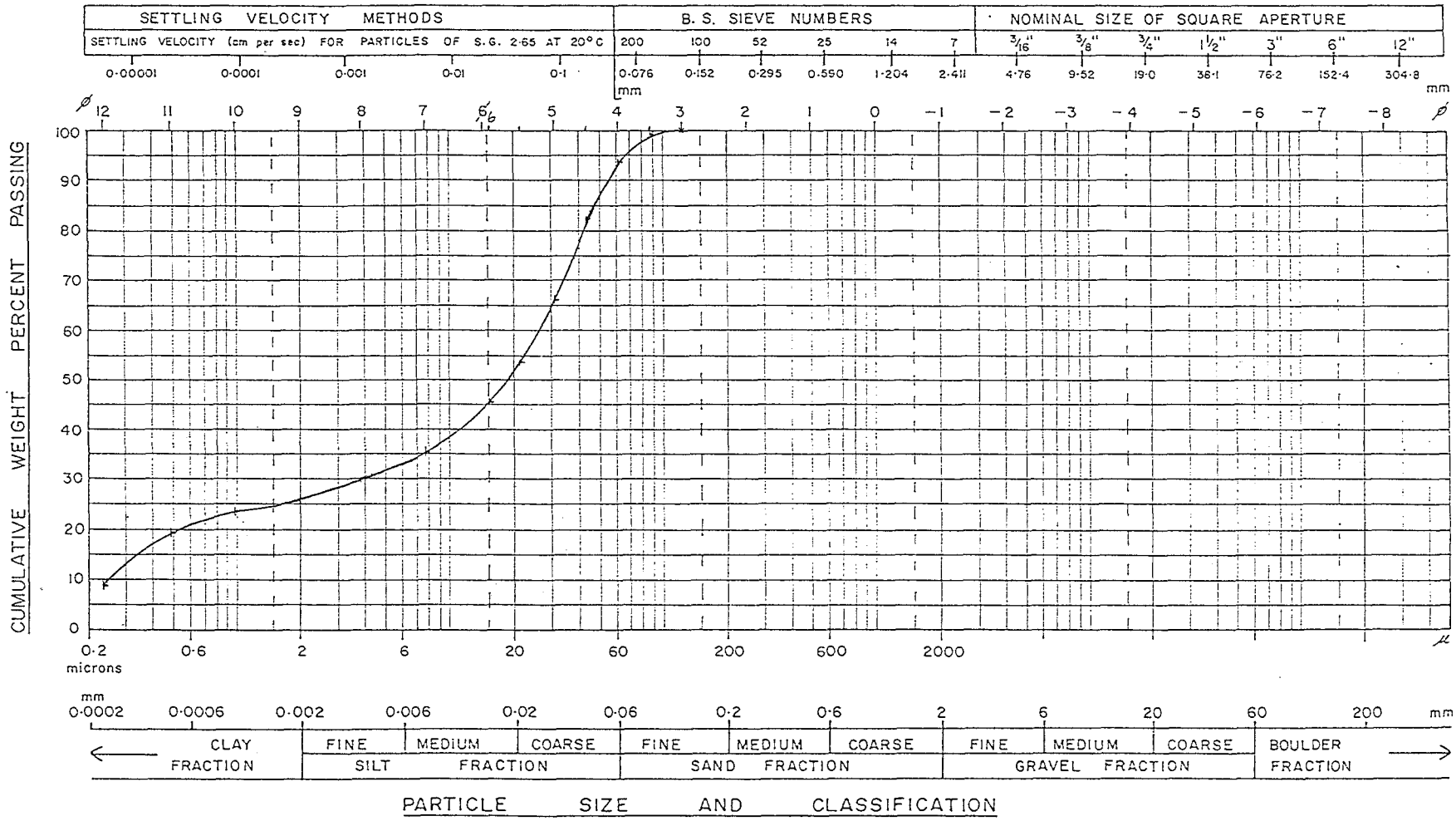

PARTICLE SIZE AND CLASSIFICATION

PARTICLE SIZE DISTRIBUTION — SEMI LOG PLOT

PROJECT ..... SAMPLE NO 2 Pq ..... SAMPLED BY ..... ANALYSED BY .....

..... LOCATION ..... DATE ..... DATE .....

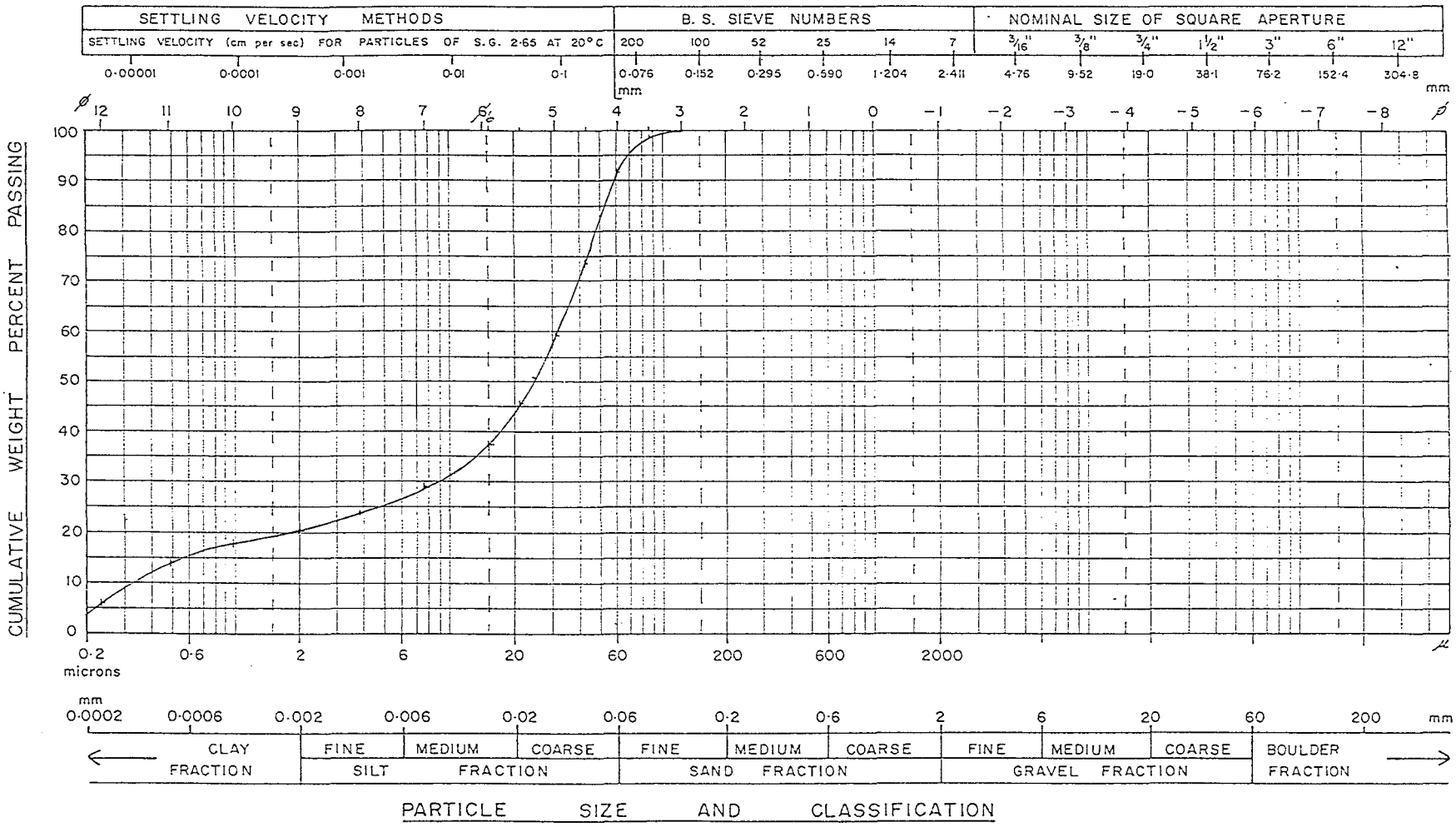

PARTICLE SIZE AND CLASSIFICATION

A4.2 Atterberg limits

Sample Pit	Field moisture Layer	content (%)	Liquid limit	Plastic limit	Plasticity index
1	T/crack	23.7	28.3	18.6	9.7
1	T/crack	25.8	28.8	19.7	9.1
1	C	16.6	24.1	17.6	6.5
1	C	16.8	24.3	16.8	7.5
1	C	17.2	24.8	16.9	7.9
2	C	19.3	28.3	19.3	9.0
2	C	21.0	28.2	19.1	9.1
2	C	19.7	25.9	19.8	6.1
2	C	20.5	26.1	19.9	6.2
5	C	23.7	30.2	19.1	11.1
1	P	19.5	N/A		
2	P		26.1	19.0	7.2
Remoulded	C		25.0	16.4	8.6
Remoulded	P		22.0	16.2	5.8

A4.3.1 In situ densities and moisture contents

Sample Pit / Layer	Bulk (t/m^3) Density	Dry (t/m^3) Density	Moisture Content(%)	Void Ratio	Saturation Ratio
1/T.Crack1	1.98	1.58	24.9	0.71	0.96
1/T.Crack2	2.03	1.63	24.8	0.66	1.01
1/T.Crack3	1.96	1.57	24.8	0.73	0.93
1/T.Crack4	2.02	1.63	23.5	0.66	0.97
1/S1	1.90	1.52	24.9	0.77	0.86
1/S2	1.96	1.59	23.4	0.70	0.90
2/S2	1.83	1.47	24.3	0.84	0.78
1/C1	2.09	1.74	20.3	0.56	0.99
1/C2	2.04	1.71	19.5	0.58	0.90
1/C3	2.14	1.83	17.1	0.48	0.97
1/C4	2.11	1.78	17.7	0.53	0.94
1/C5	2.04	1.68	21.2	0.61	0.94
1/C6	2.10	1.74	21.1	0.55	1.02
1/C7	2.10	1.75	19.8	0.55	0.99
1/C8	2.08	1.79	16.6	0.52	0.87
2/C1	1.99	1.62	22.1	0.66	0.90
1/P1	1.86	1.56	19.3	0.73	0.71
1/P2	1.99	1.71	16.7	0.60	0.77
2/P2	2.07	1.71	20.8	0.58	0.97

A4.3.2 Example Calculations

Formule used for calculating void ratio (e) and saturation ratio (S_r).

$$e = \frac{V - (Ms/Gs)}{(Ms/Gs)}$$

$$Sr = \frac{Mw}{V - (Ms/Gs)}$$

Gs = 2.71 (measured, refer appendix A4.3.3)

Mw = Vw, 1g water = 1ml

Where: V = volume
Ms = mass of solids
Mw = mass of water
Gs = specific gravity

A4.3.3 Specific Gravity Results

Sample	Specific Gravity (Gs)
1/P1a	2.71
1/P1b	2.71
1/P2a	2.67
1/P2b	2.69
1/P2	2.71
1/P1	2.73
1/C5	2.72
1/C3	2.71
1/P3a	2.71
1/P3b	2.72

A4.4.1 Laboratory unconfined compression and vane shear results.

C Layer Tests

ρ_d (t/m^3)	ϵ_f (%)	E_{tan}	w (%)	σ_f (kPa)	s_u (uu) (kPa)	s_u (vane) (kPa)	E	Cure (days)
1.76	8.0	38.0	14.86	171.45	85.73	123.83	15	0
1.76	5.9	71.7	14.82	168.71	84.36		15	10
1.76	4.5	110.3	14.44	216.09	108.04		15	100
1.66	6.6	39.8	14.85	138.71	69.36	96.91	6	0
1.66	5.8	80.0	14.83	155.19	77.59		6	10
1.66	3.7	112.2	14.36	168.31	84.15		6	100
1.65	4.0	26.7	14.09	65.37	32.68	110.37	10	0
1.60	2.5	24.6	14.13	42.48	21.24	80.76	4	0
1.80	5.0	54.6	14.27	158.49	79.24	160.17	40	0
1.63	2.2	148.1	11.87	163.61	81.80		70	0
1.63	2.2	159.9	11.96	197.93	98.96		70	10
1.63	2.7	120.5	12.04	183.06	91.53		70	100
1.46	2.6	41.5	11.93	47.99	23.99	109.03	10	0
1.46	2.6	31.2	12.01	42.22	21.11		10	10
1.46	1.8	333.3	11.75	147.67	73.83		10	100
1.58	1.1	92.9	11.72	53.58	26.79	154.79	20	0
1.64	2.1	47.6	11.66	77.68	38.84		45	0
1.73	2.5	69.5	11.72	154.76	77.38		100	0
1.56	0.9	70.9	11.59	38.21	19.10	100.95	14	0
1.64	1.8	193.9	9.97	241.27	120.63		140	0
1.64	1.8	162.3	9.94	221.14	110.57		140	10
1.64	1.6	470.6	9.98	433.39	216.69		140	100
1.53	2.1	251.3	9.87	247.93	123.96		30	0
1.53	2.0	94.7	9.91	110.46	55.23		30	100
1.49	1.1	63.7	9.49	31.56	15.78	148.06	10	0
1.46	0.8	38.6	9.74	16.18	8.09	121.14	4	0
1.46	0.8	41.4	9.73	19.86	9.93	111.72	6	0
1.76	2.2	161.3	9.73	339.10	169.55		320	0
1.60	0.8	274.5	9.82	142.68	71.34		80	0
1.45	1.0	39.5	7.80	28.63	14.32		10	0
1.45	0.8	199.4	7.77	72.82	36.41		10	10
1.45	1.2	122.7	7.80	85.79	42.89		10	100
1.63	1.4	313.6	7.60	511.24	255.62		140	0
1.63	1.2	343.0	7.70	254.92	127.46		140	10
1.63	1.4	333.3	7.80	270.50	135.25		140	100
1.70	2.1	144.3	7.47	227.88	113.94		300	0
1.54	0.8	145.6	7.84	73.55	36.77		80	0
1.75	16.3	11.8	15.91	138.32	69.16	78.07	6	0
1.75	11.8	30.0	16.20	141.31	70.66		6	10
1.75	10.5	34.3	15.98	139.37	69.68		6	100
1.80	16.5	10.9	15.59	150.75	75.37	72.68	40	0
1.80	15.8	16.6	16.10	170.65	85.32		40	10

ρ_d (t/m^3)	ϵ_f (%)	E_{tan}	w (%)	σ_f (kPa)	s_u (uu) (kPa)	s_u (vane) (kPa)	E	Cure (days)
1.80	13.1	23.7	15.98	177.06	88.53		40	100
1.80	15.2	11.9	15.72	137.39	68.69	75.37	15	0
1.78	15.0	16.4	15.74	145.98	72.99	76.72	10	0
1.73	11.9	13.4	15.81	105.32	52.66	78.07	4	0
1.80	14.5	14.1	15.78	165.57	82.78	72.68	100	0
1.76	19.7	6.5	17.57	85.57	42.78	40.38	6	0
1.76	18.4	7.57	17.40	94.57	47.28		6	10
1.76	17.1	11.6	17.40	99.89	49.94		6	100
1.76	22.3	6.6	17.38	87.51	43.76	43.07	20	0
1.76	21.8	6.5	17.55	83.47	41.73		20	10
1.76	19.7	6.6	17.62	81.55	40.77		20	100
1.76	19.7	7.3	16.91	95.84	47.92	40.38	10	0
1.75	18.4	6.5	17.38	82.29	41.14	41.73	2	0
1.77	19.7	6.8	17.38	89.88	44.94	42.40	15	0
1.68	26.3	2.0	19.62	33.33	16.66	16.15	20	0
1.67	23.7	2.0	19.29	33.39	16.69	17.50	2	0
1.67	32.9	2.2	19.10	34.83	17.42	17.50	6	0
1.63	20.0	2.3	21.88	9.26	4.63	9.42	2	0
1.57	3.9		14.11	71.62	35.81	78.07	0	0
1.65	13.1		16.05	110.10	55.05	68.64	0	0

P Layer Tests

ρ_d (t/m^3)	ϵ_f (%)	E_{tan}	w (%)	σ_f (kPa)	s_u (uu) (kPa)	s_u (vane) (kPa)	E	Cure (days)
1.67	1.5	46.7	9.49	52.38	26.19	153.44	80	0
1.67	1.3	44.4	9.48	45.10	22.55		80	10
1.67	1.2	48.0	9.62	37.76	18.88		80	100
1.80	1.5	126.0	9.42	167.98	83.99		320	0
1.80	1.8	74.4	9.43	118.83	59.42		320	10
1.80	0.9	251.0	9.57	187.54	93.77		320	100
1.75	1.0	105.9	9.44	79.11	39.56		140	0
1.80	1.4	165.8	11.41	125.01	62.51		160	0
1.56	0.8	83.0	11.50	5.52	2.76	72.68	14	0
1.64	0.6	48.2	11.31	19.09	9.54	107.68	45	0
1.74	2.2	69.2	11.37	98.35	49.17	150.75	100	0
1.74	1.8	64.8	11.60	89.39	44.69		100	10
1.74	1.7	76.3	11.59	99.86	49.93		100	100
1.57	1.6	14.1	11.40	16.94	8.47	80.76	20	0
1.57	1.3	19.6	11.60	19.17	9.58		20	10
1.57	2.0	15.2	11.66	16.57	8.28		20	100
1.76	2.8	52.2	13.71	82.33	41.16	100.95	60	0
1.76	2.7	52.8	13.69	99.40	49.70		60	10
1.76	2.3	70.4	13.73	114.84	57.42		60	100
1.61	3.3	17.6	13.66	36.48	18.24	47.78	4	0
1.61	2.6	35.7	13.74	56.79	28.39		4	10
1.61	2.9	26.9	13.75	48.26	24.13		4	100
1.59	2.0	16.6	13.67	21.08	10.54	43.07	2	0

ρ_d (t/m^3)	ϵ_f (%)	E_{tan}	w (%)	σ_f (kPa)	s_u (uu) (kPa)	s_u (vane) (kPa)	E	Cure (days)
1.81	2.2	80.5	13.62	123.03	61.52	137.29	100	0
1.68	1.8	30.3	13.66	34.01	17.0	59.22	15	0
1.62	1.7	18.5	13.55	21.49	10.75	45.76	6	0
1.67	3.1	20.3	14.63	39.06	19.53	57.21	4	0
1.76	4.5	32.4	14.73	91.93	45.96	71.34	15	0
1.86	6.0	49.7	14.62	229.76	114.88	99.60	60	0
1.83	6.2	40.8	14.69	171.89	85.94	94.89	40	0
1.83	4.9	57.0	14.71	183.50	91.75		40	10
1.83	5.0	58.0	14.75	177.51	88.75		40	100
1.71	5.8	25.1	14.63	93.44	46.72	63.93	10	0
1.71	3.9	42.2	14.70	86.58	43.29		10	10
1.71	3.1	43.0	14.69	73.97	36.98		10	100
1.71	20.0	2.2	17.83	31.25	15.62	16.15	2	0
1.70	24.0	1.8	17.82	32.48	16.24	15.48	15	0
1.70	21.0	3.4	17.71	43.84	21.92		15	10
1.70	21.0	3.1	17.89	44.93	22.46		15	100
1.66			19.43			7.67	2	0
1.66			19.47			7.78	6	0
1.63			21.05			3.72	2	0
1.63	4.3		14.84	28.93	14.46	32.30	0	0

A4.4.2 Unconfined compression strength versus axial strain graphs

Results of Unconfined Compression Testing - C layer

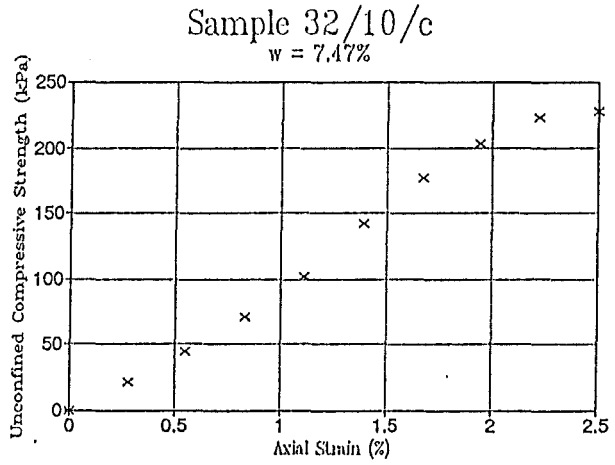

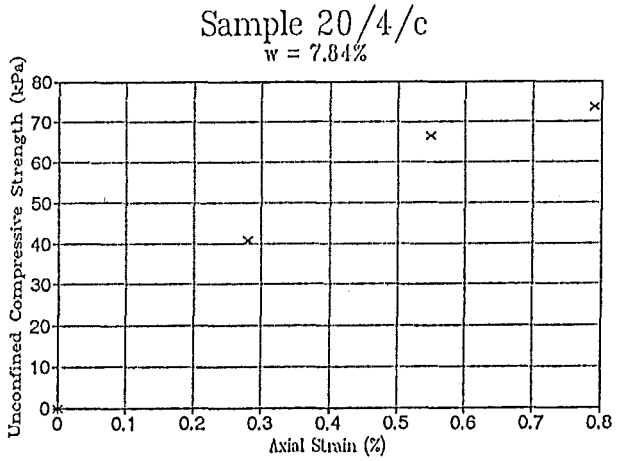

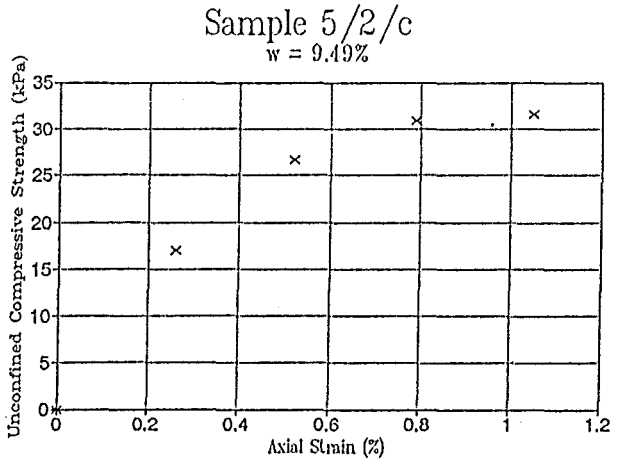

Sample 2/2/c
w = 9.74%

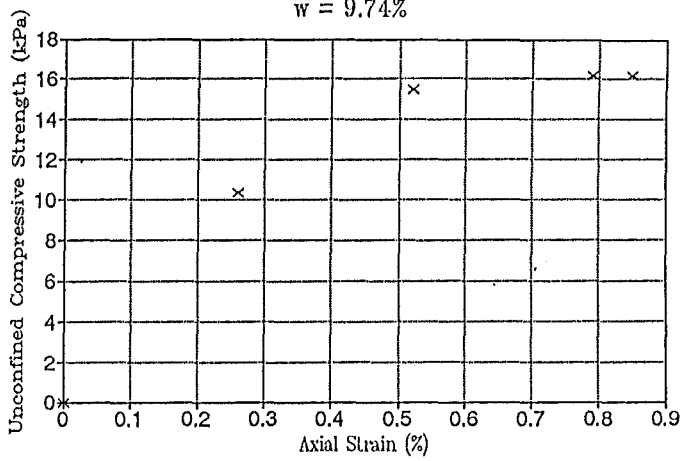

Sample 32/10/c
w = 9.73%

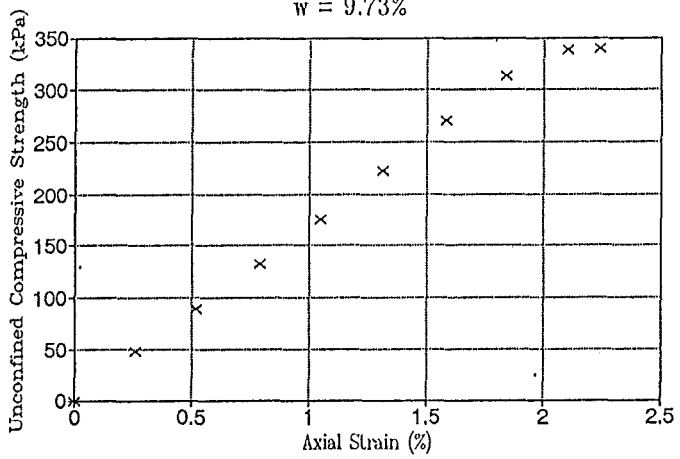

Sample 3/2/c
w = 9.73%

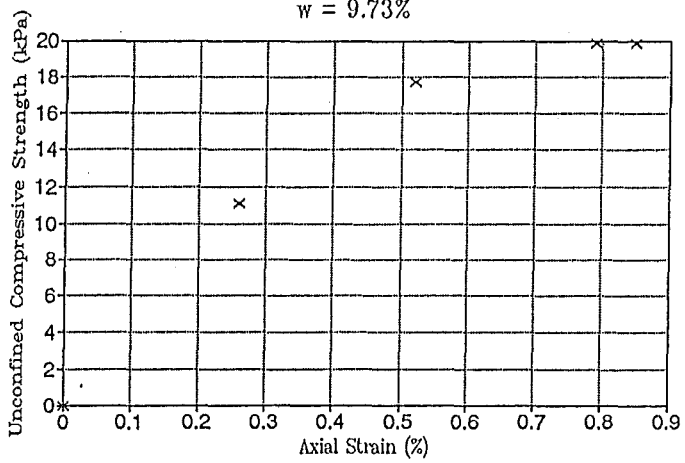

Sample 20/4/c

w = 9.82%

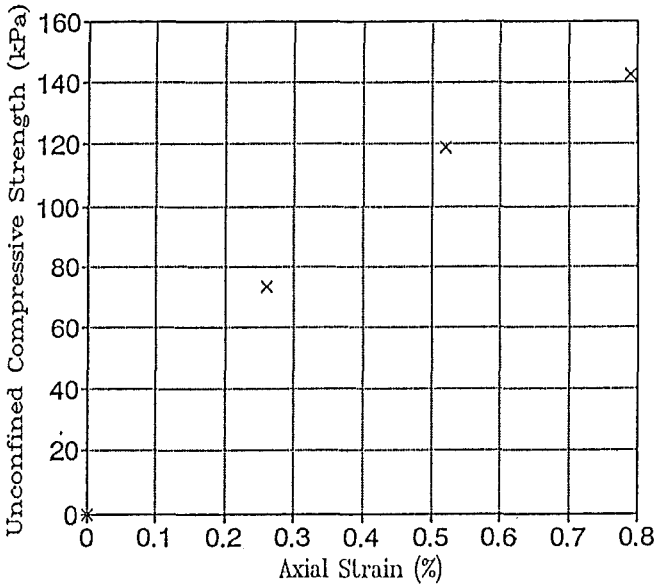

Sample 7/2/c

w = 11.59%

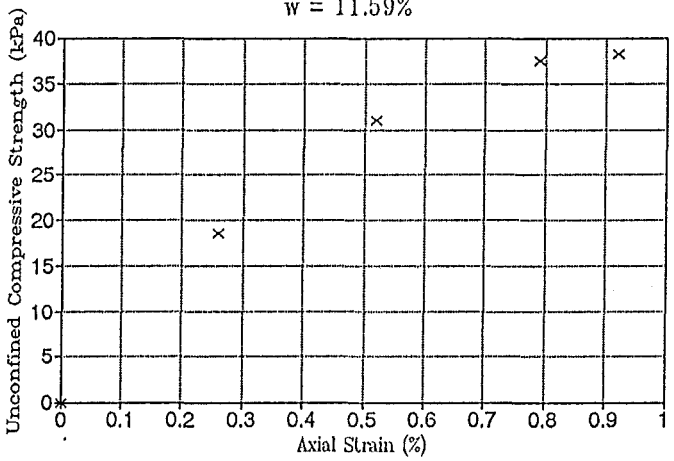

Sample 15/3/c

w = 11.66%

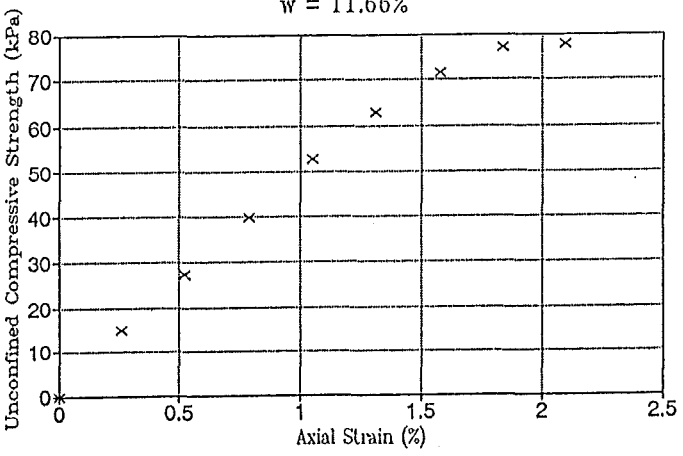

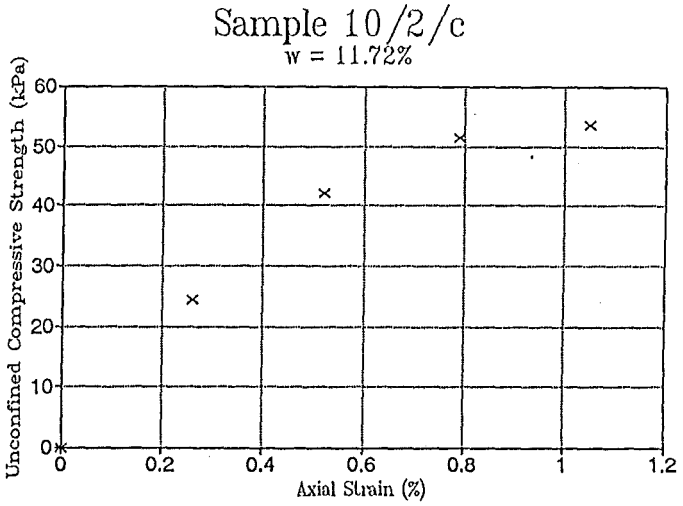
Sample 10/2/c
w = 11.72%
Unconfined Compressive Strength (kPa)
0
10
20
30
40
50
60
0
0.2
0.4
0.6
0.8
1
1.2
Axial Strain (%)

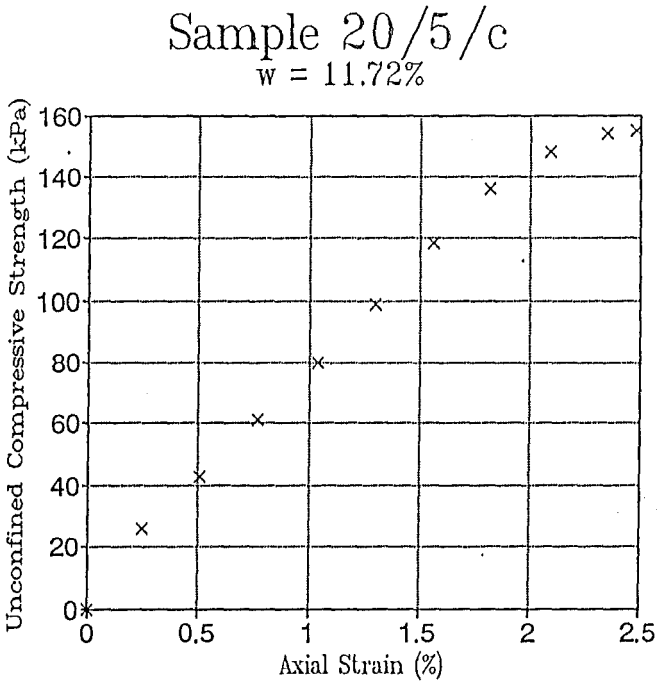
Sample 20/5/c
w = 11.72%
Unconfined Compressive Strength (kPa)
0
20
40
60
80
100
120
140
160
0
0.5
1
1.5
2
2.5
Axial Strain (%)

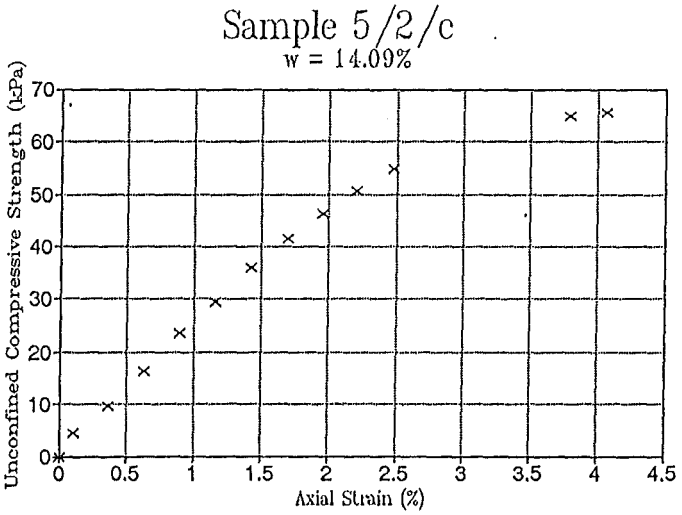
Sample 5/2/c
w = 14.09%
Unconfined Compressive Strength (kPa)
0
10
20
30
40
50
60
70
0
0.5
1
1.5
2
2.5
3
3.5
4
4.5
Axial Strain (%)

Sample 2/2/c

w = 14.13%

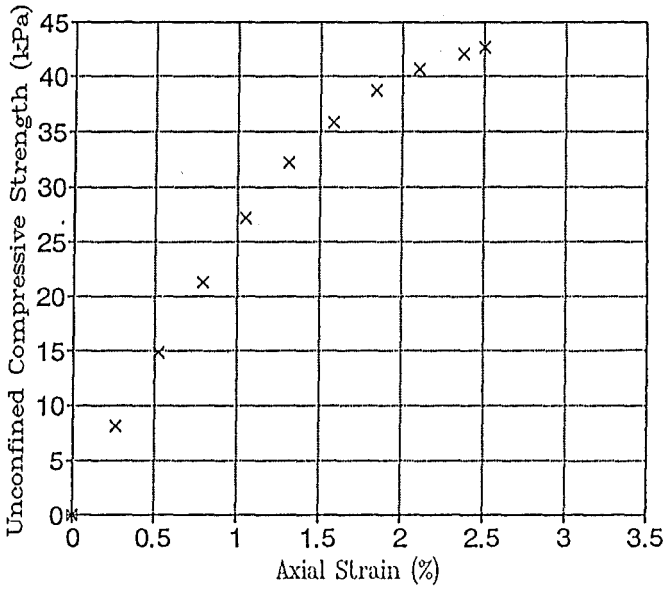

Sample 10/4/c

w = 14.27%

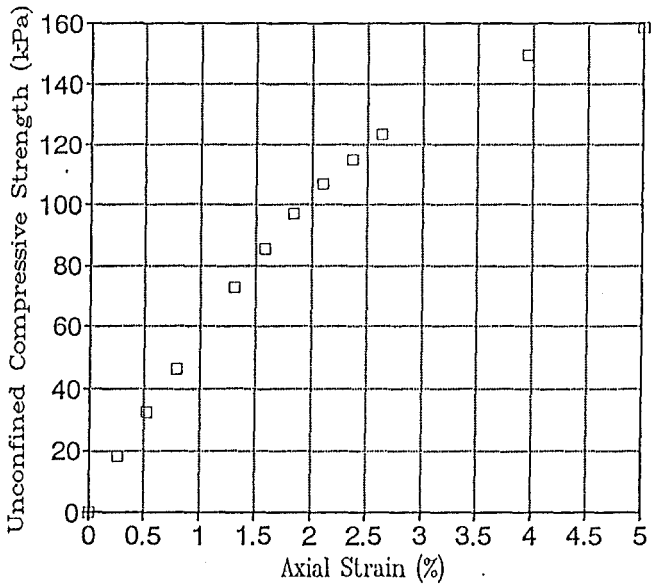

Sample 5/2/c

w = 15.74%

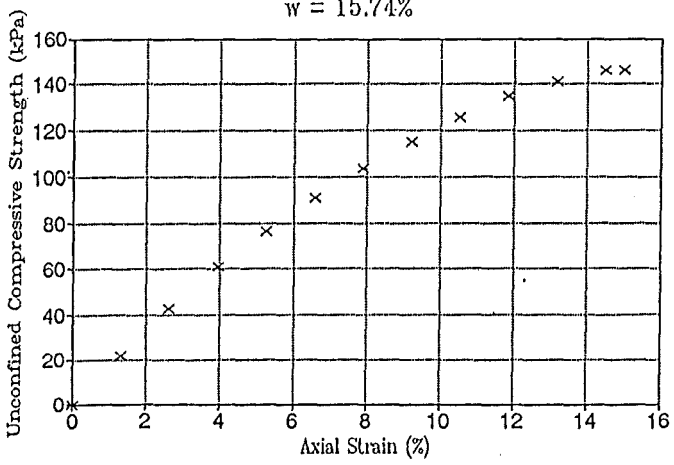

Sample 5/3/c
w = 15.72%

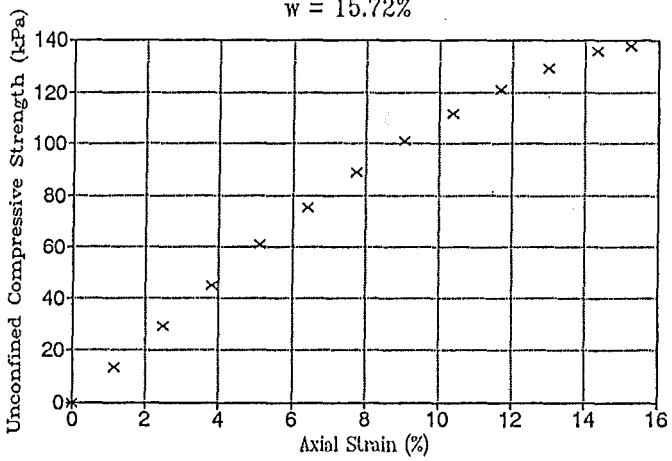

Sample 20/5/c
w = 15.78%

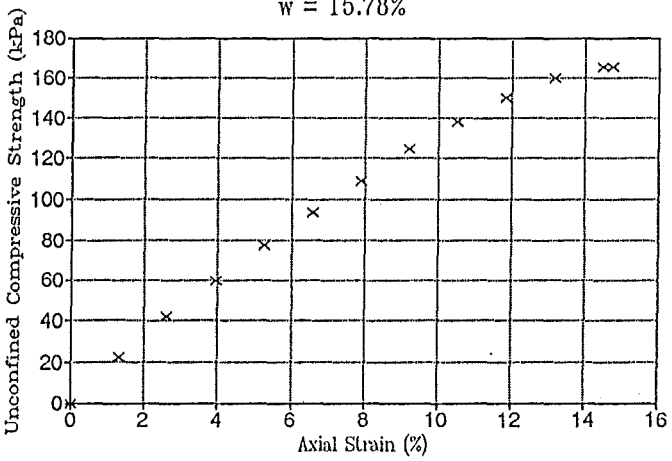

Sample 2/2/c
w = 15.81%

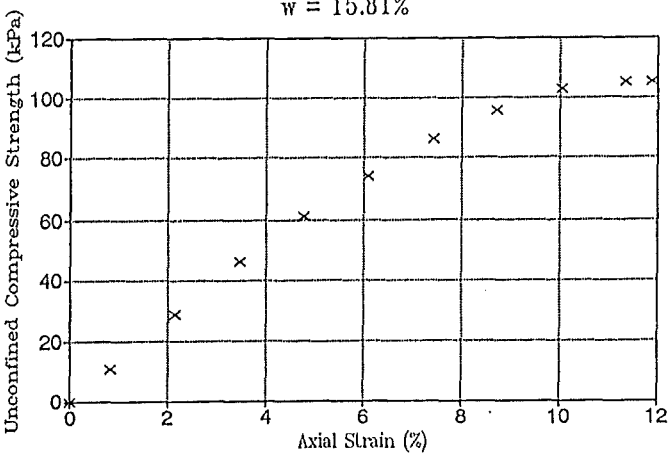

Sample 5/2/c

w = 16.91%

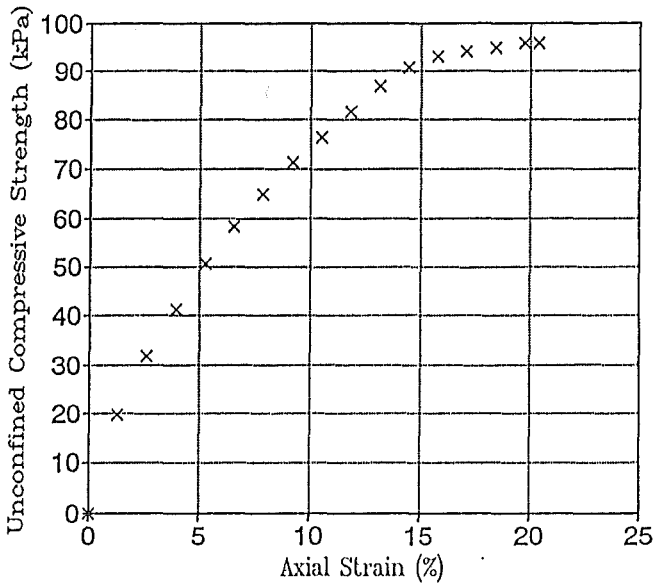

Sample 5/3/c

w = 17.38%

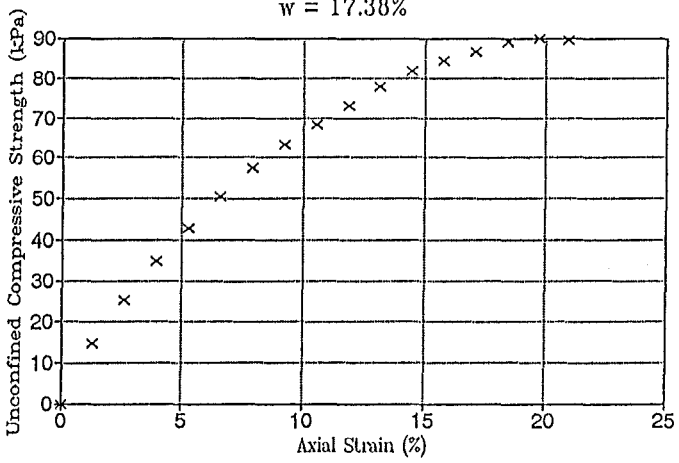

Sample 1/2/c

w = 17.38%

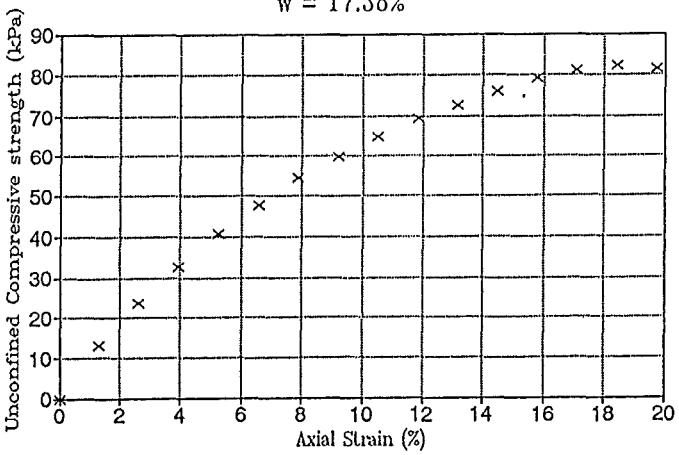

Sample 1/2/c

w = 19.29%

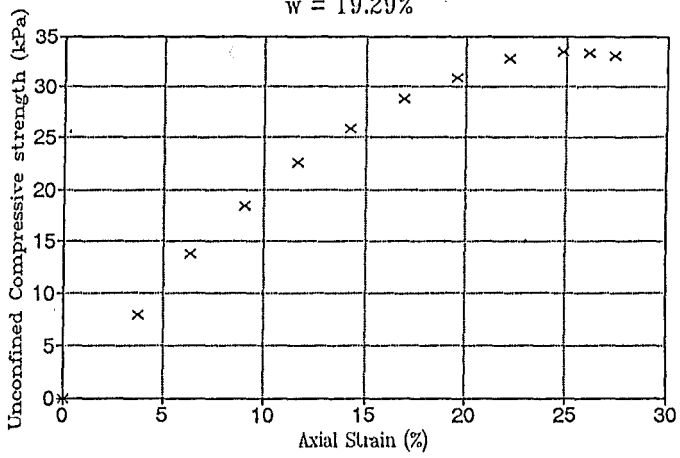

Sample 5/4/c

w = 19.62%

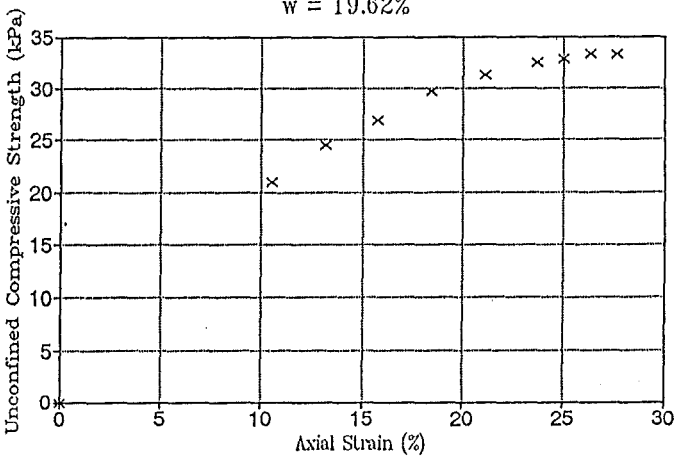

Sample 2/3/c

w = 19.10%

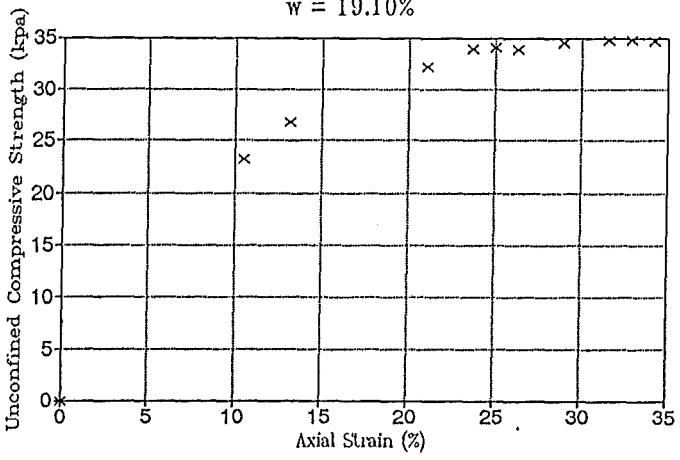

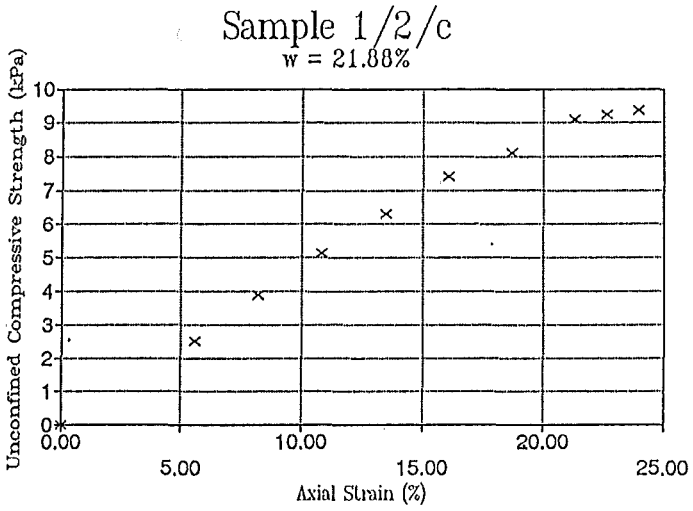
Sample 1/2/c
w = 21.88%
Unconfined Compressive Strength (kPa)
10
9
8
7
6
5
4
3
2
1
0
0.00
5.00
10.00
15.00
20.00
25.00
Axial Strain (%)

Reuslts of Curing - C layer

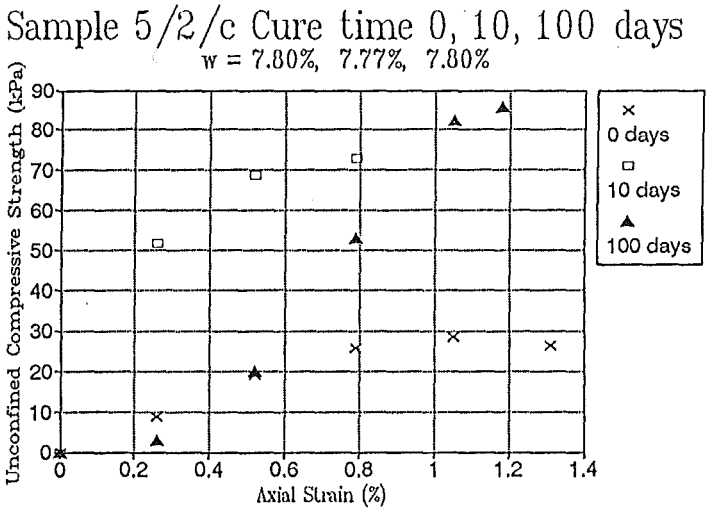

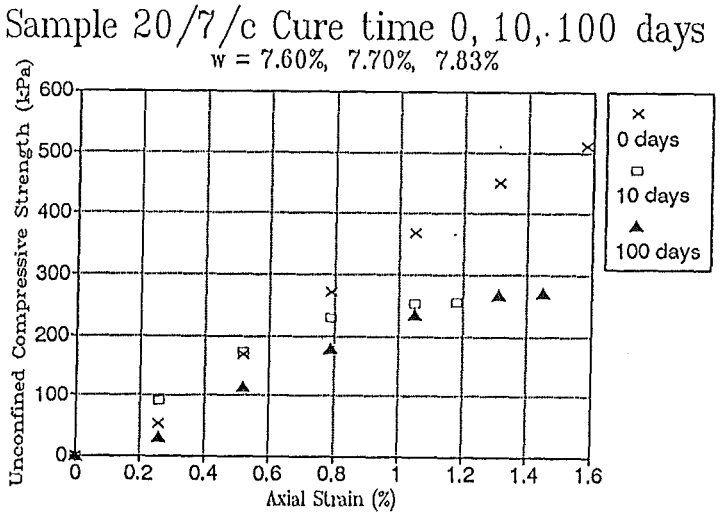

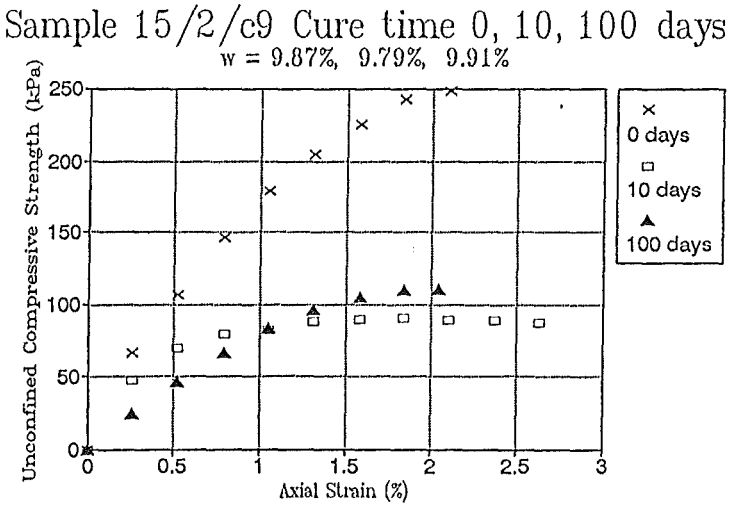

ple 20/7/c Cure time 0, 10, 100

w = 9.97%, 9.94%, 9.98%

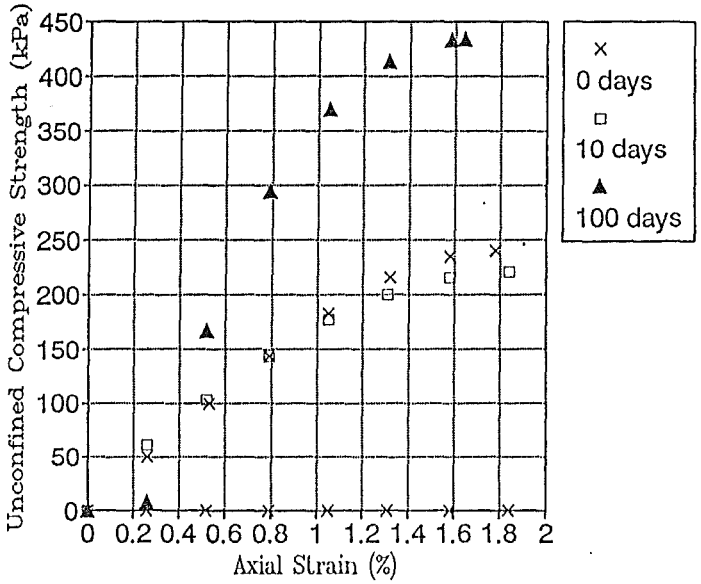

Sample 20/3.5/c Cure time 0, 10, 100 days

w = 11.87%, 11.96%, 12.04%

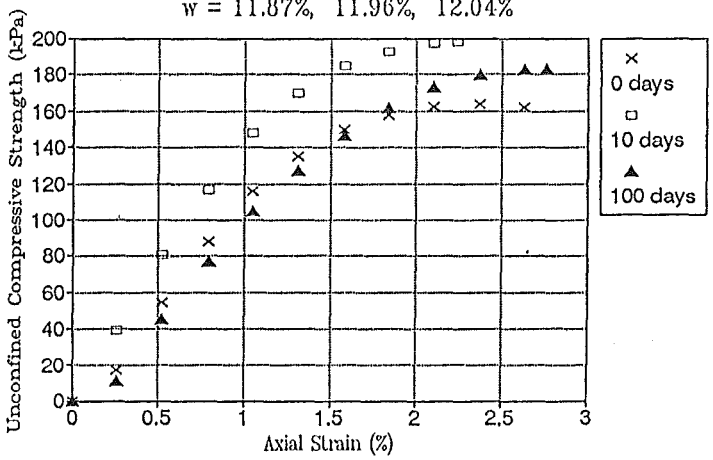

ıple 5/2/c Cure time 0, 10, 100 c

w = 11.93%, 12.01%, 11.75%

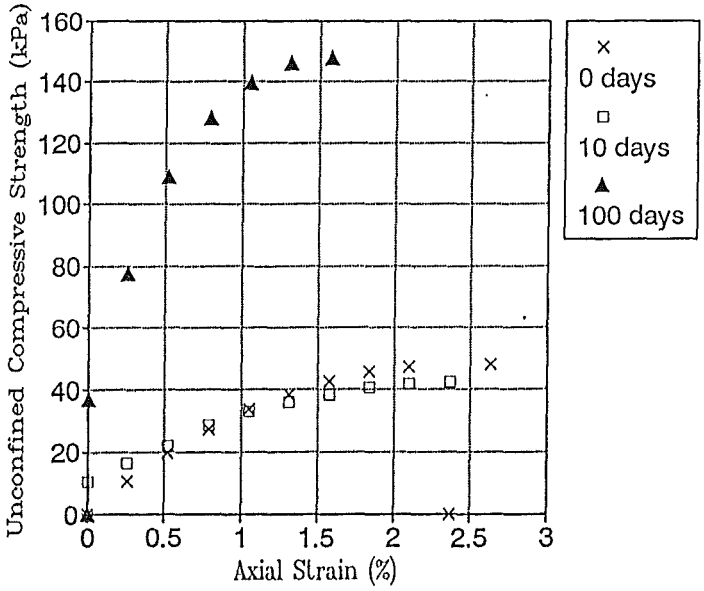

Sample 3/2/c Cure time 0, 10, 100 days

w = 14.85%, 14.83%, 14.36%

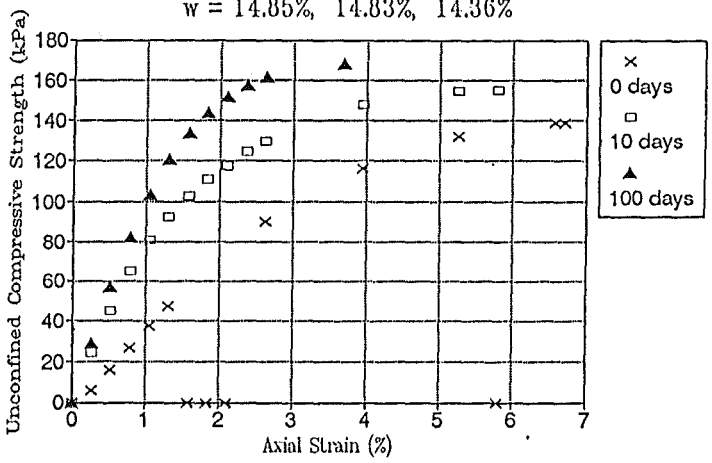

ıple 5/3/c Cure time 0, 10, 100 c

w = 14.86%, 14.82%, 14.44%

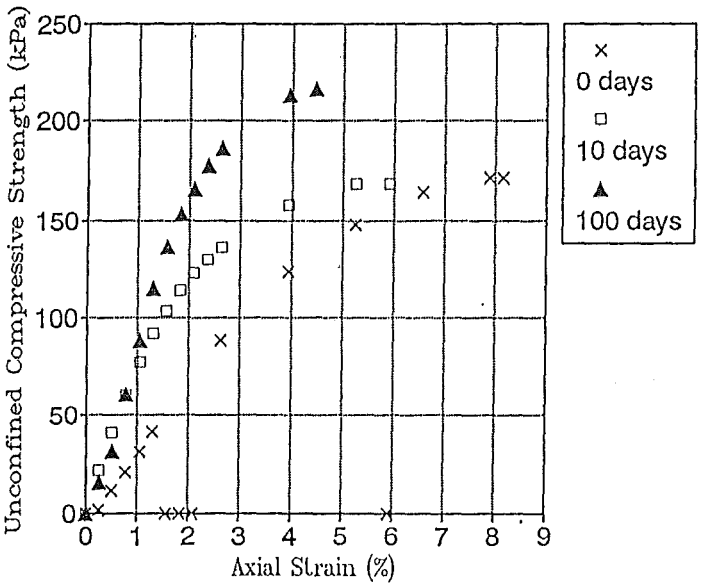

Sample 10/4/c Cure time 0, 10, 100 days

w = 15.59%, 16.10%, 15.98%

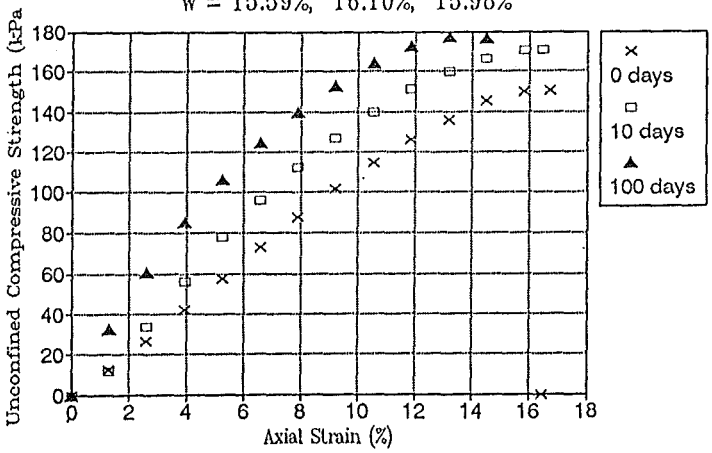

ıple 3/2/c Cure time 0, 10, 100 c
15.91%, 16.2%, 15.98%

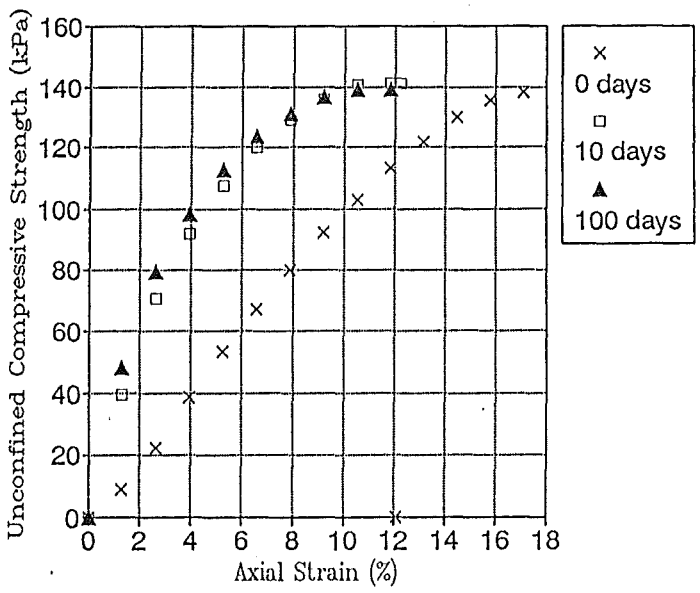

Sample 3/2/c Cure time 0, 10, 100 days
w = 17.57%, 17.40%, 17.40%

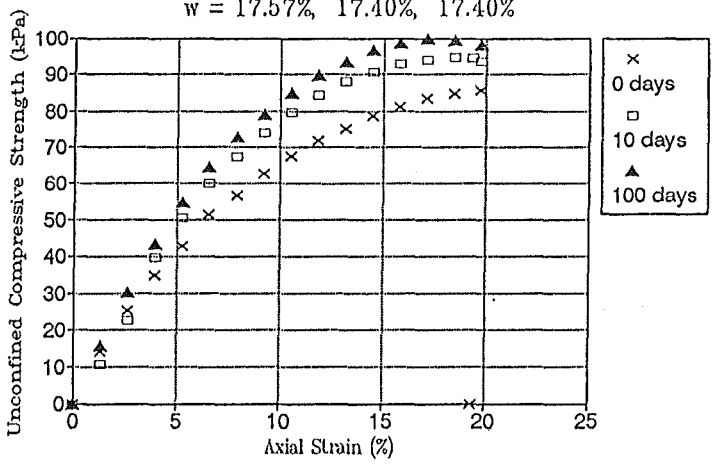

ıple 5/4/c Cure time 0, 10, 100 c
17.38%, 17.55%, 17.62%

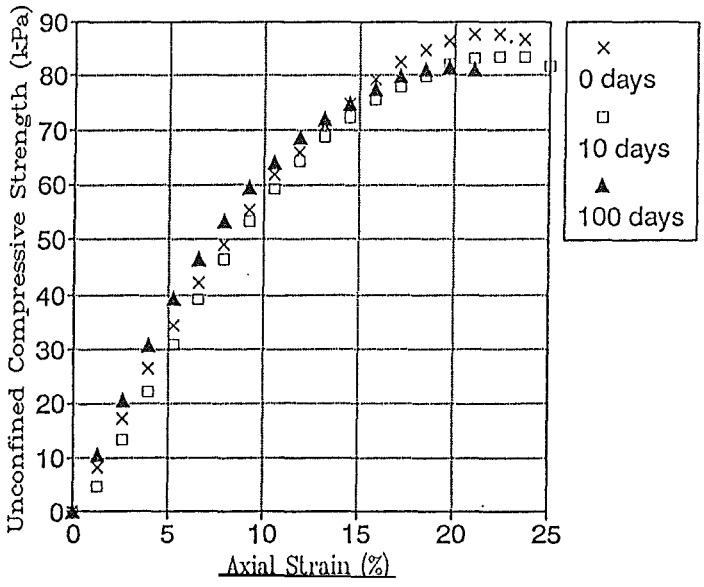

Results of Four Day Soak Test - C layer

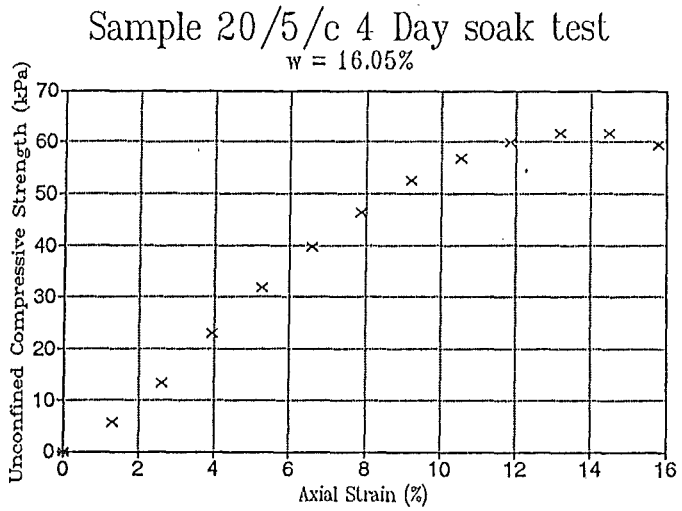

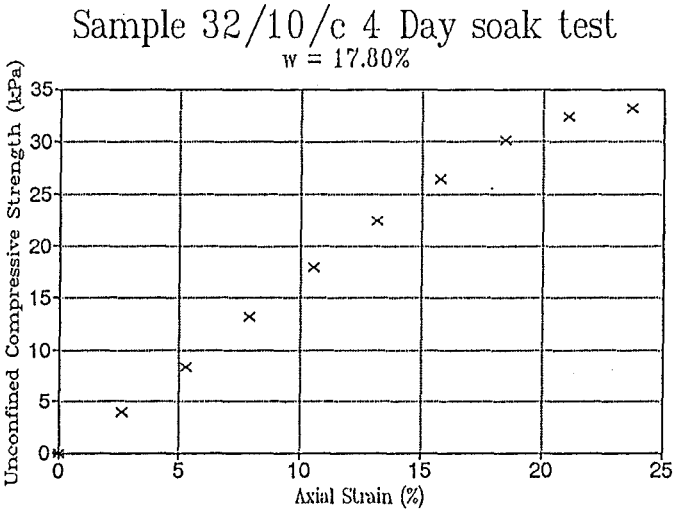

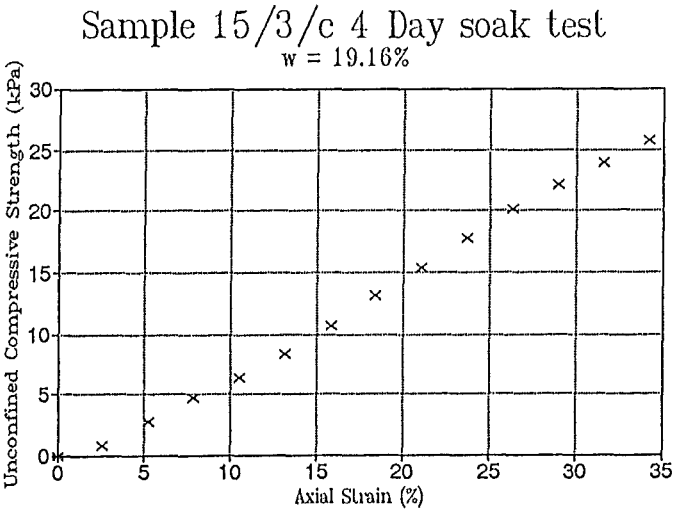

Results of Unconfined Compression Testing - P layer

Sample 20/7/p

w = 9.44%

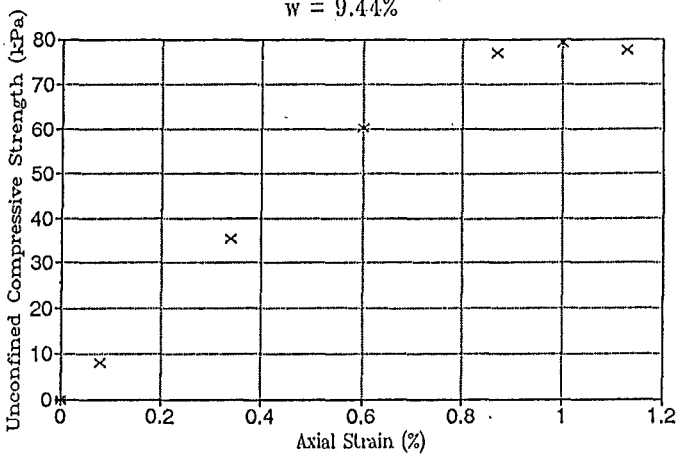

Sample 15/3/p

w = 11.31%

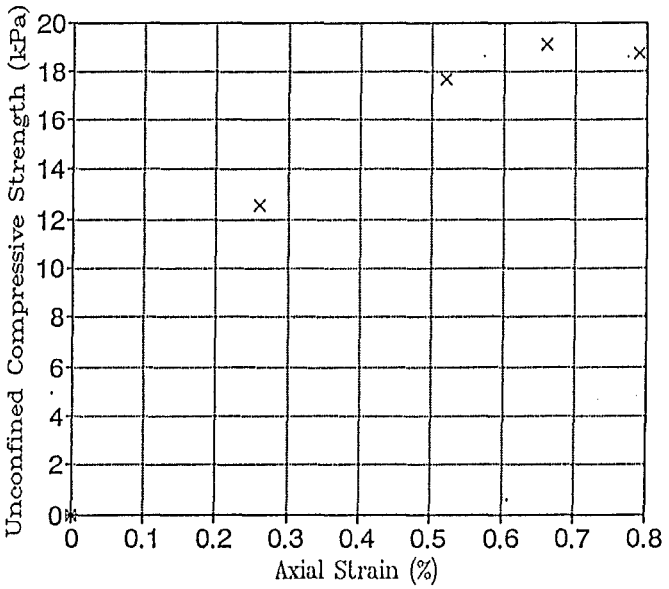

Sample 20/8/p

w = 11.41%

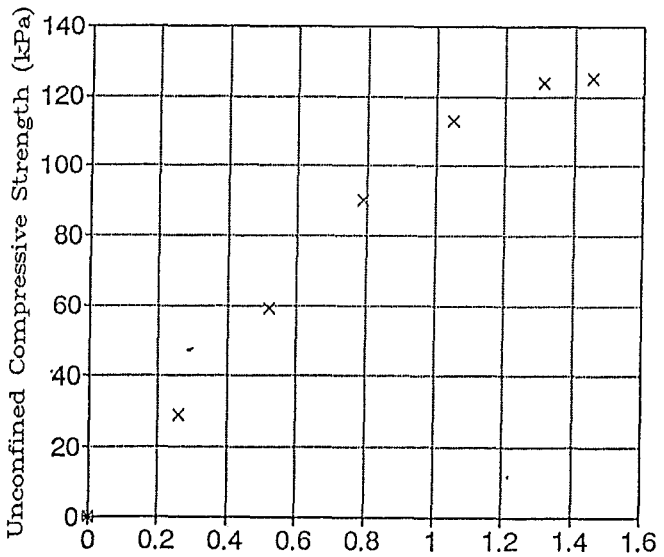

Sample 7/2/p

w = 11.50%

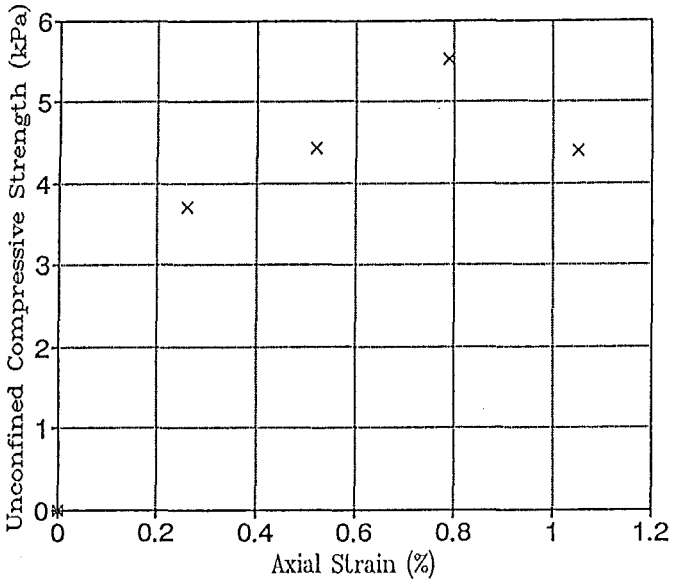

Sample 3/2/p

w = 13.55%

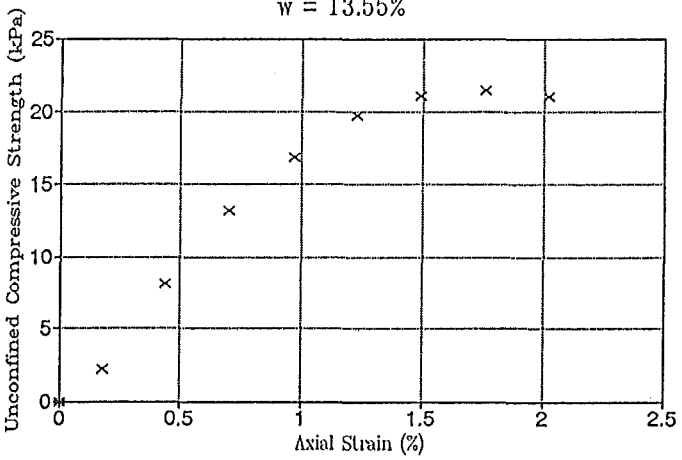

Sample 10/10/p

w = 13.62%

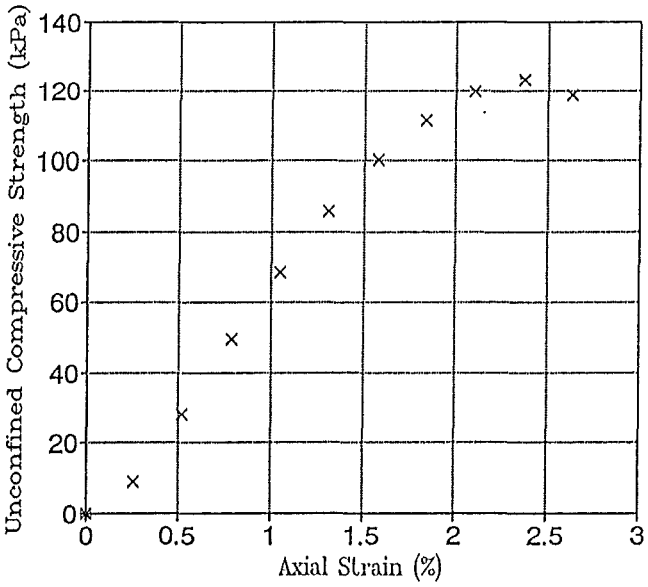

Sample 5/3/p

w = 13.66%

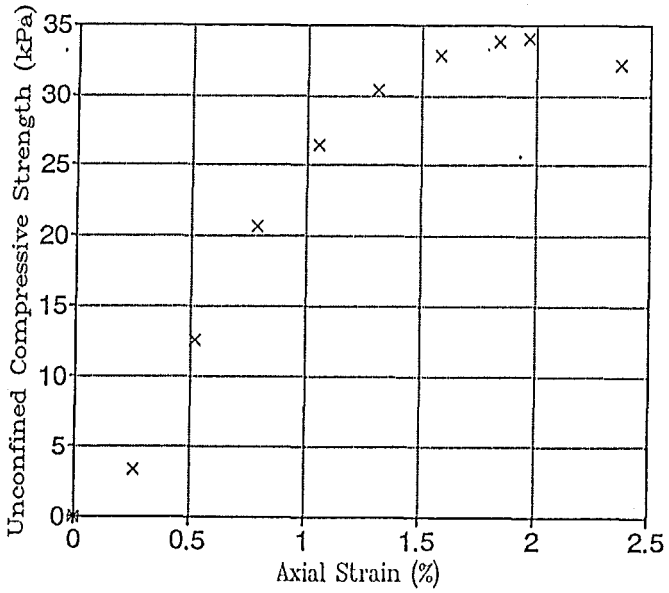

Sample 1/2/p

w = 13.67%

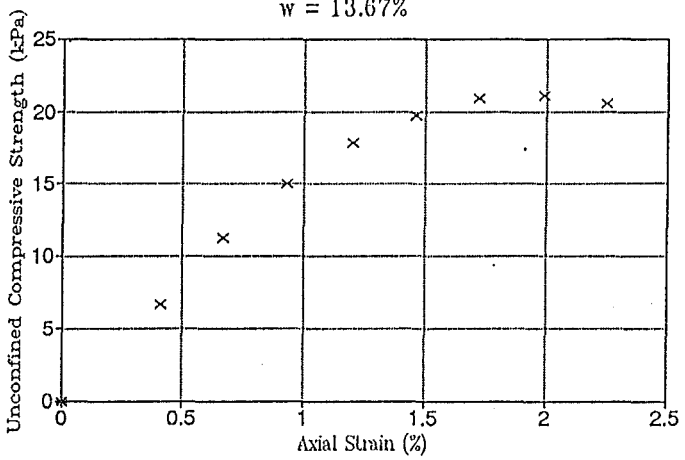

Sample 1/0/p

w = 14.66%

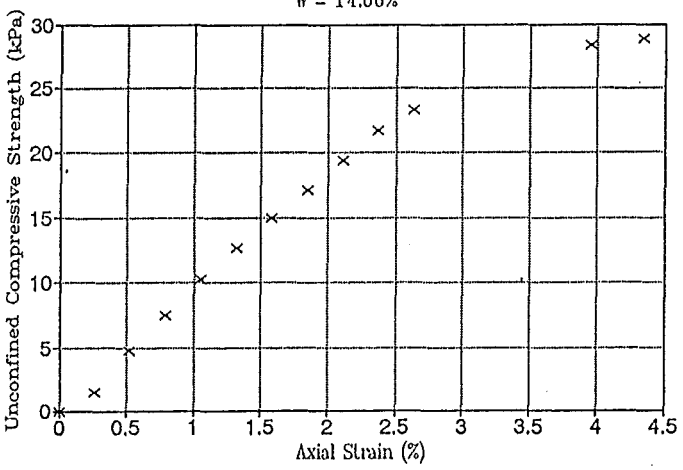

Sample 2/2/p

w = 14.63%

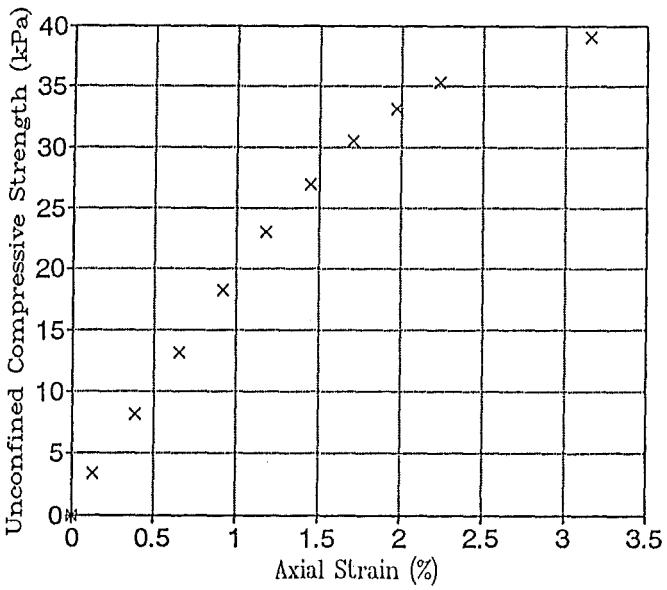

Sample 10/6/p

w = 14.62%

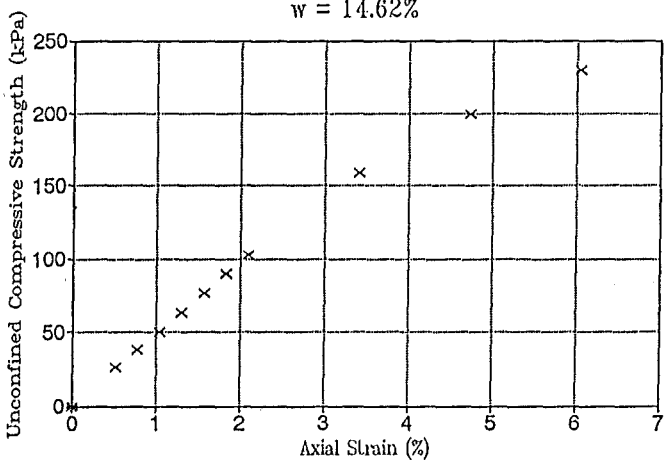

Sample 5/3/p

w = 14.73%

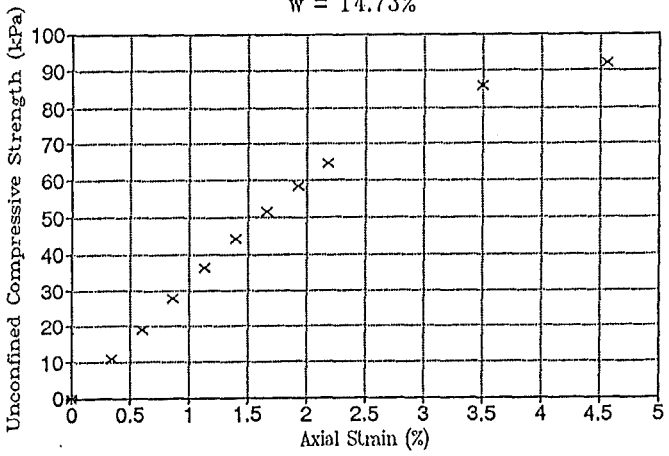

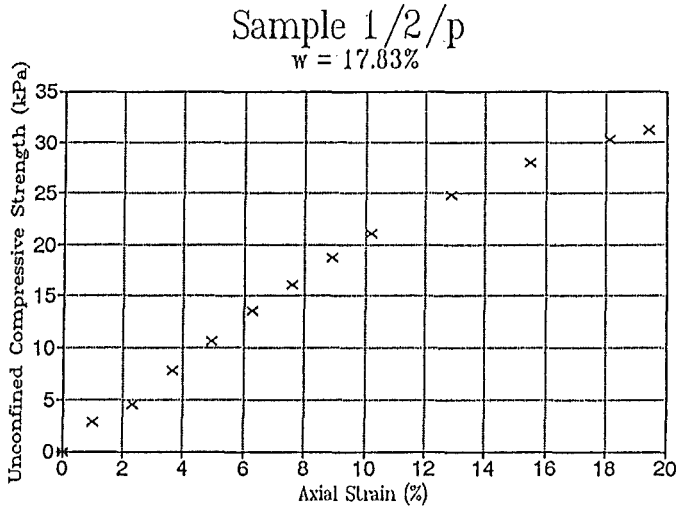
Sample 1/2/p
w = 17.83%
Unconfined Compressive Strength (kPa)
35
30
25
20
15
10
5
0
0
2
4
6
8
10
12
14
16
18
20
Axial Strain (%)

Results of Curing - P layer

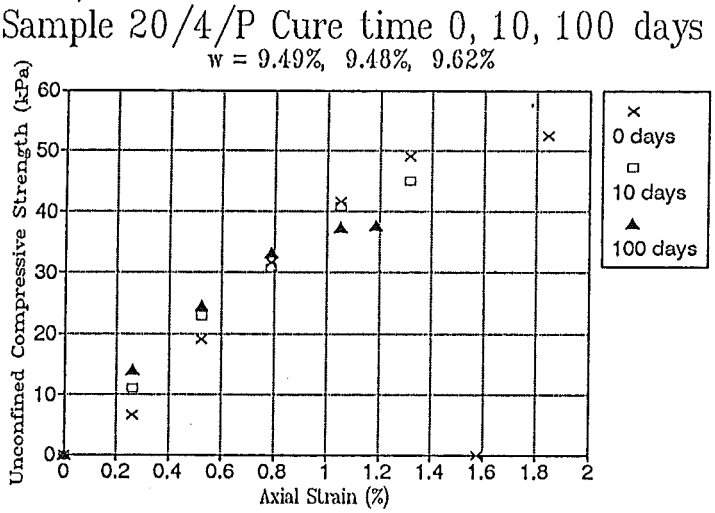

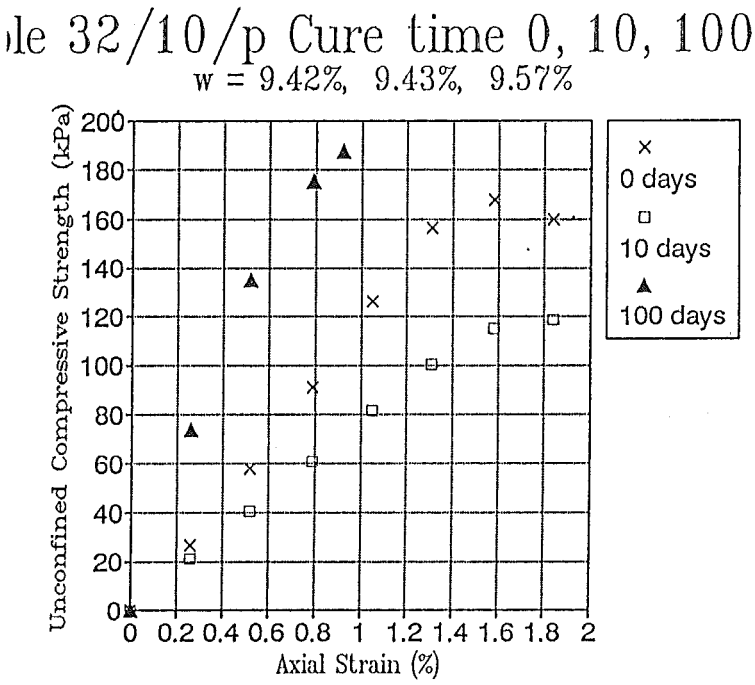

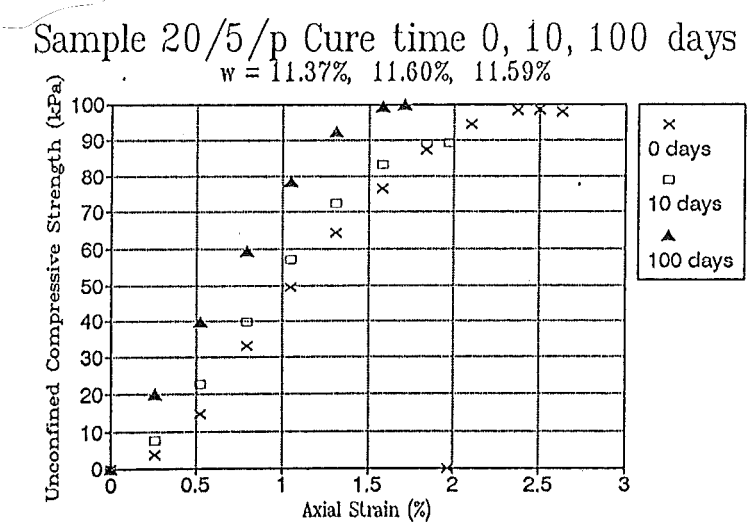

Sample 10/2/p Cure time 0, 10, 100 days

w = 11.40%, 11.60%, 11.66%

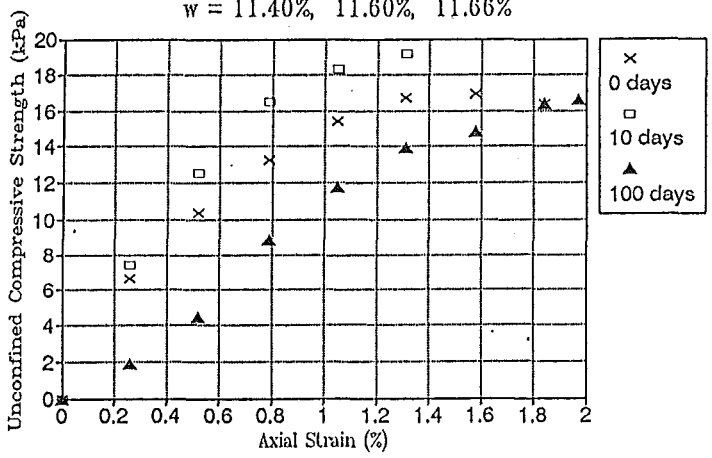

Sample 2/2/p Cure time 0, 10, 100 days

w = 13.66%, 13.74%, 13.75%

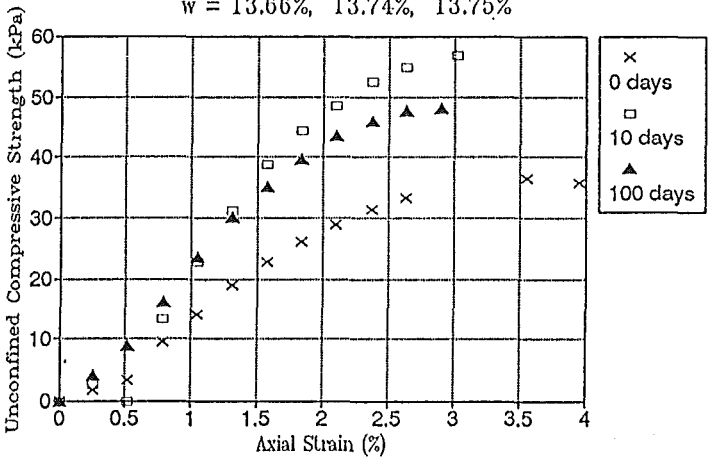

ple 10/6/p Cure time 0, 10, 100

w = 13.71%, 13.69%, 13.73%

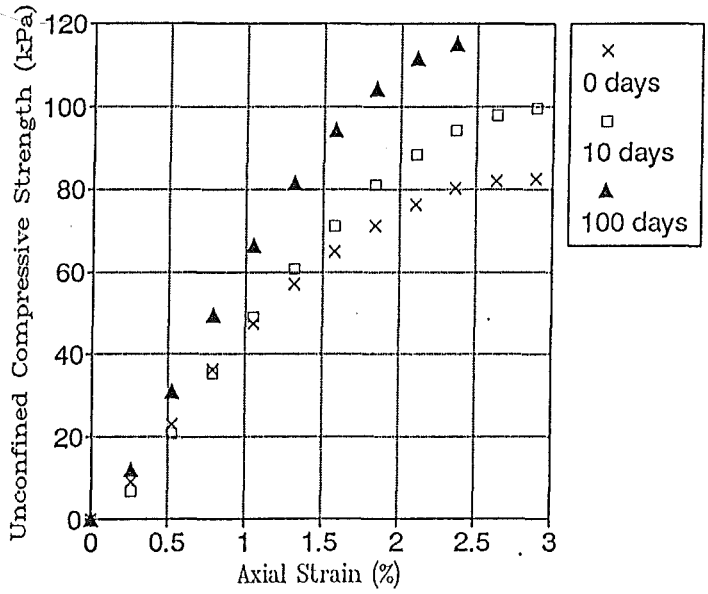

Sample 5/2/p Cure time 0, 10, 100 days

w = 14.63%, 14.70%, 14.69%

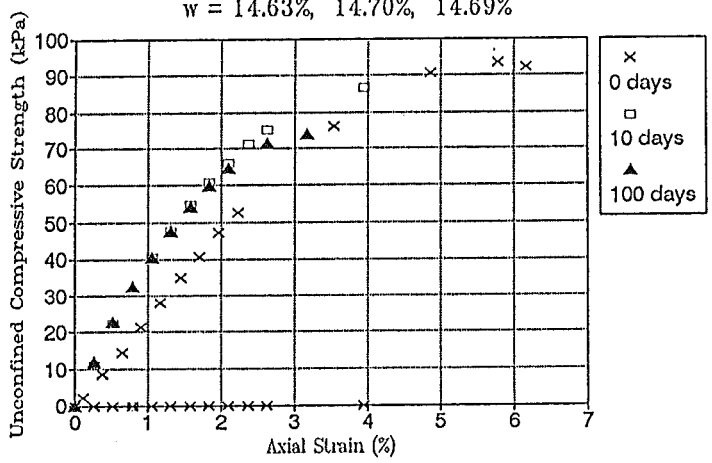

Sample 10/4/p Cure time 0, 10, 100 days

w = 14.69%, 14.71%, 14.75%

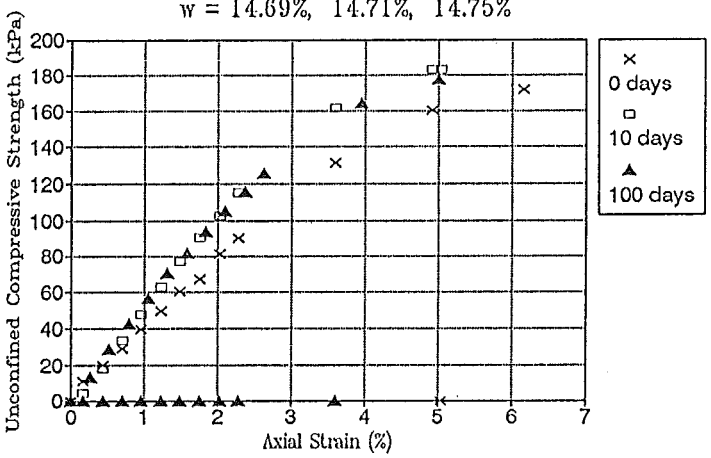

Sample 5/3/p Cure time 0, 10; 100 days

w = 17.82%, 17.71%, 17.89%

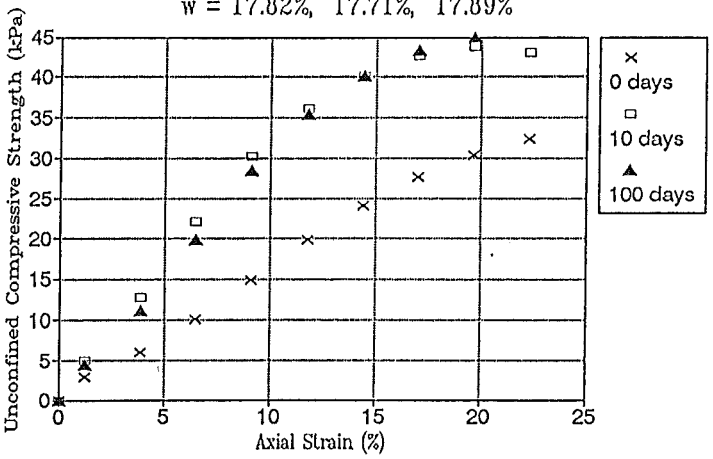

Results of Four Day Soak Test - P layer

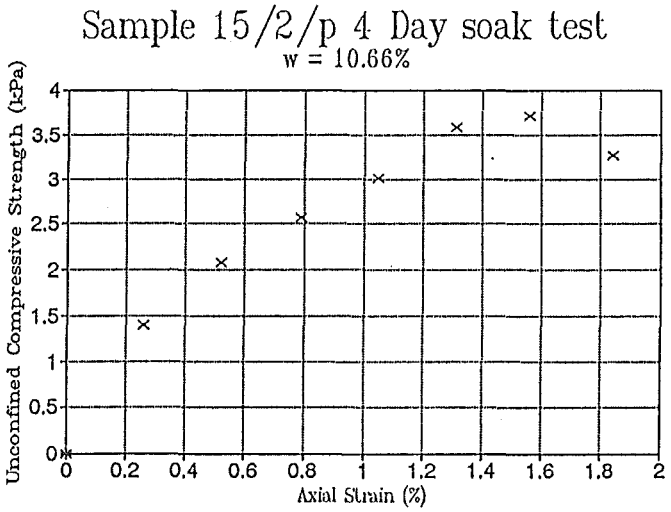

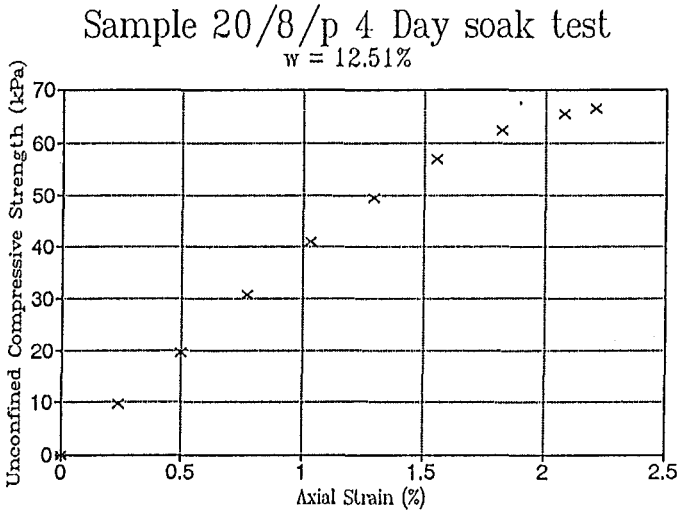

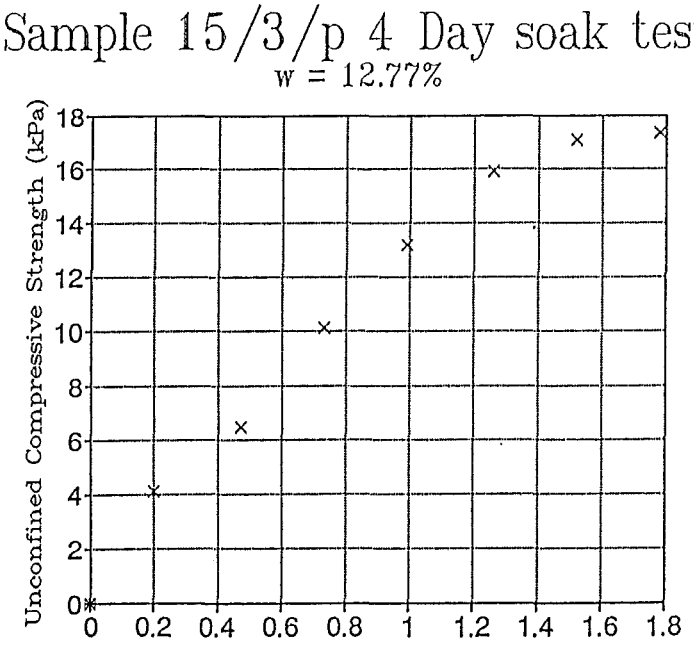

Sample 10/6/p 4 Day soak test

w = 14.99%

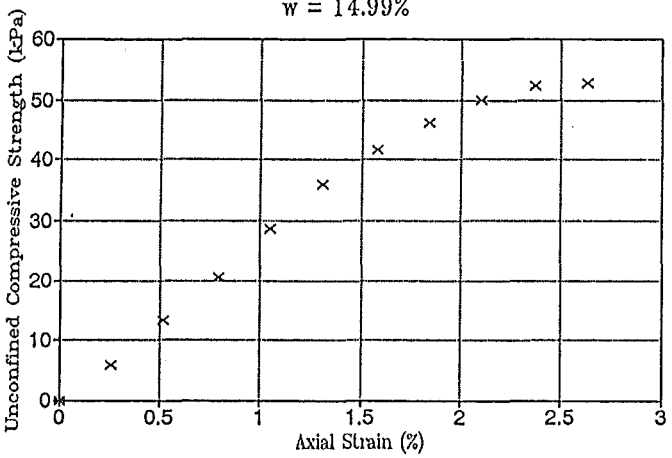

Sample 5/3/p 4 Day soak test

w = 15.17%

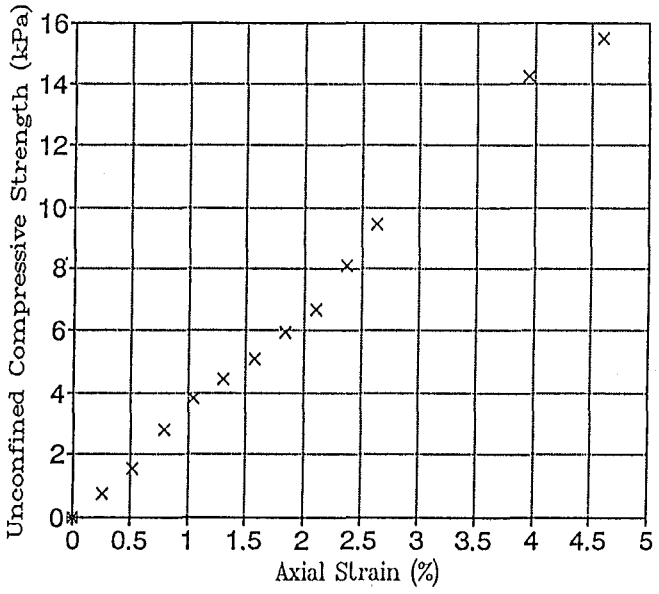

Sample 10/5/c 4 Day soak test

w = 15.52%

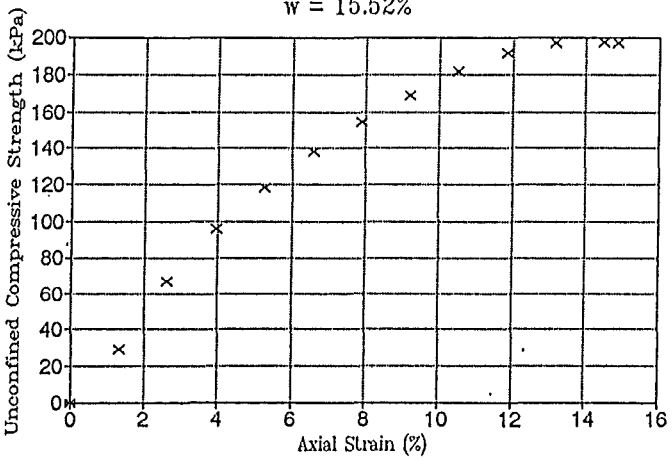

A4.4.3 N.Z. standard and heavy compaction results

Layer	Dry Density (t/m^3)	Moisture Content (%)	Compaction Type
C	1.684	10.28	Standard
C	1.856	14.50	Standard
C	1.790	16.67	Standard
C	1.714	18.75	Standard
C	1.668	20.93	Standard
C	1.830	12.54	Standard
C	1.939	10.31	Heavy
C	1.885	14.42	Heavy
C	1.791	16.57	Heavy
C	1.715	18.78	Heavy
C	1.983	12.43	Heavy
P	1.804	10.84	Standard
P	1.875	12.83	Standard
P	1.839	15.02	Standard
P	1.742	17.22	Standard
P	1.684	19.43	Standard
P	1.968	10.84	Heavy
P	1.943	12.88	Heavy
P	1.835	15.61	Heavy
P	1.740	17.16	Heavy

A4.4.4 Four Day Soak Test Results

C Layer

ρ_d (t/m^3)		w (%)		Swell	ϵ_f	s_u (UU)	s_u (vane)	Comp.
Before	After	Before	After	(mm)	(%)	(kPa)	(kPa)	Effort
1.74	1.73	12.34	16.98	0.76	12.4	30.81	125.18	20/5
1.75	1.72	9.66	18.40	3.51	23.2	16.56	69.99	32/10
1.64	1.63	12.22	19.50	0.61	34.2	12.91	30.96	15/3
1.81	1.80	14.00	15.71	0.80	14.3	98.64	175+	10/5
1.66	1.63	9.71	19.64	2.52			38.36	20/7
1.59	1.58	7.77	20.90	2.63			15.21	20/7
1.38	1.37	7.85	31.50	5.00			1.10	5/2

P Layer

ρ_d (t/m^3)		w (%)		Swell	ϵ_f	s_u (UU)	s_u (vane)	Comp.
Before	After	Before	After	(mm)	(%)	(kPa)	(kPa)	Effort
1.79	1.81	11.88	12.18	0.28	2.2	33.16	168.25	20/8
1.68	1.71	11.86	12.64	0.03	1.8	8.67	76.72	15/3
1.71	1.72	14.02	15.17	0.02	4.6	7.75	41.05	5/3
1.80	1.80	13.90	14.99	0.23	2.6	26.45	90.18	10/6
1.56	1.61	9.53	10.58	0.00	1.6	1.86	41.73	15/2
1.80	1.82	10.60	10.90	0.00				S/Comp

A4.4.5 In situ Vane Shear Testing

No.	Sample Layer	Moisture Content (%)	s_u (vane shear) (kPa)
1	S	23.95	26.92
2	S	24.17	43.07
3	T.Crack	30.99	23.56
4	T.Crack	26.74	26.25
5	S	23.65	34.73
6	S	23.48	69.99
7	C	17.68	91.53
8	C	18.22	76.72
9	T.Crack	23.72	52.49
10	T.Crack	24.09	20.19
11	C	18.69	113.06
12	C	18.57	74.70
13	S	21.01	86.82
14	C	18.63	139.98
15	C	17.87	84.80
16	C	16.48	100.95
17	P	21.93	125.18
18	P	19.44	170.94
19	P	19.12	134.60
20	P	20.86	153.44
21	P	19.67	174.98
24	P	21.15	135.95
28	Vain	22.11	34.99
29	Vain	23.36	32.30
33	C	20.43	48.45

A4.5.1 Shear box procedure

Equipment

The shear box equipment used consisted of a Wykeham and Farrance manually reversible shear box machine, a two channel Plotamatic 815M chart recorder, a single channel variable speed Rikadenki chart recorder, 10, 12 and 20 volt power supplies and potentiometers, and a 250kg load cell, as shown in figure A4.1. A 100mm diameter shear box (figure A4.2) was selected for all tests, as this accommodated remoulded samples retrieved from standard proctor moulds.

Calibration

The shear box apparatus was converted from dial gauge display of settlement and displacement, to chart recorder printout, as it was envisaged that run periods would exceed an eight hour day. This involved the installation and calibration against dial gauges of potentiometers to measure settlement and displacement. Similarly, the 250kg load cell was calibrated in compression and tension against known dead weights and showed no significant deflection (0.1mm) over its entire working range. Table A4.1 gives the calibrations for the two chart recorders and the accuracy accounting for graph line thickness.

All electrical equipment was run continuously from five days prior to the testing until the completion of all tests. Both chart recorders were tested for drift over a 24 hour period. The Plotamatic 815M chart recorder showed no drift over this period. The Rikadenki chart recorder had a random drift of up to 0.1mm (true).

Table A4.1 Calibration Data

Plotter	Parameter	Calibration	Accuracy
Plotamatic 815M	load	(50mV/cm) 1mm = 33.41N	± 16.7N
Plotamatic 815M	displacement	(0.5V/cm) 18mm=1mm	± 0.03mm
Rikadenki Plotter	settlement	(2V/cm) 1mm = 0.04mm	± 0.02mm (excl. drift)

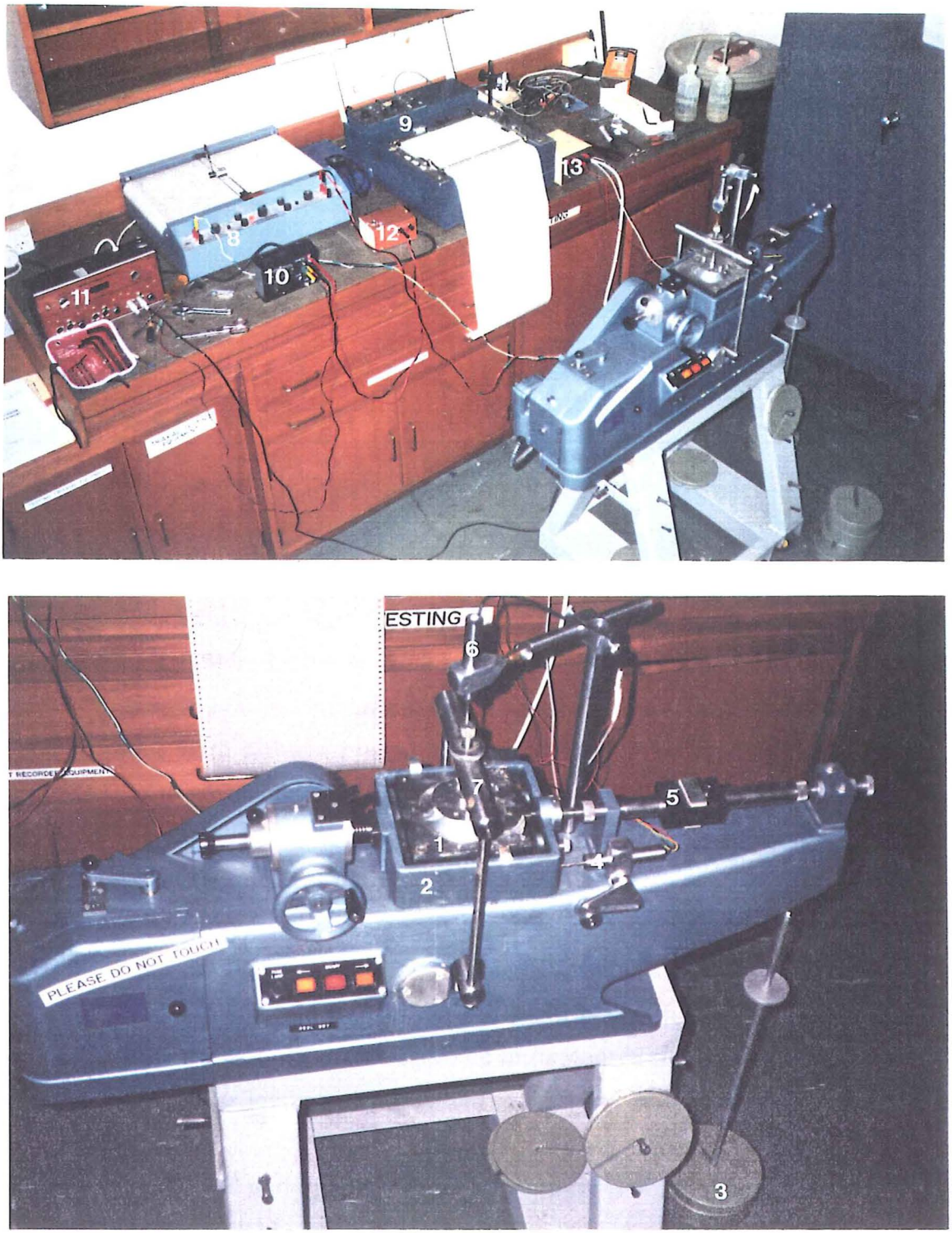

1	Shear box	8	Plotamatic 815M (Load/displ. chart recorder)
2	Shear box carriage	9	Rikadenki (time/settlement chart recorder)
3	Levered (1:10) dead weights	10	Digital readout of load cell (mV)
4	Displacement potentiometer	11	Power supply for load cell (10V)
5	250kg load cell	12	Power supply for displ. potentiometer (24V)
6	Settlement potentiometer	13	Power supply for settlement potentiometer (12V)
7	Loading arm		

Figure A4.1 Direct shear (shear box) testing equipment.

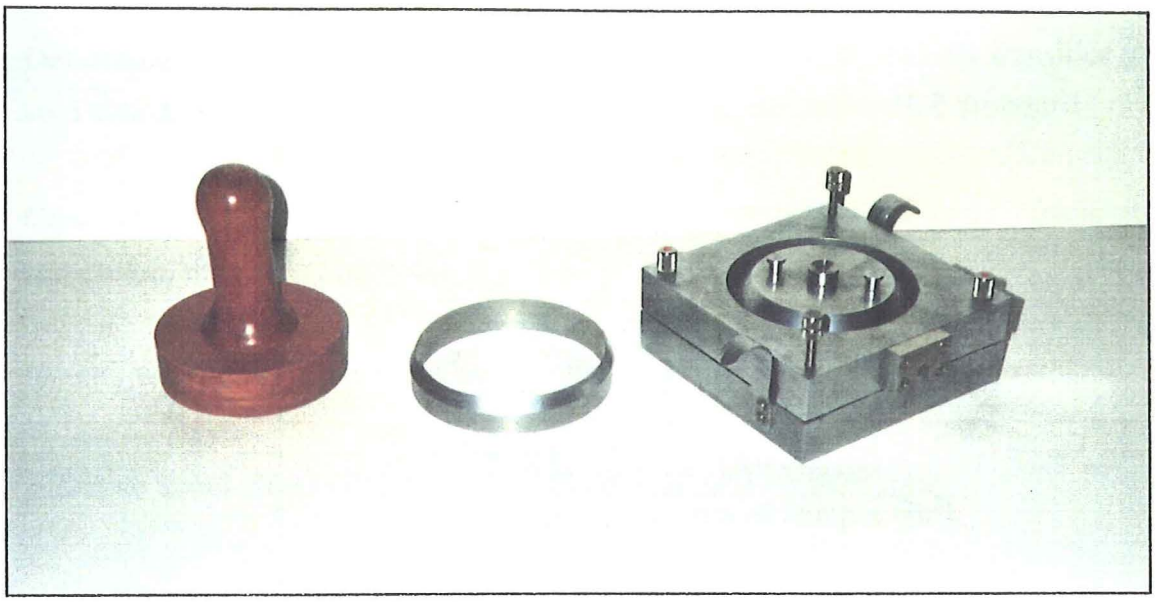

Figure A4.2 Shear box (100mm diameter) and sample extruder.

Procedure

A sample 20mm thick and 100mm diameter was placed between two saturated rough porous ceramic filters in the shear box. Free draining spacer discs were used to locate the sample mid-point adjacent to the shear box mid-point. The rough porous ceramic filters were saturated using a vacuum chamber. Weight of the shear box, saturated rough porous ceramic filters and spacer discs, with and without the sample was recorded to the nearest 0.1g. Trimmings from sample preparation were used for initial water content determination.

The shear box was then placed in the distilled water filled shear box carriage, followed by the placement of the desired weights on the lever loading arm in preparation for the consolidation stage. The settlement/time chart recorder was then zeroed and the lever loading arm released to start the 24 hour consolidation stage.

After the sample had undergone 24 hours of consolidation, the desired shearing rate selected on the variable gear box, the shear load/displacement chart recorder zeroed, and the shearing stage was started. Reversing was manually controlled after the sample had been sheared a desirable displacement.

After the shearing stage, the shear box was weighed and the sheared sample was used for final water content determination.

Determination of initial and final water contents, initial and final dry densities and void ratios, were all done in accordance with the appropriate N.Z.Standard.

Consolidation and run settlements were ascertained directly from the settlement/time chart recorder.

Shear stress and normal stress were calculated in the following manner:-

$$\text{Effective shear stress (Pa)} = \frac{\text{shear load (N)}}{\text{cross-sectional area of sample } (m^2)}$$

$$\text{Normal stress (Pa)} = \frac{\text{weight on lever arm (kg).9.81 } (m.s^{-2}) \text{ . 10 (leverage)}}{\text{cross-sectional area of sample } (m^2)}$$

Note: For the determination of effective internal angle of friction (ϕ') and cohesion (c'), area corrections need not be applied. However, area corrections should be applied if quoting effective shear strenghts on their own.

A4.5.2 Rate effects - load/displacement graphs

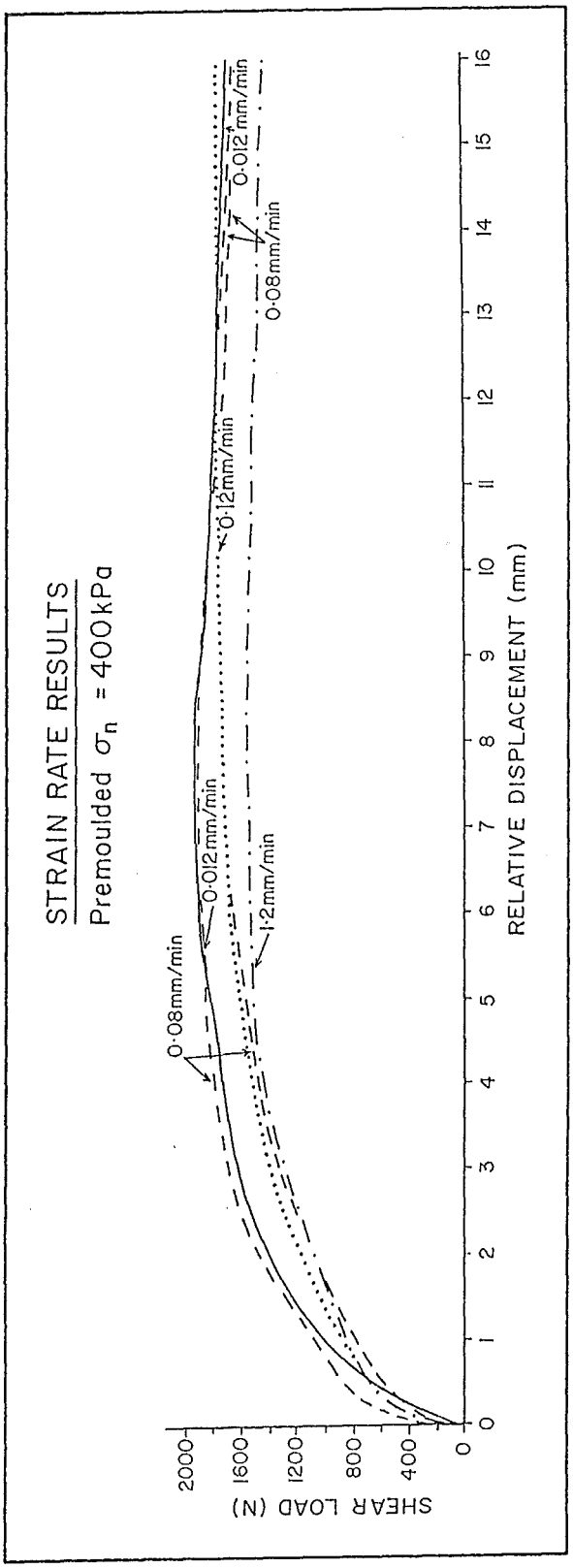

A4.5.3 Remoulded samples - load/displacement & consolidation/time graphs

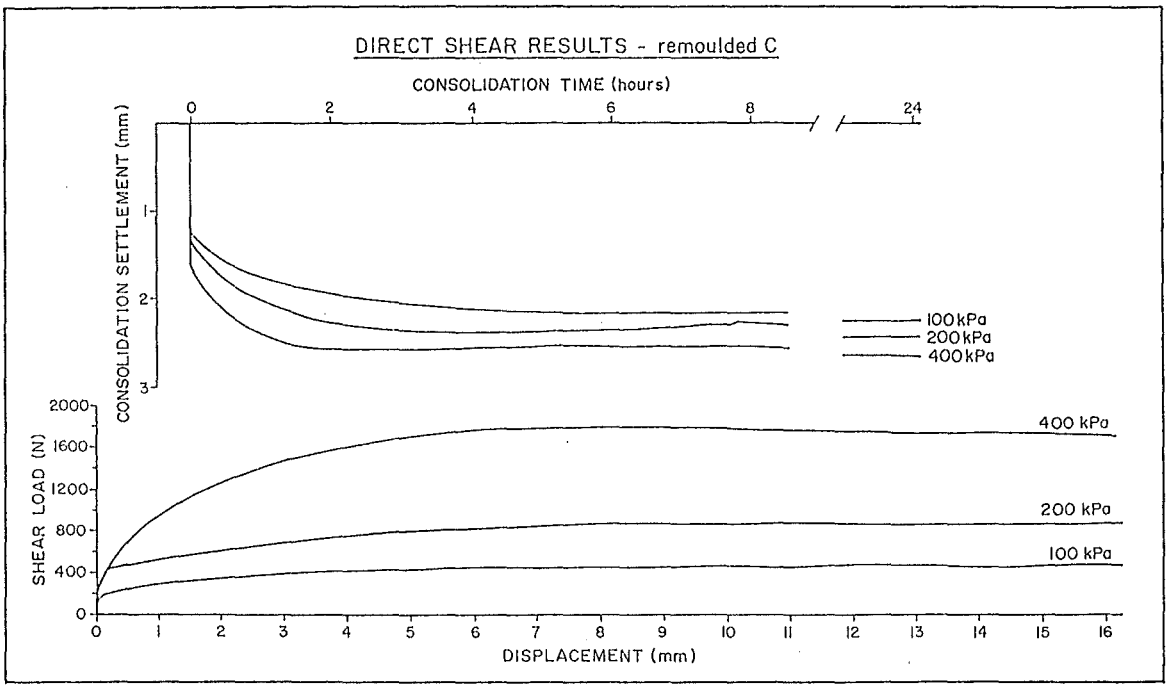

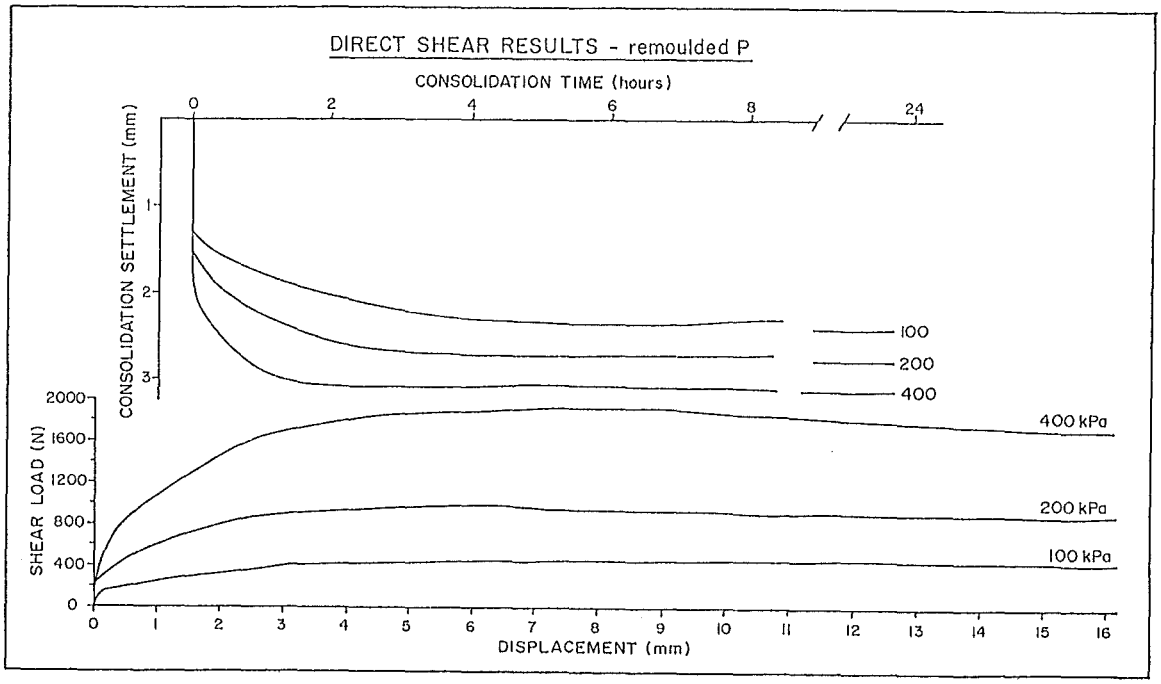

A4.5.4 Undisturbed samples - load/displacement & consolidation/time graphs

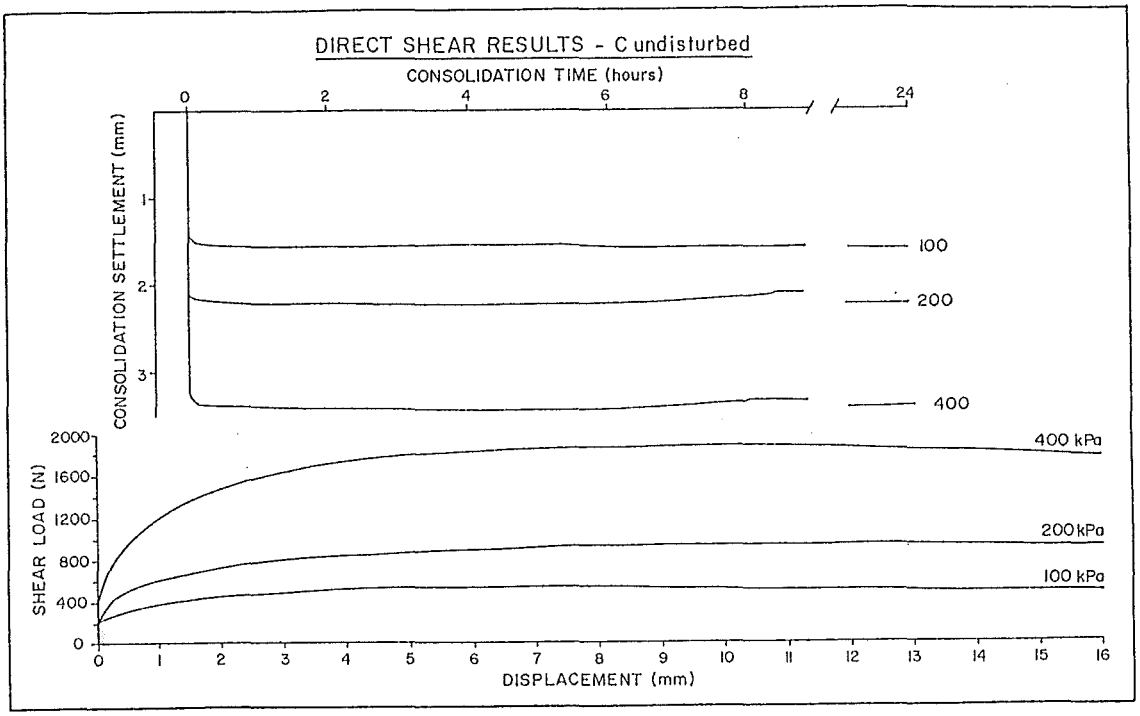

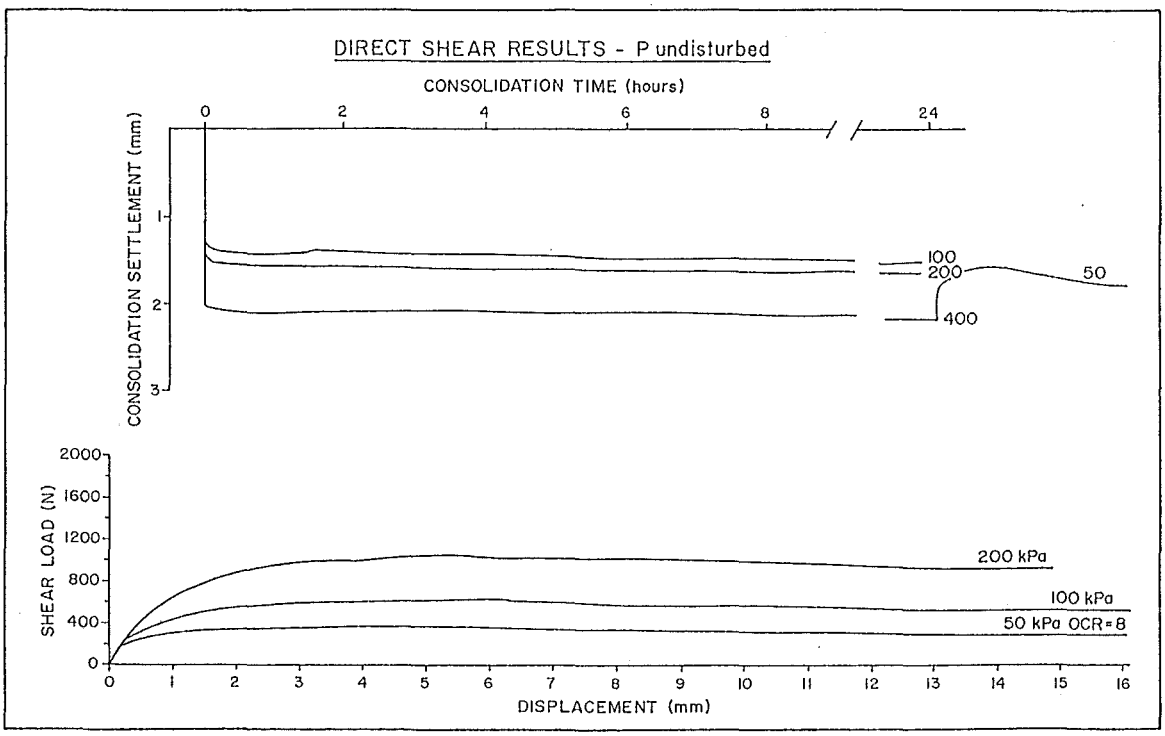

Appendix 5
Computer Modelling

Analysis of ß for 0.5, 0.75, 1.0, 1.25 and 1.5m thick wedges

SARMA NON-VERTICAL SLICE ANALYSIS

Analysis no. 0.5m thick block - wedge 5 degrees

Unit weight of water = 9.8

Side number	1	2
Coordinate xt	11.12	17.00
Coordinate yt	4.60	6.97
Coordinate xw	11.12	17.00
Coordinate yw	4.60	6.97
Coordinate xb	11.12	17.00
Coordinate yb	4.60	6.44
Friction angle	0.00	0.00
Cohesion	0.00	0.00

Slice number	1
Rock unit weight	19.62
Friction angle	28.40
Cohesion	6.00
Force T	0.00
Angle theta	0.00

Effective normal stresses

Base	2.07
Side	0.00

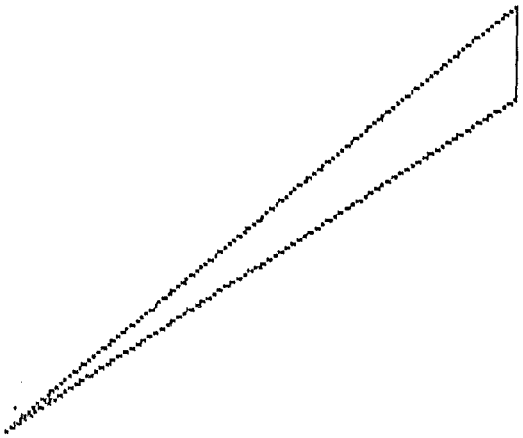

Acceleration Kc = 0.9798 Factor of Safety = 4.19

SARMA NON-VERTICAL SLICE ANALYSIS

Analysis no. 0.5m thick block - wedge 10 degrees

Unit weight of water = 9.8

Side number	1	2
Coordinate xt	14.02	17.00
Coordinate yt	5.76	6.97
Coordinate xw	14.02	17.00
Coordinate yw	5.76	6.97
Coordinate xb	14.02	17.00
Coordinate yb	5.76	6.44
Friction angle	0.00	0.00
Cohesion	0.00	0.00

Slice number	1
Rock unit weight	19.62
Friction angle	28.40
Cohesion	6.00
Force T	0.00
Angle theta	0.00

Effective normal stresses

Base	2.25
Side	0.00

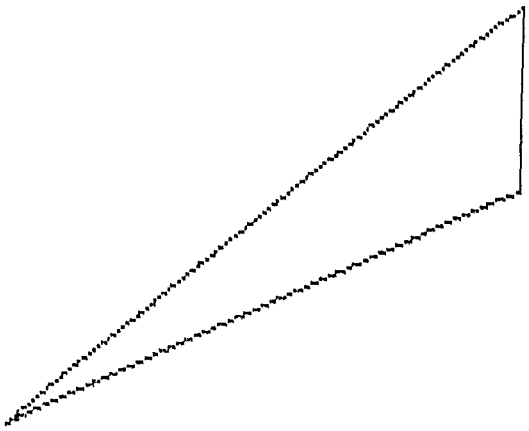

Acceleration Kc = 1.0172 Factor of Safety = 4.63

SARMA NON-VERTICAL SLICE ANALYSIS

Analysis no. 0.5m thick block - wedge 15 degrees

Unit weight of water = 9.8

Side number	1	2
Coordinate xt	15.05	17.00
Coordinate yt	6.19	6.97
Coordinate xw	15.05	17.00
Coordinate yw	6.19	6.97
Coordinate xb	15.05	17.00
Coordinate yb	6.19	6.44
Friction angle	0.00	0.00
Cohesion	0.00	0.00

Slice number	1
Rock unit weight	19.62
Friction angle	28.40
Cohesion	6.00
Force T	0.00
Angle theta	0.00

Effective normal stresses

Base	2.43
Side	0.00

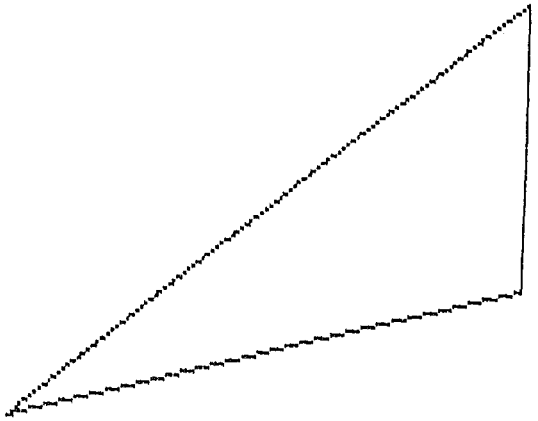

Acceleration Kc = 1.0902 Factor of Safety = 5.47

SARMA NON-VERTICAL SLICE ANALYSIS

Analysis no. 0.5m thick block - wedge 20 degrees

Unit weight of water = 9.8

Side number	1	2
Coordinate xt	15.54	17.00
Coordinate yt	6.38	6.97
Coordinate xw	15.54	17.00
Coordinate yw	6.38	6.97
Coordinate xb	15.54	17.00
Coordinate yb	6.38	6.44
Friction angle	0.00	0.00
Cohesion	0.00	0.00

Slice number	1
Rock unit weight	19.62
Friction angle	28.40
Cohesion	6.00
Force T	0.00
Angle theta	0.00

Effective normal stresses

Base	2.56
Side	0.00

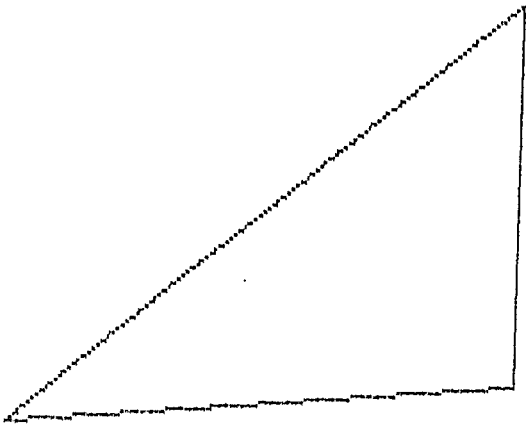

Acceleration Kc = 1.1736 Factor of Safety = 6.43

SARMA NON-VERTICAL SLICE ANALYSIS

Analysis no. 0.5m thick block - wedge 25 degrees

Unit weight of water = 9.8

Side number	1	2
Coordinate xt	15.82	17.00
Coordinate yt	6.50	6.97
Coordinate xw	15.82	17.00
Coordinate yw	6.50	6.97
Coordinate xb	15.82	17.00
Coordinate yb	6.50	6.44
Friction angle	0.00	0.00
Cohesion	0.00	0.00

Slice number	1
Rock unit weight	19.62
Friction angle	28.40
Cohesion	6.00
Force T	0.00
Angle theta	0.00

Effective normal stresses

Base	2.65
Side	0.00

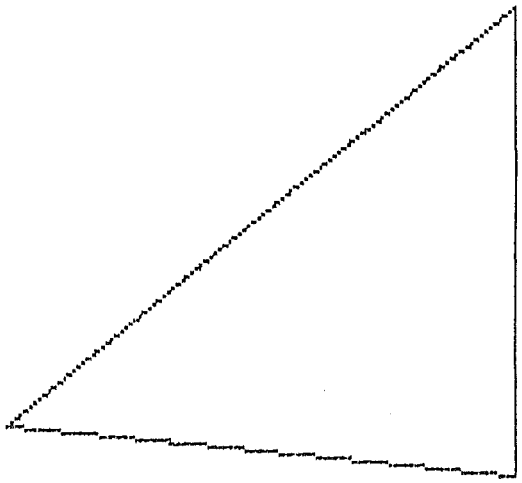

Acceleration Kc = 1.2952 Factor of Safety = 8.13
Large extrapolation - plot of fos vs K suggested to check fos

SARMA NON-VERTICAL SLICE ANALYSIS

Analysis no. 0.5m thick block - wedge 30 degrees

Unit weight of water = 9.8

Side number	1	2
Coordinate xt	16.01	17.00
Coordinate yt	6.67	6.97
Coordinate xw	16.01	17.00
Coordinate yw	6.67	6.97
Coordinate xb	16.01	17.00
Coordinate yb	6.67	6.44
Friction angle	0.00	0.00
Cohesion	0.00	0.00

Slice number	1
Rock unit weight	19.62
Friction angle	28.40
Cohesion	6.00
Force T	0.00
Angle theta	0.00

Effective normal stresses

Base	2.68
Side	0.00

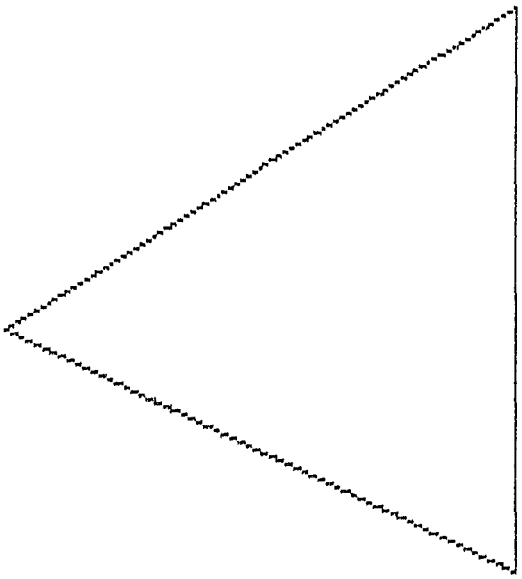

Acceleration Kc = 1.6822 Factor of Safety = 22.20
Large extrapolation - plot of fos vs K suggested to check fos

SARMA NON-VERTICAL SLICE ANALYSIS

Analysis no. 0.75m thick block - wedge 5 degrees

Unit weight of water = 9.8

Side number	1	2
Coordinate xt	8.77	17.00
Coordinate yt	3.92	7.25
Coordinate xw	8.77	17.00
Coordinate yw	3.92	7.25
Coordinate xb	8.77	17.00
Coordinate yb	3.92	6.44
Friction angle	0.00	0.00
Cohesion	0.00	0.00

Slice number	1
Rock unit weight	19.62
Friction angle	28.40
Cohesion	6.00
Force T	0.00
Angle theta	0.00

Effective normal stresses

Base	3.19
Side	0.00

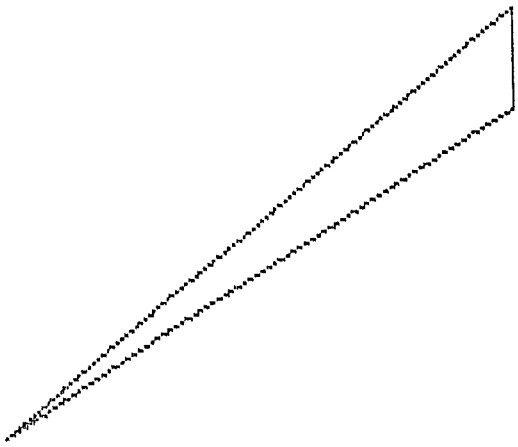

Acceleration Kc = 0.6072

Factor of Safety = 2.99

SARMA NON-VERTICAL SLICE ANALYSIS

Analysis no. 0.75m thick block - wedge 10 degrees

Unit weight of water = 9.8

Side number	1	2
Coordinate xt	12.76	17.00
Coordinate yt	5.53	7.25
Coordinate xw	12.76	17.00
Coordinate yw	5.53	7.25
Coordinate xb	12.76	17.00
Coordinate yb	5.53	6.44
Friction angle	0.00	0.00
Cohesion	0.00	0.00

Slice number	1
Rock unit weight	19.62
Friction angle	28.40
Cohesion	6.00
Force T	0.00
Angle theta	0.00

Effective normal stresses

Base	3.47
Side	0.00

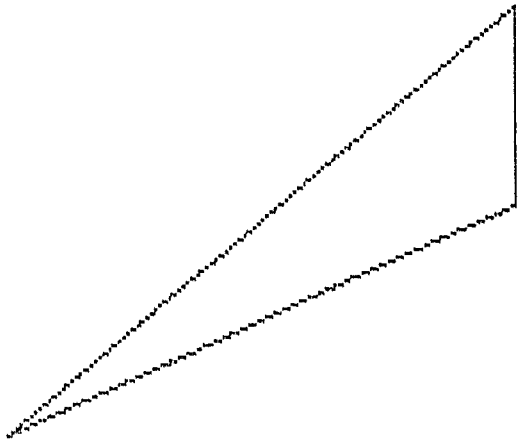

Acceleration Kc = 0.6513

Factor of Safety = 3.36

SARMA NON-VERTICAL SLICE ANALYSIS

Analysis no. 0.75m thick block - wedge 15 degrees

Unit weight of water = 9.8

Side number	1	2
Coordinate xt	14.12	17.00
Coordinate yt	6.08	7.25
Coordinate xw	14.12	17.00
Coordinate yw	6.08	7.25
Coordinate xb	14.12	17.00
Coordinate yb	6.08	6.44
Friction angle	0.00	0.00
Cohesion	0.00	0.00

Slice number	1
Rock unit weight	19.62
Friction angle	28.40
Cohesion	6.00
Force T	0.00
Angle theta	0.00

Effective normal stresses

Base	3.72
Side	0.00

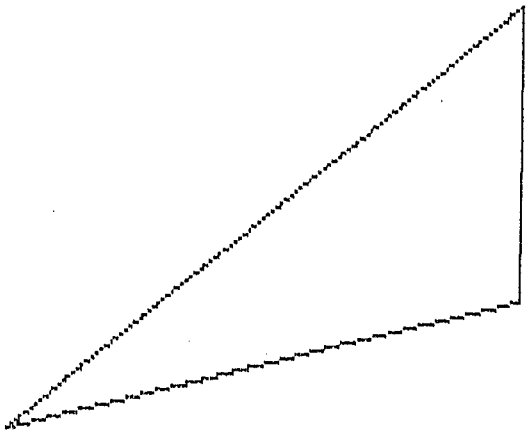

Acceleration Kc = 0.7103 Factor of Safety = 3.88

SARMA NON-VERTICAL SLICE ANALYSIS

Analysis no. 0.75m thick block - wedge 20 degrees

Unit weight of water = 9.8

Side number	1	2
Coordinate xt	14.83	17.00
Coordinate yt	6.37	7.25
Coordinate xw	14.83	17.00
Coordinate yw	6.37	7.25
Coordinate xb	14.83	17.00
Coordinate yb	6.37	6.44
Friction angle	0.00	0.00
Cohesion	0.00	0.00

Slice number	1
Rock unit weight	19.62
Friction angle	28.40
Cohesion	6.00
Force T	0.00
Angle theta	0.00

Effective normal stresses

Base	3.92
Side	0.00

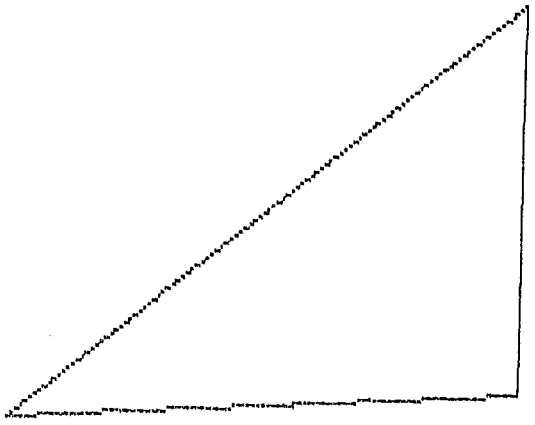

Acceleration Kc = 0.7905 Factor of Safety = 4.70

SARMA NON-VERTICAL SLICE ANALYSIS

Analysis no. 0.75m thick block - wedge 25 degrees

Unit weight of water = 9.8

Side number	1	2
Coordinate xt	15.24	17.00
Coordinate yt	6.54	7.25
Coordinate xw	15.24	17.00
Coordinate yw	6.54	7.25
Coordinate xb	15.24	17.00
Coordinate yb	6.54	6.44
Friction angle	0.00	0.00
Cohesion	0.00	0.00

Slice number	1
Rock unit weight	19.62
Friction angle	28.40
Cohesion	6.00
Force T	0.00
Angle theta	0.00

Effective normal stresses

Base	4.06
Side	0.00

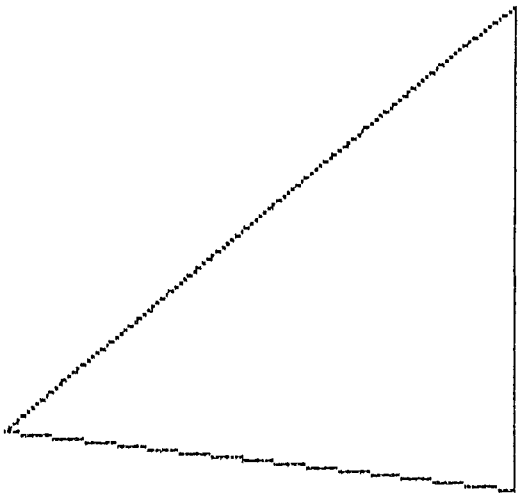

Acceleration Kc = 0.8886 Factor of Safety = 5.90

SARMA NON-VERTICAL SLICE ANALYSIS

Analysis no. 0.75m thick block - wedge 30 degrees

Unit weight of water = 9.8

Side number	1	2
Coordinate xt	15.31	17.00
Coordinate yt	6.65	7.25
Coordinate xw	15.31	17.00
Coordinate yw	6.65	7.25
Coordinate xb	15.31	17.00
Coordinate yb	6.65	6.44
Friction angle	0.00	0.00
Cohesion	0.00	0.00

Slice number	1
Rock unit weight	19.62
Friction angle	28.40
Cohesion	6.00
Force T	0.00
Angle theta	0.00

Effective normal stresses

Base	4.10
Side	0.00

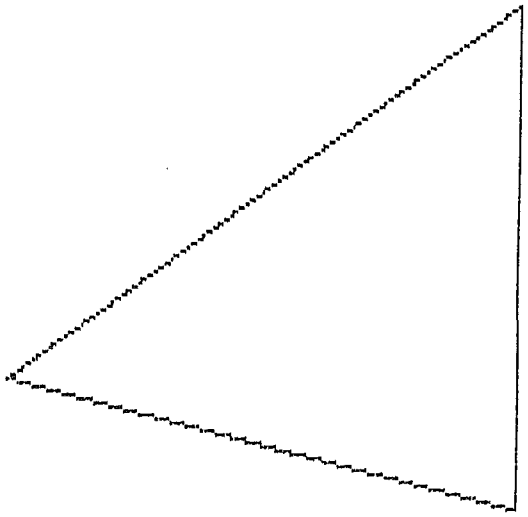

Acceleration Kc = 1.0014 Factor of Safety = 8.55
Large extrapolation - plot of fos vs K suggested to check fos

SARMA NON-VERTICAL SLICE ANALYSIS

Analysis no. 1.0m thick block - wedge 5 degrees

Unit weight of water = 9.8

Side number	1	2
Coordinate xt	6.03	17.00
Coordinate yt	3.09	7.51
Coordinate xw	6.03	17.00
Coordinate yw	3.09	7.51
Coordinate xb	6.03	17.00
Coordinate yb	3.09	6.44
Friction angle	0.00	0.00
Cohesion	0.00	0.00

Slice number	1
Rock unit weight	19.62
Friction angle	28.40
Cohesion	6.00
Force T	0.00
Angle theta	0.00

Effective normal stresses

Base	4.21
Side	0.00

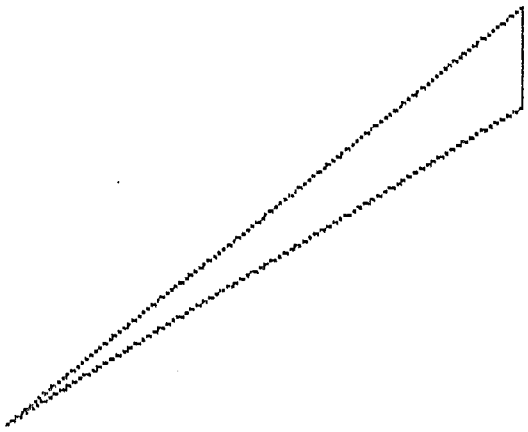

Acceleration Kc = 0.4362 Factor of Safety = 2.43

SARMA NON-VERTICAL SLICE ANALYSIS

Analysis no. 1.0m thick block - wedge 10 degrees

Unit weight of water = 9.8

Side number	1	2
Coordinate xt	11.12	17.00
Coordinate yt	5.13	7.51
Coordinate xw	11.12	17.00
Coordinate yw	5.13	7.51
Coordinate xb	11.12	17.00
Coordinate yb	5.13	6.44
Friction angle	0.00	0.00
Cohesion	0.00	0.00

Slice number	1
Rock unit weight	19.62
Friction angle	28.40
Cohesion	6.00
Force T	0.00
Angle theta	0.00

Effective normal stresses

Base	4.56
Side	0.00

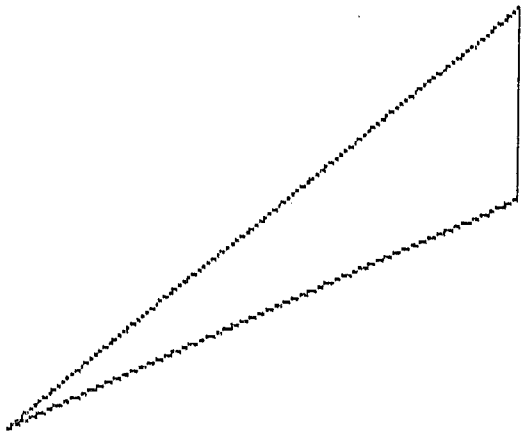

Acceleration Kc = 0.4753 Factor of Safety = 2.71

SARMA NON-VERTICAL SLICE ANALYSIS

Analysis no. 1.0m thick block - wedge 15 degrees

Unit weight of water = 9.8

Side number	1	2
Coordinate xt	13.20	17.00
Coordinate yt	5.97	7.51
Coordinate xw	13.20	17.00
Coordinate yw	5.97	7.51
Coordinate xb	13.20	17.00
Coordinate yb	5.97	6.44
Friction angle	0.00	0.00
Cohesion	0.00	0.00

Slice number	1
Rock unit weight	19.62
Friction angle	28.40
Cohesion	6.00
Force T	0.00
Angle theta	0.00

Effective normal stresses

Base	4.92
Side	0.00

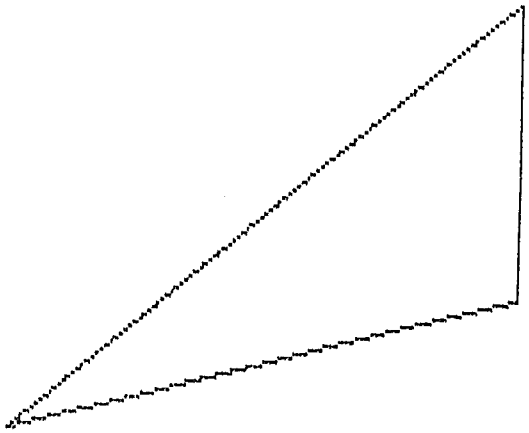

Acceleration Kc = 0.5372 Factor of Safety = 3.19

SARMA NON-VERTICAL SLICE ANALYSIS

Analysis no. 1.0m thick block - wedge 20 degrees

Unit weight of water = 9.8

Side number	1	2
Coordinate xt	14.12	17.00
Coordinate yt	6.35	7.51
Coordinate xw	14.12	17.00
Coordinate yw	6.35	7.51
Coordinate xb	14.12	17.00
Coordinate yb	6.35	6.44
Friction angle	0.00	0.00
Cohesion	0.00	0.00

Slice number	1
Rock unit weight	19.62
Friction angle	28.40
Cohesion	6.00
Force T	0.00
Angle theta	0.00

Effective normal stresses

Base	5.18
Side	0.00

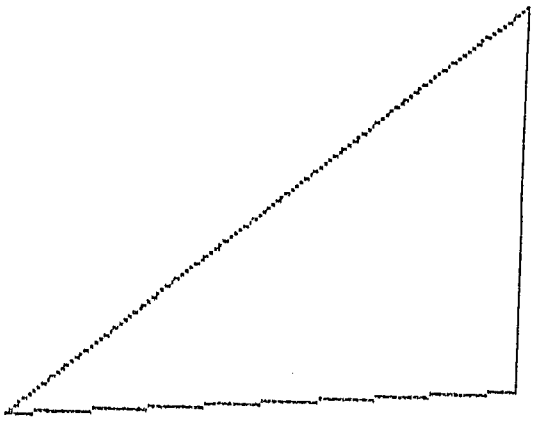

Acceleration Kc = 0.6122 Factor of Safety = 3.88

SARMA NON-VERTICAL SLICE ANALYSIS

Analysis no. 1.0m thick block - wedge 25 degrees

Unit weight of water = 9.8

Side number	1	2
Coordinate xt	14.66	17.00
Coordinate yt	6.56	7.51
Coordinate xw	14.66	17.00
Coordinate yw	6.56	7.51
Coordinate xb	14.66	17.00
Coordinate yb	6.56	6.44
Friction angle	0.00	0.00
Cohesion	0.00	0.00

Slice number	1
Rock unit weight	19.62
Friction angle	28.40
Cohesion	6.00
Force T	0.00
Angle theta	0.00

Effective normal stresses

Base	5.35
Side	0.00

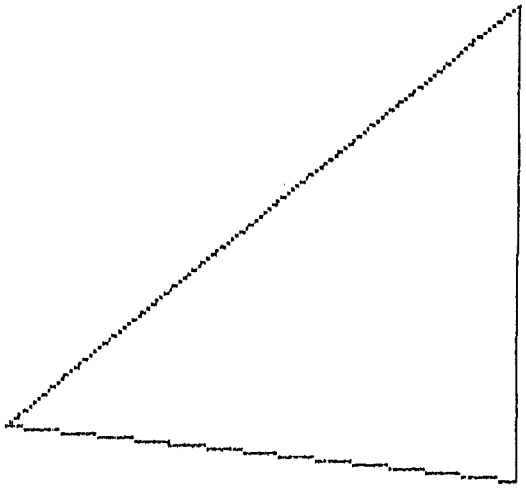

Acceleration Kc = 0.6914 Factor of Safety = 4.75

SARMA NON-VERTICAL SLICE ANALYSIS

Analysis no. 1.0m thick block - wedge 30 degrees

Unit weight of water = 9.8

Side number	1	2
Coordinate xt	15.04	17.00
Coordinate yt	6.72	7.51
Coordinate xw	15.04	17.00
Coordinate yw	6.72	7.51
Coordinate xb	15.04	17.00
Coordinate yb	6.72	6.44
Friction angle	0.00	0.00
Cohesion	0.00	0.00

Slice number	1
Rock unit weight	19.62
Friction angle	28.40
Cohesion	6.00
Force T	0.00
Angle theta	0.00

Effective normal stresses

Base	5.46
Side	0.00

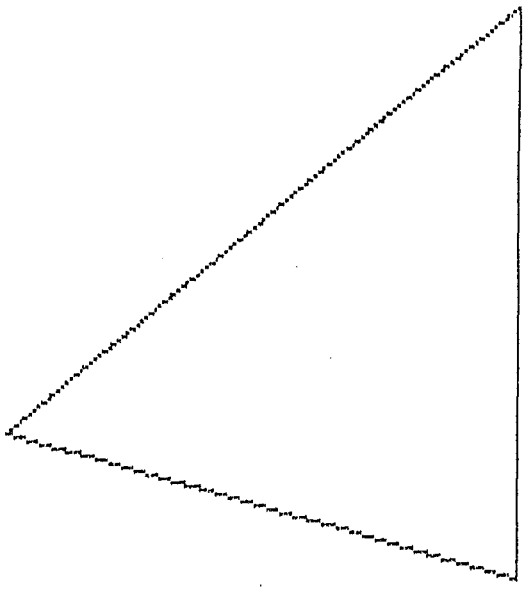

Acceleration Kc = 0.8015 Factor of Safety = 6.35
Large extrapolation - plot of fos vs K suggested to check fos

SARMA NON-VERTICAL SLICE ANALYSIS

Analysis no. 1.25m thick block - wedge 5 degrees

Unit weight of water = 9.8

Side number	1	2
Coordinate xt	3.28	17.00
Coordinate yt	2.25	7.79
Coordinate xw	3.28	17.00
Coordinate yw	2.25	7.79
Coordinate xb	3.28	17.00
Coordinate yb	2.25	6.44
Friction angle	0.00	0.00
Cohesion	0.00	0.00

Slice number	1
Rock unit weight	19.62
Friction angle	28.40
Cohesion	6.00
Force T	0.00
Angle theta	0.00

Effective normal stresses

Base	5.32
Side	0.00

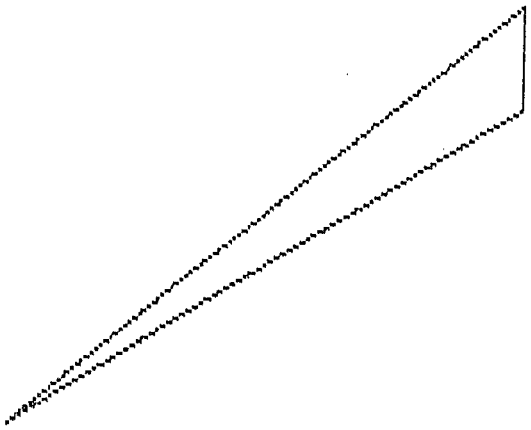

Acceleration Kc = 0.3245 Factor of Safety = 2.07

SARMA NON-VERTICAL SLICE ANALYSIS

Analysis no. 1.25m thick block - wedge 10 degrees

Unit weight of water = 9.8

Side number	1	2
Coordinate xt	9.82	17.00
Coordinate yt	4.86	7.79
Coordinate xw	9.82	17.00
Coordinate yw	4.86	7.79
Coordinate xb	9.82	17.00
Coordinate yb	4.86	6.44
Friction angle	0.00	0.00
Cohesion	0.00	0.00

Slice number	1
Rock unit weight	19.62
Friction angle	28.40
Cohesion	6.00
Force T	0.00
Angle theta	0.00

Effective normal stresses

Base	5.76
Side	0.00

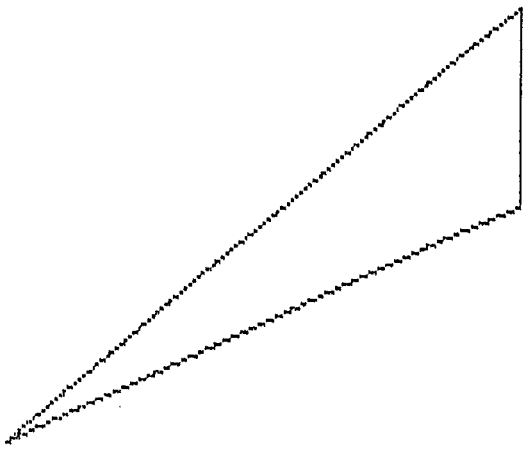

Acceleration Kc = 0.3641 Factor of Safety = 2.30

SARMA NON-VERTICAL SLICE ANALYSIS

Analysis no. 1.25m thick block - wedge 15 degrees

Unit weight of water = 9.8

Side number	1	2
Coordinate xt	12.19	17.00
Coordinate yt	5.83	7.79
Coordinate xw	12.19	17.00
Coordinate yw	5.83	7.79
Coordinate xb	12.19	17.00
Coordinate yb	5.83	6.44
Friction angle	0.00	0.00
Cohesion	0.00	0.00

Slice number	1
Rock unit weight	19.62
Friction angle	28.40
Cohesion	6.00
Force T	0.00
Angle theta	0.00

Effective normal stresses

Base	6.19
Side	0.00

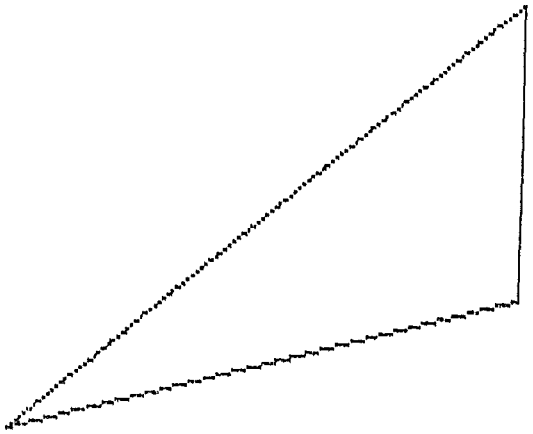

Acceleration Kc = 0.4211 Factor of Safety = 2.70

SARMA NON-VERTICAL SLICE ANALYSIS

Analysis no. 1.25m thick block - wedge 20 degrees

Unit weight of water = 9.8

Side number	1	2
Coordinate xt	13.39	17.00
Coordinate yt	6.33	7.79
Coordinate xw	13.39	17.00
Coordinate yw	6.33	7.79
Coordinate xb	13.39	17.00
Coordinate yb	6.33	6.44
Friction angle	0.00	0.00
Cohesion	0.00	0.00

Slice number	1
Rock unit weight	19.62
Friction angle	28.40
Cohesion	6.00
Force T	0.00
Angle theta	0.00

Effective normal stresses

Base	6.54
Side	0.00

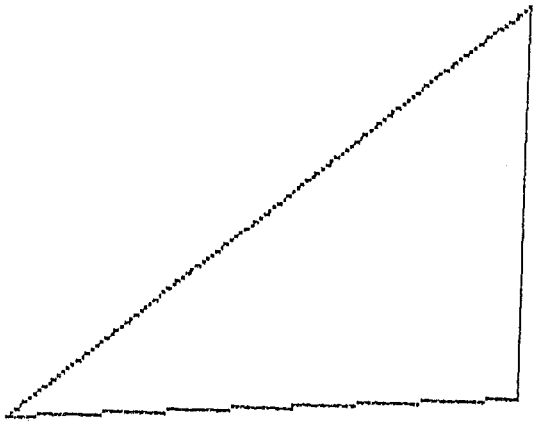

Acceleration Kc = 0.4953 Factor of Safety = 3.33

SARMA NON-VERTICAL SLICE ANALYSIS

Analysis no. 1.25m thick block - wedge 25 degrees

Unit weight of water = 9.8

Side number	1	2
Coordinate xt	14.06	17.00
Coordinate yt	6.60	7.79
Coordinate xw	14.06	17.00
Coordinate yw	6.60	7.79
Coordinate xb	14.06	17.00
Coordinate yb	6.60	6.44
Friction angle	0.00	0.00
Cohesion	0.00	0.00

Slice number	1
Rock unit weight	19.62
Friction angle	28.40
Cohesion	6.00
Force T	0.00
Angle theta	0.00

Effective normal stresses

Base	6.76
Side	0.00

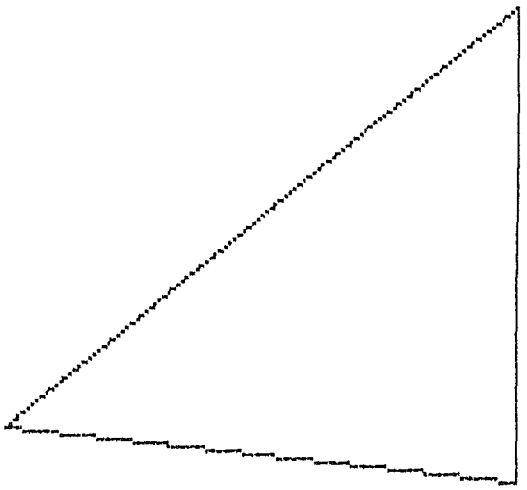

Acceleration Kc = 0.5729 Factor of Safety = 4.14

SARMA NON-VERTICAL SLICE ANALYSIS

Analysis no. 1.25m thick block - wedge 30 degrees

Unit weight of water = 9.8

Side number	1	2
Coordinate xt	14.51	17.00
Coordinate yt	6.78	7.79
Coordinate xw	14.51	17.00
Coordinate yw	6.78	7.79
Coordinate xb	14.51	17.00
Coordinate yb	6.78	6.44
Friction angle	0.00	0.00
Cohesion	0.00	0.00

Slice number	1
Rock unit weight	19.62
Friction angle	28.40
Cohesion	6.00
Force T	0.00
Angle theta	0.00

Effective normal stresses

Base	6.88
Side	0.00

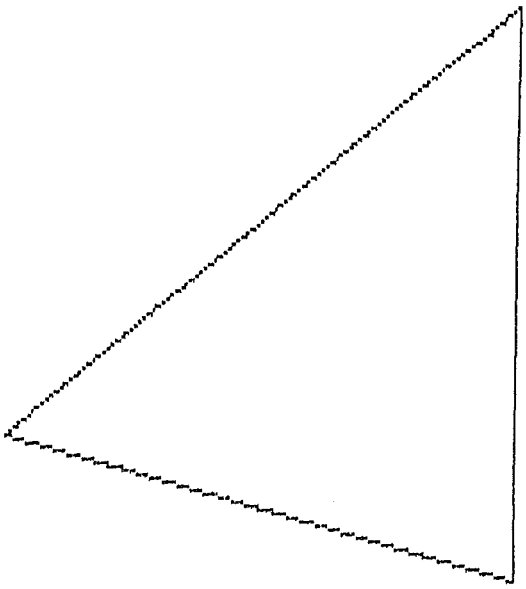

Acceleration Kc = 0.6617 Factor of Safety = 5.32
Large extrapolation - plot of fos vs K suggested to check fos

SARMA NON-VERTICAL SLICE ANALYSIS

Analysis no. 1.25m thick block - wedge 35 degrees

Unit weight of water = 9.8

Side number	1	2
Coordinate xt	14.88	17.00
Coordinate yt	6.93	7.79
Coordinate xw	14.88	17.00
Coordinate yw	6.93	7.79
Coordinate xb	14.88	17.00
Coordinate yb	6.93	6.44
Friction angle	0.00	0.00
Cohesion	0.00	0.00

Slice number	1
Rock unit weight	19.62
Friction angle	28.40
Cohesion	6.00
Force T	0.00
Angle theta	0.00

Effective normal stresses

Base	6.92
Side	0.00

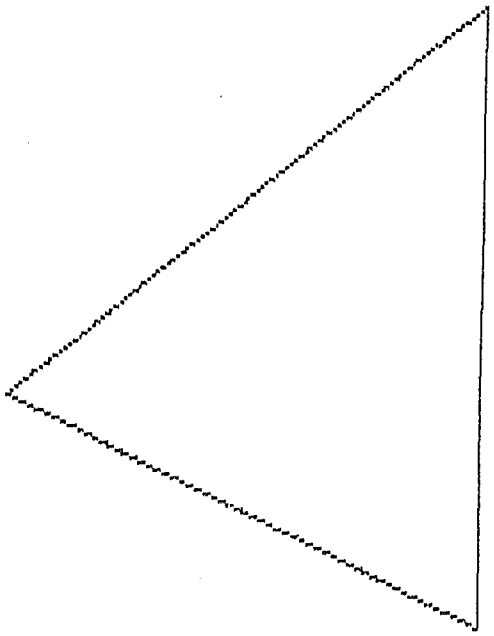

Acceleration Kc = 0.7843 Factor of Safety = 7.64

Large extrapolation - plot of fos vs K suggested to check fos

SARMA NON-VERTICAL SLICE ANALYSIS

Analysis no. 1.5m thick block - wedge 5 degrees

Unit weight of water = 9.8

Side number	1	2
Coordinate xt	0.54	17.00
Coordinate yt	1.41	7.95
Coordinate xw	0.54	17.00
Coordinate yw	1.41	7.95
Coordinate xb	0.54	17.00
Coordinate yb	1.41	6.44
Friction angle	0.00	0.00
Cohesion	0.00	0.00

Slice number	1
Rock unit weight	19.62
Friction angle	28.40
Cohesion	6.00
Force T	0.00
Angle theta	0.00

Effective normal stresses

Base	5.96
Side	0.00

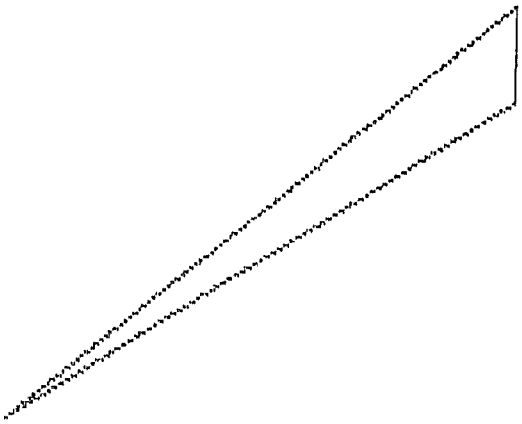

Acceleration Kc = 0.2826 Factor of Safety = 1.94

SARMA NON-VERTICAL SLICE ANALYSIS

Analysis no. 1.5m thick block - wedge 10 degrees

Unit weight of water = 9.8

Side number	1	2
Coordinate xt	7.88	17.00
Coordinate yt	4.66	7.95
Coordinate xw	7.88	17.00
Coordinate yw	4.66	7.95
Coordinate xb	7.88	17.00
Coordinate yb	4.66	6.44
Friction angle	0.00	0.00
Cohesion	0.00	0.00

Slice number	1
Rock unit weight	19.62
Friction angle	28.40
Cohesion	6.00
Force T	0.00
Angle theta	0.00

Effective normal stresses

Base	6.64
Side	0.00

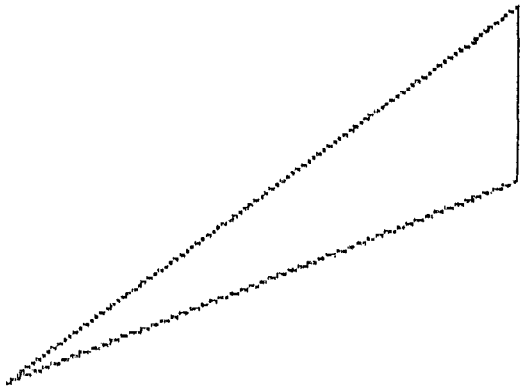

Acceleration Kc = 0.3566 Factor of Safety = 2.43

SARMA NON-VERTICAL SLICE ANALYSIS

Analysis no. 1.5m thick block - wedge 15 degrees

Unit weight of water = 9.8

Side number	1	2
Coordinate xt	11.54	17.00
Coordinate yt	5.74	7.95
Coordinate xw	11.54	17.00
Coordinate yw	5.74	7.95
Coordinate xb	11.54	17.00
Coordinate yb	5.74	6.44
Friction angle	0.00	0.00
Cohesion	0.00	0.00

Slice number	1
Rock unit weight	19.62
Friction angle	28.40
Cohesion	6.00
Force T	0.00
Angle theta	0.00

Effective normal stresses

Base	6.92
Side	0.00

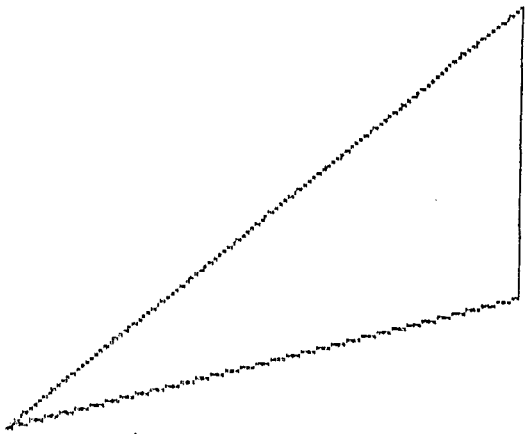

Acceleration Kc = 0.3759 Factor of Safety = 2.52

SARMA NON-VERTICAL SLICE ANALYSIS

Analysis no. 1.5m thick block - wedge 20 degrees

Unit weight of water = 9.8

Side number	1	2
Coordinate xt	12.92	17.00
Coordinate yt	6.30	7.95
Coordinate xw	12.92	17.00
Coordinate yw	6.30	7.95
Coordinate xb	12.92	17.00
Coordinate yb	6.30	6.44
Friction angle	0.00	0.00
Cohesion	0.00	0.00

Slice number	1
Rock unit weight	19.62
Friction angle	28.40
Cohesion	6.00
Force T	0.00
Angle theta	0.00

Effective normal stresses

Base	7.30
Side	0.00

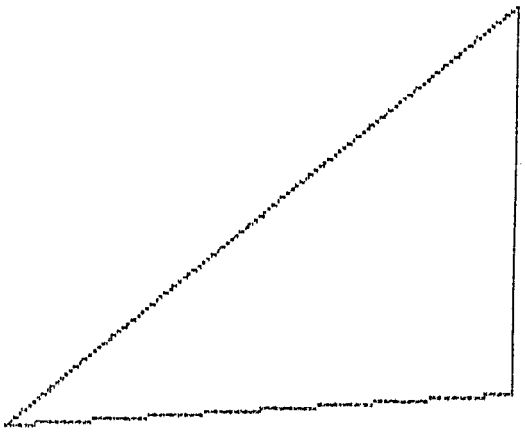

Acceleration Kc = 0.4450 Factor of Safety = 3.08

SARMA NON-VERTICAL SLICE ANALYSIS

Analysis no. 1.5m thick block - wedge 25 degrees

Unit weight of water = 9.8

Side number	1	2
Coordinate xt	13.68	17.00
Coordinate yt	6.60	7.95
Coordinate xw	13.68	17.00
Coordinate yw	6.60	7.95
Coordinate xb	13.68	17.00
Coordinate yb	6.60	6.44
Friction angle	0.00	0.00
Cohesion	0.00	0.00

Slice number	1
Rock unit weight	19.62
Friction angle	28.40
Cohesion	6.00
Force T	0.00
Angle theta	0.00

Effective normal stresses

Base	7.54
Side	0.00

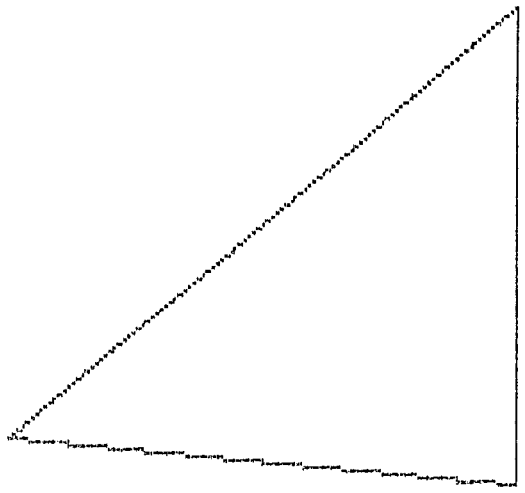

Acceleration Kc = 0.5164 Factor of Safety = 3.78

SARMA NON-VERTICAL SLICE ANALYSIS

Analysis no. 1.5m thick block - wedge 30 degrees

Unit weight of water = 9.8

Side number	1	2
Coordinate xt	14.21	17.00
Coordinate yt	6.82	7.95
Coordinate xw	14.21	17.00
Coordinate yw	6.82	7.95
Coordinate xb	14.21	17.00
Coordinate yb	6.82	6.44
Friction angle	0.00	0.00
Cohesion	0.00	0.00

Slice number	1
Rock unit weight	19.62
Friction angle	28.40
Cohesion	6.00
Force T	0.00
Angle theta	0.00

Effective normal stresses

Base	7.69
Side	0.00

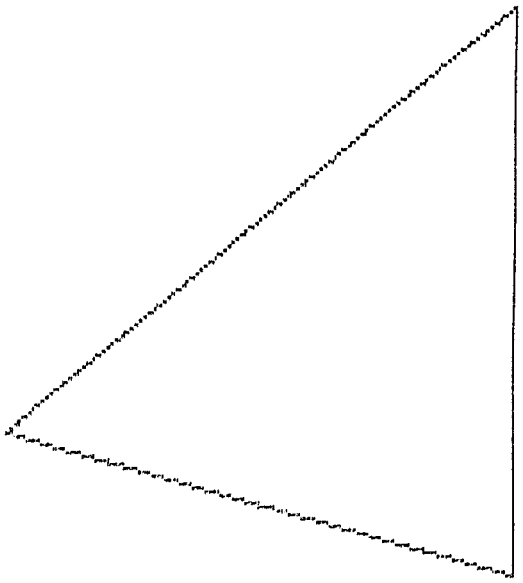

Acceleration Kc = 0.6088 Factor of Safety = 4.99

SARMA NON-VERTICAL SLICE ANALYSIS

Analysis no. 1.5m thick block - wedge 35 degrees

Unit weight of water = 9.8

Side number	1	2
Coordinate xt	14.61	17.00
Coordinate yt	6.98	7.95
Coordinate xw	14.61	17.00
Coordinate yw	6.98	7.95
Coordinate xb	14.61	17.00
Coordinate yb	6.98	6.44
Friction angle	0.00	0.00
Cohesion	0.00	0.00

Slice number	1
Rock unit weight	19.62
Friction angle	28.40
Cohesion	6.00
Force T	0.00
Angle theta	0.00

Effective normal stresses

Base	7.74
Side	0.00

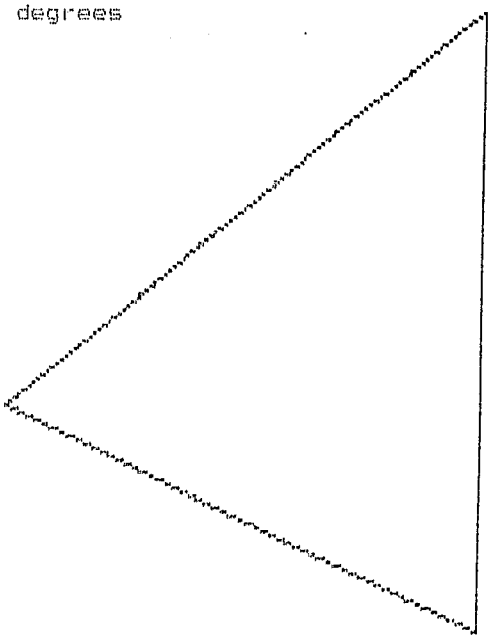

Acceleration Kc = 0.7194 Factor of Safety = 7.00
Large extrapolation - plot of fos vs K suggested to check fos

Analysis of ß for 0.5m to 1.5m thick wedges plus an additional 2m long block

SARMA NON-VERTICAL SLICE ANALYSIS

Analysis no. 0.75m thick block with 2m block - wedge 5 degrees

Unit weight of water = 9.8

Side number	1	2	3
Coordinate xt	8.77	17.00	19.00
Coordinate yt	3.92	7.25	8.05
Coordinate xw	8.77	17.00	19.00
Coordinate yw	3.92	7.25	8.05
Coordinate xb	8.77	17.00	19.00
Coordinate yb	3.92	6.44	7.24
Friction angle	0.00	28.40	0.00
Cohesion	0.00	6.00	0.00

Slice number	1	2
Rock unit weight	19.62	19.62
Friction angle	28.40	28.40
Cohesion	6.00	6.00
Force T	0.00	0.00
Angle theta	0.00	0.00

Effective normal stresses

Base		3.36	5.22
Side	0.00	4.45	

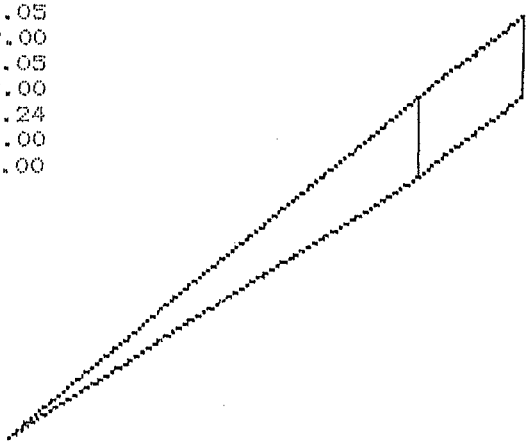

Acceleration Kc = 0.4889 Factor of Safety = 2.54

SARMA NON-VERTICAL SLICE ANALYSIS

Analysis no. 0.75m thick block with 2m block - wedge 10 degrees

Unit weight of water = 9.8

Side number	1	2	3
Coordinate xt	12.76	17.00	19.00
Coordinate yt	5.53	7.25	8.05
Coordinate xw	12.76	17.00	19.00
Coordinate yw	5.53	7.25	8.05
Coordinate xb	12.76	17.00	19.00
Coordinate yb	5.53	6.44	7.24
Friction angle	0.00	28.40	0.00
Cohesion	0.00	6.00	0.00

Slice number	1	2
Rock unit weight	19.62	19.62
Friction angle	28.40	28.40
Cohesion	6.00	6.00
Force T	0.00	0.00
Angle theta	0.00	0.00

Effective normal stresses

Base		3.91	5.19
Side	0.00	4.24	

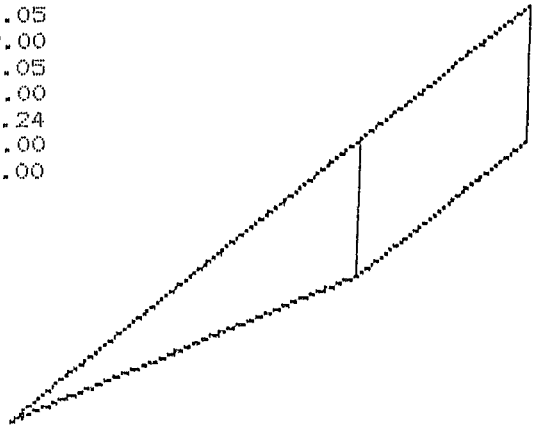

Acceleration Kc = 0.4674 Factor of Safety = 2.49

SARMA NON-VERTICAL SLICE ANALYSIS

Analysis no. 0.75m thick block with 2m block - wedge 15 degrees

Unit weight of water = 9.8

Side number	1	2	3
Coordinate xt	14.12	17.00	19.00
Coordinate yt	6.08	7.25	8.05
Coordinate xw	14.12	17.00	19.00
Coordinate yw	6.08	7.25	8.05
Coordinate xb	14.12	17.00	19.00
Coordinate yb	6.08	6.44	7.24
Friction angle	0.00	28.40	0.00
Cohesion	0.00	6.00	0.00

Slice number	1	2
Rock unit weight	19.62	19.62
Friction angle	28.40	28.40
Cohesion	6.00	6.00
Force T	0.00	0.00
Angle theta	0.00	0.00

Effective normal stresses

Base		4.49	5.19
Side	0.00	4.27	

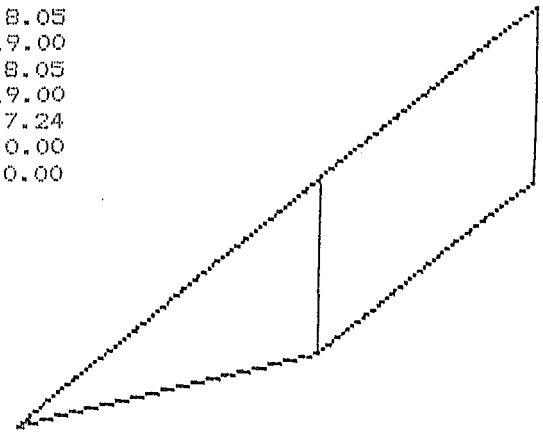

Acceleration Kc = 0.4736 Factor of Safety = 2.50

SARMA NON-VERTICAL SLICE ANALYSIS

Analysis no. 0.75m thick block with 2m block - wedge 20 degrees

Unit weight of water = 9.8

Side number	1	2	3
Coordinate xt	14.83	17.00	19.00
Coordinate yt	6.37	7.25	8.05
Coordinate xw	14.83	17.00	19.00
Coordinate yw	6.37	7.25	8.05
Coordinate xb	14.83	17.00	19.00
Coordinate yb	6.37	6.44	7.24
Friction angle	0.00	28.40	0.00
Cohesion	0.00	6.00	0.00

Slice number	1	2
Rock unit weight	19.62	19.62
Friction angle	28.40	28.40
Cohesion	6.00	6.00
Force T	0.00	0.00
Angle theta	0.00	0.00

Effective normal stresses

Base		5.10	5.23
Side	0.00	4.45	

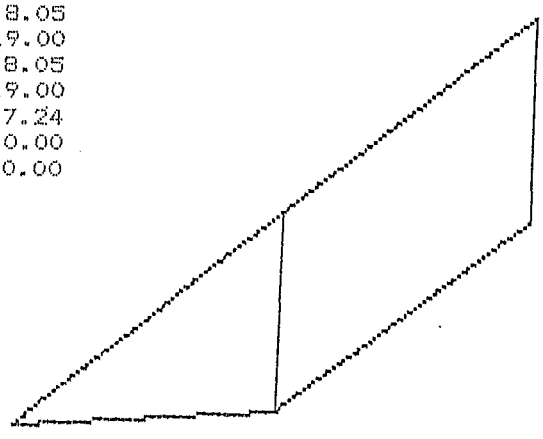

Acceleration Kc = 0.5006 Factor of Safety = 2.55

SARMA NON-VERTICAL SLICE ANALYSIS

Analysis no. 0.75m thick block with 2m block - wedge 25 degrees

Unit weight of water = 9.8

Side number	1	2	3
Coordinate xt	15.24	17.00	19.00
Coordinate yt	6.54	7.25	8.05
Coordinate xw	15.24	17.00	19.00
Coordinate yw	6.54	7.25	8.05
Coordinate xb	15.24	17.00	19.00
Coordinate yb	6.54	6.44	7.24
Friction angle	0.00	28.40	0.00
Cohesion	0.00	6.00	0.00

Slice number	1	2
Rock unit weight	19.62	19.62
Friction angle	28.40	28.40
Cohesion	6.00	6.00
Force T	0.00	0.00
Angle theta	0.00	0.00

Effective normal stresses

Base		5.67	5.29
Side	0.00	4.72	

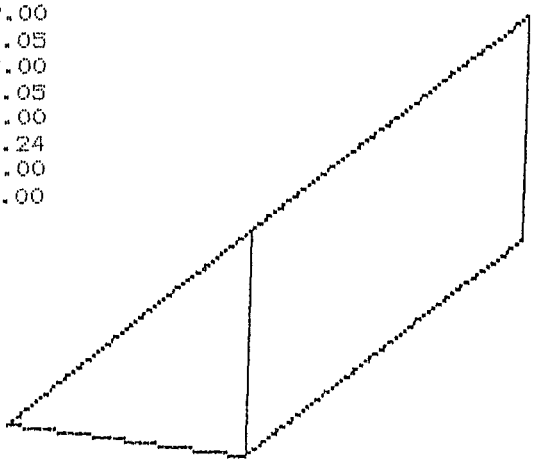

Acceleration Kc = 0.5454

Factor of Safety = 2.63

SARMA NON-VERTICAL SLICE ANALYSIS

Analysis no. 0.75m thick block with 2m block - wedge 30 degrees

Unit weight of water = 9.8

Side number	1	2	3
Coordinate xt	15.31	17.00	19.00
Coordinate yt	6.65	7.25	8.05
Coordinate xw	15.31	17.00	19.00
Coordinate yw	6.65	7.25	8.05
Coordinate xb	15.31	17.00	19.00
Coordinate yb	6.65	6.44	7.24
Friction angle	0.00	28.40	0.00
Cohesion	0.00	6.00	0.00

Slice number	1	2
Rock unit weight	19.62	19.62
Friction angle	28.40	28.40
Cohesion	6.00	6.00
Force T	0.00	0.00
Angle theta	0.00	0.00

Effective normal stresses

Base		5.88	5.43
Side	0.00	5.36	

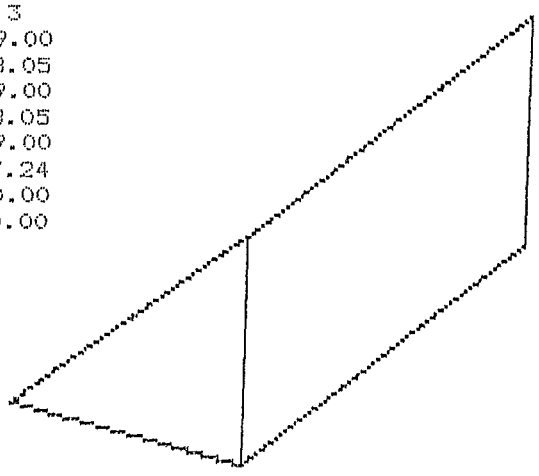

Acceleration Kc = 0.6155

Factor of Safety = 2.84

SARMA NON-VERTICAL SLICE ANALYSIS

Analysis no. 0.5m thick block with 2m long block - wedge 5 degrees

Unit weight of water = 9.8

Side number	1	2	3
Coordinate xt	11.12	17.00	19.00
Coordinate yt	4.60	6.97	7.77
Coordinate xw	11.12	17.00	19.00
Coordinate yw	4.60	6.97	7.77
Coordinate xb	11.12	17.00	19.00
Coordinate yb	4.60	6.44	7.24
Friction angle	0.00	28.40	0.00
Cohesion	0.00	6.00	0.00

Slice number	1	2
Rock unit weight	19.62	19.62
Friction angle	28.40	28.40
Cohesion	6.00	6.00
Force T	0.00	0.00
Angle theta	0.00	0.00

Effective normal stresses

Base		2.16	3.60
Side	0.00	4.43	

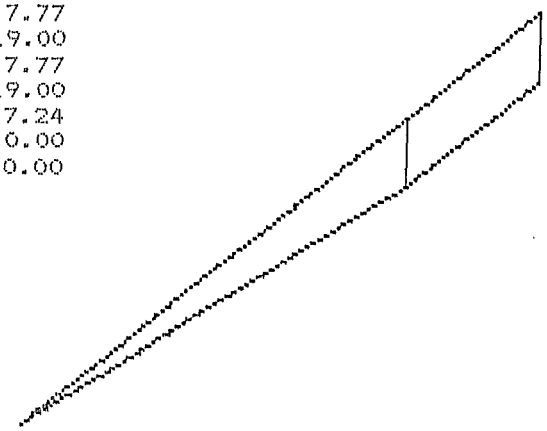

Acceleration Kc = 0.7602 Factor of Safety = 3.36

SARMA NON-VERTICAL SLICE ANALYSIS

Analysis no. 0.5m thick block with 2m long block - wedge 10 degrees

Unit weight of water = 9.8

Side number	1	2	3
Coordinate xt	14.02	17.00	19.00
Coordinate yt	5.76	6.97	7.77
Coordinate xw	14.02	17.00	19.00
Coordinate yw	5.76	6.97	7.77
Coordinate xb	14.02	17.00	19.00
Coordinate yb	5.76	6.44	7.24
Friction angle	0.00	28.40	0.00
Cohesion	0.00	6.00	0.00

Slice number	1	2
Rock unit weight	19.62	19.62
Friction angle	28.40	28.40
Cohesion	6.00	6.00
Force T	0.00	0.00
Angle theta	0.00	0.00

Effective normal stresses

Base		2.53	3.54
Side	0.00	3.83	

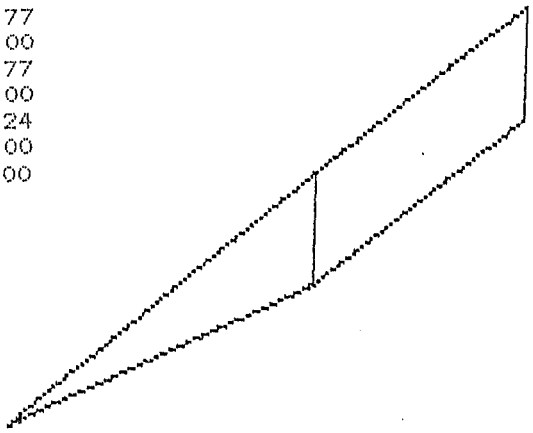

Acceleration Kc = 0.6991 Factor of Safety = 3.18

SARMA NON-VERTICAL SLICE ANALYSIS

Analysis no. 0.5m thick block with 2m long block - wedge 15 degrees

Unit weight of water = 9.8

Side number	1	2	3
Coordinate xt	15.05	17.00	19.00
Coordinate yt	6.19	6.97	7.77
Coordinate xw	15.05	17.00	19.00
Coordinate yw	6.19	6.97	7.77
Coordinate xb	15.05	17.00	19.00
Coordinate yb	6.19	6.44	7.24
Friction angle	0.00	28.40	0.00
Cohesion	0.00	6.00	0.00

Slice number	1	2
Rock unit weight	19.62	19.62
Friction angle	28.40	28.40
Cohesion	6.00	6.00
Force T	0.00	0.00
Angle theta	0.00	0.00

Effective normal stresses

Base	2.98	3.52
Side	0.00	3.68

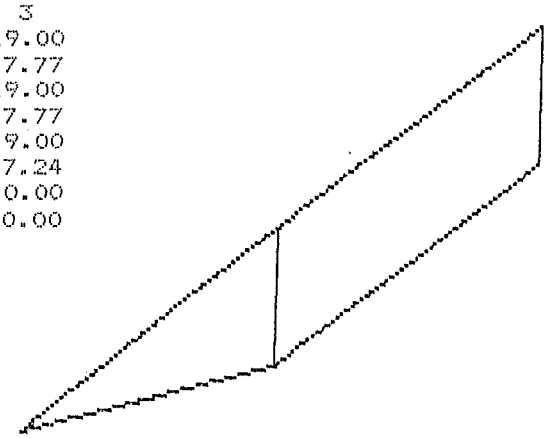

Acceleration Kc = 0.6911 Factor of Safety = 3.14

SARMA NON-VERTICAL SLICE ANALYSIS

Analysis no. 0.5m thick block with 2m long block - wedge 20 degrees

Unit weight of water = 9.8

Side number	1	2	3
Coordinate xt	15.54	17.00	19.00
Coordinate yt	6.38	6.97	7.77
Coordinate xw	15.54	17.00	19.00
Coordinate yw	6.38	6.97	7.77
Coordinate xb	15.54	17.00	19.00
Coordinate yb	6.38	6.44	7.24
Friction angle	0.00	28.40	0.00
Cohesion	0.00	6.00	0.00

Slice number	1	2
Rock unit weight	19.62	19.62
Friction angle	28.40	28.40
Cohesion	6.00	6.00
Force T	0.00	0.00
Angle theta	0.00	0.00

Effective normal stresses

Base	3.42	3.52
Side	0.00	3.63

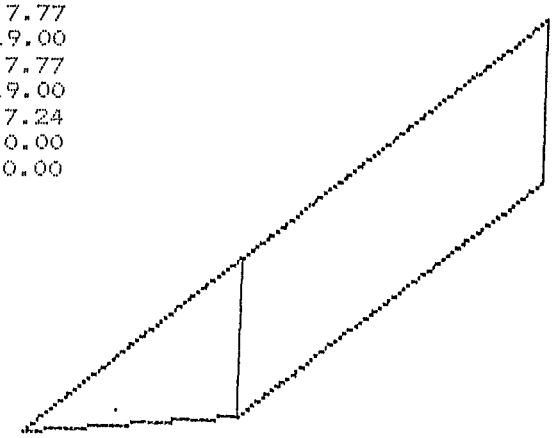

Acceleration Kc = 0.7042 Factor of Safety = 3.12

SARMA NON-VERTICAL SLICE ANALYSIS

Analysis no. 0.5m thick block with 2m long block - wedge 25 degrees

Unit weight of water = 9.8

Side number	1	2	3
Coordinate xt	15.82	17.00	19.00
Coordinate yt	6.50	6.97	7.77
Coordinate xw	15.82	17.00	19.00
Coordinate yw	6.50	6.97	7.77
Coordinate xb	15.82	17.00	19.00
Coordinate yb	6.50	6.44	7.24
Friction angle	0.00	28.40	0.00
Cohesion	0.00	6.00	0.00

Slice number	1	2
Rock unit weight	19.62	19.62
Friction angle	28.40	28.40
Cohesion	6.00	6.00
Force T	0.00	0.00
Angle theta	0.00	0.00

Effective normal stresses

Base		3.87	3.54
Side	0.00	3.80	

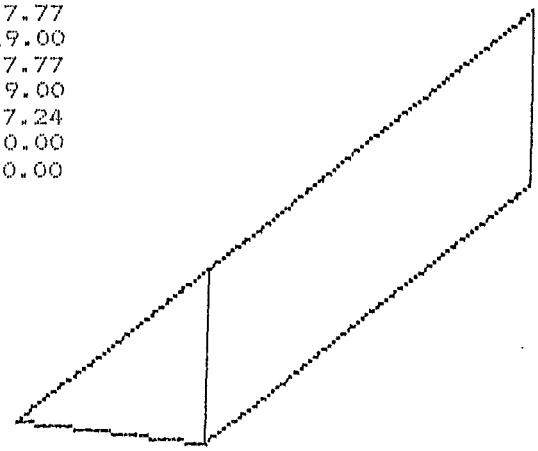

Acceleration Kc = 0.7467 Factor of Safety = 3.18

SARMA NON-VERTICAL SLICE ANALYSIS

Analysis no. 0.5m thick block with 2m long block - wedge 30 degrees

Unit weight of water = 9.8

Side number	1	2	3
Coordinate xt	16.01	17.00	19.00
Coordinate yt	6.67	6.97	7.77
Coordinate xw	16.01	17.00	19.00
Coordinate yw	6.67	6.97	7.77
Coordinate xb	16.01	17.00	19.00
Coordinate yb	6.67	6.44	7.24
Friction angle	0.00	28.40	0.00
Cohesion	0.00	6.00	0.00

Slice number	1	2
Rock unit weight	19.62	19.62
Friction angle	28.40	28.40
Cohesion	6.00	6.00
Force T	0.00	0.00
Angle theta	0.00	0.00

Effective normal stresses

Base		4.41	3.69
Side	0.00	4.83	

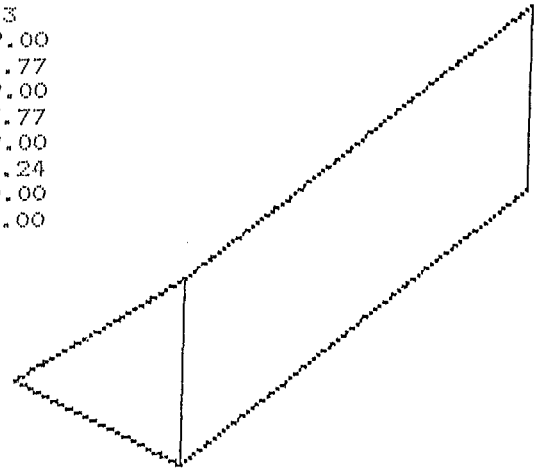

Acceleration Kc = 0.9562 Factor of Safety = 3.62

SARMA NON-VERTICAL SLICE ANALYSIS

Analysis no. 1.25m thick block with 2m long block - wedge 5 degrees

Unit weight of water = 9.8

Side number	1	2	3
Coordinate xt	3.28	17.00	19.00
Coordinate yt	2.25	7.79	8.59
Coordinate xw	3.28	17.00	19.00
Coordinate yw	2.25	7.79	8.59
Coordinate xb	3.28	17.00	19.00
Coordinate yb	2.25	6.44	7.24
Friction angle	0.00	28.40	0.00
Cohesion	0.00	6.00	0.00

Slice number	1	2
Rock unit weight	19.62	19.62
Friction angle	28.40	28.40
Cohesion	6.00	6.00
Force T	0.00	0.00
Angle theta	0.00	0.00

Effective normal stresses

Base		5.60	8.02
Side	0.00	4.43	

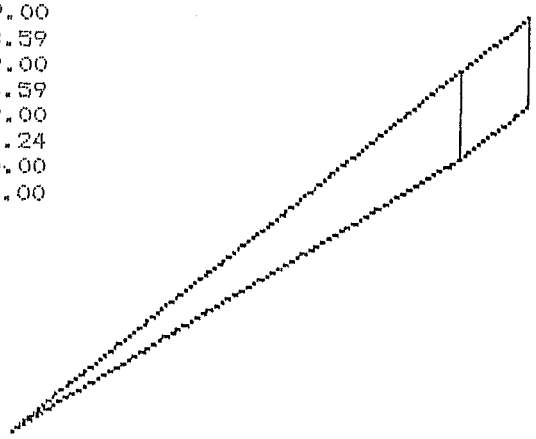

Acceleration Kc = 0.2734 Factor of Safety = 1.87

SARMA NON-VERTICAL SLICE ANALYSIS

Analysis no. 1.25m thick block with 2m long block - wedge 10 degrees

Unit weight of water = 9.8

Side number	1	2	3
Coordinate xt	9.82	17.00	19.00
Coordinate yt	4.86	7.79	8.59
Coordinate xw	9.82	17.00	19.00
Coordinate yw	4.86	7.79	8.59
Coordinate xb	9.82	17.00	19.00
Coordinate yb	4.86	6.44	7.24
Friction angle	0.00	28.40	0.00
Cohesion	0.00	6.00	0.00

Slice number	1	2
Rock unit weight	19.62	19.62
Friction angle	28.40	28.40
Cohesion	6.00	6.00
Force T	0.00	0.00
Angle theta	0.00	0.00

Effective normal stresses

Base		6.37	8.08
Side	0.00	4.56	

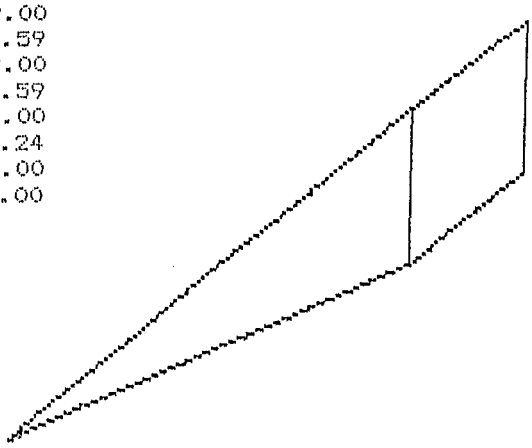

Acceleration Kc = 0.2775 Factor of Safety = 1.90

SARMA NON-VERTICAL SLICE ANALYSIS

Analysis no. 1.25m thick block with 2m long block - wedge 15 degrees

Unit weight of water = 9.8

Side number	1	2	3
Coordinate xt	12.19	17.00	19.00
Coordinate yt	5.83	7.79	8.59
Coordinate xw	12.19	17.00	19.00
Coordinate yw	5.83	7.79	8.59
Coordinate xb	12.19	17.00	19.00
Coordinate yb	5.83	6.44	7.24
Friction angle	0.00	28.40	0.00
Cohesion	0.00	6.00	0.00

Slice number	1	2
Rock unit weight	19.62	19.62
Friction angle	28.40	28.40
Cohesion	6.00	6.00
Force T	0.00	0.00
Angle theta	0.00	0.00

Effective normal stresses

Base		7.22	8.21
Side	0.00	4.91	

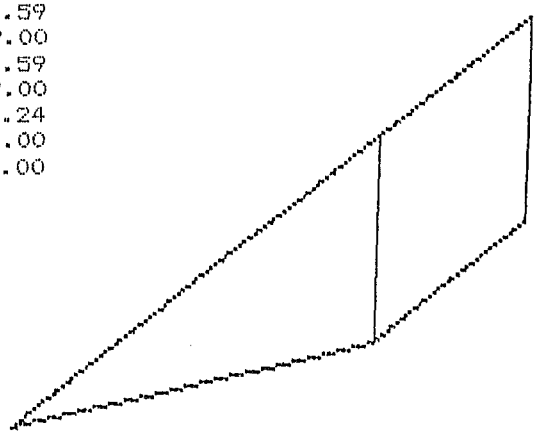

Acceleration Kc = 0.2997 Factor of Safety = 1.98

SARMA NON-VERTICAL SLICE ANALYSIS

Analysis no. 1.25m thick block with 2m long block - wedge 20 degrees

Unit weight of water = 9.8

Side number	1	2	3
Coordinate xt	13.39	17.00	19.00
Coordinate yt	6.33	7.79	8.59
Coordinate xw	13.39	17.00	19.00
Coordinate yw	6.33	7.79	8.59
Coordinate xb	13.39	17.00	19.00
Coordinate yb	6.33	6.44	7.24
Friction angle	0.00	28.40	0.00
Cohesion	0.00	6.00	0.00

Slice number	1	2
Rock unit weight	19.62	19.62
Friction angle	28.40	28.40
Cohesion	6.00	6.00
Force T	0.00	0.00
Angle theta	0.00	0.00

Effective normal stresses

Base		8.06	8.39
Side	0.00	5.38	

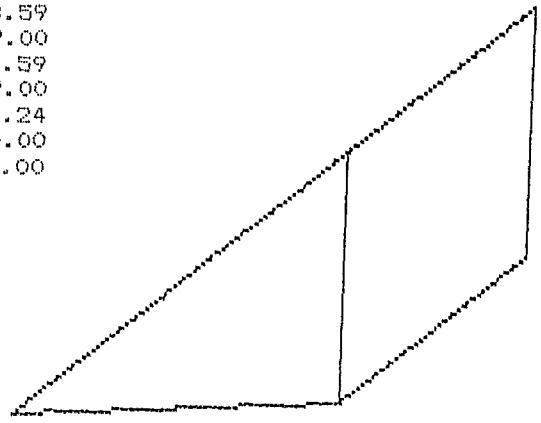

Acceleration Kc = 0.3380 Factor of Safety = 2.10

SARMA NON-VERTICAL SLICE ANALYSIS

Analysis no. 1.25m thick block with 2m long block - wedge 25 degrees

Unit weight of water = 9.8

Side number	1	2	3
Coordinate xt	14.06	17.00	19.00
Coordinate yt	6.60	7.79	8.59
Coordinate xw	14.06	17.00	19.00
Coordinate yw	6.60	7.79	8.59
Coordinate xb	14.06	17.00	19.00
Coordinate yb	6.60	6.44	7.24
Friction angle	0.00	28.40	0.00
Cohesion	0.00	6.00	0.00

Slice number	1	2
Rock unit weight	19.62	19.62
Friction angle	28.40	28.40
Cohesion	6.00	6.00
Force T	0.00	0.00
Angle theta	0.00	0.00

Effective normal stresses

Base	8.78	8.56
Side	0.00	5.79

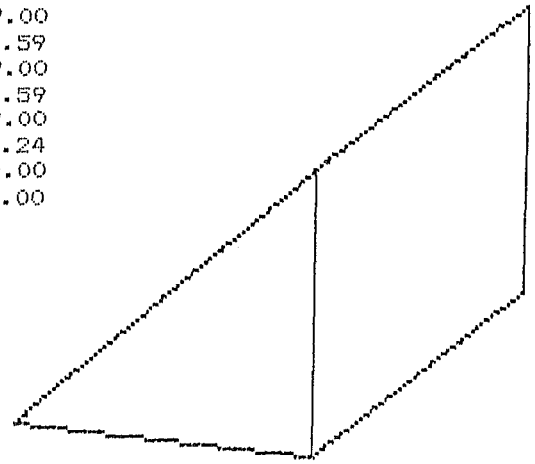

Acceleration Kc = 0.3833 Factor of Safety = 2.22

SARMA NON-VERTICAL SLICE ANALYSIS

Analysis no. 1.25m thick block with 2m long block - wedge 30 degrees

Unit weight of water = 9.8

Side number	1	2	3
Coordinate xt	14.51	17.00	19.00
Coordinate yt	6.78	7.79	8.59
Coordinate xw	14.51	17.00	19.00
Coordinate yw	6.78	7.79	8.59
Coordinate xb	14.51	17.00	19.00
Coordinate yb	6.78	6.44	7.24
Friction angle	0.00	28.40	0.00
Cohesion	0.00	6.00	0.00

Slice number	1	2
Rock unit weight	19.62	19.62
Friction angle	28.40	28.40
Cohesion	6.00	6.00
Force T	0.00	0.00
Angle theta	0.00	0.00

Effective normal stresses

Base	9.43	8.74
Side	0.00	6.19

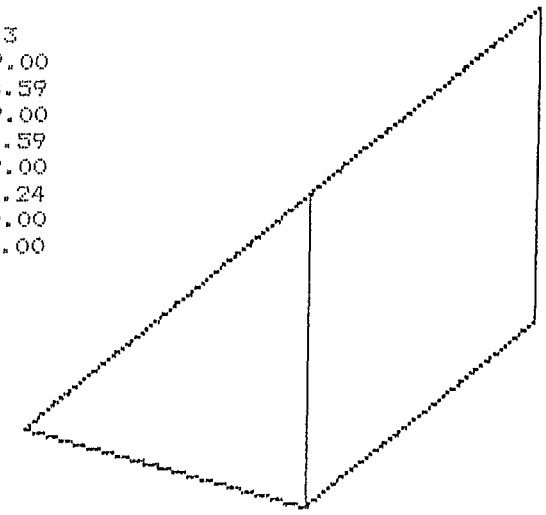

Acceleration Kc = 0.4419 Factor of Safety = 2.35

SARMA NON-VERTICAL SLICE ANALYSIS

Analysis no. 1.25m thick block with 2m long block - wedge 35 degrees

Unit weight of water = 9.8

Side number	1	2	3
Coordinate xt	14.88	17.00	19.00
Coordinate yt	6.93	7.79	8.59
Coordinate xw	14.88	17.00	19.00
Coordinate yw	6.93	7.79	8.59
Coordinate xb	14.88	17.00	19.00
Coordinate yb	6.93	6.44	7.24
Friction angle	0.00	28.40	0.00
Cohesion	0.00	6.00	0.00

Slice number	1	2
Rock unit weight	19.62	19.62
Friction angle	28.40	28.40
Cohesion	6.00	6.00
Force T	0.00	0.00
Angle theta	0.00	0.00

Effective normal stresses

Base		10.08	8.99
Side	0.00	6.63	

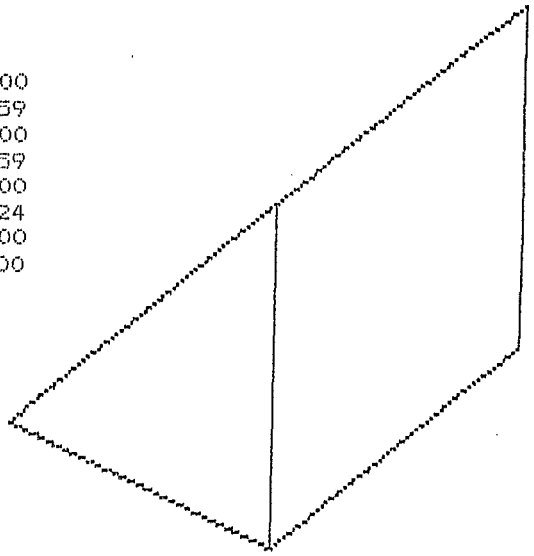

Acceleration Kc = 0.5350 Factor of Safety = 2.54

SARMA NON-VERTICAL SLICE ANALYSIS

Analysis no. 1.0m thick block with 2m long block - wedge 5 degrees

Unit weight of water = 9.8

Side number	1	2	3
Coordinate xt	6.03	17.00	19.00
Coordinate yt	3.09	7.51	8.31
Coordinate xw	6.03	17.00	19.00
Coordinate yw	3.09	7.51	8.31
Coordinate xb	6.03	17.00	19.00
Coordinate yb	3.09	6.44	7.24
Friction angle	0.00	28.40	0.00
Cohesion	0.00	6.00	0.00

Slice number	1	2
Rock unit weight	19.62	19.62
Friction angle	28.40	28.40
Cohesion	6.00	6.00
Force T	0.00	0.00
Angle theta	0.00	0.00

Effective normal stresses

Base		4.44	6.62
Side	0.00	4.48	

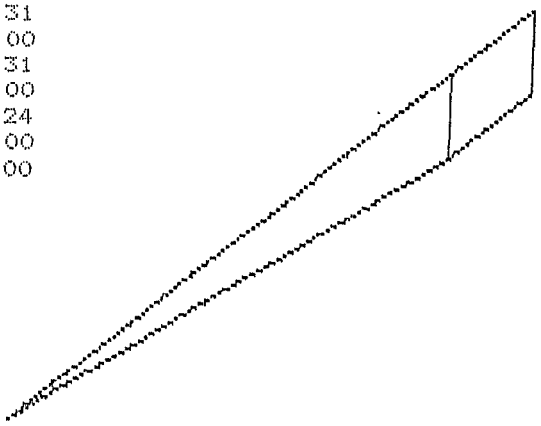

Acceleration Kc = 0.3614 Factor of Safety = 2.15

SARMA NON-VERTICAL SLICE ANALYSIS

Analysis no. 1.0m thick block with 2m long block - wedge 10 degrees

Unit weight of water = 9.8

Side number	1	2	3
Coordinate xt	11.12	17.00	19.00
Coordinate yt	5.13	7.51	8.31
Coordinate xw	11.12	17.00	19.00
Coordinate yw	5.13	7.51	8.31
Coordinate xb	11.12	17.00	19.00
Coordinate yb	5.13	6.44	7.24
Friction angle	0.00	28.40	0.00
Cohesion	0.00	6.00	0.00

Slice number	1	2
Rock unit weight	19.62	19.62
Friction angle	28.40	28.40
Cohesion	6.00	6.00
Force T	0.00	0.00
Angle theta	0.00	0.00

Effective normal stresses

Base	5.06	6.63
Side	0.00	4.47

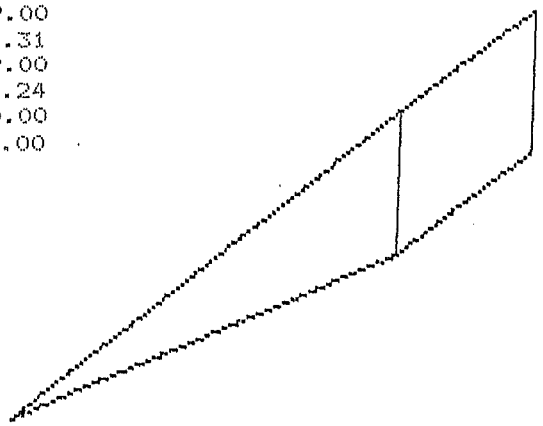

Acceleration Kc = 0.3557 Factor of Safety = 2.15

SARMA NON-VERTICAL SLICE ANALYSIS

Analysis no. 1.0m thick block with 2m long block - wedge 15 degrees

Unit weight of water = 9.8

Side number	1	2	3
Coordinate xt	13.20	17.00	19.00
Coordinate yt	5.97	7.51	8.31
Coordinate xw	13.20	17.00	19.00
Coordinate yw	5.97	7.51	8.31
Coordinate xb	13.20	17.00	19.00
Coordinate yb	5.97	6.44	7.24
Friction angle	0.00	28.40	0.00
Cohesion	0.00	6.00	0.00

Slice number	1	2
Rock unit weight	19.62	19.62
Friction angle	28.40	28.40
Cohesion	6.00	6.00
Force T	0.00	0.00
Angle theta	0.00	0.00

Effective normal stresses

Base	5.83	6.68
Side	0.00	4.67

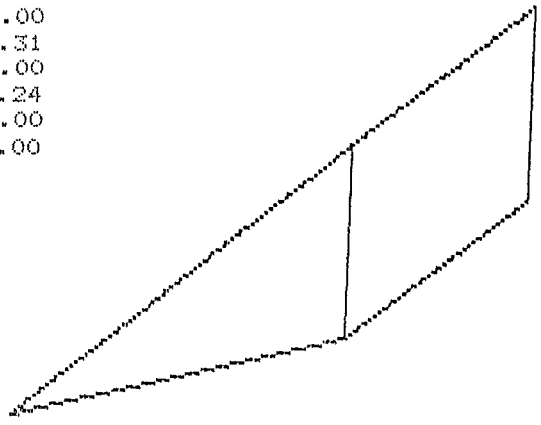

Acceleration Kc = 0.3713 Factor of Safety = 2.20

SARMA NON-VERTICAL SLICE ANALYSIS

Analysis no. 1.0m thick block with 2m long block - wedge 20 degrees

Unit weight of water = 9.8

Side number	1	2	3
Coordinate xt	14.12	17.00	19.00
Coordinate yt	6.35	7.51	8.31
Coordinate xw	14.12	17.00	19.00
Coordinate yw	6.35	7.51	8.31
Coordinate xb	14.12	17.00	19.00
Coordinate yb	6.35	6.44	7.24
Friction angle	0.00	28.40	0.00
Cohesion	0.00	6.00	0.00

Slice number	1	2
Rock unit weight	19.62	19.62
Friction angle	28.40	28.40
Cohesion	6.00	6.00
Force T	0.00	0.00
Angle theta	0.00	0.00

Effective normal stresses

Base		6.54	6.78
Side	0.00	5.00	

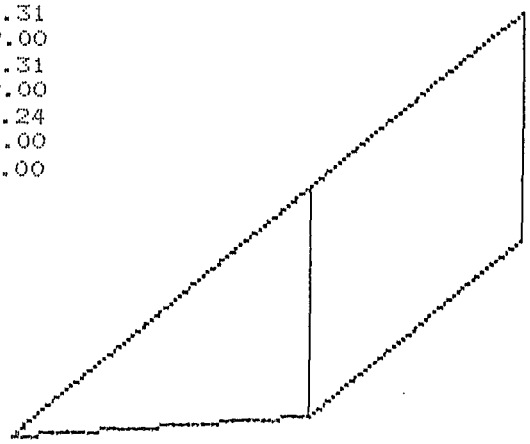

Acceleration Kc = 0.4041

Factor of Safety = 2.28

SARMA NON-VERTICAL SLICE ANALYSIS

Analysis no. 1.0m thick block with 2m long block - wedge 25 degrees

Unit weight of water = 9.8

Side number	1	2	3
Coordinate xt	14.66	17.00	19.00
Coordinate yt	6.56	7.51	8.31
Coordinate xw	14.66	17.00	19.00
Coordinate yw	6.56	7.51	8.31
Coordinate xb	14.66	17.00	19.00
Coordinate yb	6.56	6.44	7.24
Friction angle	0.00	28.40	0.00
Cohesion	0.00	6.00	0.00

Slice number	1	2
Rock unit weight	19.62	19.62
Friction angle	28.40	28.40
Cohesion	6.00	6.00
Force T	0.00	0.00
Angle theta	0.00	0.00

Effective normal stresses

Base		7.18	6.87
Side	0.00	5.29	

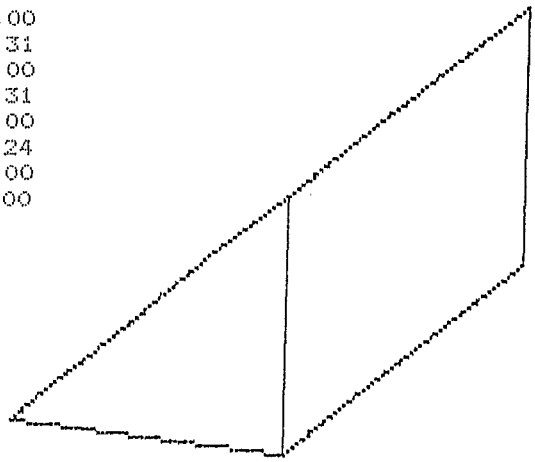

Acceleration Kc = 0.4448

Factor of Safety = 2.37

SARMA NON-VERTICAL SLICE ANALYSIS

Analysis no. 1.0m thick block with 2m long block - wedge 30 degrees

Unit weight of water = 9.8

Side number	1	2	3
Coordinate xt	15.04	17.00	19.00
Coordinate yt	6.72	7.51	8.31
Coordinate xw	15.04	17.00	19.00
Coordinate yw	6.72	7.51	8.31
Coordinate xb	15.04	17.00	19.00
Coordinate yb	6.72	6.44	7.24
Friction angle	0.00	28.40	0.00
Cohesion	0.00	6.00	0.00

Slice number	1	2
Rock unit weight	19.62	19.62
Friction angle	28.40	28.40
Cohesion	6.00	6.00
Force T	0.00	0.00
Angle theta	0.00	0.00

Effective normal stresses

Base		7.81	7.01
Side	0.00	5.69	

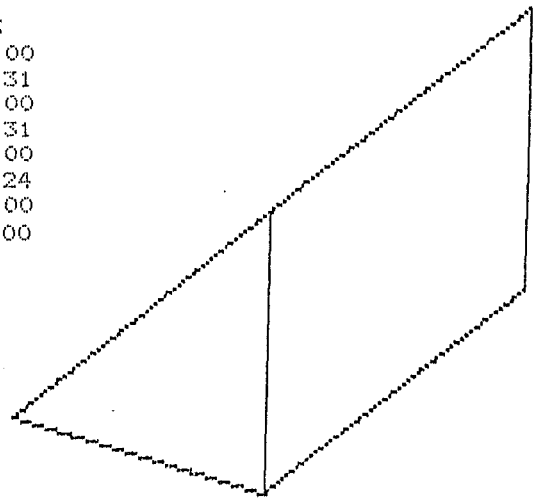

Acceleration Kc = 0.5120 Factor of Safety = 2.51

SARMA NON-VERTICAL SLICE ANALYSIS

Analysis no. 1.5m thick block with 2m long block - wedge 5 degrees

Unit weight of water = 9.8

Side number	1	2	3
Coordinate xt	0.54	17.00	19.00
Coordinate yt	1.41	7.95	8.75
Coordinate xw	0.54	17.00	19.00
Coordinate yw	1.41	7.95	8.75
Coordinate xb	0.54	17.00	19.00
Coordinate yb	1.41	6.44	7.24
Friction angle	0.00	28.40	0.00
Cohesion	0.00	6.00	0.00

Slice number	1	2
Rock unit weight	19.62	19.62
Friction angle	28.40	28.40
Cohesion	6.00	6.00
Force T	0.00	0.00
Angle theta	0.00	0.00

Effective normal stresses

Base		6.24	8.83
Side	0.00	4.51	

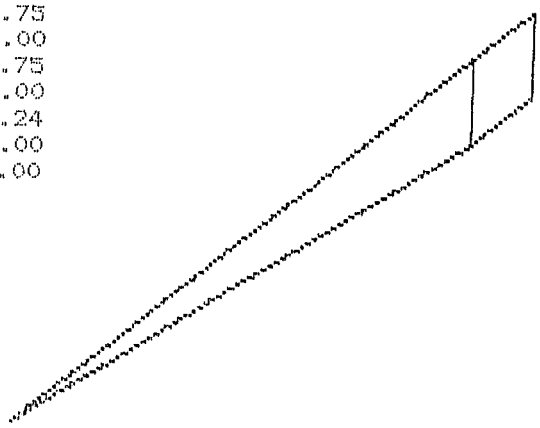

Acceleration Kc = 0.2420 Factor of Safety = 1.78

SARMA NON-VERTICAL SLICE ANALYSIS

Analysis no. 1.5m thick block with 2m long block - wedge 10 degrees

Unit weight of water = 9.8

Side number	1	2	3
Coordinate xt	7.88	17.00	19.00
Coordinate yt	4.66	7.95	8.75
Coordinate xw	7.88	17.00	19.00
Coordinate yw	4.66	7.95	8.75
Coordinate xb	7.88	17.00	19.00
Coordinate yb	4.66	6.44	7.24
Friction angle	0.00	28.40	0.00
Cohesion	0.00	6.00	0.00

Slice number	1	2
Rock unit weight	19.62	19.62
Friction angle	28.40	28.40
Cohesion	6.00	6.00
Force T	0.00	0.00
Angle theta	0.00	0.00

Effective normal stresses

Base	7.19	9.24
Side	0.00	5.41

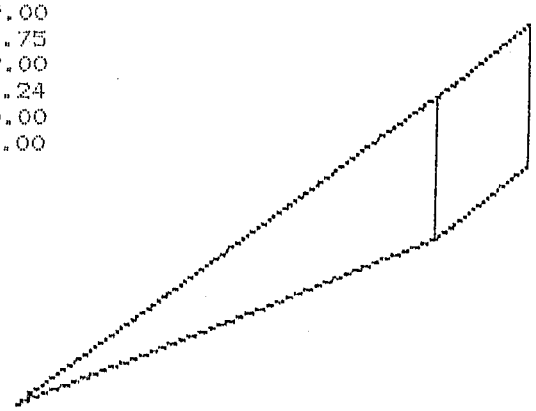

Acceleration Kc = 0.2812 Factor of Safety = 1.99

SARMA NON-VERTICAL SLICE ANALYSIS

Analysis no. 1.5m thick block with 2m long block - wedge 15 degrees

Unit weight of water = 9.8

Side number	1	2	3
Coordinate xt	11.54	17.00	19.00
Coordinate yt	5.74	7.95	8.75
Coordinate xw	11.54	17.00	19.00
Coordinate yw	5.74	7.95	8.75
Coordinate xb	11.54	17.00	19.00
Coordinate yb	5.74	6.44	7.24
Friction angle	0.00	28.40	0.00
Cohesion	0.00	6.00	0.00

Slice number	1	2
Rock unit weight	19.62	19.62
Friction angle	28.40	28.40
Cohesion	6.00	6.00
Force T	0.00	0.00
Angle theta	0.00	0.00

Effective normal stresses

Base	7.99	9.07
Side	0.00	5.06

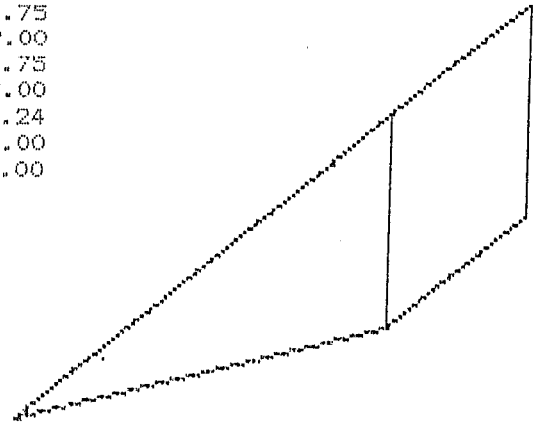

Acceleration Kc = 0.2718 Factor of Safety = 1.90

SARMA NON-VERTICAL SLICE ANALYSIS

Analysis no. 1.5m thick block with 2m long block - wedge 20 degrees

Unit weight of water = 9.8

Side number	1	2	3
Coordinate xt	12.92	17.00	19.00
Coordinate yt	6.30	7.95	8.75
Coordinate xw	12.92	17.00	19.00
Coordinate yw	6.30	7.95	8.75
Coordinate xb	12.92	17.00	19.00
Coordinate yb	6.30	6.44	7.24
Friction angle	0.00	28.40	0.00
Cohesion	0.00	6.00	0.00

Slice number	1	2
Rock unit weight	19.62	19.62
Friction angle	28.40	28.40
Cohesion	6.00	6.00
Force T	0.00	0.00
Angle theta	0.00	0.00

Effective normal stresses

Base		8.88	9.29
Side	0.00	5.53	

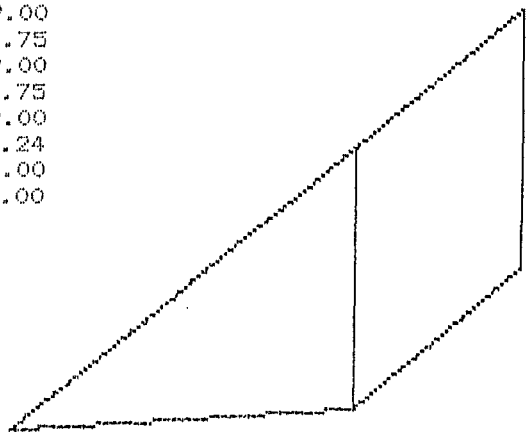

Acceleration Kc = 0.3089

Factor of Safety = 2.02

SARMA NON-VERTICAL SLICE ANALYSIS

Analysis no. 1.5m thick block with 2m long block - wedge 25 degrees

Unit weight of water = 9.8

Side number	1	2	3
Coordinate xt	13.68	17.00	19.00
Coordinate yt	6.60	7.95	8.75
Coordinate xw	13.68	17.00	19.00
Coordinate yw	6.60	7.95	8.75
Coordinate xb	13.68	17.00	19.00
Coordinate yb	6.60	6.44	7.24
Friction angle	0.00	28.40	0.00
Cohesion	0.00	6.00	0.00

Slice number	1	2
Rock unit weight	19.62	19.62
Friction angle	28.40	28.40
Cohesion	6.00	6.00
Force T	0.00	0.00
Angle theta	0.00	0.00

Effective normal stresses

Base		9.63	9.48
Side	0.00	5.95	

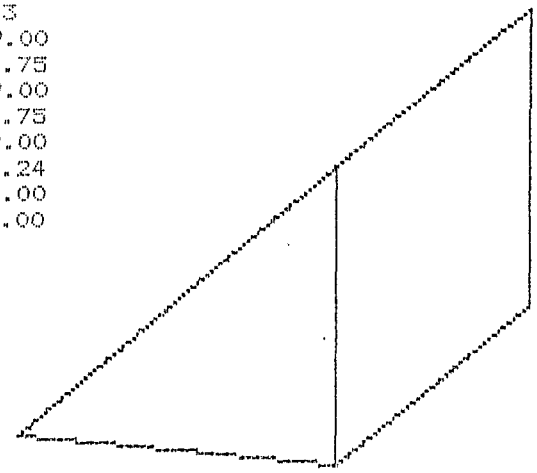

Acceleration Kc = 0.3522

Factor of Safety = 2.14

SARMA NON-VERTICAL SLICE ANALYSIS

Analysis no. 1.5m thick block with 2m long block - wedge 30 degrees

Unit weight of water = 9.8

Side number	1	2	3
Coordinate xt	14.21	17.00	19.00
Coordinate yt	6.82	7.95	8.75
Coordinate xw	14.21	17.00	19.00
Coordinate yw	6.82	7.95	8.75
Coordinate xb	14.21	17.00	19.00
Coordinate yb	6.82	6.44	7.24
Friction angle	0.00	28.40	0.00
Cohesion	0.00	6.00	0.00

Slice number	1	2
Rock unit weight	19.62	19.62
Friction angle	28.40	28.40
Cohesion	6.00	6.00
Force T	0.00	0.00
Angle theta	0.00	0.00

Effective normal stresses

Base		10.34	9.74
Side	0.00	6.44	

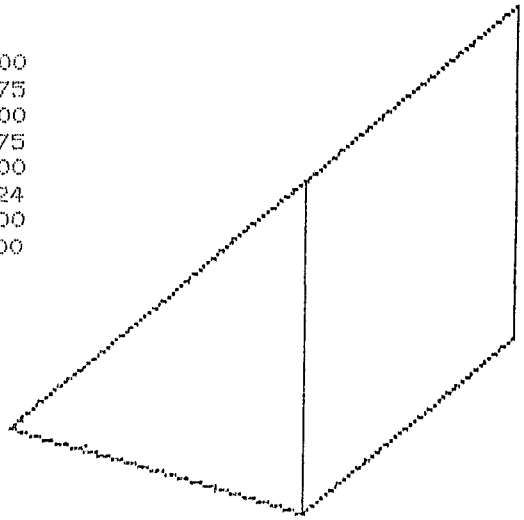

Acceleration Kc = 0.4156 Factor of Safety = 2.29

SARMA NON-VERTICAL SLICE ANALYSIS

Analysis no. 1.5m thick block with 2m long block - wedge 35 degrees

Unit weight of water = 9.8

Side number	1	2	3
Coordinate xt	14.61	17.00	19.00
Coordinate yt	6.98	7.95	8.75
Coordinate xw	14.61	17.00	19.00
Coordinate yw	6.98	7.95	8.75
Coordinate xb	14.61	17.00	19.00
Coordinate yb	6.98	6.44	7.24
Friction angle	0.00	28.40	0.00
Cohesion	0.00	6.00	0.00

Slice number	1	2
Rock unit weight	19.62	19.62
Friction angle	28.40	28.40
Cohesion	6.00	6.00
Force T	0.00	0.00
Angle theta	0.00	0.00

Effective normal stresses

Base		10.98	10.02
Side	0.00	6.89	

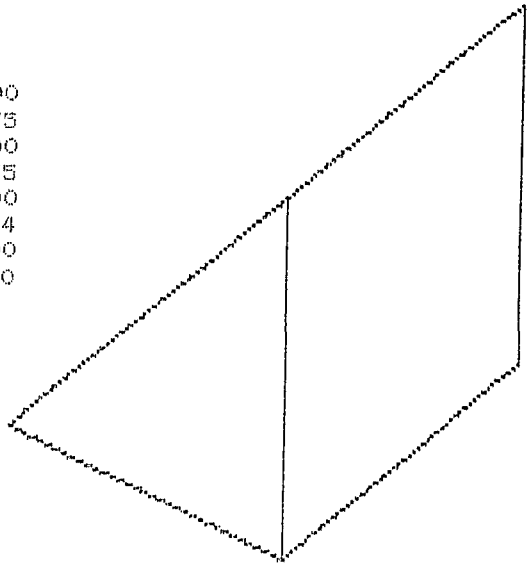

Acceleration Kc = 0.5017 Factor of Safety = 2.48

Analysis of ß for 0.5m to 1.5m thick wedges plus additional 4m long block.

SARMA NON-VERTICAL SLICE ANALYSIS

Analysis no. 1.25m thick block with 4m long block - wedge 5 degrees

Unit weight of water = 9.8

Side number	1	2	3
Coordinate xt	3.28	17.00	21.00
Coordinate yt	2.25	7.79	9.39
Coordinate xw	3.28	17.00	21.00
Coordinate yw	2.25	7.79	9.39
Coordinate xb	3.28	17.00	21.00
Coordinate yb	2.25	6.44	8.04
Friction angle	0.00	28.40	0.00
Cohesion	0.00	6.00	0.00

Slice number	1	2
Rock unit weight	19.62	19.62
Friction angle	28.40	28.40
Cohesion	6.00	6.00
Force T	0.00	0.00
Angle theta	0.00	0.00

Effective normal stresses

Base		5.63	8.81
Side	0.00	7.91	

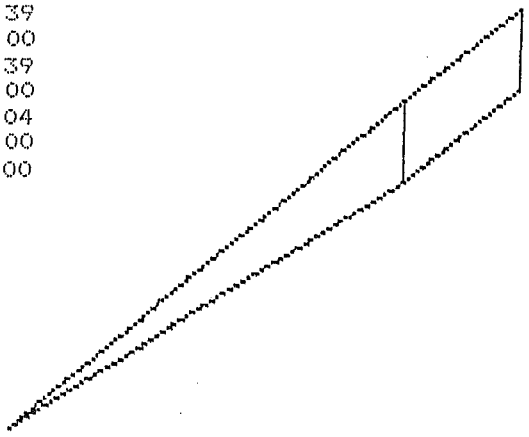

Acceleration Kc = 0.2379 Factor of Safety = 1.75

SARMA NON-VERTICAL SLICE ANALYSIS

Analysis no. 1.25m thick block with 4m long block - wedge 10 degrees

Unit weight of water = 9.8

Side number	1	2	3
Coordinate xt	9.82	17.00	21.00
Coordinate yt	4.86	7.79	9.39
Coordinate xw	9.82	17.00	21.00
Coordinate yw	4.86	7.79	9.39
Coordinate xb	9.82	17.00	21.00
Coordinate yb	4.86	6.44	8.04
Friction angle	0.00	28.40	0.00
Cohesion	0.00	6.00	0.00

Slice number	1	2
Rock unit weight	19.62	19.62
Friction angle	28.40	28.40
Cohesion	6.00	6.00
Force T	0.00	0.00
Angle theta	0.00	0.00

Effective normal stresses

Base		6.51	8.77
Side	0.00	7.53	

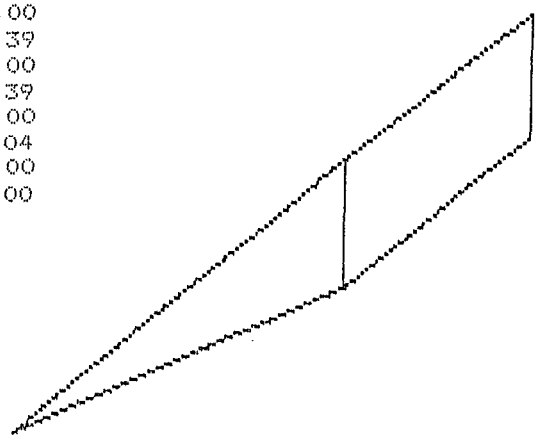

Acceleration Kc = 0.2265 Factor of Safety = 1.71

SARMA NON-VERTICAL SLICE ANALYSIS

Analysis no. 1.25m thick block with 4m long block - wedge 15 degrees

Unit weight of water = 9.8

Side number	1	2	3
Coordinate xt	12.19	17.00	21.00
Coordinate yt	5.83	7.79	9.39
Coordinate xw	12.19	17.00	21.00
Coordinate yw	5.83	7.79	9.39
Coordinate xb	12.19	17.00	21.00
Coordinate yb	5.83	6.44	8.04
Friction angle	0.00	28.40	0.00
Cohesion	0.00	6.00	0.00

Slice number	1	2
Rock unit weight	19.62	19.62
Friction angle	28.40	28.40
Cohesion	6.00	6.00
Force T	0.00	0.00
Angle theta	0.00	0.00

Effective normal stresses

Base		7.54	8.79
Side	0.00	7.71	

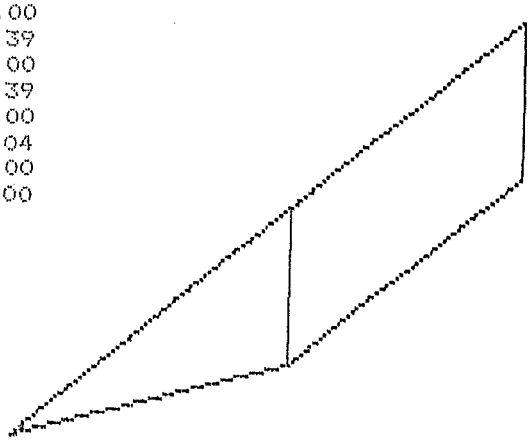

Acceleration Kc = 0.2339

Factor of Safety = 1.73

SARMA NON-VERTICAL SLICE ANALYSIS

Analysis no. 1.25m thick block with 4m long block - wedge 20 degrees

Unit weight of water = 9.8

Side number	1	2	3
Coordinate xt	13.39	17.00	21.00
Coordinate yt	6.33	7.79	9.39
Coordinate xw	13.39	17.00	21.00
Coordinate yw	6.33	7.79	9.39
Coordinate xb	13.39	17.00	21.00
Coordinate yb	6.33	6.44	8.04
Friction angle	0.00	28.40	0.00
Cohesion	0.00	6.00	0.00

Slice number	1	2
Rock unit weight	19.62	19.62
Friction angle	28.40	28.40
Cohesion	6.00	6.00
Force T	0.00	0.00
Angle theta	0.00	0.00

Effective normal stresses

Base		8.64	8.85
Side	0.00	8.19	

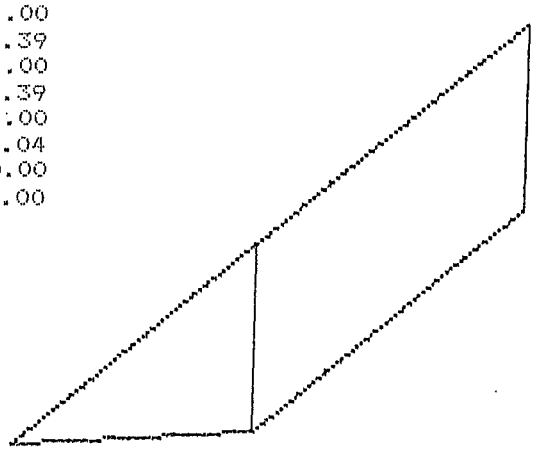

Acceleration Kc = 0.2545

Factor of Safety = 1.78

SARMA NON-VERTICAL SLICE ANALYSIS

Analysis no. 1.25m thick block with 4m long block - wedge 25 degrees

Unit weight of water = 9.8

Side number	1	2	3
Coordinate xt	14.06	17.00	21.00
Coordinate yt	6.60	7.79	9.39
Coordinate xw	14.06	17.00	21.00
Coordinate yw	6.60	7.79	9.39
Coordinate xb	14.06	17.00	21.00
Coordinate yb	6.60	6.44	8.04
Friction angle	0.00	28.40	0.00
Cohesion	0.00	6.00	0.00

Slice number	1	2
Rock unit weight	19.62	19.62
Friction angle	28.40	28.40
Cohesion	6.00	6.00
Force T	0.00	0.00
Angle theta	0.00	0.00

Effective normal stresses

Base		9.65	8.92
Side	0.00	8.68	

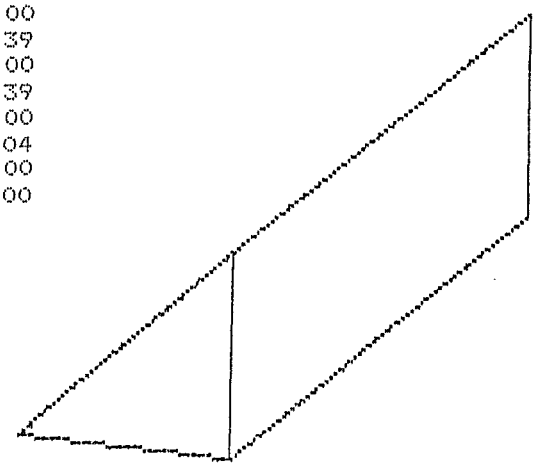

Acceleration Kc = 0.2813 Factor of Safety = 1.83

SARMA NON-VERTICAL SLICE ANALYSIS

Analysis no. 1.25m thick block with 4m long block - wedge 30 degrees

Unit weight of water = 9.8

Side number	1	2	3
Coordinate xt	14.51	17.00	21.00
Coordinate yt	6.78	7.79	9.39
Coordinate xw	14.51	17.00	21.00
Coordinate yw	6.78	7.79	9.39
Coordinate xb	14.51	17.00	21.00
Coordinate yb	6.78	6.44	8.04
Friction angle	0.00	28.40	0.00
Cohesion	0.00	6.00	0.00

Slice number	1	2
Rock unit weight	19.62	19.62
Friction angle	28.40	28.40
Cohesion	6.00	6.00
Force T	0.00	0.00
Angle theta	0.00	0.00

Effective normal stresses

Base		10.62	9.01
Side	0.00	9.20	

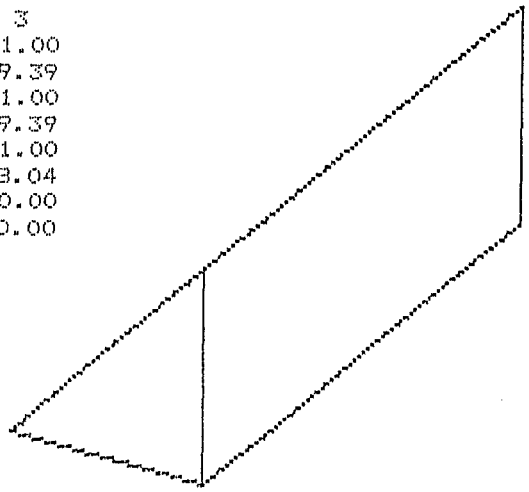

Acceleration Kc = 0.3179 Factor of Safety = 1.89

SARMA NON-VERTICAL SLICE ANALYSIS

Analysis no. 1.25m thick block with 4m long block - wedge 35 degrees

Unit weight of water = 9.8

Side number	1	2	3
Coordinate xt	14.88	17.00	21.00
Coordinate yt	6.93	7.79	9.39
Coordinate xw	14.88	17.00	21.00
Coordinate yw	6.93	7.79	9.39
Coordinate xb	14.88	17.00	21.00
Coordinate yb	6.93	6.44	8.04
Friction angle	0.00	28.40	0.00
Cohesion	0.00	6.00	0.00

Slice number	1	2
Rock unit weight	19.62	19.62
Friction angle	28.40	28.40
Cohesion	6.00	6.00
Force T	0.00	0.00
Angle theta	0.00	0.00

Effective normal stresses

Base	11.66	9.15
Side	0.00	9.82

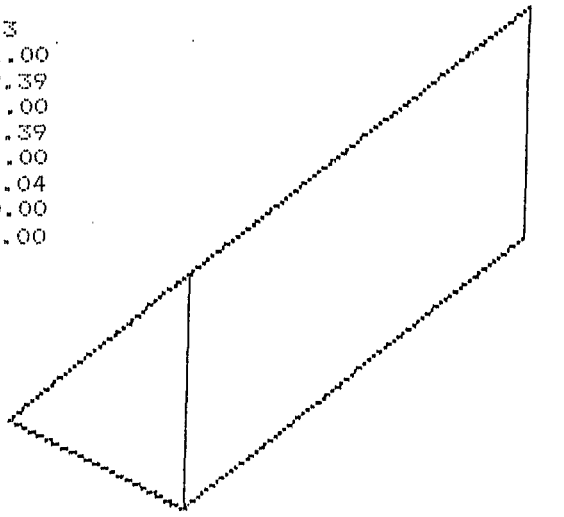

Acceleration Kc = 0.3788 Factor of Safety = 2.00

SARMA NON-VERTICAL SLICE ANALYSIS

Analysis no. 0.75m thick block with 4m block - wedge 5 degrees

Unit weight of water = 9.8

Side number	1	2	3
Coordinate xt	8.77	17.00	21.00
Coordinate yt	3.92	7.25	8.85
Coordinate xw	8.77	17.00	21.00
Coordinate yw	3.92	7.25	8.85
Coordinate xb	8.77	17.00	21.00
Coordinate yb	3.92	6.44	8.04
Friction angle	0.00	28.40	0.00
Cohesion	0.00	6.00	0.00

Slice number	1	2
Rock unit weight	19.62	19.62
Friction angle	28.40	28.40
Cohesion	6.00	6.00
Force T	0.00	0.00
Angle theta	0.00	0.00

Effective normal stresses

Base	3.37	5.52
Side	0.00	7.48

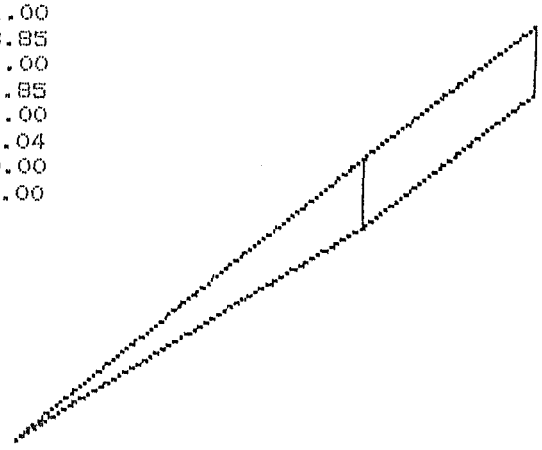

Acceleration Kc = 0.4239 Factor of Safety = 2.31

SARMA NON-VERTICAL SLICE ANALYSIS

Analysis no. 0.75m thick block with 4m block - wedge 10 degrees

Unit weight of water = 9.8

Side number	1	2	3
Coordinate xt	12.76	17.00	21.00
Coordinate yt	5.53	7.25	8.85
Coordinate xw	12.76	17.00	21.00
Coordinate yw	5.53	7.25	8.85
Coordinate xb	12.76	17.00	21.00
Coordinate yb	5.53	6.44	8.04
Friction angle	0.00	28.40	0.00
Cohesion	0.00	6.00	0.00

Slice number	1	2
Rock unit weight	19.62	19.62
Friction angle	28.40	28.40
Cohesion	6.00	6.00
Force T	0.00	0.00
Angle theta	0.00	0.00

Effective normal stresses

Base	4.00	5.46
Side	0.00	6.45

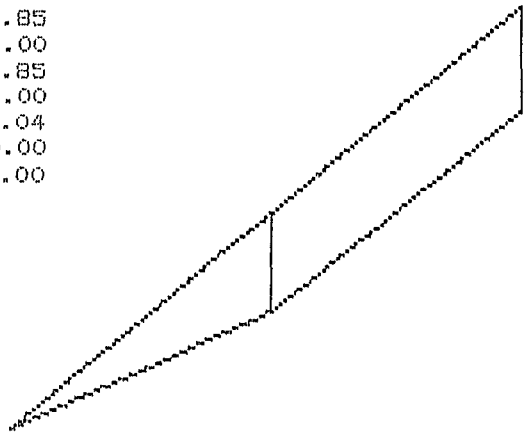

Acceleration Kc = 0.3890 Factor of Safety = 2.20

SARMA NON-VERTICAL SLICE ANALYSIS

Analysis no. 0.75m thick block with 4m block - wedge 15 degrees

Unit weight of water = 9.8

Side number	1	2	3
Coordinate xt	14.12	17.00	21.00
Coordinate yt	6.08	7.25	8.85
Coordinate xw	14.12	17.00	21.00
Coordinate yw	6.08	7.25	8.85
Coordinate xb	14.12	17.00	21.00
Coordinate yb	6.08	6.44	8.04
Friction angle	0.00	28.40	0.00
Cohesion	0.00	6.00	0.00

Slice number	1	2
Rock unit weight	19.62	19.62
Friction angle	28.40	28.40
Cohesion	6.00	6.00
Force T	0.00	0.00
Angle theta	0.00	0.00

Effective normal stresses

Base	4.69	5.44
Side	0.00	6.14

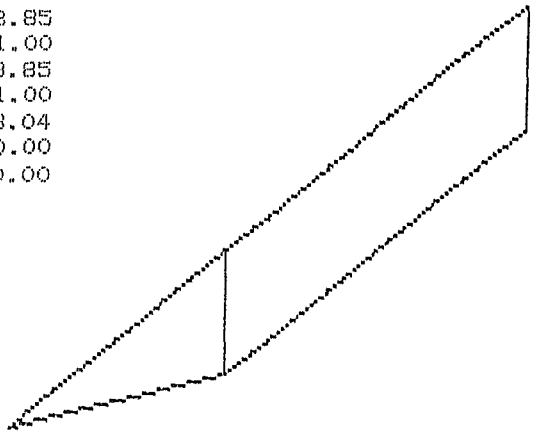

Acceleration Kc = 0.3841 Factor of Safety = 2.17

SARMA NON-VERTICAL SLICE ANALYSIS

Analysis no. 0.75m thick block with 4m block - wedge 20 degrees

Unit weight of water = 9.8

Side number	1	2	3
Coordinate xt	14.83	17.00	21.00
Coordinate yt	6.37	7.25	8.85
Coordinate xw	14.83	17.00	21.00
Coordinate yw	6.37	7.25	8.85
Coordinate xb	14.83	17.00	21.00
Coordinate yb	6.37	6.44	8.04
Friction angle	0.00	28.40	0.00
Cohesion	0.00	6.00	0.00

Slice number	1	2
Rock unit weight	19.62	19.62
Friction angle	28.40	28.40
Cohesion	6.00	6.00
Force T	0.00	0.00
Angle theta	0.00	0.00

Effective normal stresses

Base		5.45	5.44
Side	0.00	6.20	

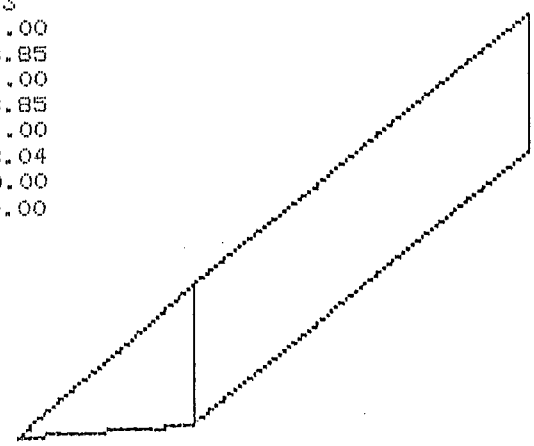

Acceleration Kc = 0.3959

Factor of Safety = 2.18

SARMA NON-VERTICAL SLICE ANALYSIS

Analysis no. 0.75m thick block with 4m block - wedge 25 degrees

Unit weight of water = 9.8

Side number	1	2	3
Coordinate xt	15.24	17.00	21.00
Coordinate yt	6.54	7.25	8.85
Coordinate xw	15.24	17.00	21.00
Coordinate yw	6.54	7.25	8.85
Coordinate xb	15.24	17.00	21.00
Coordinate yb	6.54	6.44	8.04
Friction angle	0.00	28.40	0.00
Cohesion	0.00	6.00	0.00

Slice number	1	2
Rock unit weight	19.62	19.62
Friction angle	28.40	28.40
Cohesion	6.00	6.00
Force T	0.00	0.00
Angle theta	0.00	0.00

Effective normal stresses

Base		6.19	5.47
Side	0.00	6.47	

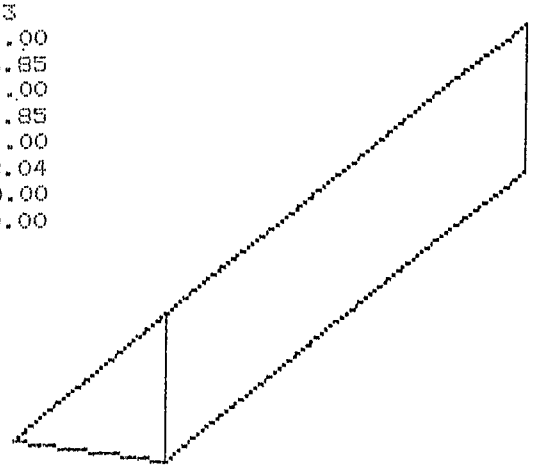

Acceleration Kc = 0.4204

Factor of Safety = 2.21

SARMA NON-VERTICAL SLICE ANALYSIS

Analysis no. 0.75m thick block with 4m block - wedge 30 degrees

Unit weight of water = 9.8

Side number	1	2	3
Coordinate xt	15.31	17.00	21.00
Coordinate yt	6.65	7.25	8.85
Coordinate xw	15.31	17.00	21.00
Coordinate yw	6.65	7.25	8.85
Coordinate xb	15.31	17.00	21.00
Coordinate yb	6.65	6.44	8.04
Friction angle	0.00	28.40	0.00
Cohesion	0.00	6.00	0.00

Slice number	1	2
Rock unit weight	19.62	19.62
Friction angle	28.40	28.40
Cohesion	6.00	6.00
Force T	0.00	0.00
Angle theta	0.00	0.00

Effective normal stresses

Base		6.55	5.53
Side	0.00	7.36	

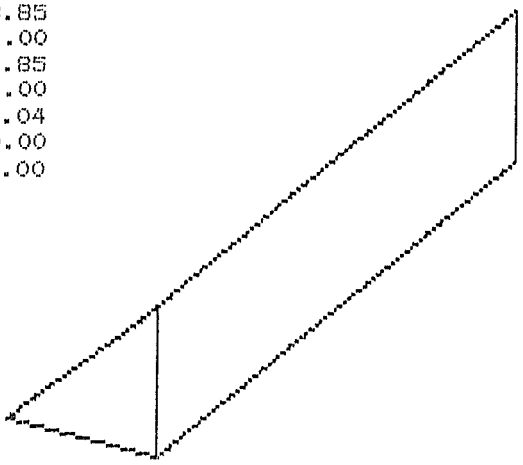

Acceleration Kc = 0.4652 Factor of Safety = 2.32

SARMA NON-VERTICAL SLICE ANALYSIS

Analysis no. 0.5m thick block with 4m long block - wedge 5 degrees

Unit weight of water = 9.8

Side number	1	2	3
Coordinate xt	11.12	17.00	21.00
Coordinate yt	4.60	6.97	8.57
Coordinate xw	11.12	17.00	21.00
Coordinate yw	4.60	6.97	8.57
Coordinate xb	11.12	17.00	21.00
Coordinate yb	4.60	6.44	8.04
Friction angle	0.00	28.40	0.00
Cohesion	0.00	6.00	0.00

Slice number	1	2
Rock unit weight	19.62	19.62
Friction angle	28.40	28.40
Cohesion	6.00	6.00
Force T	0.00	0.00
Angle theta	0.00	0.00

Effective normal stresses

Base		2.15	3.72
Side	0.00	7.07	

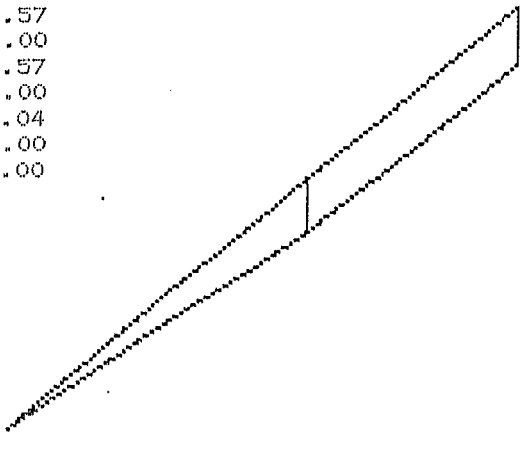

Acceleration Kc = 0.6608 Factor of Safety = 3.02

SARMA NON-VERTICAL SLICE ANALYSIS

Analysis no. 0.5m thick block with 4m long block - wedge 10 degrees

Unit weight of water = 9.8

Side number	1	2	3
Coordinate xt	14.02	17.00	21.00
Coordinate yt	5.76	6.97	8.57
Coordinate xw	14.02	17.00	21.00
Coordinate yw	5.76	6.97	8.57
Coordinate xb	14.02	17.00	21.00
Coordinate yb	5.76	6.44	8.04
Friction angle	0.00	28.40	0.00
Cohesion	0.00	6.00	0.00

Slice number	1	2
Rock unit weight	19.62	19.62
Friction angle	28.40	28.40
Cohesion	6.00	6.00
Force T	0.00	0.00
Angle theta	0.00	0.00

Effective normal stresses

Base		2.57	3.65
Side	0.00	5.47	

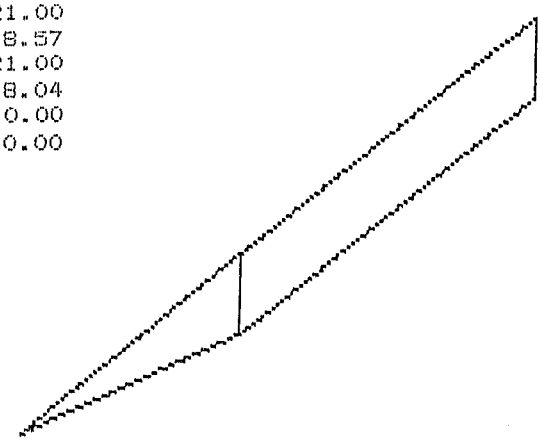

Acceleration Kc = 0.5961 Factor of Safety = 2.82

SARMA NON-VERTICAL SLICE ANALYSIS

Analysis no. 0.5m thick block with 4m long block - wedge 15 degrees

Unit weight of water = 9.8

Side number	1	2	3
Coordinate xt	15.05	17.00	21.00
Coordinate yt	6.19	6.97	8.57
Coordinate xw	15.05	17.00	21.00
Coordinate yw	6.19	6.97	8.57
Coordinate xb	15.05	17.00	21.00
Coordinate yb	6.19	6.44	8.04
Friction angle	0.00	28.40	0.00
Cohesion	0.00	6.00	0.00

Slice number	1	2
Rock unit weight	19.62	19.62
Friction angle	28.40	28.40
Cohesion	6.00	6.00
Force T	0.00	0.00
Angle theta	0.00	0.00

Effective normal stresses

Base		3.10	3.63
Side	0.00	4.94	

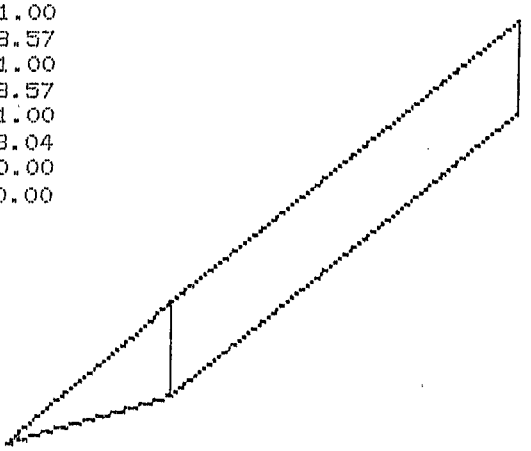

Acceleration Kc = 0.5814 Factor of Safety = 2.75

SARMA NON-VERTICAL SLICE ANALYSIS

Analysis no. 0.5m thick block with 4m long block - wedge 20 degrees

Unit weight of water = 9.8

Side number	1	2	3
Coordinate xt	15.54	17.00	21.00
Coordinate yt	6.38	6.97	8.57
Coordinate xw	15.54	17.00	21.00
Coordinate yw	6.38	6.97	8.57
Coordinate xb	15.54	17.00	21.00
Coordinate yb	6.38	6.44	8.04
Friction angle	0.00	28.40	0.00
Cohesion	0.00	6.00	0.00

Slice number	1	2
Rock unit weight	19.62	19.62
Friction angle	28.40	28.40
Cohesion	6.00	6.00
Force T	0.00	0.00
Angle theta	0.00	0.00

Effective normal stresses

Base		3.62	3.62
Side	0.00	4.71	

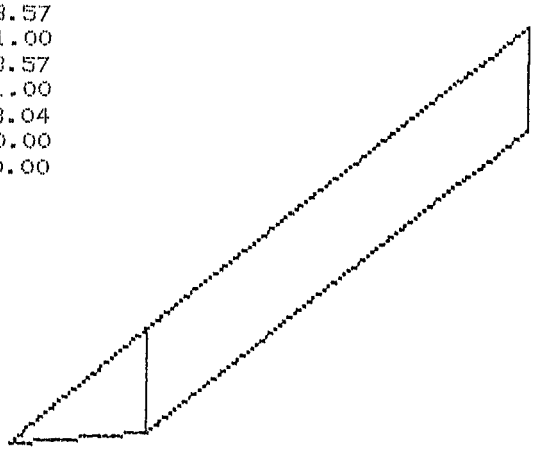

Acceleration Kc = 0.5842 Factor of Safety = 2.73

SARMA NON-VERTICAL SLICE ANALYSIS

Analysis no. 0.5m thick block with 4m long block - wedge 25 degrees

Unit weight of water = 9.8

Side number	1	2	3
Coordinate xt	15.82	17.00	21.00
Coordinate yt	6.50	6.97	8.57
Coordinate xw	15.82	17.00	21.00
Coordinate yw	6.50	6.97	8.57
Coordinate xb	15.82	17.00	21.00
Coordinate yb	6.50	6.44	8.04
Friction angle	0.00	28.40	0.00
Cohesion	0.00	6.00	0.00

Slice number	1	2
Rock unit weight	19.62	19.62
Friction angle	28.40	28.40
Cohesion	6.00	6.00
Force T	0.00	0.00
Angle theta	0.00	0.00

Effective normal stresses

Base		4.16	3.63
Side	0.00	4.84	

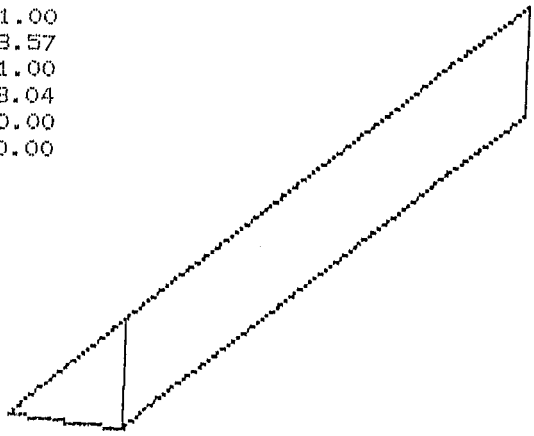

Acceleration Kc = 0.6064 Factor of Safety = 2.75

SARMA NON-VERTICAL SLICE ANALYSIS

Analysis no. 0.5m thick block with 4m long block - wedge 30 degrees

Unit weight of water = 9.8

Side number	1	2	3
Coordinate xt	16.01	17.00	21.00
Coordinate yt	6.57	6.97	8.57
Coordinate xw	16.01	17.00	21.00
Coordinate yw	6.57	6.97	8.57
Coordinate xb	16.01	17.00	21.00
Coordinate yb	6.57	6.44	8.04
Friction angle	0.00	28.40	0.00
Cohesion	0.00	6.00	0.00

Slice number	1	2
Rock unit weight	19.62	19.62
Friction angle	28.40	28.40
Cohesion	6.00	6.00
Force T	0.00	0.00
Angle theta	0.00	0.00

Effective normal stresses

Base		4.68	3.64
Side	0.00	4.94	

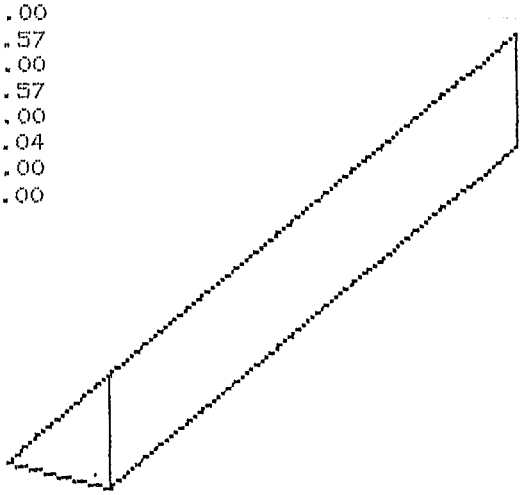

Acceleration Kc = 0.6350 Factor of Safety = 2.77

SARMA NON-VERTICAL SLICE ANALYSIS

Analysis no. 1.0m thick block with 4m long block - wedge 5 degrees

Unit weight of water = 9.8

Side number	1	2	3
Coordinate xt	6.03	17.00	21.00
Coordinate yt	3.09	7.51	9.11
Coordinate xw	6.03	17.00	21.00
Coordinate yw	3.09	7.51	9.11
Coordinate xb	6.03	17.00	21.00
Coordinate yb	3.09	6.44	8.04
Friction angle	0.00	28.40	0.00
Cohesion	0.00	6.00	0.00

Slice number	1	2
Rock unit weight	19.62	19.62
Friction angle	28.40	28.40
Cohesion	6.00	6.00
Force T	0.00	0.00
Angle theta	0.00	0.00

Effective normal stresses

Base		4.46	7.14
Side	0.00	7.81	

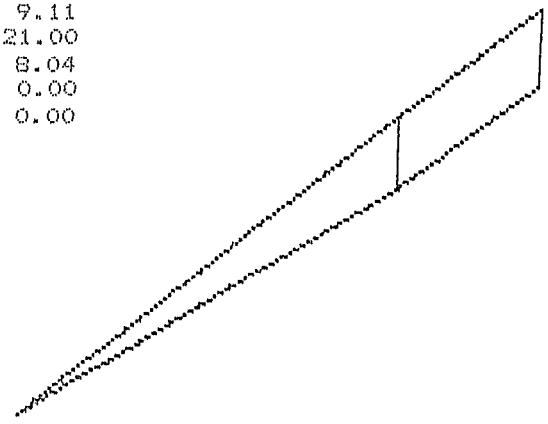

Acceleration Kc = 0.3142 Factor of Safety = 1.98

SARMA NON-VERTICAL SLICE ANALYSIS

Analysis no. 1.0m thick block with 4m long block - wedge 10 degrees

Unit weight of water = 9.8

Side number	1	2	3
Coordinate xt	11.12	17.00	21.00
Coordinate yt	5.13	7.51	9.11
Coordinate xw	11.12	17.00	21.00
Coordinate yw	5.13	7.51	9.11
Coordinate xb	11.12	17.00	21.00
Coordinate yb	5.13	6.44	8.04
Friction angle	0.00	28.40	0.00
Cohesion	0.00	6.00	0.00

Slice number	1	2
Rock unit weight	19.62	19.62
Friction angle	28.40	28.40
Cohesion	6.00	6.00
Force T	0.00	0.00
Angle theta	0.00	0.00

Effective normal stresses

Base	5.17	7.08
Side	0.00	7.16

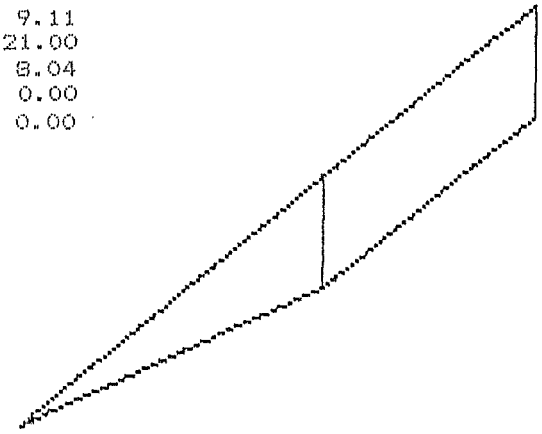

Acceleration Kc = 0.2937 Factor of Safety = 1.92

SARMA NON-VERTICAL SLICE ANALYSIS

Analysis no. 1.0m thick block with 4m long block - wedge 15 degrees

Unit weight of water = 9.8

Side number	1	2	3
Coordinate xt	13.20	17.00	21.00
Coordinate yt	5.97	7.51	9.11
Coordinate xw	13.20	17.00	21.00
Coordinate yw	5.97	7.51	9.11
Coordinate xb	13.20	17.00	21.00
Coordinate yb	5.97	6.44	8.04
Friction angle	0.00	28.40	0.00
Cohesion	0.00	6.00	0.00

Slice number	1	2
Rock unit weight	19.62	19.62
Friction angle	28.40	28.40
Cohesion	6.00	6.00
Force T	0.00	0.00
Angle theta	0.00	0.00

Effective normal stresses

Base	6.10	7.07
Side	0.00	7.05

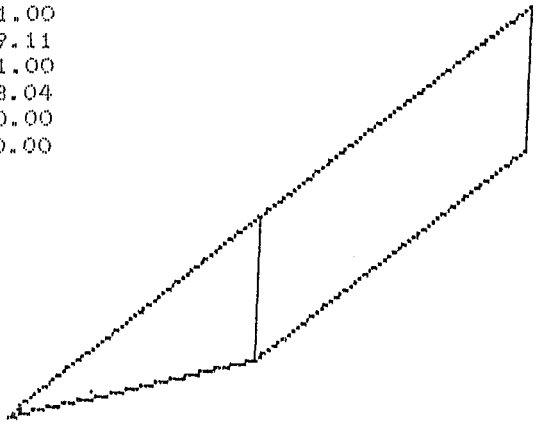

Acceleration Kc = 0.2944 Factor of Safety = 1.91

SARMA NON-VERTICAL SLICE ANALYSIS

Analysis no. 1.0m thick block with 4m long block - wedge 20 degrees

Unit weight of water = 9.8

Side number	1	2	3
Coordinate xt	14.12	17.00	21.00
Coordinate yt	6.35	7.51	9.11
Coordinate xw	14.12	17.00	21.00
Coordinate yw	6.35	7.51	9.11
Coordinate xb	14.12	17.00	21.00
Coordinate yb	6.35	6.44	8.04
Friction angle	0.00	28.40	0.00
Cohesion	0.00	6.00	0.00

Slice number	1	2
Rock unit weight	19.62	19.62
Friction angle	28.40	28.40
Cohesion	6.00	6.00
Force T	0.00	0.00
Angle theta	0.00	0.00

Effective normal stresses

Base		7.01	7.10
Side	0.00	7.32	

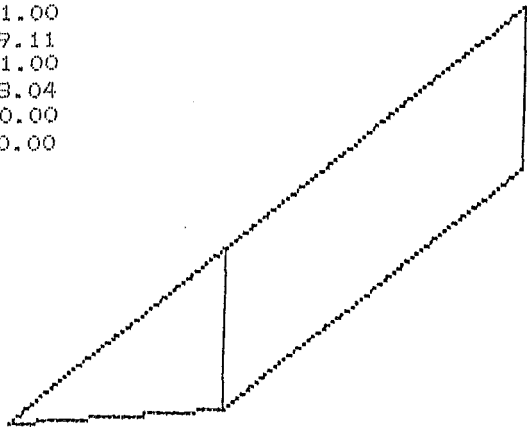

Acceleration Kc = 0.3107 Factor of Safety = 1.94

SARMA NON-VERTICAL SLICE ANALYSIS

Analysis no. 1.0m thick block with 4m long block - wedge 25 degrees

Unit weight of water = 9.8

Side number	1	2	3
Coordinate xt	14.66	17.00	21.00
Coordinate yt	6.56	7.51	9.11
Coordinate xw	14.66	17.00	21.00
Coordinate yw	6.56	7.51	9.11
Coordinate xb	14.66	17.00	21.00
Coordinate yb	6.56	6.44	8.04
Friction angle	0.00	28.40	0.00
Cohesion	0.00	6.00	0.00

Slice number	1	2
Rock unit weight	19.62	19.62
Friction angle	28.40	28.40
Cohesion	6.00	6.00
Force T	0.00	0.00
Angle theta	0.00	0.00

Effective normal stresses

Base		7.87	7.13
Side	0.00	7.62	

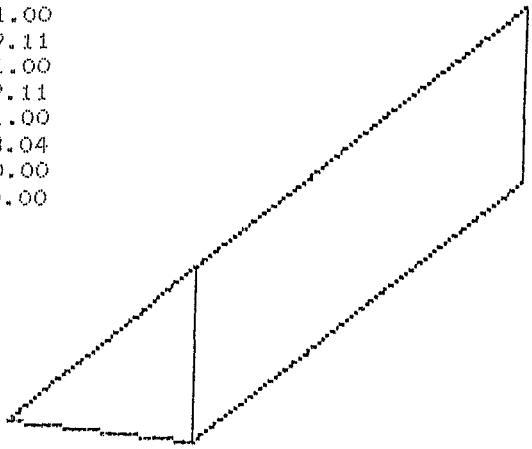

Acceleration Kc = 0.3333 Factor of Safety = 1.97

SARMA NON-VERTICAL SLICE ANALYSIS

Analysis no. 1.0m thick block with 4m long block - wedge 30 degrees

Unit weight of water = 9.8

Side number	1	2	3
Coordinate xt	15.04	17.00	21.00
Coordinate yt	6.72	7.51	9.11
Coordinate xw	15.04	17.00	21.00
Coordinate yw	6.72	7.51	9.11
Coordinate xb	15.04	17.00	21.00
Coordinate yb	6.72	6.44	8.04
Friction.angle	0.00	28.40	0.00
Cohesion	0.00	6.00	0.00

Slice number	1	2
Rock unit weight	19.62	19.62
Friction angle	28.40	28.40
Cohesion	6.00	6.00
Force T	0.00	0.00
Angle theta	0.00	0.00

Effective normal stresses

Base		8.79	7.20
Side	0.00	8.14	

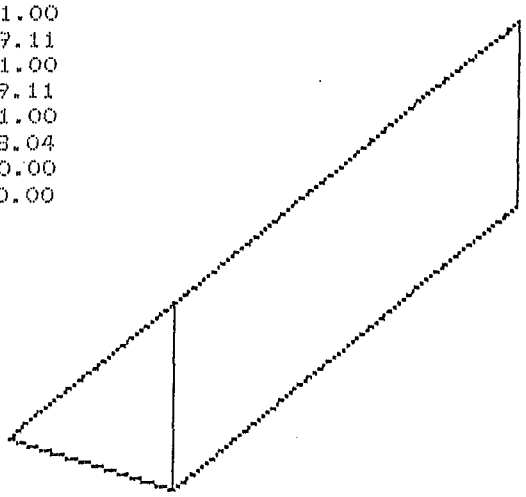

Acceleration Kc = 0.3742 Factor of Safety = 2.04

SARMA NON-VERTICAL SLICE ANALYSIS

Analysis no. 1.5m thick block with 4m long block - wedge 5 degrees

Unit weight of water = 9.8

Side number	1	2	3
Coordinate xt	0.54	17.00	21.00
Coordinate yt	1.41	7.95	9.55
Coordinate xw	0.54	17.00	21.00
Coordinate yw	1.41	7.95	9.55
Coordinate xb	0.54	17.00	21.00
Coordinate yb	1.41	6.44	8.04
Friction angle	0.00	28.40	0.00
Cohesion	0.00	6.00	0.00

Slice number	1	2
Rock unit weight	19.62	19.62
Friction angle	28.40	28.40
Cohesion	6.00	6.00
Force T	0.00	0.00
Angle theta	0.00	0.00

Effective normal stresses

Base		6.27	9.78
Side	0.00	8.20	

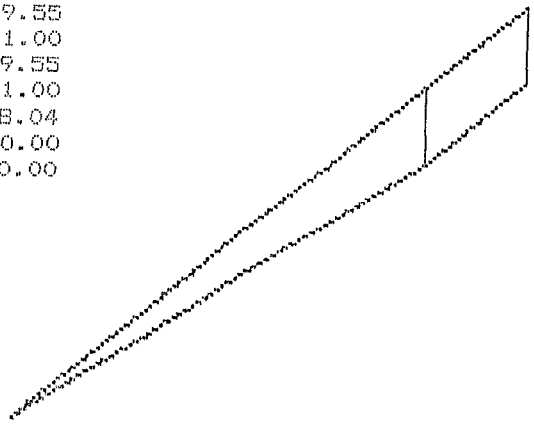

Acceleration Kc = 0.2118 Factor of Safety = 1.67

SARMA NON-VERTICAL SLICE ANALYSIS

Analysis no. 1.5m thick block with 4m long block - wedge 10 degrees

Unit weight of water = 9.8

Side number	1	2	3
Coordinate xt	7.88	17.00	21.00
Coordinate yt	4.66	7.95	9.55
Coordinate xw	7.88	17.00	21.00
Coordinate yw	4.66	7.95	9.55
Coordinate xb	7.88	17.00	21.00
Coordinate yb	4.66	6.44	8.04
Friction angle	0.00	28.40	0.00
Cohesion	0.00	6.00	0.00

Slice number	1	2
Rock unit weight	19.62	19.62
Friction angle	28.40	29.40
Cohesion	6.00	6.00
Force T	0.00	0.00
Angle theta	0.00	0.00

Effective normal stresses

Base		7.34	9.92
Side	0.00	9.20	

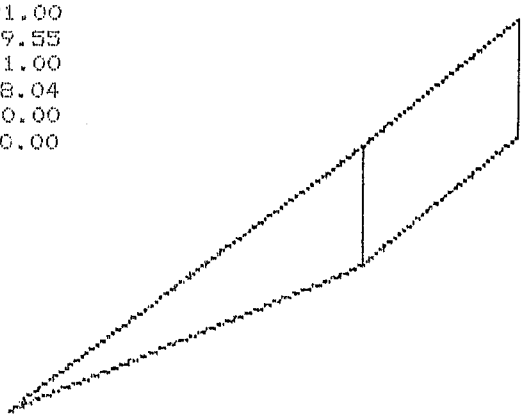

Acceleration Kc = 0.2309 Factor of Safety = 1.77

SARMA NON-VERTICAL SLICE ANALYSIS

Analysis no. 1.5m thick block with 4m long block - wedge 15 degrees

Unit weight of water = 9.8

Side number	1	2	3
Coordinate xt	11.54	17.00	21.00
Coordinate yt	5.74	7.95	9.55
Coordinate xw	11.54	17.00	21.00
Coordinate yw	5.74	7.95	9.55
Coordinate xb	11.54	17.00	21.00
Coordinate yb	5.74	6.44	8.04
Friction angle	0.00	28.40	0.00
Cohesion	0.00	6.00	0.00

Slice number	1	2
Rock unit weight	19.62	19.62
Friction angle	28.40	28.40
Cohesion	6.00	6.00
Force T	0.00	0.00
Angle theta	0.00	0.00

Effective normal stresses

Base		8.33	9.77
Side	0.00	8.10	

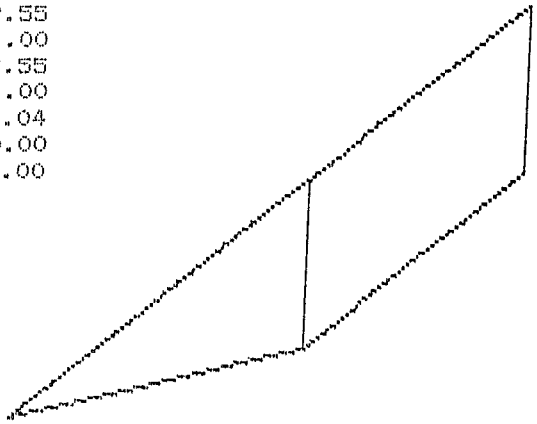

Acceleration Kc = 0.2108 Factor of Safety = 1.67

SARMA NON-VERTICAL SLICE ANALYSIS

Analysis no. 1.5m thick block with 4m long block - wedge 20 degrees

Unit weight of water = 9.8

Side number	1	2	3
Coordinate xt	12.92	17.00	21.00
Coordinate yt	6.30	7.95	9.55
Coordinate xw	12.92	17.00	21.00
Coordinate yw	6.30	7.95	9.55
Coordinate xb	12.92	17.00	21.00
Coordinate yb	6.30	6.44	8.04
Friction angle	0.00	28.40	0.00
Cohesion	0.00	6.00	0.00

Slice number	1	2
Rock unit weight	19.62	19.62
Friction angle	28.40	28.40
Cohesion	6.00	6.00
Force T	0.00	0.00
Angle theta	0.00	0.00

Effective normal stresses

Base		9.49	9.84
Side	0.00	8.60	

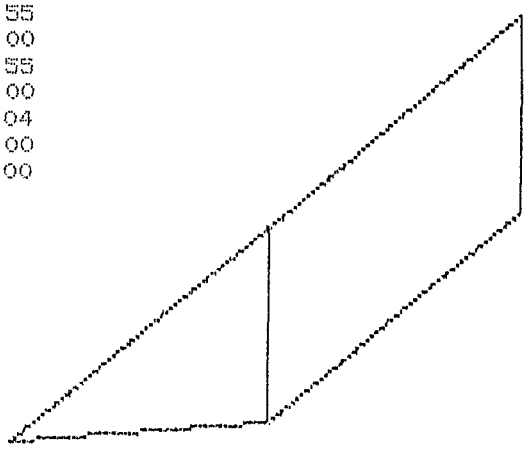

Acceleration Kc = 0.2310 Factor of Safety = 1.71

SARMA NON-VERTICAL SLICE ANALYSIS

Analysis no. 1.5m thick block with 4m long block - wedge 25 degrees

Unit weight of water = 9.8

Side number	1	2	3
Coordinate xt	13.68	17.00	21.00
Coordinate yt	6.60	7.95	9.55
Coordinate xw	13.68	17.00	21.00
Coordinate yw	6.60	7.95	9.55
Coordinate xb	13.68	17.00	21.00
Coordinate yb	6.60	6.44	8.04
Friction angle	0.00	28.40	0.00
Cohesion	0.00	6.00	0.00

Slice number	1	2
Rock unit weight	19.62	19.62
Friction angle	28.40	28.40
Cohesion	6.00	6.00
Force T	0.00	0.00
Angle theta	0.00	0.00

Effective normal stresses

Base		10.55	9.92
Side	0.00	9.10	

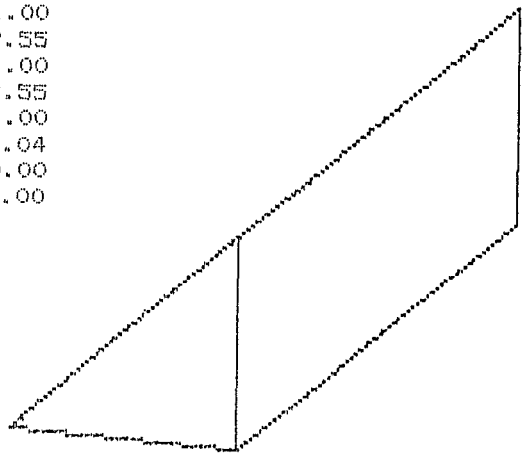

Acceleration Kc = 0.2568 Factor of Safety = 1.76

SARMA NON-VERTICAL SLICE ANALYSIS

Analysis no. 1.5m thick block with 4m long block - wedge 30 degrees

Unit weight of water = 9.8

Side number	1	2	3
Coordinate xt	14.21	17.00	21.00
Coordinate yt	6.82	7.95	9.55
Coordinate xw	14.21	17.00	21.00
Coordinate yw	6.82	7.95	9.55
Coordinate xb	14.21	17.00	21.00
Coordinate yb	6.82	6.44	8.04
Friction angle	0.00	28.40	0.00
Cohesion	0.00	6.00	0.00

Slice number	1	2
Rock unit weight	19.62	19.62
Friction angle	28.40	28.40
Cohesion	6.00	6.00
Force T	0.00	0.00
Angle theta	0.00	0.00

Effective normal stresses

Base	11.63	10.04
Side	0.00	9.75

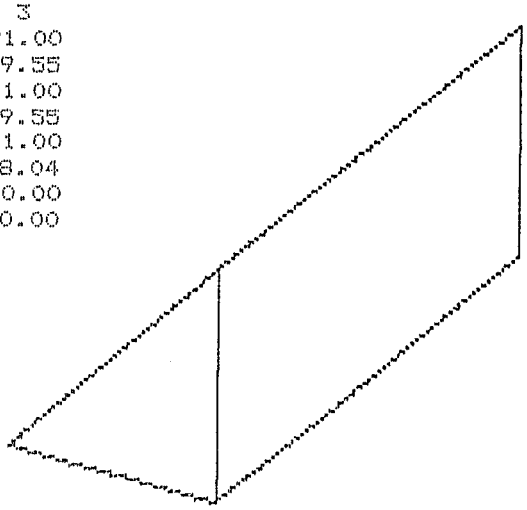

Acceleration Kc = 0.2973

Factor of Safety = 1.84

SARMA NON-VERTICAL SLICE ANALYSIS

Analysis no. 1.5m thick block with 4m long block - wedge 35 degrees

Unit weight of water = 9.8

Side number	1	2	3
Coordinate xt	14.61	17.00	21.00
Coordinate yt	6.98	7.95	9.55
Coordinate xw	14.61	17.00	21.00
Coordinate yw	6.98	7.95	9.55
Coordinate xb	14.61	17.00	21.00
Coordinate yb	6.98	6.44	8.04
Friction angle	0.00	28.40	0.00
Cohesion	0.00	6.00	0.00

Slice number	1	2
Rock unit weight	19.62	19.62
Friction angle	28.40	28.40
Cohesion	6.00	6.00
Force T	0.00	0.00
Angle theta	0.00	0.00

Effective normal stresses

Base	12.68	10.20
Side	0.00	10.38

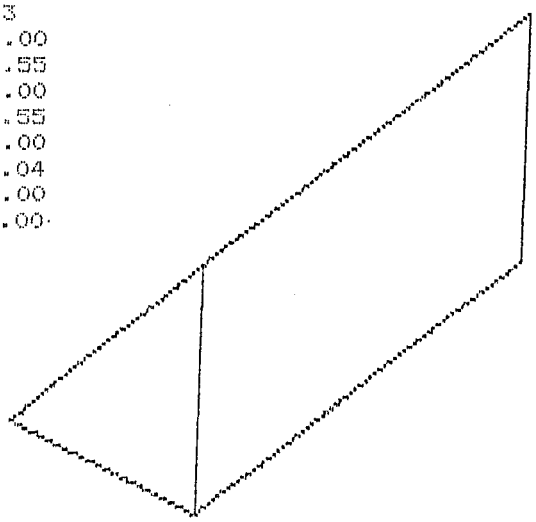

Acceleration Kc = 0.3546

Factor of Safety = 1.94

Analysis of ß for 0.5m to 1.5m thick wedges plus additional 40m long block.

SARMA NON-VERTICAL SLICE ANALYSIS

Analysis no. 0.5m thick block with 40m long block - wedge 5 degrees

Unit weight of water = 9.8

Side number	1	2	3
Coordinate xt	11.12	17.00	62.00
Coordinate yt	4.60	6.97	23.13
Coordinate xw	11.12	17.00	62.00
Coordinate yw	4.60	6.97	23.13
Coordinate xb	11.12	17.00	62.00
Coordinate yb	4.60	6.44	22.60
Friction angle	0.00	28.40	0.00
Cohesion	0.00	6.00	0.00

Slice number	1	2
Rock unit weight	19.62	19.62
Friction angle	28.40	28.40
Cohesion	6.00	6.00
Force T	0.00	0.00
Angle theta	0.00	0.00

Effective normal stresses

Base		2.16	4.01
Side	0.00	11.72	

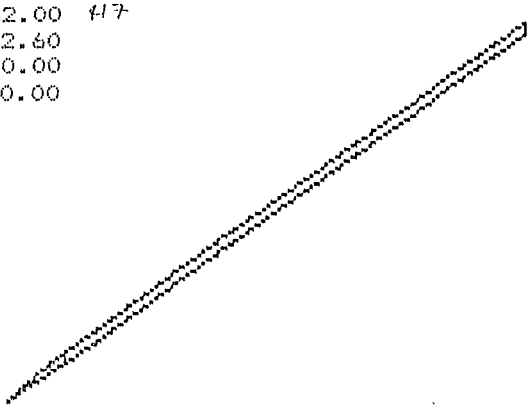

Acceleration Kc = 0.4763

SARMA NON-VERTICAL SLICE ANALYSIS

Analysis no. 0.5m thick block with 40m long block - wedge 10 degrees

Unit weight of water = 9.8

Side number	1	2	3
Coordinate xt	14.02	17.00	62.00
Coordinate yt	5.76	6.97	23.13
Coordinate xw	14.02	17.00	62.00
Coordinate yw	5.76	6.97	23.13
Coordinate xb	14.02	17.00	62.00
Coordinate yb	5.76	6.44	22.60
Friction angle	0.00	28.40	0.00
Cohesion	0.00	6.00	0.00

Slice number	1	2
Rock unit weight	19.62	19.62
Friction angle	28.40	28.40
Cohesion	6.00	6.00
Force T	0.00	0.00
Angle theta	0.00	0.00

Effective normal stresses

Base		2.63	4.00
Side	0.00	7.15	

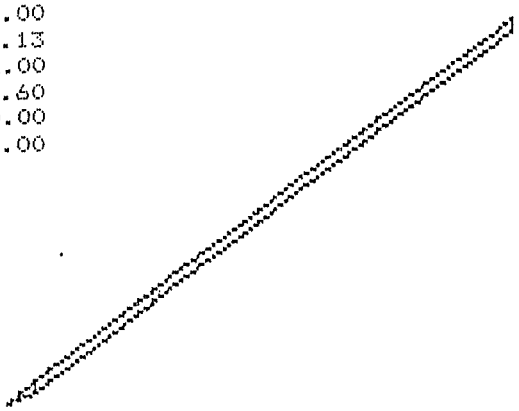

Acceleration Kc = 0.4631

Factor of Safety = 2.54

SARMA NON-VERTICAL SLICE ANALYSIS

Analysis no. 0.5m thick block with 40m long block - wedge 15 degrees

Unit weight of water = 9.8

Side number	1	2	3
Coordinate xt	15.05	17.00	62.00
Coordinate yt	6.19	6.97	23.13
Coordinate xw	15.05	17.00	62.00
Coordinate yw	6.19	6.97	23.13
Coordinate xb	15.05	17.00	62.00
Coordinate yb	6.19	6.44	22.60
Friction angle	0.00	28.40	0.00
Cohesion	0.00	6.00	0.00

Slice number	1	2
Rock unit weight	19.62	19.62
Friction angle	28.40	28.40
Cohesion	6.00	6.00
Force T	0.00	0.00
Angle theta	0.00	0.00

Effective normal stresses

Base		3.20	4.00
Side	0.00	5.93	

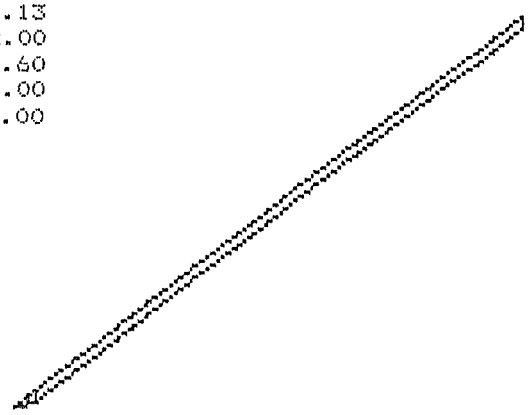

Acceleration Kc = 0.4601 Factor of Safety = 2.52

SARMA NON-VERTICAL SLICE ANALYSIS

Analysis no. 0.5m thick block with 40m long block - wedge 20 degrees

Unit weight of water = 9.8

Side number	1	2	3
Coordinate xt	15.54	17.00	62.00
Coordinate yt	6.38	6.97	23.13
Coordinate xw	15.54	17.00	62.00
Coordinate yw	6.38	6.97	23.13
Coordinate xb	15.54	17.00	62.00
Coordinate yb	6.38	6.44	22.60
Friction angle	0.00	28.40	0.00
Cohesion	0.00	6.00	0.00

Slice number	1	2
Rock unit weight	19.62	19.62
Friction angle	28.40	28.40
Cohesion	6.00	6.00
Force T	0.00	0.00
Angle theta	0.00	0.00

Effective normal stresses

Base		3.76	4.00
Side	0.00	5.46	

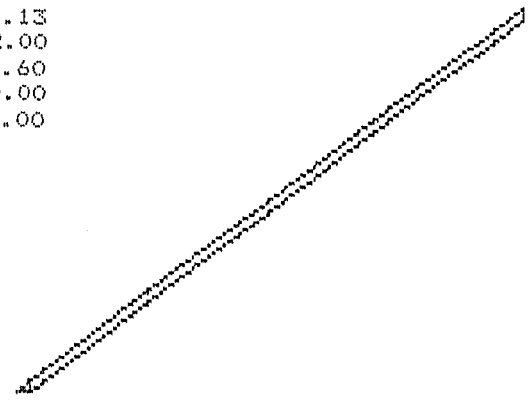

Acceleration Kc = 0.4598 Factor of Safety = 2.52

SARMA NON-VERTICAL SLICE ANALYSIS

Analysis no. 0.5m thick block with 40m long block - wedge 25 degrees

Unit weight of water = 9.8

Side number	1	2	3
Coordinate xt	15.82	17.00	62.00
Coordinate yt	6.50	6.97	23.13
Coordinate xw	15.82	17.00	62.00
Coordinate yw	6.50	6.97	23.13
Coordinate xb	15.82	17.00	62.00
Coordinate yb	6.50	6.44	22.60
Friction angle	0.00	28.40	0.00
Cohesion	0.00	6.00	0.00

Slice number	1	2
Rock unit weight	19.62	19.62
Friction angle	28.40	28.40
Cohesion	6.00	6.00
Force T	0.00	0.00
Angle theta	0.00	0.00

Effective normal stresses

Base	4.38	4.00
Side	0.00	5.58

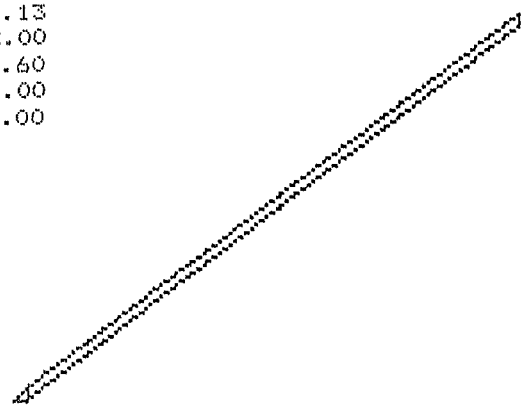

Acceleration Kc = 0.4618 Factor of Safety = 2.52

SARMA NON-VERTICAL SLICE ANALYSIS

Analysis no. 0.5m thick block with 40m long block - wedge 30 degrees

Unit weight of water = 9.8

Side number	1	2	3
Coordinate xt	16.01	17.00	62.00
Coordinate yt	6.57	6.97	23.13
Coordinate xw	16.01	17.00	62.00
Coordinate yw	6.57	6.97	23.13
Coordinate xb	16.01	17.00	62.00
Coordinate yb	6.57	6.44	22.60
Friction angle	0.00	28.40	0.00
Cohesion	0.00	6.00	0.00

Slice number	1	2
Rock unit weight	19.62	19.62
Friction angle	28.40	28.40
Cohesion	6.00	6.00
Force T	0.00	0.00
Angle theta	0.00	0.00

Effective normal stresses

Base	4.98	4.00
Side	0.00	5.70

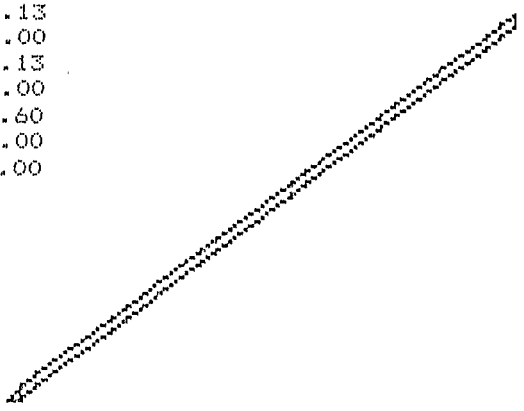

Acceleration Kc = 0.4645 Factor of Safety = 2.52

SARMA NON-VERTICAL SLICE ANALYSIS

Analysis no. 0.75m thick block with 40m block- wedge 5 degrees

Unit weight of water = 9.8

Side number	1	2	3	
Coordinate xt	8.77	17.00	62.00	117
Coordinate yt	3.92	7.25	23.41	47.65
Coordinate xw	8.77	17.00	62.00	117
Coordinate yw	3.92	7.25	23.41	47.65
Coordinate xb	8.77	17.00	62.00	117
Coordinate yb	3.92	6.44	22.60	46.94
Friction angle	0.00	28.40	0.00	
Cohesion	0.00	6.00	0.00	

Slice number	1	2
Rock unit weight	19.62	19.62
Friction angle	28.40	28.40
Cohesion	6.00	6.00
Force T	0.00	0.00
Angle theta	0.00	0.00

Effective normal stresses

Base		3.43	6.11
Side	0.00	14.11	

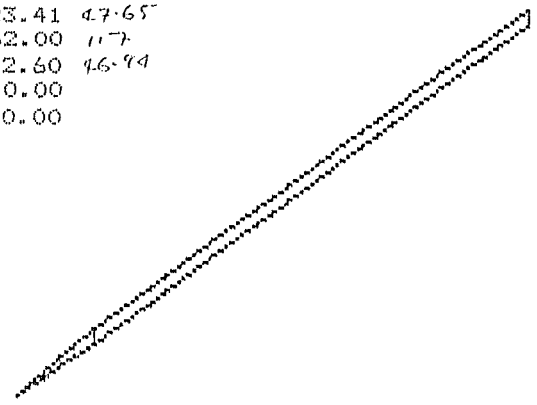

Acceleration Kc = 0.2844 Factor of Safety = 1.94

SARMA NON-VERTICAL SLICE ANALYSIS

Analysis no. 0.75m thick block with 40m block- wedge 10 degrees

Unit weight of water = 9.8

Side number	1	2	3
Coordinate xt	12.76	17.00	62.00
Coordinate yt	5.53	7.25	23.41
Coordinate xw	12.76	17.00	62.00
Coordinate yw	5.53	7.25	23.41
Coordinate xb	12.76	17.00	62.00
Coordinate yb	5.53	6.44	22.60
Friction angle	0.00	28.40	0.00
Cohesion	0.00	6.00	0.00

Slice number	1	2
Rock unit weight	19.62	19.62
Friction angle	28.40	28.40
Cohesion	6.00	6.00
Force T	0.00	0.00
Angle theta	0.00	0.00

Effective normal stresses

Base		4.16	6.10
Side	0.00	9.52	

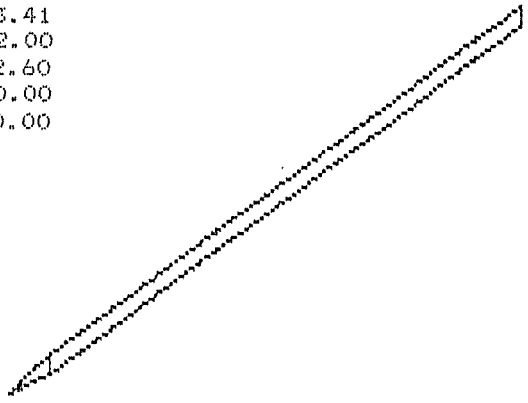

Acceleration Kc = 0.2742 Factor of Safety = 1.91

SARMA NON-VERTICAL SLICE ANALYSIS

Analysis no. 0.75m thick block with 40m block- wedge 15 degrees

Unit weight of water = 9.8

Side number	1	2	3
Coordinate xt	14.12	17.00	62.00
Coordinate yt	6.08	7.25	23.41
Coordinate xw	14.12	17.00	62.00
Coordinate yw	6.08	7.25	23.41
Coordinate xb	14.12	17.00	62.00
Coordinate yb	6.08	6.44	22.60
Friction angle	0.00	28.40	0.00
Cohesion	0.00	6.00	0.00

Slice number	1	2
Rock unit weight	19.62	19.62
Friction angle	28.40	28.40
Cohesion	6.00	6.00
Force T	0.00	0.00
Angle theta	0.00	0.00

Effective normal stresses

Base		4.96	6.10
Side	0.00	8.30	

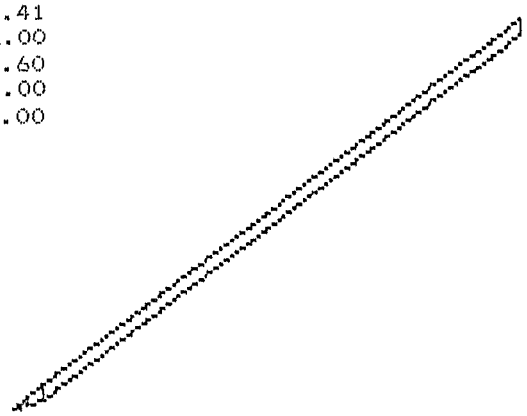

Acceleration Kc = 0.2720 Factor of Safety = 1.90

SARMA NON-VERTICAL SLICE ANALYSIS

Analysis no. 0.75m thick block with 40m block- wedge 20 degrees

Unit weight of water = 9.8

Side number	1	2	3
Coordinate xt	14.83	17.00	62.00
Coordinate yt	6.37	7.25	23.41
Coordinate xw	14.83	17.00	62.00
Coordinate yw	6.37	7.25	23.41
Coordinate xb	14.83	17.00	62.00
Coordinate yb	6.37	6.44	22.60
Friction angle	0.00	28.40	0.00
Cohesion	0.00	6.00	0.00

Slice number	1	2
Rock unit weight	19.62	19.62
Friction angle	28.40	28.40
Cohesion	6.00	6.00
Force T	0.00	0.00
Angle theta	0.00	0.00

Effective normal stresses

Base		5.86	6.10
Side	0.00	8.12	

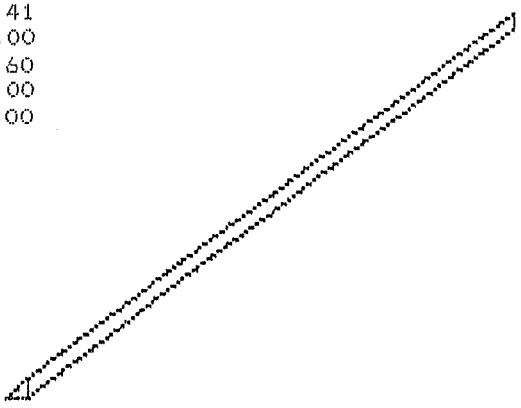

Acceleration Kc = 0.2726 Factor of Safety = 1.90

SARMA NON-VERTICAL SLICE ANALYSIS

Analysis no. 0.75m thick block with 40m block- wedge 25 degrees

Unit weight of water = 9.8

Side number	1	2	3
Coordinate xt	15.24	17.00	62.00
Coordinate yt	6.54	7.25	23.41
Coordinate xw	15.24	17.00	62.00
Coordinate yw	6.54	7.25	23.41
Coordinate xb	15.24	17.00	62.00
Coordinate yb	6.54	6.44	22.60
Friction angle	0.00	28.40	0.00
Cohesion	0.00	6.00	0.00

Slice number	1	2
Rock unit weight	19.62	19.62
Friction angle	28.40	28.40
Cohesion	6.00	6.00
Force T	0.00	0.00
Angle theta	0.00	0.00

Effective normal stresses

Base		6.82	6.10
Side	0.00	8.44	

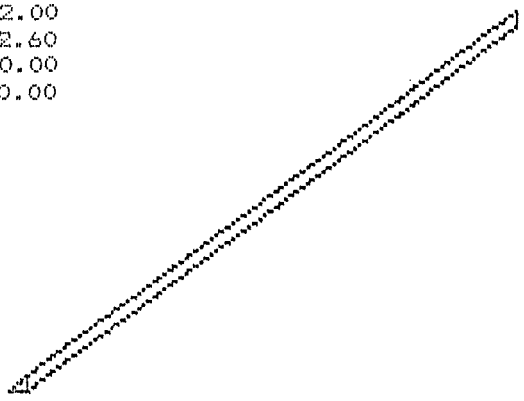

Acceleration Kc = 0.2749 Factor of Safety = 1.90

SARMA NON-VERTICAL SLICE ANALYSIS

Analysis no. 0.75m thick block with 40m block- wedge 30 degrees

Unit weight of water = 9.8

Side number	1	2	3
Coordinate xt	15.31	17.00	62.00
Coordinate yt	6.65	7.25	23.41
Coordinate xw	15.31	17.00	62.00
Coordinate yw	6.65	7.25	23.41
Coordinate xb	15.31	17.00	62.00
Coordinate yb	6.65	6.44	22.60
Friction angle	0.00	28.40	0.00
Cohesion	0.00	6.00	0.00

Slice number	1	2
Rock unit weight	19.62	19.62
Friction angle	28.40	28.40
Cohesion	6.00	6.00
Force T	0.00	0.00
Angle theta	0.00	0.00

Effective normal stresses

Base		7.49	6.10
Side	0.00	9.97	

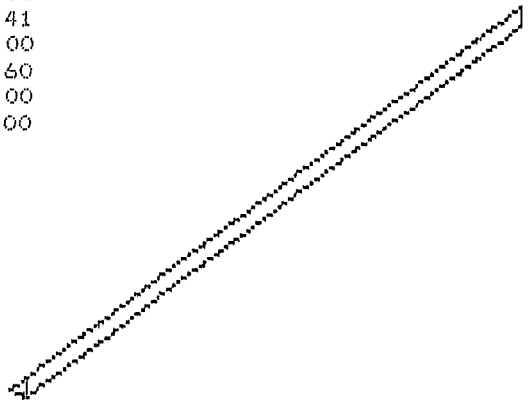

Acceleration Kc = 0.2801 Factor of Safety = 1.91

SARMA NON-VERTICAL SLICE ANALYSIS

Analysis no. 1.0m thick block with 40m long block - wedge 5 degrees

Unit weight of water = 9.8

Side number	1	2	3
Coordinate xt	6.03	17.00	62.00
Coordinate yt	3.09	7.51	23.67
Coordinate xw	6.03	17.00	62.00
Coordinate yw	3.09	7.51	23.67
Coordinate xb	6.03	17.00	62.00
Coordinate yb	3.09	6.44	22.60
Friction angle	0.00	28.40	0.00
Cohesion	0.00	6.00	0.00

Slice number	1	2
Rock unit weight	19.62	19.62
Friction angle	28.40	28.40
Cohesion	6.00	6.00
Force T	0.00	0.00
Angle theta	0.00	0.00

Effective normal stresses

Base	4.57	8.04
Side	0.00	16.57

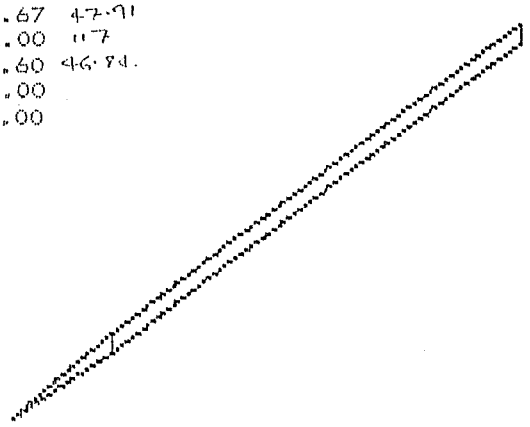

Acceleration Kc = 0.1973 Factor of Safety = 1.65

SARMA NON-VERTICAL SLICE ANALYSIS

Analysis no. 1.0m thick block with 40m long block - wedge 10 degrees

Unit weight of water = 9.8

Side number	1	2	3
Coordinate xt	11.12	17.00	62.00
Coordinate yt	5.13	7.51	23.67
Coordinate xw	11.12	17.00	62.00
Coordinate yw	5.13	7.51	23.67
Coordinate xb	11.12	17.00	62.00
Coordinate yb	5.13	6.44	22.60
Friction angle	0.00	28.40	0.00
Cohesion	0.00	6.00	0.00

Slice number	1	2
Rock unit weight	19.62	19.62
Friction angle	28.40	28.40
Cohesion	6.00	6.00
Force T	0.00	0.00
Angle theta	0.00	0.00

Effective normal stresses

Base	5.42	8.04
Side	0.00	11.92

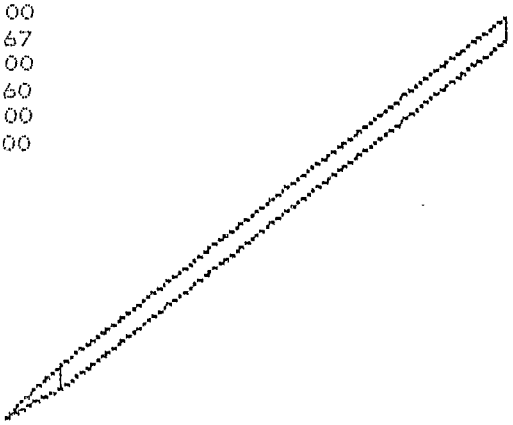

Acceleration Kc = 0.1883 Factor of Safety = 1.62

SARMA NON-VERTICAL SLICE ANALYSIS

Analysis no. 1.0m thick block with 40m long block - wedge 15 degrees

Unit weight of water = 9.8

Side number	1	2	3
Coordinate xt	13.20	17.00	62.00
Coordinate yt	5.97	7.51	23.67
Coordinate xw	13.20	17.00	62.00
Coordinate yw	5.97	7.51	23.67
Coordinate xb	13.20	17.00	62.00
Coordinate yb	5.97	6.44	22.60
Friction angle	0.00	28.40	0.00
Cohesion	0.00	6.00	0.00

Slice number	1	2
Rock unit weight	19.62	19.62
Friction angle	28.40	28.40
Cohesion	6.00	6.00
Force T	0.00	0.00
Angle theta	0.00	0.00

Effective normal stresses

Base		6.56	8.04
Side	0.00	10.55	

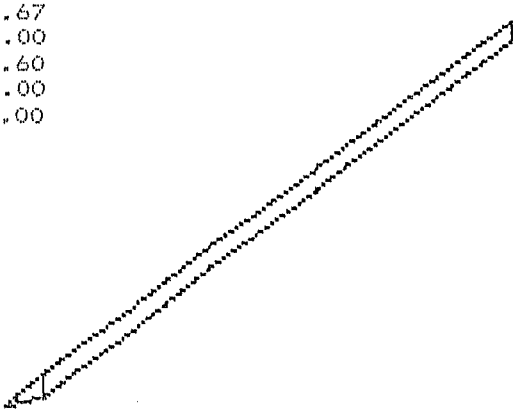

Acceleration Kc = 0.1862 Factor of Safety = 1.62

SARMA NON-VERTICAL SLICE ANALYSIS

Analysis no. 1.0m thick block with 40m long block - wedge 20 degrees

Unit weight of water = 9.8

Side number	1	2	3
Coordinate xt	14.12	17.00	62.00
Coordinate yt	6.35	7.51	23.67
Coordinate xw	14.12	17.00	62.00
Coordinate yw	6.35	7.51	23.67
Coordinate xb	14.12	17.00	62.00
Coordinate yb	6.35	6.44	22.60
Friction angle	0.00	28.40	0.00
Cohesion	0.00	6.00	0.00

Slice number	1	2
Rock unit weight	19.62	19.62
Friction angle	28.40	28.40
Cohesion	6.00	6.00
Force T	0.00	0.00
Angle theta	0.00	0.00

Effective normal stresses

Base		7.76	8.04
Side	0.00	10.64	

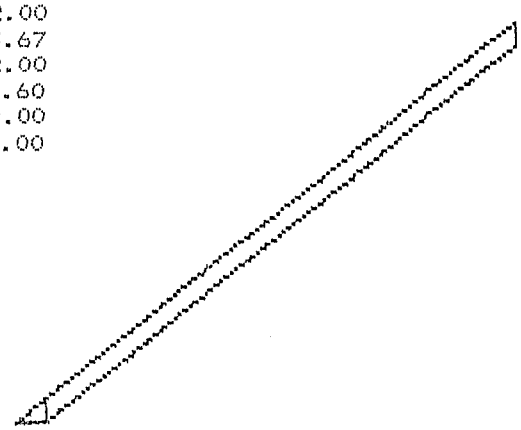

Acceleration Kc = 0.1873 Factor of Safety = 1.62

SARMA NON-VERTICAL SLICE ANALYSIS

Analysis no. 1.0m thick block with 40m long block - wedge 25 degrees

Unit weight of water = 9.8

Side number	1	2	3
Coordinate xt	14.66	17.00	62.00
Coordinate yt	6.56	7.51	23.67
Coordinate xw	14.66	17.00	62.00
Coordinate yw	6.56	7.51	23.67
Coordinate xb	14.66	17.00	62.00
Coordinate yb	6.56	6.44	22.60
Friction angle	0.00	28.40	0.00
Cohesion	0.00	6.00	0.00

Slice number	1	2
Rock unit weight	19.62	19.62
Friction angle	28.40	28.40
Cohesion	6.00	6.00
Force T	0.00	0.00
Angle theta	0.00	0.00

Effective normal stresses

Base		8.98	8.04
Side	0.00	11.01	

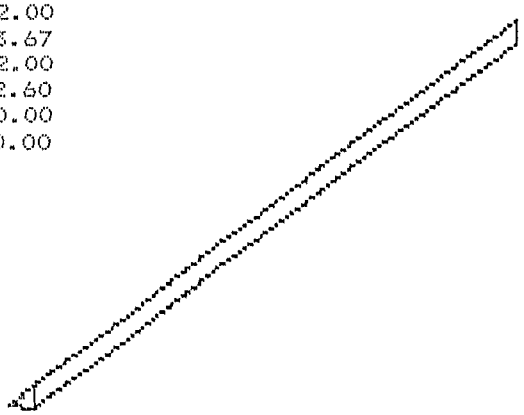

Acceleration Kc = 0.1894 Factor of Safety = 1.62

SARMA NON-VERTICAL SLICE ANALYSIS

Analysis no. 1.0m thick block with 40m long block - wedge 30 degrees

Unit weight of water = 9.8

Side number	1	2	3
Coordinate xt	15.04	17.00	62.00
Coordinate yt	6.72	7.51	23.67
Coordinate xw	15.04	17.00	62.00
Coordinate yw	6.72	7.51	23.67
Coordinate xb	15.04	17.00	62.00
Coordinate yb	6.72	6.44	22.60
Friction angle	0.00	28.40	0.00
Cohesion	0.00	6.00	0.00

Slice number	1	2
Rock unit weight	19.62	19.62
Friction angle	28.40	28.40
Cohesion	6.00	6.00
Force T	0.00	0.00
Angle theta	0.00	0.00

Effective normal stresses

Base		10.48	8.04
Side	0.00	12.03	

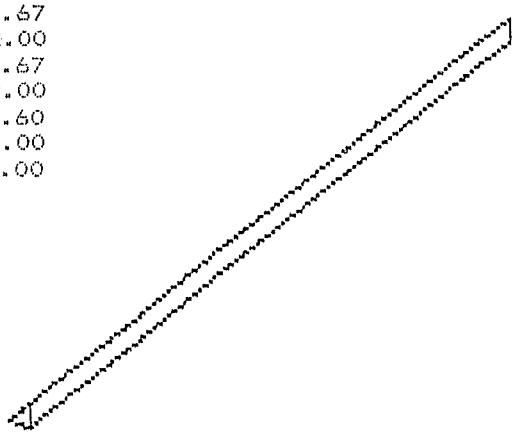

Acceleration Kc = 0.1939 Factor of Safety = 1.62

SARMA NON-VERTICAL SLICE ANALYSIS

Analysis no. 1.25m thick block with 40m long block- wedge 5 degrees

Unit weight of water = 9.8

Side number	1	2	3	
Coordinate xt	3.28	17.00	62.00	117
Coordinate yt	2.25	7.79	23.95	48.19
Coordinate xw	3.28	17.00	62.00	117
Coordinate yw	2.25	7.79	23.95	48.19
Coordinate xb	3.28	17.00	62.00	117
Coordinate yb	2.25	6.44	22.60	46.84
Friction angle	0.00	28.40	0.00	
Cohesion	0.00	6.00	0.00	

Slice number	1	2
Rock unit weight	19.62	19.62
Friction angle	28.40	28.40
Cohesion	6.00	6.00
Force T	0.00	0.00
Angle theta	0.00	0.00

Effective normal stresses

Base		5.79	10.12
Side	0.00	18.28	

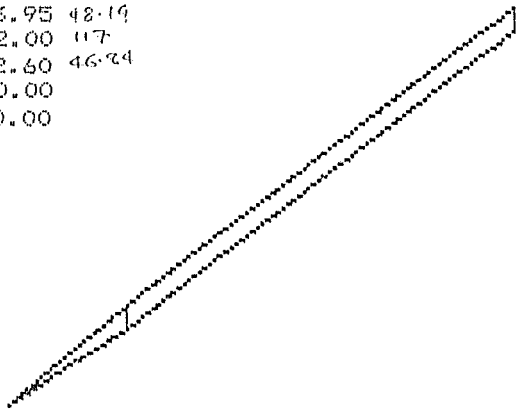

Acceleration Kc = 0.1402 Factor of Safety = 1.46

SARMA NON-VERTICAL SLICE ANALYSIS

Analysis no. 1.25m thick block with 40m long block- wedge 10 degrees

Unit weight of water = 9.8

Side number	1	2	3
Coordinate xt	9.82	17.00	62.00
Coordinate yt	4.86	7.79	23.95
Coordinate xw	9.82	17.00	62.00
Coordinate yw	4.86	7.79	23.95
Coordinate xb	9.82	17.00	62.00
Coordinate yb	4.86	6.44	22.60
Friction angle	0.00	28.40	0.00
Cohesion	0.00	6.00	0.00

Slice number	1	2
Rock unit weight	19.62	19.62
Friction angle	28.40	28.40
Cohesion	6.00	6.00
Force T	0.00	0.00
Angle theta	0.00	0.00

Effective normal stresses

Base		6.88	10.11
Side	0.00	13.55	

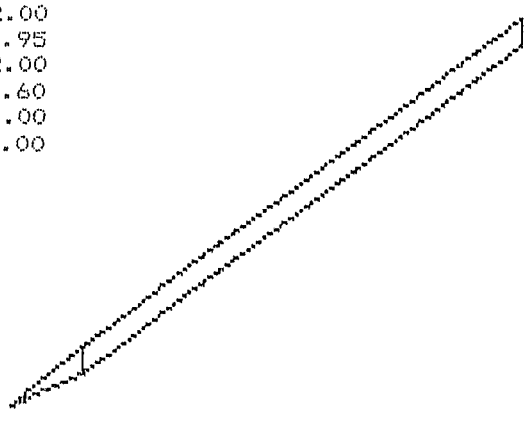

Acceleration Kc = 0.1321 Factor of Safety = 1.44

SARMA NON-VERTICAL SLICE ANALYSIS

Analysis no. 1.25m thick block with 40m long block- wedge 15 degrees

Unit weight of water = 9.8

Side number	1	2	3
Coordinate xt	12.19	17.00	62.00
Coordinate yt	5.83	7.79	23.95
Coordinate xw	12.19	17.00	62.00
Coordinate yw	5.83	7.79	23.95
Coordinate xb	12.19	17.00	62.00
Coordinate yb	5.83	6.44	22.60
Friction angle	0.00	28.40	0.00
Cohesion	0.00	6.00	0.00

Slice number	1	2
Rock unit weight	19.62	19.62
Friction angle	28.40	28.40
Cohesion	6.00	6.00
Force T	0.00	0.00
Angle theta	0.00	0.00

Effective normal stresses

Base		8.22	10.11
Side	0.00	12.65	

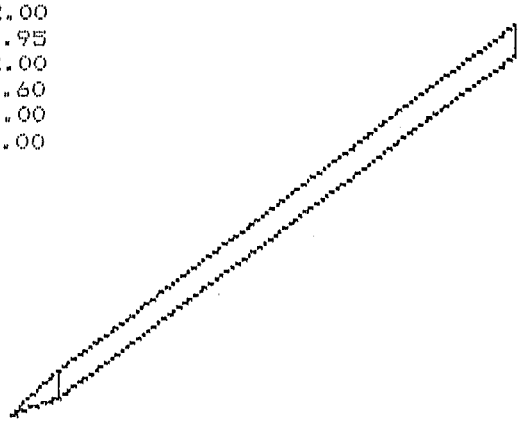

Acceleration Kc = 0.1309 Factor of Safety = 1.43

SARMA NON-VERTICAL SLICE ANALYSIS

Analysis no. 1.25m thick block with 40m long block- wedge 20 degrees

Unit weight of water = 9.8

Side number	1	2	3
Coordinate xt	13.39	17.00	62.00
Coordinate yt	6.33	7.79	23.95
Coordinate xw	13.39	17.00	62.00
Coordinate yw	6.33	7.79	23.95
Coordinate xb	13.39	17.00	62.00
Coordinate yb	6.33	6.44	22.60
Friction angle	0.00	28.40	0.00
Cohesion	0.00	6.00	0.00

Slice number	1	2
Rock unit weight	19.62	19.62
Friction angle	28.40	28.40
Cohesion	6.00	6.00
Force T	0.00	0.00
Angle theta	0.00	0.00

Effective normal stresses

Base		9.80	10.11
Side	0.00	13.10	

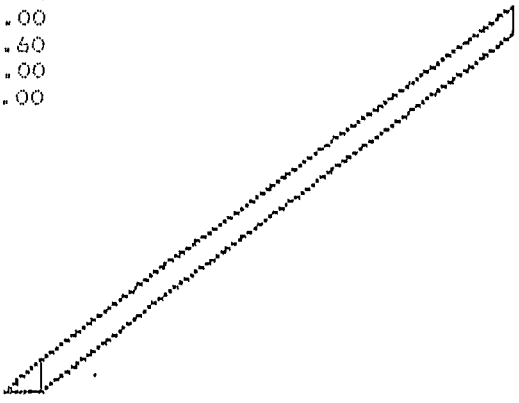

Acceleration Kc = 0.1325 Factor of Safety = 1.44

SARMA NON-VERTICAL SLICE ANALYSIS

Analysis no. 1.25m thick block with 40m long block- wedge 25 degrees

Unit weight of water = 9.8

Side number	1	2	3
Coordinate xt	14.06	17.00	62.00
Coordinate yt	6.60	7.79	23.95
Coordinate xw	14.06	17.00	62.00
Coordinate yw	6.60	7.79	23.95
Coordinate xb	14.06	17.00	62.00
Coordinate yb	6.60	6.44	22.60
Friction angle	0.00	28.40	0.00
Cohesion	0.00	6.00	0.00

Slice number	1	2
Rock unit weight	19.62	19.62
Friction angle	28.40	28.40
Cohesion	6.00	6.00
Force T	0.00	0.00
Angle theta	0.00	0.00

Effective normal stresses

Base	11.40	10.11
Side	0.00	13.93

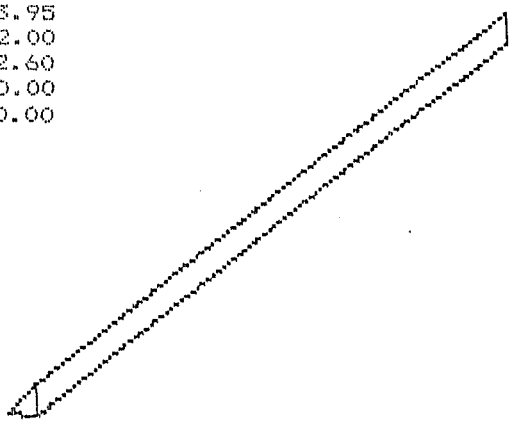

Acceleration Kc = 0.1352 Factor of Safety = 1.44

SARMA NON-VERTICAL SLICE ANALYSIS

Analysis no. 1.25m thick block with 40m long block- wedge 30 degrees

Unit weight of water = 9.8

Side number	1	2	3
Coordinate xt	14.51	17.00	62.00
Coordinate yt	6.78	7.79	23.95
Coordinate xw	14.51	17.00	62.00
Coordinate yw	6.78	7.79	23.95
Coordinate xb	14.51	17.00	62.00
Coordinate yb	6.78	6.44	22.60
Friction angle	0.00	28.40	0.00
Cohesion	0.00	6.00	0.00

Slice number	1	2
Rock unit weight	19.62	19.62
Friction angle	28.40	28.40
Cohesion	6.00	6.00
Force T	0.00	0.00
Angle theta	0.00	0.00

Effective normal stresses

Base	13.18	10.11
Side	0.00	15.12

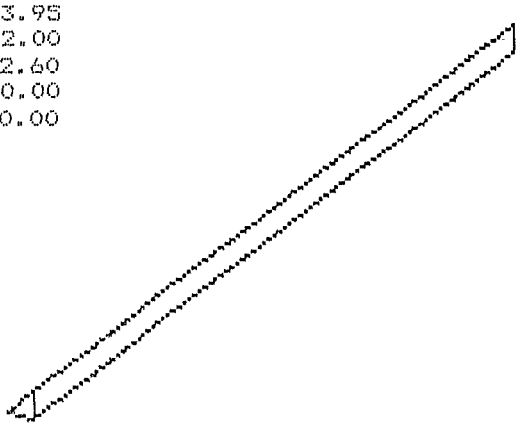

Acceleration Kc = 0.1393 Factor of Safety = 1.45

SARMA NON-VERTICAL SLICE ANALYSIS

Analysis no. 1.25m thick block with 40m long block- wedge 35 degrees

Unit weight of water = 9.8

Side number	1	2	3
Coordinate xt	14.88	17.00	62.00
Coordinate yt	6.93	7.79	23.95
Coordinate xw	14.88	17.00	62.00
Coordinate yw	6.93	7.79	23.95
Coordinate xb	14.88	17.00	62.00
Coordinate yb	6.93	6.44	22.60
Friction angle	0.00	28.40	0.00
Cohesion	0.00	6.00	0.00

Slice number	1	2
Rock unit weight	19.62	19.62
Friction angle	28.40	28.40
Cohesion	6.00	6.00
Force T	0.00	0.00
Angle theta	0.00	0.00

Effective normal stresses

Base		15.55	10.12
Side	0.00	16.97	

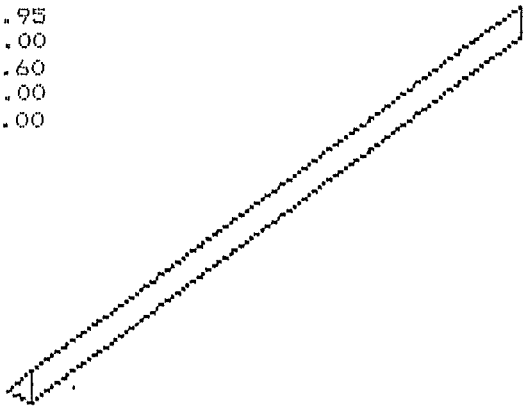

Acceleration Kc = 0.1467 Factor of Safety = 1.46

SARMA NON-VERTICAL SLICE ANALYSIS

Analysis no. 1.5m thick block with 40m long block- wedge 5 degrees

Unit weight of water = 9.8

Side number	1	2	3	
Coordinate xt	0.54	17.00	62.00	117
Coordinate yt	1.41	7.95	24.11	48.35
Coordinate xw	0.54	17.00	62.00	117
Coordinate yw	1.41	7.95	24.11	48.35
Coordinate xb	0.54	17.00	62.00	117
Coordinate yb	1.41	6.44	22.60	46.84
Friction angle	0.00	28.40	0.00	
Cohesion	0.00	6.00	0.00	

Slice number	1	2
Rock unit weight	19.62	19.62
Friction angle	28.40	28.40
Cohesion	6.00	6.00
Force T	0.00	0.00
Angle theta	0.00	0.00

Effective normal stresses

Base		6.46	11.30
Side	0.00	20.61	

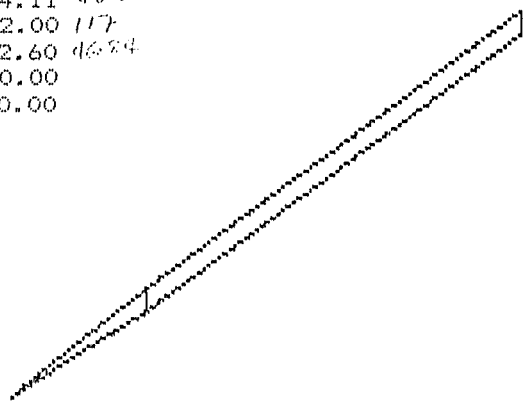

Acceleration Kc = 0.1193 Factor of Safety = 1.39

SARMA NON-VERTICAL SLICE ANALYSIS

Analysis no. 1.5m thick block with 40m long block- wedge 10 degrees

Unit weight of water = 9.8

Side number	1	2	3
Coordinate xt	7.88	17.00	62.00
Coordinate yt	4.66	7.95	24.11
Coordinate xw	7.88	17.00	62.00
Coordinate yw	4.66	7.95	24.11
Coordinate xb	7.88	17.00	62.00
Coordinate yb	4.66	6.44	22.60
Friction angle	0.00	28.40	0.00
Cohesion	0.00	6.00	0.00

Slice number	1	2
Rock unit weight	19.62	19.62
Friction angle	28.40	28.40
Cohesion	6.00	6.00
Force T	0.00	0.00
Angle theta	0.00	0.00

Effective normal stresses

Base		7.93	11.30
Side	0.00	19.29	

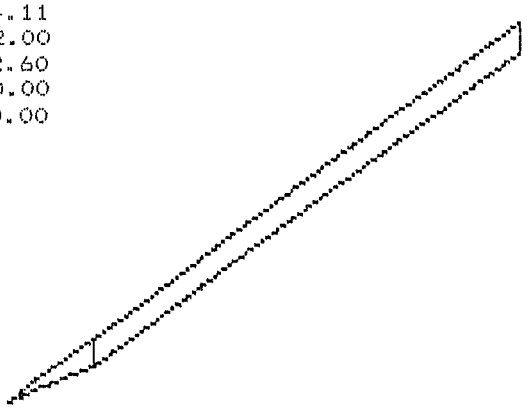

Acceleration Kc = 0.1164 Factor of Safety = 1.39

SARMA NON-VERTICAL SLICE ANALYSIS

Analysis no. 1.5m thick block with 40m long block- wedge 15 degrees

Unit weight of water = 9.8

Side number	1	2	3
Coordinate xt	11.54	17.00	62.00
Coordinate yt	5.74	7.95	24.11
Coordinate xw	11.54	17.00	62.00
Coordinate yw	5.74	7.95	24.11
Coordinate xb	11.54	17.00	62.00
Coordinate yb	5.74	6.44	22.60
Friction angle	0.00	28.40	0.00
Cohesion	0.00	6.00	0.00

Slice number	1	2
Rock unit weight	19.62	19.62
Friction angle	28.40	28.40
Cohesion	6.00	6.00
Force T	0.00	0.00
Angle theta	0.00	0.00

Effective normal stresses

Base		9.14	11.30
Side	0.00	14.02	

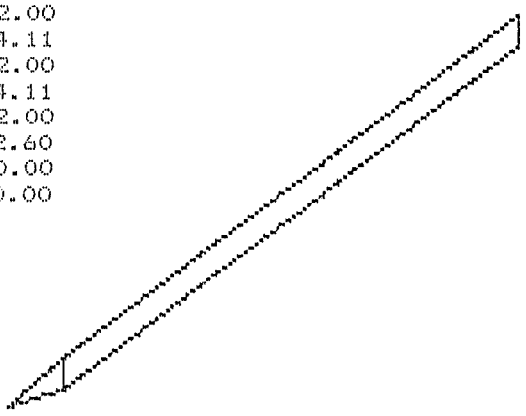

Acceleration Kc = 0.1090 Factor of Safety = 1.36

SARMA NON-VERTICAL SLICE ANALYSIS

Analysis no. 1.5m thick block with 40m long block- wedge 20 degrees

Unit weight of water = 9.8

Side number	1	2	3
Coordinate xt	12.92	17.00	62.00
Coordinate yt	6.30	7.95	24.11
Coordinate xw	12.92	17.00	62.00
Coordinate yw	6.30	7.95	24.11
Coordinate xb	12.92	17.00	62.00
Coordinate yb	6.30	6.44	22.60
Friction angle	0.00	28.40	0.00
Cohesion	0.00	6.00	0.00

Slice number	1	2
Rock unit weight	19.62	19.62
Friction angle	28.40	28.40
Cohesion	6.00	6.00
Force T	0.00	0.00
Angle theta	0.00	0.00

Effective normal stresses

Base		10.87	11.30
Side	0.00	14.46	

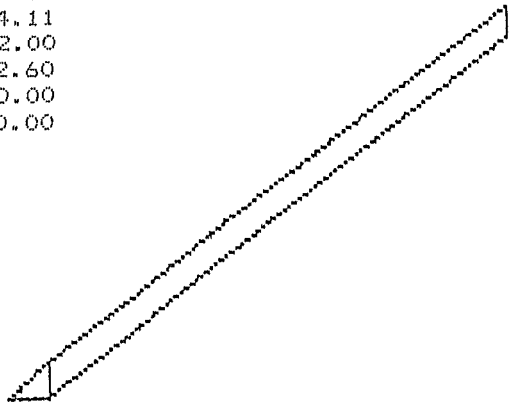

Acceleration Kc = 0.1104 Factor of Safety = 1.36

SARMA NON-VERTICAL SLICE ANALYSIS

Analysis no. 1.5m thick block with 40m long block- wedge 25 degrees

Unit weight of water = 9.8

Side number	1	2	3
Coordinate xt	13.68	17.00	62.00
Coordinate yt	6.60	7.95	24.11
Coordinate xw	13.68	17.00	62.00
Coordinate yw	6.60	7.95	24.11
Coordinate xb	13.68	17.00	62.00
Coordinate yb	6.60	6.44	22.60
Friction angle	0.00	28.40	0.00
Cohesion	0.00	6.00	0.00

Slice number	1	2
Rock unit weight	19.62	19.62
Friction angle	28.40	28.40
Cohesion	6.00	6.00
Force T	0.00	0.00
Angle theta	0.00	0.00

Effective normal stresses

Base		12.62	11.30
Side	0.00	15.35	

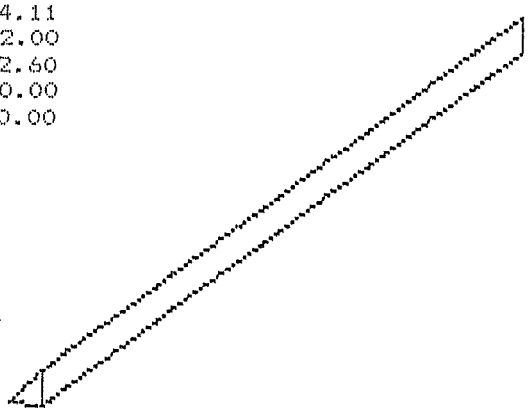

Acceleration Kc = 0.1131 Factor of Safety = 1.37

SARMA NON-VERTICAL SLICE ANALYSIS

Analysis no. 1.5m thick block with 40m long block- wedge 30 degrees

Unit weight of water = 9.8

Side number	1	2	3
Coordinate xt	14.21	17.00	62.00
Coordinate yt	6.82	7.95	24.11
Coordinate xw	14.21	17.00	62.00
Coordinate yw	6.82	7.95	24.11
Coordinate xb	14.21	17.00	62.00
Coordinate yb	6.82	6.44	22.60
Friction angle	0.00	28.40	0.00
Cohesion	0.00	6.00	0.00

Slice number	1	2
Rock unit weight	19.62	19.62
Friction angle	28.40	28.40
Cohesion	6.00	6.00
Force T	0.00	0.00
Angle theta	0.00	0.00

Effective normal stresses

Base		14.77	11.30
Side	0.00	16.97	

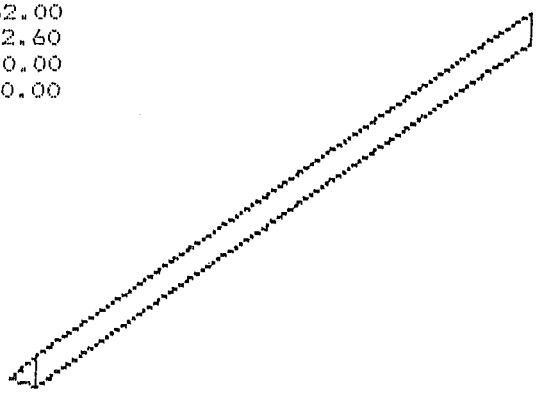

Acceleration Kc = 0.1178 Factor of Safety = 1.38

SARMA NON-VERTICAL SLICE ANALYSIS

Analysis no. 1.5m thick block with 40m long block- wedge 35 degrees

Unit weight of water = 9.8

Side number	1	2	3
Coordinate xt	14.61	17.00	62.00
Coordinate yt	6.98	7.95	24.11
Coordinate xw	14.61	17.00	62.00
Coordinate yw	6.98	7.95	24.11
Coordinate xb	14.61	17.00	62.00
Coordinate yb	6.98	6.44	22.60
Friction angle	0.00	28.40	0.00
Cohesion	0.00	6.00	0.00

Slice number	1	2
Rock unit weight	19.62	19.62
Friction angle	28.40	28.40
Cohesion	6.00	6.00
Force T	0.00	0.00
Angle theta	0.00	0.00

Effective normal stresses

Base		17.33	11.30
Side	0.00	19.00	

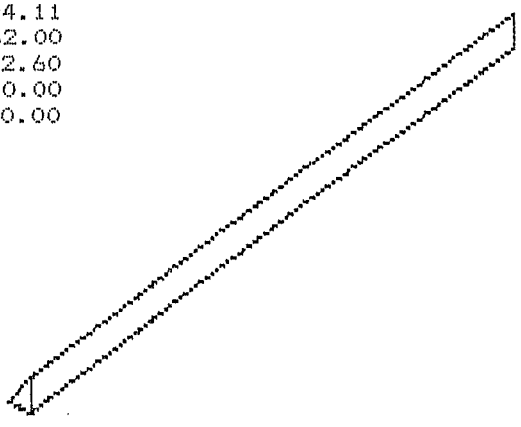

Acceleration Kc = 0.1249 Factor of Safety = 1.39

Analysis of Sarma "infinite" slope for 0.5m to 1.5m thick blocks.

SARMA NON-VERTICAL SLICE ANALYSIS

Analysis no. infinite slope 100m long 0.50m thick block

Unit weight of water = 9.8

Side number	1	2
Coordinate xt	17.00	117.00
Coordinate yt	6.97	47.37
Coordinate xw	17.00	117.00
Coordinate yw	6.97	47.37
Coordinate xb	17.00	117.00
Coordinate yb	6.44	46.84
Friction angle	0.00	0.00
Cohesion	0.00	0.00

Slice number	1
Rock unit weight	19.62
Friction angle	28.40
Cohesion	6.00
Force T	0.00
Angle theta	0.00

Effective normal stresses

Base	3.74
Side	0.00

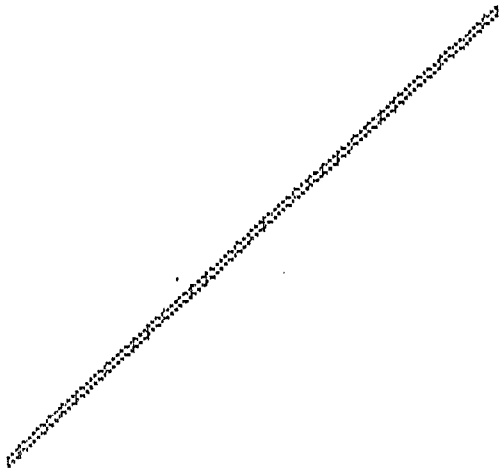

Acceleration Kc = 0.4052 Factor of Safety = 2.21

SARMA NON-VERTICAL SLICE ANALYSIS

Analysis no. infinite slope 100m long 0.75m thick block

Unit weight of water = 9.8

Side number	1	2
Coordinate xt	17.00	117.00
Coordinate yt	7.25	47.65
Coordinate xw	17.00	117.00
Coordinate yw	7.25	47.65
Coordinate xb	17.00	117.00
Coordinate yb	6.44	46.84
Friction angle	0.00	0.00
Cohesion	0.00	0.00

Slice number	1
Rock unit weight	19.62
Friction angle	28.40
Cohesion	6.00
Force T	0.00
Angle theta	0.00

Effective normal stresses

Base	5.72
Side	0.00

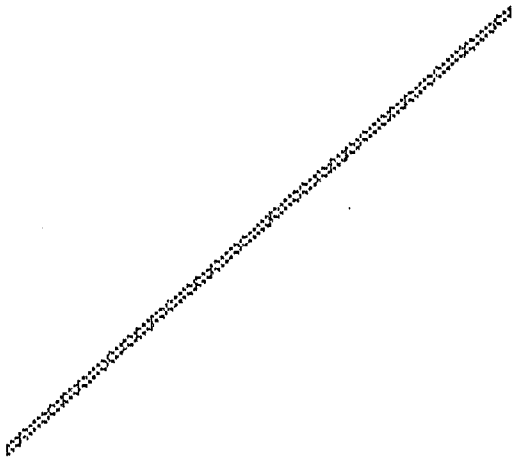

Acceleration Kc = 0.2148 Factor of Safety = 1.64

SARMA NON-VERTICAL SLICE ANALYSIS

Analysis no. infinite slope 100m long 1.00m thick block

Unit weight of water = 9.8

Side number	1	2
Coordinate xt	17.00	117.00
Coordinate yt	7.51	47.91
Coordinate xw	17.00	117.00
Coordinate yw	7.51	47.91
Coordinate xb	17.00	117.00
Coordinate yb	6.44	46.84
Friction angle	0.00	0.00
Cohesion	0.00	0.00

Slice number	1
Rock unit weight	19.62
Friction angle	28.40
Cohesion	6.00
Force T	0.00
Angle theta	0.00

Effective normal stresses

Base	7.56
Side	0.00

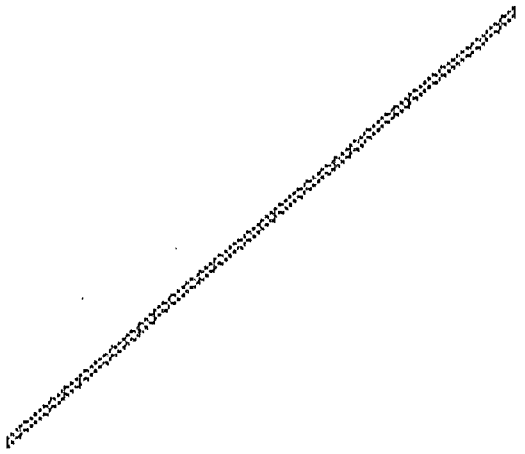

Acceleration Kc = 0.1272 Factor of Safety = 1.38

SARMA NON-VERTICAL SLICE ANALYSIS

Analysis no. infinite slope 100m long 1.25m thick block

Unit weight of water = 9.8

Side number	1	2
Coordinate xt	17.00	117.00
Coordinate yt	7.79	48.19
Coordinate xw	17.00	117.00
Coordinate yw	7.79	48.19
Coordinate xb	17.00	117.00
Coordinate yb	6.44	46.84
Friction angle	0.00	0.00
Cohesion	0.00	0.00

Slice number	1
Rock unit weight	19.62
Friction angle	28.40
Cohesion	6.00
Force T	0.00
Angle theta	0.00

Effective normal stresses

Base	9.54
Side	0.00

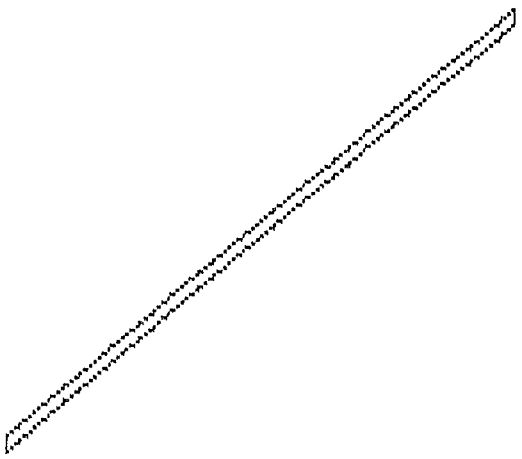

Acceleration Kc = 0.0706 Factor of Safety = 1.21

SARMA NON-VERTICAL SLICE ANALYSIS

Analysis no. infinite slope 100m long 1.5m thick block

Unit weight of water = 9.8

Side number	1	2
Coordinate xt	17.00	117.00
Coordinate yt	7.95	48.35
Coordinate xw	17.00	117.00
Coordinate yw	7.95	48.35
Coordinate xb	17.00	117.00
Coordinate yb	6.44	46.84
Friction angle	0.00	0.00
Cohesion	0.00	0.00

Slice number	1
Rock unit weight	19.62
Friction angle	28.40
Cohesion	6.00
Force T	0.00
Angle theta	0.00

Effective normal stresses

Base	10.67
Side	0.00

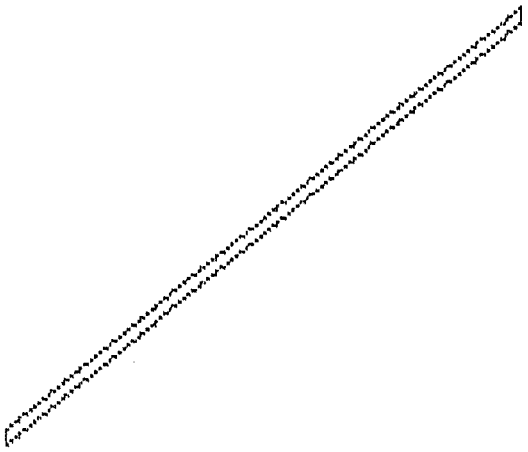

Acceleration Kc = 0.0477

Factor of Safety = 1.14

Undrained back analysis for a 0.53m thick block.

SARMA NON-VERTICAL SLICE ANALYSIS

Analysis no. F.O.S.=1, Block thickness=0.53m, phi=0, G.W.L.=0.26m

Unit weight of water = 9.8

Side number	1	2	3
Coordinate xt	15.05	17.00	27.00
Coordinate yt	6.19	6.97	11.01
Coordinate xw	15.05	17.00	27.00
Coordinate yw	6.19	6.71	10.75
Coordinate xb	15.05	17.00	27.00
Coordinate yb	6.19	6.44	10.48
Friction angle	0.00	0.00	0.00
Cohesion	0.00	3.17	0.00

Slice number	1	2
Rock unit weight	19.62	19.62
Friction angle	0.00	0.00
Cohesion	3.17	3.17
Force T	0.00	0.00
Angle theta	0.00	0.00

Effective normal stresses

Base		4.33	6.30
Side	0.00	8.33	

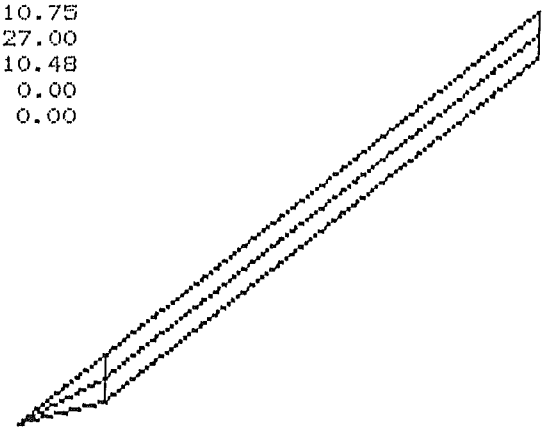

Acceleration Kc = -0.0004 Factor of Safety = 1.00

SARMA NON-VERTICAL SLICE ANALYSIS

Analysis no. F.O.S.=1, Block thickness=0.53m, phi=0, G.W.L.=0.53m

Unit weight of water = 9.8

Side number	1	2	3
Coordinate xt	15.05	17.00	27.00
Coordinate yt	6.19	6.97	11.01
Coordinate xw	15.05	17.00	27.00
Coordinate yw	6.19	6.97	11.01
Coordinate xb	15.05	17.00	27.00
Coordinate yb	6.19	6.44	10.48
Friction angle	0.00	0.00	0.00
Cohesion	0.00	3.25	0.00

Slice number	1	2
Rock unit weight	19.62	19.62
Friction angle	0.00	0.00
Cohesion	3.25	3.25
Force T	0.00	0.00
Angle theta	0.00	0.00

Effective normal stresses

Base		3.07	3.72
Side	0.00	6.68	

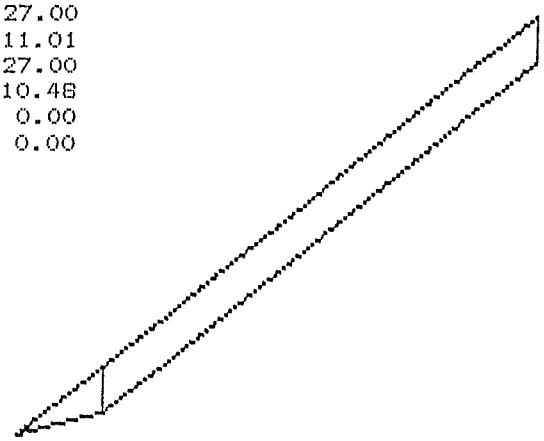

Acceleration Kc = 0.0003 Factor of Safety = 1.00

SARMA NON-VERTICAL SLICE ANALYSIS

Analysis no. F.O.S.=1, Block thickness=0.53m, phi=0, G.W.L.=0m

Unit weight of water = 9.8

Side number	1	2	3
Coordinate xt	15.05	17.00	27.00
Coordinate yt	6.19	6.97	11.01
Coordinate xw	15.05	17.00	27.00
Coordinate yw	6.19	6.44	10.48
Coordinate xb	15.05	17.00	27.00
Coordinate yb	6.19	6.44	10.48
Friction angle	0.00	0.00	0.00
Cohesion	0.00	3.15	0.00

Slice number	1	2
Rock unit weight	19.62	19.62
Friction angle	0.00	0.00
Cohesion	3.15	3.15
Force T	0.00	0.00
Angle theta	0.00	0.00

Effective normal stresses

Base		5.65	8.96
Side	0.00	8.91	

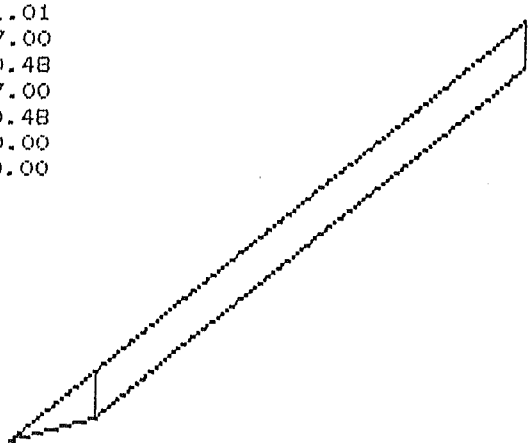

Acceleration Kc = 0.0003

Factor of Safety = 1.00

Drained back analysis for a 0.53m thick block.

SARMA NON-VERTICAL SLICE ANALYSIS

Analysis no. F.O.S.=1, Block thickness=0.53m, phi=28.4, G.W.L.=0.53m

Unit weight of water = 9.8

Side number	1	2	3
Coordinate xt	15.05	17.00	27.00
Coordinate yt	6.19	6.97	11.01
Coordinate xw	15.05	17.00	27.00
Coordinate yw	6.19	6.97	11.01
Coordinate xb	15.05	17.00	27.00
Coordinate yb	6.19	6.44	10.48
Friction angle	0.00	28.40	0.00
Cohesion	0.00	1.28	0.00

Slice number	1	2
Rock unit weight	19.62	19.62
Friction angle	28.40	28.40
Cohesion	1.28	1.28
Force T	0.00	0.00
Angle theta	0.00	0.00

Effective normal stresses

Base		3.44	3.65
Side	0.00	6.10	

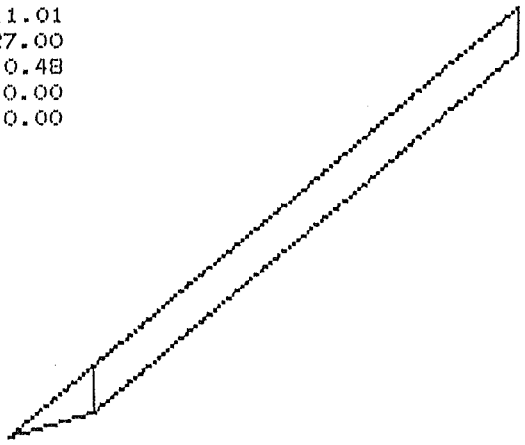

Acceleration Kc = 0.0004 Factor of Safety = 1.00

SARMA NON-VERTICAL SLICE ANALYSIS

Analysis no. F.O.S.=1, Block thickness=0.53m, phi=28.4, G.W.L.=0.26m

Unit weight of water = 9.8

Side number	1	2	3
Coordinate xt	15.05	17.00	27.00
Coordinate yt	6.19	6.97	11.01
Coordinate xw	15.05	17.00	27.00
Coordinate yw	6.19	6.71	10.75
Coordinate xb	15.05	17.00	27.00
Coordinate yb	6.19	6.44	10.48
Friction angle	0.00	28.40	0.00
Cohesion	0.00	-0.06	0.00

Slice number	1	2
Rock unit weight	19.62	19.62
Friction angle	28.40	28.40
Cohesion	-0.06	-0.06
Force T	0.00	0.00
Angle theta	0.00	0.00

Effective normal stresses

Base		4.31	6.26
Side	0.00	5.04	

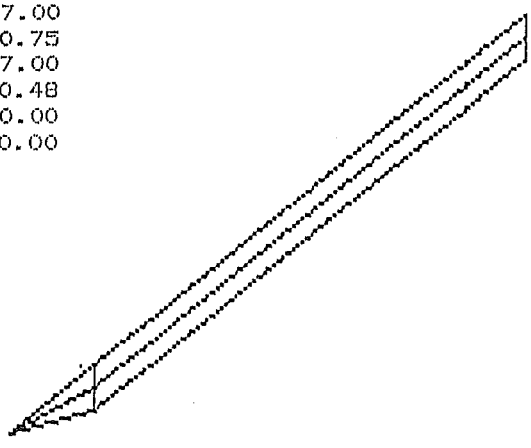

Acceleration Kc = -0.0005 Factor of Safety = 1.00

SARMA NON-VERTICAL SLICE ANALYSIS

Analysis no. F.O.S.=1, Block thickness=0.53m, phi=28.4, G.W.L.=0m

Unit weight of water = 9.8

Side number	1	2	3
Coordinate xt	15.05	17.00	27.00
Coordinate yt	6.19	6.97	11.01
Coordinate xw	15.05	17.00	27.00
Coordinate yw	6.19	6.44	10.48
Coordinate xb	15.05	17.00	27.00
Coordinate yb	6.19	6.44	10.48
Friction angle	0.00	28.40	0.00
Cohesion	0.00	-1.37	0.00

Slice number	1	2
Rock unit weight	19.62	19.62
Friction angle	28.40	28.40
Cohesion	-1.37	-1.37
Force T	0.00	0.00
Angle theta	0.00	0.00

Effective normal stresses

Base		5.04	8.99
Side	0.00	2.61	

Acceleration Kc = -0.0003 Factor of Safety = 1.00

Undrained back analysis for a 1.4m thick block.

SARMA NON-VERTICAL SLICE ANALYSIS

Analysis no. F.O.S.=1, Block thickness=1.4m, phi=0, G.W.L.= 1.4m

Unit weight of water = 9.8

Side number	1	2	3
Coordinate xt	11.54	17.00	27.00
Coordinate yt	5.74	7.95	11.99
Coordinate xw	11.54	17.00	27.00
Coordinate yw	5.74	7.95	11.99
Coordinate xb	11.54	17.00	27.00
Coordinate yb	5.74	6.44	10.48
Friction angle	0.00	0.00	0.00
Cohesion	0.00	8.03	0.00

Slice number	1	2
Rock unit weight	19.62	19.62
Friction angle	0.00	0.00
Cohesion	8.03	8.03
Force T	0.00	0.00
Angle theta	0.00	0.00

Effective normal stresses

Base		8.60	10.37
Side	0.00	14.20	

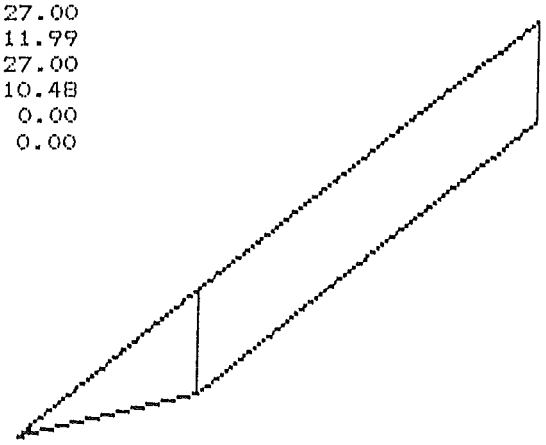

Acceleration Kc = 0.0002 Factor of Safety = 1.00

SARMA NON-VERTICAL SLICE ANALYSIS

Analysis no. F.O.S.=1, Block thickness=1.4m, phi=0, G.W.L.= 0.7m

Unit weight of water = 9.8

Side number	1	2	3
Coordinate xt	11.54	17.00	27.00
Coordinate yt	5.74	7.95	11.99
Coordinate xw	11.54	17.00	27.00
Coordinate yw	5.74	7.25	11.29
Coordinate xb	11.54	17.00	27.00
Coordinate yb	5.74	6.44	10.48
Friction angle	0.00	0.00	0.00
Cohesion	0.00	7.57	0.00

Slice number	1	2
Rock unit weight	19.62	19.62
Friction angle	0.00	0.00
Cohesion	7.57	7.57
Force T	0.00	0.00
Angle theta	0.00	0.00

Effective normal stresses

Base		11.97	17.49
Side	0.00	17.87	

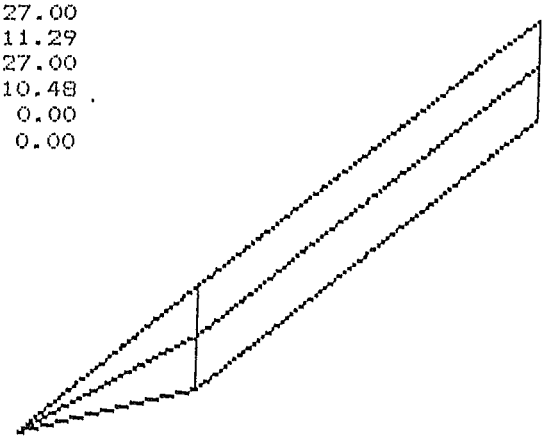

Acceleration Kc = -0.0001 Factor of Safety = 1.00

SARMA NON-VERTICAL SLICE ANALYSIS

Analysis no. F.O.S.=1, Block thickness=1.4m, phi=0, G.W.L.= 0m

Unit weight of water = 9.8

Side number	1	2	3
Coordinate xt	11.54	17.00	27.00
Coordinate yt	5.74	7.95	11.99
Coordinate xw	11.54	17.00	27.00
Coordinate yw	5.74	6.44	10.48
Coordinate xb	11.54	17.00	27.00
Coordinate yb	5.74	6.44	10.48
Friction angle	0.00	0.00	0.00
Cohesion	0.00	7.39	0.00

Slice number	1	2
Rock unit weight	19.62	19.62
Friction angle	0.00	0.00
Cohesion	7.39	7.39
Force T	0.00	0.00
Angle theta	0.00	0.00

Effective normal stresses

Base		15.91	25.52
Side	0.00	19.35	

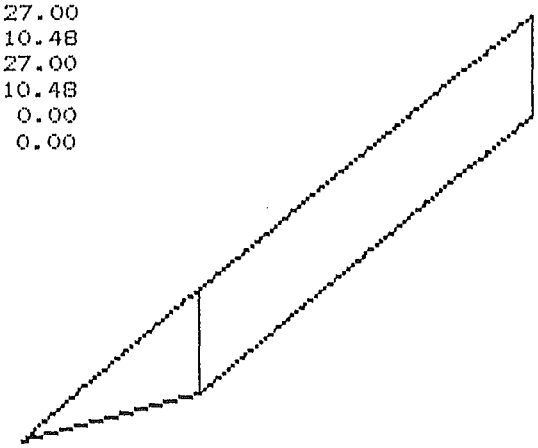

Acceleration Kc = -0.0000

Factor of Safety = 1.00

Drained back analysis for a 1.4m thick block.

SARMA NON-VERTICAL SLICE ANALYSIS

Analysis no. F.O.S.=1, Block thickness=1.4m, phi=28.4, G.W.L.= 1.4m

Unit weight of water = 9.8

Side number	1	2	3
Coordinate xt	11.54	17.00	27.00
Coordinate yt	5.74	7.95	11.99
Coordinate xw	11.54	17.00	27.00
Coordinate yw	5.74	7.95	11.99
Coordinate xb	11.54	17.00	27.00
Coordinate yb	5.74	6.44	10.48
Friction angle	0.00	28.40	0.00
Cohesion	0.00	2.71	0.00

Slice number	1	2
Rock unit weight	19.62	19.62
Friction angle	28.40	28.40
Cohesion	2.71	2.71
Force T	0.00	0.00
Angle theta	0.00	0.00

Effective normal stresses

Base		9.06	10.10
Side	0.00	12.49	

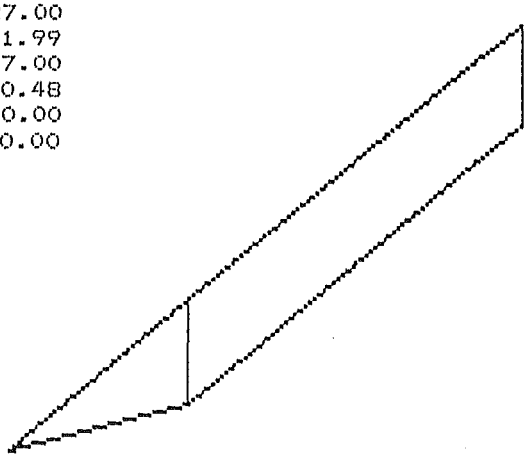

Acceleration Kc = -0.0001 Factor of Safety = 1.00

SARMA NON-VERTICAL SLICE ANALYSIS

Analysis no. F.O.S.=1, Block thickness=1.4m, phi=28.4, G.W.L.= 0.7m

Unit weight of water = 9.8

Side number	1	2	3
Coordinate xt	11.54	17.00	27.00
Coordinate yt	5.74	7.95	11.99
Coordinate xw	11.54	17.00	27.00
Coordinate yw	5.74	7.25	11.29
Coordinate xb	11.54	17.00	27.00
Coordinate yb	5.74	6.44	10.48
Friction angle	0.00	28.40	0.00
Cohesion	0.00	-0.76	0.00

Slice number	1	2
Rock unit weight	19.62	19.62
Friction angle	28.40	28.40
Cohesion	-0.76	-0.76
Force T	0.00	0.00
Angle theta	0.00	0.00

Effective normal stresses

Base		11.50	17.44
Side	0.00	10.44	

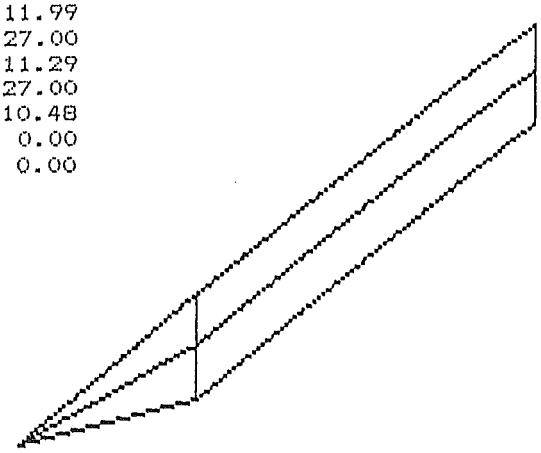

Acceleration Kc = -0.0002 Factor of Safety = 1.00

SARMA NON-VERTICAL SLICE ANALYSIS

Analysis no. F.O.S.=1, Block thickness=1.4m, phi=28.4, G.W.L.= 0m

Unit weight of water = 9.8

Side number	1	2	3
Coordinate xt	11.54	17.00	27.00
Coordinate yt	5.74	7.95	11.99
Coordinate xw	11.54	17.00	27.00
Coordinate yw	5.74	6.44	10.48
Coordinate xb	11.54	17.00	27.00
Coordinate yb	5.74	6.44	10.48
Friction angle	0.00	28.40	0.00
Cohesion	0.00	-4.33	0.00

Slice number	1	2
Rock unit weight	19.62	19.62
Friction angle	28.40	28.40
Cohesion	-4.33	-4.33
Force T	0.00	0.00
Angle theta	0.00	0.00

Effective normal stresses

Base	13.98	25.94
Side	0.00	5.19

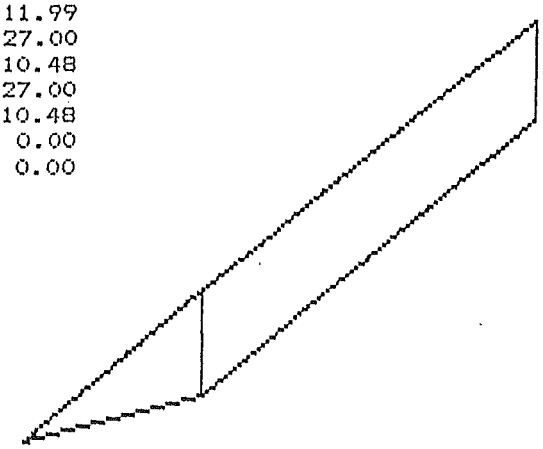

Acceleration Kc = -0.0000 Factor of Safety = 1.00

Undrained back analysis (infinite slope equation) for a 0.53m thick block.

```
INFINITE SLOPE CALCULATIONS FOR ANY GENERALISED SLOPE WITH SEIS
                    [without artesian pressures]
INPUT PARAMETERS

SLOPE ANGLE (DEG)          22.00     COS = .93 SIN = .37 COS SQ =
THICKNESS (H in M)           .53                         TAN =
WATER LEVEL (Hw in M)        .53                         COTAN =
RATIO, Hw/H                 1.00
UNIT WT WATER               9.80
AVERAGE UNIT WT, SOIL      19.62
ANGLE OF FRICTION           0.00     TAN = .00
COHESION                    3.62
SEISMIC COEFF. (K)          0.00

SOIL FORCE                  8.94
WATER FORCE                 4.47
FRICTONAL STRENGTH           .00
TOTAL STRENGTH (ie + C)     3.62
SHEAR STRESS                3.61

FACTOR OF SAFETY            1.00

   Kcrit =                   .00    (-1.00       1.00          .00
```

```
INFINITE SLOPE CALCULATIONS FOR ANY GENERALISED SLOPE WITH SEIS
                    [without artesian pressures]
INPUT PARAMETERS

SLOPE ANGLE (DEG)          22.00     COS = .93 SIN = .37 COS SQ =
THICKNESS (H in M)           .53                         TAN =
WATER LEVEL (Hw in M)        0.00                        COTAN =
RATIO, Hw/H                  ERR
UNIT WT WATER               9.80
AVERAGE UNIT WT, SOIL      19.62
ANGLE OF FRICTION          28.40     TAN = .54
COHESION                   -1.23
SEISMIC COEFF. (K)          0.00

SOIL FORCE                  8.94
WATER FORCE                  .00
FRICTONAL STRENGTH          4.83
TOTAL STRENGTH (ie + C)     3.60
SHEAR STRESS                3.61

FACTOR OF SAFETY            1.00

   Kcrit =                  -.00    (  .34       -.34          -.00
```

Drained back analysis (infinite slope equation) for a 0.53m thick block.

```
INFINITE SLOPE CALCULATIONS FOR ANY GENERALISED SLOPE WITH SEIS
                    [without artesian pressures]
INPUT PARAMETERS

SLOPE ANGLE (DEG)          22.00     COS = .93 SIN = .37 COS SQ =
THICKNESS (H in M)           .53                         TAN =
WATER LEVEL (Hw in M)        .26                         COTAN =
RATIO, Hw/H                 2.04
UNIT WT WATER               9.80
AVERAGE UNIT WT, SOIL      19.62
ANGLE OF FRICTION          28.40     TAN = .54
COHESION                    -.03
SEISMIC COEFF. (K)          0.00

SOIL FORCE                  8.94
WATER FORCE                 2.19
FRICTONAL STRENGTH          3.65
TOTAL STRENGTH (ie + C)     3.62
SHEAR STRESS                3.61

FACTOR OF SAFETY            1.00

   Kcrit =                   .00    (  .01        -.01           .00
```

```
INFINITE SLOPE CALCULATIONS FOR ANY GENERALISED SLOPE WITH SEIS
                    [without artesian pressures]
INPUT PARAMETERS

SLOPE ANGLE (DEG)          22.00     COS = .93 SIN = .37 COS SQ =
THICKNESS (H in M)           .53                         TAN =
WATER LEVEL (Hw in M)        .53                         COTAN =
RATIO, Hw/H                 1.00
UNIT WT WATER               9.80
AVERAGE UNIT WT, SOIL      19.62
ANGLE OF FRICTION          28.40     TAN = .54
COHESION                    1.20
SEISMIC COEFF. (K)          0.00

SOIL FORCE                  8.94
WATER FORCE                 4.47
FRICTONAL STRENGTH          2.42
TOTAL STRENGTH (ie + C)     3.62
SHEAR STRESS                3.61

FACTOR OF SAFETY            1.00

   Kcrit =                   .00    ( -.33        .33            .00
```

Undrained back analysis (infinite slope equation) for a 1.4m thick block.

```
INFINITE SLOPE CALCULATIONS FOR ANY GENERALISED SLOPE WITH SEIS
                    [without artesian pressures]
F.O.S.=1, Block thickness=1.4m, phi=0    , G.W.L.= =0m

INPUT PARAMETERS

SLOPE ANGLE (DEG)          22.00    COS = .93 SIN = .37 COS SQ =
THICKNESS (H in M)          1.40                         TAN =
WATER LEVEL (Hw in M)       0.00                         COTAN =
RATIO, Hw/H                  ERR
UNIT WT WATER               9.80
AVERAGE UNIT WT, SOIL      19.62
ANGLE OF FRICTION           0.00    TAN = .00
COHESION                    9.54
SEISMIC COEFF. (K)          0.00

SOIL FORCE                 23.61
WATER FORCE                  .00
FRICTONAL STRENGTH           .00
TOTAL STRENGTH (ie + C)     9.54
SHEAR STRESS                9.54

FACTOR OF SAFETY            1.00

   Kcrit =                   .00   (-1.00   .    1.00          .00
```

```
INFINITE SLOPE CALCULATIONS FOR ANY GENERALISED SLOPE WITH SEIS
                    [without artesian pressures]
F.O.S.=1, Block thickness=1.4m, phi=28.4, G.W.L.= =0m

INPUT PARAMETERS

SLOPE ANGLE (DEG)          22.00    COS = .93 SIN = .37 COS SQ =
THICKNESS (H in M)          1.40                         TAN =
WATER LEVEL (Hw in M)       0.00                         COTAN =
RATIO, Hw/H .                ERR
UNIT WT WATER               9.80
AVERAGE UNIT WT, SOIL      19.62
ANGLE OF FRICTION          28.40    TAN = .54
COHESION                   -3.22
SEISMIC COEFF. (K)          0.00

SOIL FORCE                 23.61
WATER FORCE                  .00
FRICTONAL STRENGTH         12.77
TOTAL STRENGTH (ie + C)     9.55
SHEAR STRESS                9.54

FACTOR OF SAFETY            1.00

   Kcrit =                   .00   (  .34      -.34          .00
```

Drained back analysis (infinite slope equation) for a 1.4m thick block.

```
INFINITE SLOPE CALCULATIONS FOR ANY GENERALISED SLOPE WITH SEIS
                    [without artesian pressures]
F.O.S.=1, Block thickness=1.4m, phi=28.4, G.W.L.= 0.7m

INPUT PARAMETERS

SLOPE ANGLE (DEG)          22.00    COS = .93 SIN = .37 COS SQ =
THICKNESS (H in M)          1.40                         TAN =
WATER LEVEL (Hw in M)        .70                         COTAN =
RATIO, Hw/H                 2.00
UNIT WT WATER               9.80
AVERAGE UNIT WT, SOIL      19.62
ANGLE OF FRICTION          28.40    TAN = .54
COHESION                    -.03
SEISMIC COEFF. (K)          0.00

SOIL FORCE                 23.61
WATER FORCE                 5.90
FRICTONAL STRENGTH          9.58
TOTAL STRENGTH (ie + C)     9.55
SHEAR STRESS                9.54

FACTOR OF SAFETY            1.00

   Kcrit =                   .00   (  .00       -.00          .00
```

```
INFINITE SLOPE CALCULATIONS FOR ANY GENERALISED SLOPE WITH SEIS
                    [without artesian pressures]
F.O.S.=1, Block thickness=1.4m, phi=28.4, G.W.L.=1.4

INPUT PARAMETERS

SLOPE ANGLE (DEG)          22.00    COS = .93 SIN = .37 COS SQ =
THICKNESS (H in M)          1.40                         TAN =
WATER LEVEL (Hw in M)       1.40                         COTAN =
RATIO, Hw/H                 1.00
UNIT WT WATER               9.80
AVERAGE UNIT WT, SOIL      19.62
ANGLE OF FRICTION          28.40    TAN = .54
COHESION                    3.15
SEISMIC COEFF. (K)          0.00

SOIL FORCE                 23.61
WATER FORCE                11.80
FRICTONAL STRENGTH          6.39
TOTAL STRENGTH (ie + C)     9.54
SHEAR STRESS                9.54

FACTOR OF SAFETY            1.00

   Kcrit =                   .00   ( -.33       .33          .00
```